Antarctic Meteorites XXI

Papers presented to the Twentyfirst Symposium on Antarctic Meteorites

June 5-7, 1996

NATIONAL INSTITUTE OF POLAR RESEARCH,
TOKYO

国立極地研究所

Wednesday, June 5, 1996

0900 - 1200 Registration — Auditorium (6th Floor)

0925 - 0930 Opening Address — **Takeo Hirasawa**, Director-General, National Institute of Polar Research

*Speaker

Chairmen: Fukuoka T. and Noguchi T. **Page**

1200 - 1300 Lunch Time

Chairmen: Yamaguchi A. and Ebihara M. **Page**

1510 - 1540 Tea Time

-- Special Lecture (I) --

1700 - 1900 Reception Lecture room (2F)

Thursday, June 6, 1996

Chairmen: Sugiura N. and Nagao K. **Page**

Chairmen: Tsuchiyama A. and Mikouchi T. **Page**

Friday, June 7, 1996

Chairmen: Funaki M. and Kimura M. **Page**

1200 - 1300 Lunch Time & Poster Session

ABSTRACTS

New descriptions and re-examinations on thermal metamorphisms in several Antarctic CM2 carbonaceous chondrites : Preliminary reports

Akai ,J. , Tari,S. and Tanaka ,H.
Department of Geology , Faculty of Science , Niigata University
Ikarashi 2-nocho, 8050, Niigata 950-21, Japan

Introduction: Antaractic carbonaceous chondrites often have characteristic features of thermal metamorphism (Akai, 1984,1988, 1990; Kojima et al.,1984; Tomeoka, 1989a,b ; Ikeda, 1991; Zolensky, et al.,1989). It is very characteristic in contrast to non-Antarctic carbonaceous chondrites. The cause of this metamorphism has also variously estimated (Kimura,1992; Miyamoto,1990, Hiroi et al.,1995). Some shock effect experiments have been carried out to ascertain these possibility, using shock experiment (Akai and Sekine, 1994). However the possiblity of heating by shock events was considered to be less. Hiroi et al (1993,1995) suggested possible thermal metamorphism in many of the C,G,B and Ftype asteroids. Hiroi et al. interpreted thermal metamorphism after extensive aqueous alteration in parent body. The different degrees of thermal metamorphism may partly depend on the different degrees of water contents and depths. More data are necessary to ascertain these scenarios or have the other. The ratio of thermally metamorphosed C meteorites / unheated C meteorites may become fundamental data. So, using as many Antarctic CM2 type carbonaceous chondrite specimens available as posible , we wanted to obtain the ratio in Antarctic meteorites. In this study we searched for the metamrophic evidences in the constituent minerlas, especially phyllosilicates in CM2 carbonaceous chondrites . Some specimens which have already been examined were re-examined because checking the phyllosilcates by TEM is in some cases difficult and confusing. The phyllosilicates are sometimes easily damaged to electron beam and/or to argon ion beam which is often used in TEM specimen preparation. We performed the checking such artifiacts of defect in detail by using non-ion thinned specimens. Thus, examined results made us to give some correction for the the results on Y-82042 which was reported last year (Akai,1995).

Specimens and general features: The following new CM2 specimens and Y-82042 were examined. But the examination is not fully completed, and the results are preliminarily reported here. Description of the bulk specimen and the other characteristics which have been reported by NIPR (1994) are as follows :

	type	total weight	Fa in olivine	Fs in px	Other characteristics
Y-793595	CM2	48.22g	18.1 (17.3-18.8)	2.4(1.0-3.8)	Pl($An_{6.3}$ $Or_{7.4}$)$En_{59.3}Fs_{0.9}Wo_{39.8}$ ap.
Y-82042	CM2	37.08	(0.2- 35.4)		
Y-82054	CM2	76.34	10.1(0.2-37.9)	2.1(0.5-7.1)	$En_{60.7}Fs_{18.5}Wo_{5.6}$
Y-82098	CM2	94.48	18.1(0.2-53.1)	4.4(0.5-42.4)	
Y-86695	CM2	59.59	10.6(0.1-53.4)	1.4(0.5-3.7)	
A-881334	CM2	34.05	4.8(0.2-32.1)	1.7(0.6-6.3)	
A-881458	CM2	56.84	16.4(0.2-54.0)	1.6(0.5-4.4)	
A-881955	CM2	40.0	(0.3-51.5)	(0.6-5.0)	

TEM observations : TEM observations of phyllosilicates for all samples were carried out. Fig. 1 shows four examples of lattice images of phyllosilicates of Y-82098 (Fig.1a) , A-881955 (Fig.1b), Y-793595 (Fig.1c) and Y-82042 (Fig.1d) .

All the phyllosilicates or transformed minerals were originally serpentine type. Thier compositions were Fe-rich type. However, two types may be present according to the iron contents; one , Fe »» Mg, and the other, Fe≃Mg or Fe ≧ Mg types.

Y-82054, Y-82098,Y-86695 and A-881334 were estimated to be thermally metamorphosed specimens. Thermal metamorphism can be decided by combined results of CTEM , HRTEM lattice images, ED patterns and AEM spectra. The characteristics are different based on the degrees of thermal metamorphism. For example, in metamorphism of 300 -500 C characteristic halo diffraction and ~10 -13A degraded lattices in HRTEM images are the features (cf.Y-82098 : Fig. Fig.1a).

On the other hand, non-metamorphosed CM2 chondrite is ,for example, A-881955. In specimens A-891955, phyllosilicates are found sharply (Fig. 1b).

Y-793595 is also very similar to that of unheated (non-metamorphosed) CM2 chondrites but characteristic HRTEM images and ED pattern were found in this specimen. In the ED pattern of phyllosilicates extra 14 A diffuse spots with streaks between systematic 7 A diffraction spot series were found. HRTEM images of layer structures showed partial 14 A periodicity in the 7 A lattice arrangements. Another patch-like pattern which may be more clear damaged structure is also found in wide area of 7 A lattice images (Fig.1c). The cause of this degraded features cannot be uniquely determined yet, but one possibility is that they were formed by weak thermal metamorphism or the other factor with equivalent effects. Planar or tube-like tochilinite was also found.

We reported last year that Y82042 is thermally metamorphosed one, but detailed re-examination has shown that the lattice image of the phyllosilciates are not so sharp but frequently wavy although 7 A spacing is recognized. ED pattern in some case showed halo pattern . In these points interpretation was a little confusing. The reasons for them are not yet clarified : whether it is originally degraded for example in the early stage of thermal metamorphism, or it is susceptible to electron damage and so on. This study showed that Y-82042 may be fundamentally slightly metamorphosed ~ non-metamorphosed type and the phyllosilicates are a little damaged.

Summarized results: Preliminary results are summarized as follows:

Y-793595	non-metamorphosed ~ slightly metamorphosed
Y-82042	slightly metamorphosed ~ non-metamorphosed
Y-82054	metamorphosed
Y-82098	metamorphosed
Y-86695	metamorphosed
A-881334	metamorphosed
A-881458	very weakly metamorphosed ~ non-metamorphosed
A-881955	non-metamorphosed

From these preliminary results, it can be at least said that several metamorphosed specimens are present in the examined eight CM2 specimens. The half is apparantly thermally metamorphosed among the examined specimens. The degree of thermal metamorphism on the four specimens are roughly similar to that of Y-793321; that is, 300~ 500 C. Another finding in this study is that phyllosilicate layer structure is not always simple even if its d- spacing maintains 7 A of serpentine structure. Sometimes its layer structure is wavy or has patch- like defect pattern in TEM image, and shows 14 A

extra spots in ED pattern. These characteristic can be interpreted variously but one possibility is that these are due to initial stage of weak thermal metamorphism in which fundamental phyllosilicate structure is not fully decomposed but some change starts. Thus, the following features were confirmed that (1) Antarctic carbonaceous chondrites are often and generally thermally metamorphosed and that (2) the metamorphic degrees are various and apparently continuous. At present, There still exist various possible models for the heating events: for example, parent body processes, interplanetary heating processes and so on. One possibility is that differences of these thermal metamorphism may be due to characteristics in various water (ice) contents and various depths in CM2 parent bodies processes.

References: AkaiJ.(1984) Pap.9th NIPR Symp.Ant.Met.59; ··· (1988) GCA,52,1593;··· (1990) Proc.NIPR Symp.Ant.Met., 3,55;··· (1992a) Pap.9th NIPR Symp.Ant.Met.;··· (1992b) Proc.NIPR Symp. Ant.Met.,5,120; ··· (1995) Pap. 20th NIPR Symp.Ant. Met, 1; Akai, J. and Sekine, T. (1994) Proc. NIPR Symp. Antarctic meteorites, 7 ,101; Hiroi, et al.,(1993) Science 261,1076; Hiroi, et al.,(1995) Pap. 20th NIPR Symp.Ant. Met,72; Ikeda, Y. (1991) Proc.NIPR Symp.Ant. Met.,4,187; Kimura,M. et al.(1992) Proc.NIPR Symp. Ant.Met.5,74; Kojima, et al.,(1984) Mem.NIPR Sp.Iss.35,184.; Miyamoto,M. (1990) Pap.15th NIPR Symp. Ant. Met.89; NIPR (1995) Catalog of the Antarctic meteorites;Tomeoka,K. (1989a) Proc. NIPR Symp.Ant.Met. , 2,36; ··· (1989b) Proc.NIPR Symp.Ant.Met.2,55; Zolensky, et al.(1989) Pap.14th NIPR Symp.Ant.Met.24.

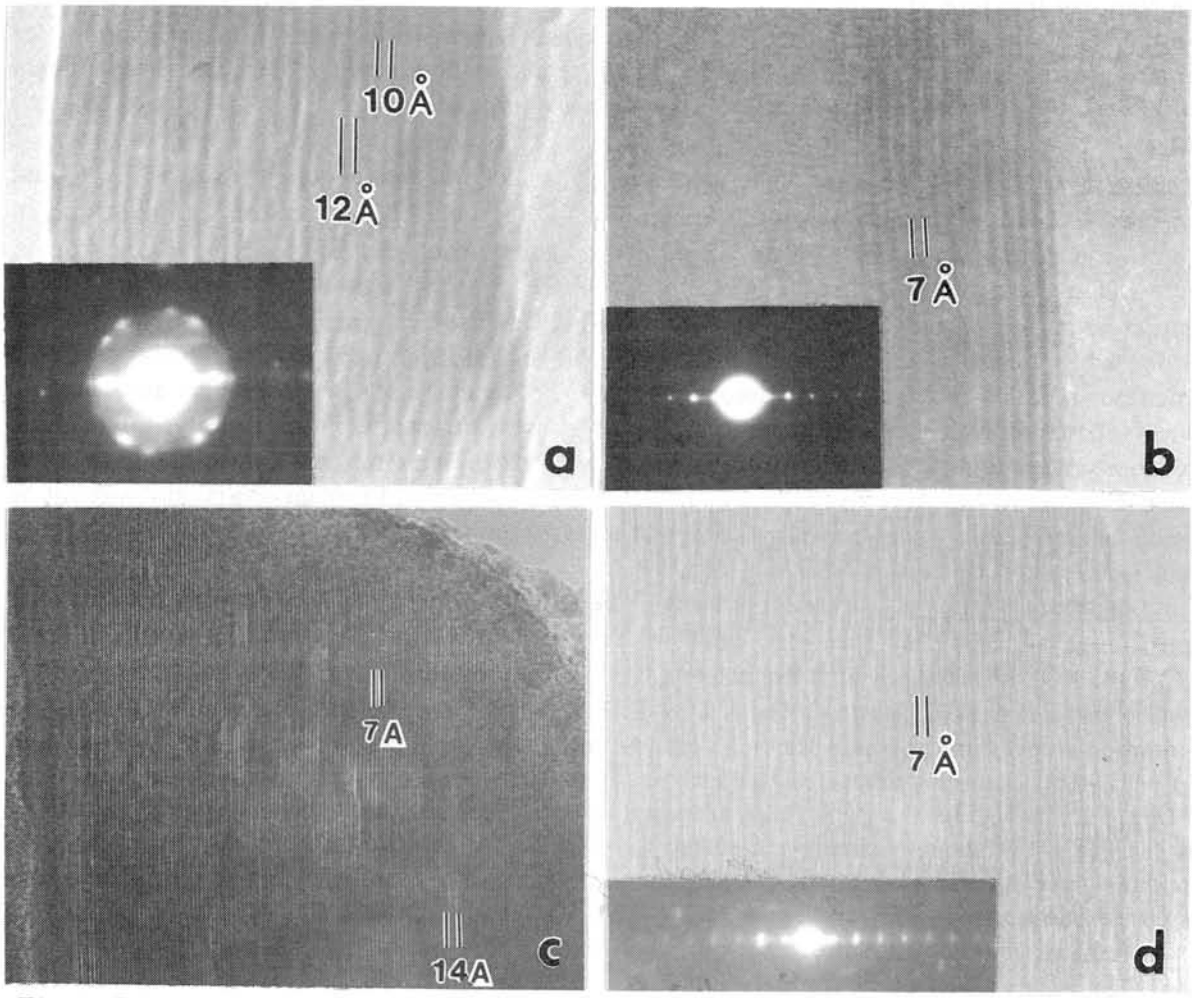

Fig.1 TEM images of phyllosilicates or transformed phyllosilicates in CM2 chondrites. a: Y-82098 ; b: A-881955 ; c: Y-793595 ; d : Y-82042.

VLT-mare glasses of probable pyroclastic origin in lunar meteorite breccias Yamato 793274 and QUE94281

TOMOKO ARAI[1] AND PAUL H. WARREN[1,2]

[1]Mineralogical Institute, Graduate School of Science, University of Tokyo, Hongo Tokyo,
[2]Institute of Geophysics, UCLA, Los Angeles, CA 90095-1567, U.S.A.

Introduction: Among Apollo samples, two kinds of glasses have been recognized: impact glasses and pristine (pyroclastic) glasses. Pristine lunar glasses are thought to have been erupted on the Moon's surface directly from lunar mantle, since they appear to be geochemically less evolved than crystalline mare basalts [1,2]. They could play a significant role in deciphering lunar mantle petrology. Their compositions are diverse, for instance, TiO_2 ranges from 0.4 to 16.4 wt%, and they probably represent a wide variety of primary magma types, and thus imply considerable heterogeneity among their mantle source regions [1].

Antarctic meteorites Yamato 793274 and QUE94281 are regolith breccias dominated by VLT mare basalt (bulk-breccia TiO_2 = 0.6 wt%) [3,4]. Whole-rock chemistries, mineral chemistries, textures, and exposure histories of these two breccias are remarkably similar and source-crater pairing has been proposed [5,6,7,8]. Even though glass spherules are rare by regolith standards in both breccias, they include some probably pristine volcanic glasses.

Samples and Methods: We studied three PTSs of Y793274, 91-2, 95-1, and 95-2, kindly supplied by the National Institute of Polar Research, and two PTSs of QUE94281, 6 and ,8, supplied by the Antarctic Meteorite Working Group. We probed glass composition with a focused beam for information on the heterogeneity within the spherule, and with a slightly defocused beam (beam diameter = 10 μm) to get the best data for bulk-spherule composition.

Results:

Glass populations: Most of glass spherules and spherule fragments found in Y793274 and QUE94281 tend to be brownish with a few exceptions of clear ones. Most are from 30 to 60 μm in diameter. In addition, several pale green glasses of probable pyroclastic origin occur as large (up to 240 μm) angular fragments in Y793274. Compositionally these glasses are indistinguishable from the intact spherules (including representatives from both of the Ti groups discussed below). Some spherules are apparently zoned from core to rim, or include microcrystals and inclusions. We screened out possibly pristine glasses among all Y793274 and QUE94281 spherules and spherule fragments, based on Delano's criteria for pristinity of glasses: intrasample homogeneity, intersample homogeneity (clustering), high Mg/Al ratio (>1.5), absence of schlieren and exotic inclusions, etc. [1]. Glasses with low Mg/Al ratio (Al_2O_3 = 13-32 wt%) are probably of impact origin, and will not be discussed further. Table 1 shows average compositions from nine probably pristine individual glasses in QUE94281 and sixteen in Y793274.

Compositional variations: Pristine glasses from the two breccias show remarkably similar compositional trends. They are very poor in Ti (TiO_2 = 0.37-1.22 wt%). However, in both Y793274 and QUE94281 two distinct clusters can be recognized: a lower-Ti group (TiO_2 = 0.37-0.67wt%) and a higher-Ti group (TiO_2 = 0.99-1.22 wt%) (Fig. 1a). In the higher-TiO_2 group, the fractionation trend starts at a less Mg-rich composition (MgO = 14 wt%) than in the lower-Ti one (MgO = 16 wt%). In both groups, CaO steadily increases (CaO = 10.72-8.19 wt%) with decreasing of MgO (Fig. 1b). In Fig. 1c, the two groups are again manifest, as two divergent trends. The glasses of the higher-Ti group show markedly increasing Al_2O_3 with decreasing MgO and the lower-Ti glass group shows level or decreasing Al_2O_3 with decreasing MgO. To simplify the following discussion, we arbitrarily designate the lower-Ti group as "group YQ1" and the higher-Ti group as "group YQ2" (the Y stands for Y793274 and the Q for QUE94281; note that group YQ1 is more numerous than group YQ2). Analyses of one extremely heterogeneous spherule (thus rejected as not confidently

pristine) suggest that possibly QUE94281 includes a minor component of glass with relatively high (1.4-5.5 wt%) TiO_2.

Discussion:

Comparison with Apollo/Luna glasses: Until recently, only the pristine glasses having the highest MgO composition within each of the 25 distinct Apollo+Luna suites were considered to have formed as primary magma, unmodified by low-pressure processing. Nearly all intra-group compositional variations were thought to be driven by a low-pressure process, such as olivine fractionation [1,2]. However, dynamic polybaric melting has recently been recognized as an important process in generation of primary magmas on the Earth [9,10], it appears more likely that intra-group compositional trends of lunar pyroclastic glasses generally reflect incomplete mixing of aggregated melts from different regions of ascending mantle diapir [11,12].

Compared with the 25 different pristine glasses identified for Apollo glasses [1], the glass compositions of Y793274 and QUE94281 appear to scatter toward relatively MgO-poor compositions (Fig. 2a). That is just because 25 glass compositions represent only MgO-rich end within the groups, as mentioned above. Taking 1.5 wt% as the maximum TiO_2 content for classification as VLT (sometimes 1.0 wt% has been used), both YQ1 and YQ2 represent VLT types. These glasses show remarkably similar compositions and fractionation trends to those of an Apollo 14 VLT glass suite [13] and to a slightly lesser degree the Apollo 17 VLT glass suites of [13,14]. However, the Y793274/QUE94281 glasses are distinctive, in two respects: (1) they appear separated into two independent suites, based on the bimodality of their TiO_2 contents (Fig. 1a), and (2) while in the Apollo 14 and 17 VLT glass suites (and also in YQ1) Al_2O_3 markedly increases with the decrease of MgO, in YQ2 decreasing MgO is accompanied by a slight decrease in Al_2O_3 (Fig. 1c).

Fractionation trends: Conceivably, the increase of CaO with decreasing of MgO in both YQ1 and YQ2 (Fig. 1b) and the development of a separate trend (YQ2) with slightly higher TiO_2 (Fig. 1a) may have been caused by crystallization of microcrystals of olivines during pyroclastic eruption. However, the near-constancy of TiO_2 across the wide range of MgO and Al_2O_3 in YQ1, and the constant or slightly decreasing Al_2O_3 with decreasing MgO in YQ2, are both inconsistent with simple olivine control. It seems far more likely that the YQ1 and YQ2 fractionation trends resulted from deep-seated processes in the lunar mantle, such as dynamic melting. If so, each of these fractionation trends probably reflects a range of melt compositions produced primarily by mixing of aggregated melts from different regions of ascending mantle diapir, as proposed by Delano [1].

Mantle (?) arrays: Two apparent "arrays" of Apollo/Luna glasses on MgO - Al_2O_3 plots have been explained as the product of assimilative processes involving two discrete cumulate components in a grossly heterogeneous lunar mantle [1,15]. If this array concept is valid, new discoveries of lunar pyroclastic glasses should not fill the space between the two arrays. The YQ1 and YQ2 pristine glasses both plot entirely within Delano's [1] high- Al_2O_3, low-MgO array (Fig. 2b and c).

Pairing of Y793274 and QUE94281: Pristine glasses from Y793274 and QUE94281 show nearly identical glass populations, involving two clusters on the MgO vs. TiO_2 plot (Fig. 1a). The two clusters presumably reflect two different aggregate primary magmas. It would be miraculous to find such a high degree of similarity between breccias from two widely separated points on the Moon's surface. Our glass compositional data, added to other strong evidence from petrology, mineralogy, exposure history, etc. [5,6,7,8], make Y793274 and QUE94281 the most compelling case ever for meteorites discovered at great distant apart (2500 km) having been derived from a common source crater on the ultimate parent body.

Relationship between VLT glasses and VLT basalts: Longhi [2] inferred that none of the Apollo/Luna picritic glass types is a suitable parent for any known variety of crystalline mare basalt, except in the case of Apollo 17 VLT glass, which in principle could be parental to Luna 24 VLT basalt. The Y793274/QUE94281 glasses (both YQ1 and YQ2) closely resemble the Apollo 17 VLT glass. Based on systematic crystallization trends of Ti/(Ti+Cr) vs. Fe/(Fe+Mg) ratios within pyroxenes, the dominant mare clasts and mineral fragments in both Y793724 and QUE94281 were

probably derived from VLT-type basalt with primary TiO_2 (by extrapolation) = roughly 0.8 wt% [16]. The occurrence in these breccias of dominantly VLT primary crystalline basalt (inferred TiO_2 = 0.8 wt%) and dominantly VLT pristine glasses (TiO_2 = 0.4-1.2 wt%) is consistent with the possibility that the glasses and the crystalline basalts were derived from the same or closely related magma systems. We cannot draw any firm inference, however, because the detailed composition of the crystalline basalt has been obscured by mixing with other breccia components, and VLT crystalline basalts and VLT glasses possibly became mingled in these breccias simply by a fortuitous juxtaposition of unrelated materials.

Conclusions: (1) Y793724 and QUE94281 include remarkably similar compositional varieties of pristine glasses, forming two distinct clusters, based mainly on TiO_2. This detailed similarity strongly confirms a pairing of these two breccias. Although found 2500 km apart in Antarctica, they apparently came from a common source crater on the Moon. (2) These glasses are very low in TiO_2 (VLT) and their compositions are closely analogous to those of Apollo 14 and Apollo 17 VLT glasses. (3) Both VLT glass types belong to the high-Al_2O_3, low-MgO array of Delano [1]. (4) The coincidence of VLT compositions for the dominant glasses and VLT inferred compositions for the dominant crystalline basalt components in Y793274 and QUE94281 suggests the possibility that the glasses and the crystalline basalts were derived from closely related magmas.

References: [1] Delano J. W. (1986) Proc. Lunar Planet. Sci. Conf., 16th, D201-D213. [2] Longhi J. (1987) J. Geophys. Res. 92, E349-E360.[3] Takeda et al. (1991) Proc. NIPR Symp. Antarct. Meteorites 4,3-11.[4] Warren P. H. and Kallemeyn G. W. (1993) Proc. NIPR Symp. Antarct. Meteorites 6, 35-37.[5] Arai T., Warren P. H., and Kallemeyn G. W. (1996) Lunar and Planet. Sci., XXVII, 34-35.[6] Eugster O. and Polnau E. (1996) Lunar and Planet. Sci., XXVII, 761-762.[7] Lindstrom M. M., Mittlefehldt, D. W., Morris R. V., and Martinez R. R. (1996) Lunar and Planet. Sci., XXVII, 343-344.[8] Nishiizumi K. and Caffee M. W. (1996) Lunar and Planet. Sci., XXVII, 959-960.[9] Longhi J. (1992) Geoch. Cosmoch. Acta, 56, 2235-2251.[10] Longhi J. (1995) Geoch. Cosmoch. Acta, 59, 2375-2386.[11] Delano J. W. (1990) Proc. Lunar Planet. Sci. Conf., 20th, 3-12.[12] Delano J. W. (1996) Lunar and Planet. Sci., XXVII, 301-302.[13] Chen H. -K., Delano J. W., and Lindsley D. H. (1982) Proc. Lunar Planet. Sci. Conf., 13th, A171-A181. [14] Lindstrom D. et al. (1994) Geoch. Cosmoch. Acta, 58, 1367-1375. [15] Ringwood A. E. and Kesson S. E. (1976) Proc. Lunar Planet. Sci. Conf.,7th, 1697-1722. [16] Arai T., Warren P. H., and Takeda H. (1995) Meteoritics PS, submitted.

Table 1 Average compositions (wt%) of pristine glasses in Y793274 and QUE94281.

	QUE94281					Y793274								
SiO_2	44.59	44.98	46.13	46.23	45.47	44.28	45.24	46.48	45.51	46.76	45.26	46.05	46.43	46.89
TiO_2	0.37	0.51	1.06	0.48	1.19	0.49	0.40	0.99	0.45	1.22	0.51	0.48	0.45	1.09
Al_2O_3	9.71	9.46	8.60	10.16	8.69	9.19	9.98	9.12	9.92	8.90	9.30	10.08	9.99	8.77
FeO	18.77	18.94	19.20	18.50	19.23	21.76	18.63	18.20	19.08	19.06	19.56	18.29	19.04	19.17
MnO	0.26	0.27	0.26	0.24	0.28	0.27	0.27	0.27	0.29	0.27	0.28	0.24	0.27	0.26
MgO	15.67	15.17	13.23	13.74	12.52	14.21	14.52	13.81	14.72	12.63	14.81	14.69	15.69	13.48
CaO	9.14	9.21	9.41	10.20	9.69	8.52	9.37	9.15	9.29	9.57	8.99	9.56	8.19	9.42
Na_2O	0.26	0.22	0.35	0.20	0.31	0.25	0.25	0.31	0.24	0.32	0.23	0.23	0.22	0.32
K_2O	0.03	0.02	0.04	0.07	0.04	0.03	0.06	0.04	0.03	0.05	0.02	0.02	0.21	0.04
Cr_2O_3	0.49	0.50	0.56	0.47	0.50	0.39	0.45	0.60	0.47	0.51	0.59	0.49	0.47	0.54
V_2O_5	0.03	0.02	0.03	0.00	0.02	0.03	0.02	0.01	0.03	0.05	0.06	0.03	0.02	0.02
NiO	0.02	0.01	0.03	0.00	0.05	0.01	0.01	0.02	0.03	0.03	0.02	0.04	0.03	0.03
total	99.36	99.31	98.90	100.28	98.00	99.42	99.20	98.99	100.07	99.38	99.62	100.20	101.01	100.02

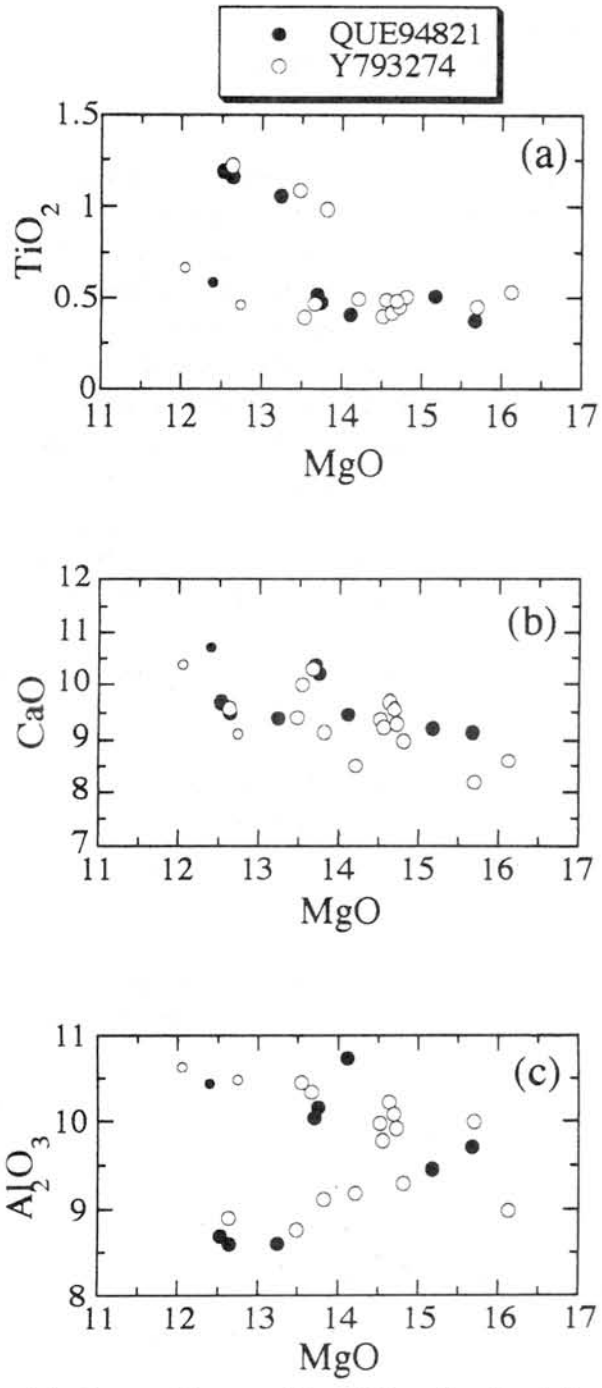

Fig.1a-c. Compositional trends of pristine glasses in Y793274 and QUE94281: smaller symbols (open and solid circles) represent glasses with critically lower Mg/Al ratio.

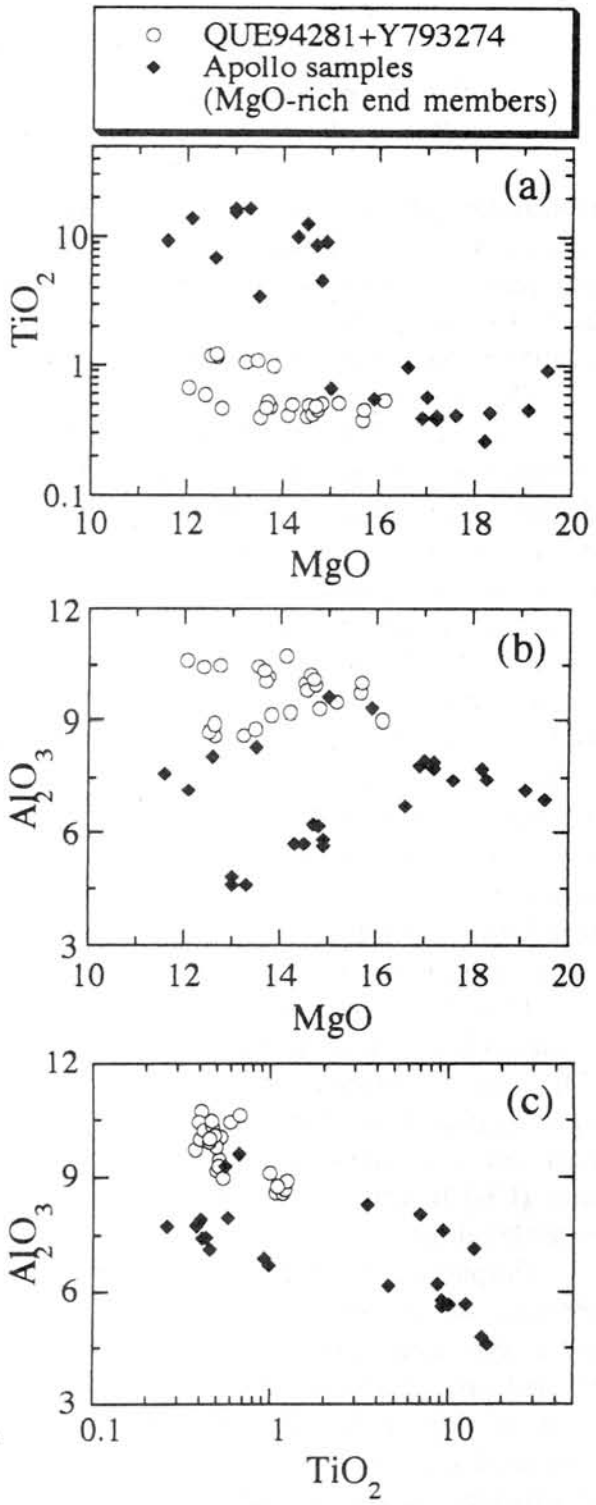

Fig.2a-c. Compositional trends of pristine glasses in Apollo samples, Y793274, and QUE94281.

High temperature components of Antarctic meteorite PCA91082 (CR2) and their nebular evolution.

Biryukov, V.V., and Ulyanov, A.A.
Division of Mineralogy, Geological Department of M.V. Lomonosov Moscow State University, Vorobievy Gory, Moscow, 119899, Russia.

Introduction. Discovering of many specimens of CR chondrites and related meteorites in deserts of Africa and Antarctica produces a great interest to studying of this meteorite group in last years. Some unique features of CR meteorites such as isotopic composition of O, N; solar Ni:Co ratio in Fe-Ni metal, and specific character of secondary alteration [Weisberg et al., 1995] probably indicates to formation in local nebular and planetary environment.

Our investigation is concerned with studying of high temperature components of recently recovered CR2 chondrite PCA91082 by SEM EPMA analytical technique. PCA91082 consists of high temperature silicate components (refractory inclusions, chondrules and their fragments), opaque components (metal and sulfides) and low temperature components: (matrix and dark inclusions). We concentrate focus of our research to nebular stage of evolution and respectively to studying of high temperature silicate components because metal and minerals of matrix and dark inclusions were investigated detail early [Noguchi, 1995; Weisberg et al., 1995].

Results. Studied thin polish section of PCA91082,12 contains only one refractory inclusion (INC1) and no dark inclusions. Brief petrologic description of this section was given in [Birjukov and Ulyanov, 1996].

INC1 is a fine-grained object of amoeboid shape with average diameter 1.4 mm. It consists of isolated melilite-anorthite-Al-diopside clusters 50-70 μm in diameter distributed in olivine matrix (Fa_3, 0.3 wt.% Cr_2O_3). Melilite (Ak_{21}) and Al-diopside (1.7-2.8 wt.% Al_2O_3; without detectable Cr_2O_3) form regular grains with interstitial rims of anorthitic plagioclase. Inclusion contains also small grains of troilite and Mg-Al-spinel.

Chondrules and their fragments are main constituent of PCA91082 and occupy more than 50 vol.% of meteorite matter. We studied 22 magnesian chondrules (Type I [MacSween, 1979]) and 5 ferroan objects (Type II). Porphiritic chondrules dominate (23 from 27); barred olivine chondrules are rare (3), one object (CH10) can be classified as radial olivine chondrule.

Porphiritic chondrules in PCA91082 is composed of olivine, olivine+pyroxene or low-Ca pyroxene with variable amount of glass and opaque phases. Type I chondrules consist of Mg-olivine (Fa_{0-4}) and low-Ca pyroxene (Fs_{0-8}); interstices between olivine and pyroxene grains are filled by glass of plagioclase-pyroxene composition. Type II chondrules consist of ferroan olivine (Fa_{34-55}) and Na-Fe rich glass; pyroxene is absent. Chondrules contain abundant Fe-Ni metal as large spherical inclusions, tiny grains with phyllosilicates in the outer parts of chondrules, and "dusty olivine" grains.

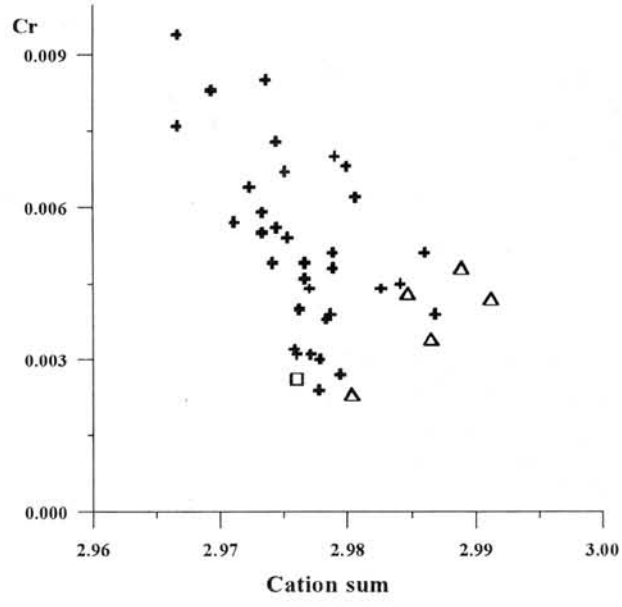

Fig. 1. Cation sum vs. Cr contents in olivines
□ INC1; ✚ Type I chondrules; △ Type II chondrules

Olivines from Type I chondrules show strong negative correlation between cation sum and contents of Cr (Fig. 1). Probably this effect is determined by presence of Cr^{2+} in olivines. Similar feature is observed for clinopyroxenes from magnesian chondrules, they contain Ti^{3+} and Cr^{2+} as well as normal Ti^{4+} and Cr^{3+} [Birjukov and Ulyanov, 1996].

One compound chondrule (CH10) of Type II shows extreme enrichment in Fe, Na, K, P and some other volatile elements (Fig. 2). It consists of two unzonal spherical objects (1 and 0.7 mm in diameter). Structure (similar to the fine-grained dendritic or skeletal) and composition of both objects is identical. Olivine lathes (length up to 150 μm, width 1-2 μm) form radial clusters of different orientation. Interstices between olivine lathes are filled by glass; μm-sized chromite grains are disorderly distributed. Chondrule consists of 49.9 vol.% of olivine, 48.4 vol.% of glass and 1.7 vol.% of opaque phases. Olivine (Fa_{42-46}) contains P_2O_5 (0.26-1.25 wt.%), CaO and MnO. Glass of average composition $Na_{1.97}Mg_{1.92}Fe_{2.16}Si_{8.59}O_{24}$ contains also P_2O_5 (up to 3.21 wt.%), CaO, Al_2O_3, K_2O and MnO.

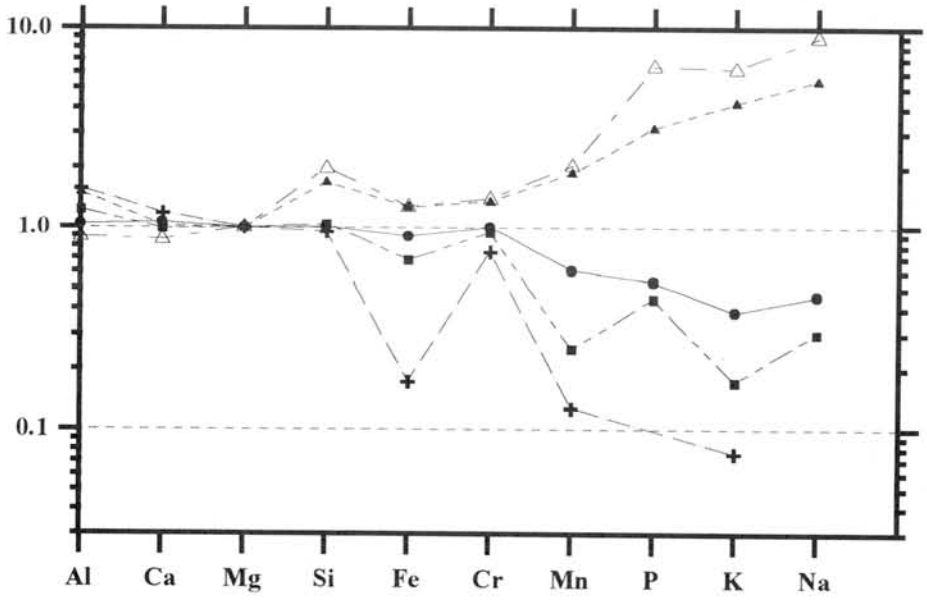

Fig 2. Mg-normalized bulk composition/CI

● average for CR chondrites [Kallemein et al., 1994]; [Weisberg et al., 1993];

■ bulk PCA91082;

✚ Type I chondrules;

▲ Type II chondrules;

△ CH10 chondrule.

Discussion. Specific features of CR chondrites constitute the great interest for discussion. According [Weisberg et al., 1995] most of them (related to high temperature components) are: magnesian character of anhydrous silicates in chondrules; solar abundance of refractory and moderately volatile lithophiles and strong depletion in volatile elements.

Fig. 2 shows that average composition of Type I chondrules in PCA91082 is very similar to bulk CR composition, but Type II chondrules has complementary consistency and enriched in volatile elements (this tendency is especially expressed for CH10 chondrule). Abundance of magnesian chondrules and lack of ferroan objects produce resulting depletion in volatile elements. Probably chondrules of both types can have corporate origin. Possible genetic relationship between Type I and Type II chondrules are:

1. Formation of Type I chondrules from volatile-rich material during heating and volatile loss.

2. Formation of Type II chondrules during crystallization differentiation of liquid or secondary alteration of matter of Type I chondrules.

3. Differentiation of matter of solar composition to two complement fractions.

The first model was proposed by Sears D.W.G. (1994) for ordinary and carbonaceous chondrites, but probably it is not reflect conditions of chondrule formation for CR meteorites. Type I chondrules in ordinary chondrites are less in average size than Type II objects [Sears et al., 1995]; this is not true for PCA91082. Bulk composition of Type I chondrules in

PCA91082 is not controlled by elements volatility, because refractory and moderately volatile elements patterns are almost unfractionated (Fig. 2). Enrichment of CR chondrites in ^{15}N that is usually interpreted as evidence of presence of presolar grains [Weisberg et al, 1995]. If more than 50 % of meteorite matter was undergone intensive heating, presolar grains would be evaporated and isotope anomalies would be reset.

The second model of crystallization differentiation explains enrichment of Type II chondrules in incompatible Na, K, Fe, P but they also enriched in compatible Cr and Mn. This model also requires evolution of liquid in large reservoir that can be realized only in planetary environment.

Formation of matter of Type II chondrules under secondary alteration of precursor with bulk composition of CR chondrites looks more likely, although enrichment in P is not typical for this process. According considered model, outer parts of chondrules must be enriched in volatile elements. This tendency is not observed for studied ferroan chondrules in PCA91082, therefore chondrules was melted after secondary alteration. Cooling rates for CH10 may be enough high to preserve it from volatile loss. This suggestion is confirmed by fine-grained skeletal structure of chondrule material and significant quantity of P_2O_5 in olivine. Cooling rates for other Type II PO and BO chondrules must be lower and it determines resulting less degree of volatile enrichment.

The last model suggests differentiation of matter of approximately solar composition into volatile-rich and volatile-poor fractions. Possible abundance of magnesian chondrules in nebular region of CR chondrites formation produces total bulk consistency. At present time there is no clearness in the problem of the priority of formation of bulk chondrite composition or chondrules composition [see e.g. Wood, 1994]. However some arguments, such as domination of chondrules of limitary structural types and sizes for each chondrite group let us to propose significant impact of fractionation of chondrules matter to chondrite composition. It is especially likely for CR meteorites which contain important amount of chondrules.

Presence of low valent forms of Ti and Cr in olivines and clinopyroxenes from magnesian chondrules in PCA91082 probable determined by formation of minerals in reduced environment or postformational reducing. Abundant "dusty olivine" grains confirm last suggestion. Clinopyroxene from INC1 does not contain detectable amounts of Cr, while Al-diopside from chondrules contains up to 2-3 wt.% of Cr_2O_3. Possible reason is preferred entering of Cr into structure of spinel in refractory inclusion. Similar situation is observed for pyroxenes from other carbonaceous chondrite group [Birjukov and Ulyanov, 1996].

Acknowledgments. We thank NASA Johnson Space Center for samples. Our research was made possible in part by grant No. 96-05-65144 of Russian Fund of Fundamental Research and grant No. a1081-H of International Soros Science Education Program.

References.

1. Birjukov, V. V. and Ulyanov, A.A. (1996): Proc. NIPR Symp. Antarct. Meteorites, **9**, 8-19.
2. Kallemein, G.W. *et al.* (1994): GCA, **58**, 2873-2888.
3. McSween, H. Y., Jr. (1979): Rev. Geophys. Space Phys., **43**, 1059-1078.
4. Noguchi, T. (1995): Proc. NIPR Symp. Antarct. Meteorites, **8**, 33-62.
5. Sears, D.W.G. *et al.* (1995): Earth Planet. Sci. Lett., **131**, 27-39.
6. Weisberg, M.K *et al.* (1993): GCA, **57**, 1567-1586.
7. Weisberg, M.K. *et al.* (1995): Proc. NIPR Symp. Antarct. Meteorites, **8**, 11-32.
8. Wood, J.A. (1994): Proc. Chondrules and Protoplanetary Disk. Harvard-Smithsonian Center for Astrophysics, Preprint series No. 4024, Cambridge.

STATISTICS OF IRON GRAINS IN THE SEQUENCE OF PETROLOGIC CLASSES OF LL TYPE ANTARCTIC NIPR CHONDRITES

Sz. Bérczi[1,2], Adrienn Kiss[2] & B. Lukács[3]

[1] Eötvös University, Dean's Office, H-1088 Budapest, Rákóczi út 5. Hungary
[2] Eötvös University, Dept. of Petrology, H-1088 Budapest, Múzeum krt 4\a. Hungary
[3] CRIP-RMKI, H-1525 Bp. 114. Pf. 49. Budapest, Hungary

ABSTRACT

In order to see direct signals of the suspected oxidation-reduction competition in chondrites we investigate the dependence of iron grain size distribution on petrologic classes for LL chondrites, as carried out on a sequence of LL type chondrites from Antarctica, on loan from NIPR, Tokyo. The statistical chi-square probe of the iron grain size distributions of the LL-3 to LL-7 chondrites were calculated.

INTRODUCTION

Petrologic classes in the Van Schmus-Wood classification sheme of chondritic meteorites (1967) represent final stages of thermal evolution of meteorite parent bodies. This thermal evolution causes observable changes in the texture of the chondrites. One of these changes is in the number and grain size distribution of iron grains. This change is the result of the oxidation-reduction chemical reactions in a system, where iron-oxide, carbon and H_2O are present and react with each other in a complex process depending on the temperature, and the ratio of the components. Different stages of the complex oxidation-reduction competition between carbon and H_2O have been preserved in meteorites. The most direct signals of reduction and oxidation are the new iron grains, their growth or shrinking, or disappearance. We checked this on grain size distributions of LL chondrites. It seems that the statistics of the present, first, investigation should be doubled or trebled; but even now some evolutionary effects are seen.

THE LL TYPE ANTARCTIC METEORITE SAMPLES FROM NIPR: MEASURING THE DISTRIBUTIONS

For determining the size distribution of iron grains we used two groups of Antarctic Meteorite Samples on loan from NIPR, Tokyo. One was a sequence of LL3, LL5 and LL7 petrologic types (ALH-77304, 83-4, Y-74022, 92-2, and Y-791067, 73-1), the other one was taken from the Antarctic Meteorite Thin Section Set of NIPR, the samples of 24, 25 and 26, LL4, LL5 and LL6, (Y-74442, 83-6, ALH-78109, 88-1, and Y-75258, 97-8), respectively. Number of grains were counted in petrographic microscope (Nicon-type) belonging to 1: 0-25 μm, 2: 25-50 μm, ... up to 8: >175 μm size ranges. (In order to receive a more smooth averages, all 25 μm ranges were subdivided into three smaller intervals and counts were carried out for these shorter diameter ranges, then three of them were summed up.)

The measurements resulted in 6 iron grain size distributions. One for LL3, LL4, LL6 and LL7 petrologic types and two for LL5 one. The normalized distributions are shown in Figs. 1-6. Looking at these column graphs it was noticeable that LL4 and

both LL5's had "tails" at large grain sizes. It seemed very consistent with our observation that in the LL group at the final stage of their evolutionary path some iron loss is suspected; maybe at high temperature the substantial iron grains percolated and Fe flowed out. Indeed, the "tail" is missing at LL6 and LL7.

THE STATISTICAL ANALYSES: THE CHI²-PROBE

We checked if there are statistically significant differences between the Fe grain distributions. In the lack of any serious theory for the shape of the distribution we used a chi²-type test. Our first null hypothesis is that all distributions are the same, and differences come purely from statistical fluctuations. This null hypothesis is disproven on a quite satisfactory significance level.

If in size range $_i$ the actual grain size is n_i, then its statistical mean deviation is $\approx n_i^{1/2}$. Then

$$chi^2_{12} = \Sigma_i \, (n_{1i}/N_1 - n_{2i}/N_2)^2 / (n_{1i}/N_1^2 + n_{2i}/N_2^2) \qquad (1)$$

N being the total grain number. We measured at 8 points, so the degree of freedom is 7. The chi² values for various pairs are:

(34) = 18.5; (35) = 23.8; (36) = 31.5; (37) = 51.3
(45) = 23.2; (46) = 20.2; (47) = 47.8
(56) = 21.8; (57) = 21.2; (67) = 16.6

Here 5 stands for the united distribution of 2 LL5's. None of these values are conform with a uniform distribution considering that the expectation value is 7, and the mean deviation is $\sqrt{14}$. For more details of the test see Janossy (1965).

However it is possible that not only statistical fluctuations are present; there may be moderate differences within the same van Schmus-Wood class too. We checked this possibility on the 2 LL5 samples, with the result

$$chi^2_{55} = 12.2$$

compatible with no difference at all at slightly more than 1σ level.

CONCLUSIONS

Taking the numbers in face value, we can conclude that the two LL5's are undistinguishable at any fair significance level while any two samples of different classes can be; the differences are the smallest for neighbours. However $chi^2_{55} = 12.2$ does not rule out moderate non-statistical differences within a van-Schmus-Wood class. Therefore for *classes* the denominators in eq. (1) may moderately increase. Even then our guess is that no more than 3 different thin sections for each class would suffice for settle the question if the classes are distinguishable for grain size distributions. Possibly LL5 is an exception; earlier we saw that oxidation takes over at LL5, so trends change there and the diversity may be higher.

ACKNOWLEDGEMENTS

We thank to NIPR for lending the Antarctic samples investigated here. Partly supported by Mec/P-2113 & -1330/95/96, MÜI/TP.55/96 and OTKA T014958.

REFERENCES

Bérczi Sz., Holba Ágnes & Lukács B. 1995: Acta Min. Petr. Szeged, **XXXVI**, 143.

Janossy L. 1965: Theory and Practice of Evaluation of Measurements. Oxford University Press, Oxford

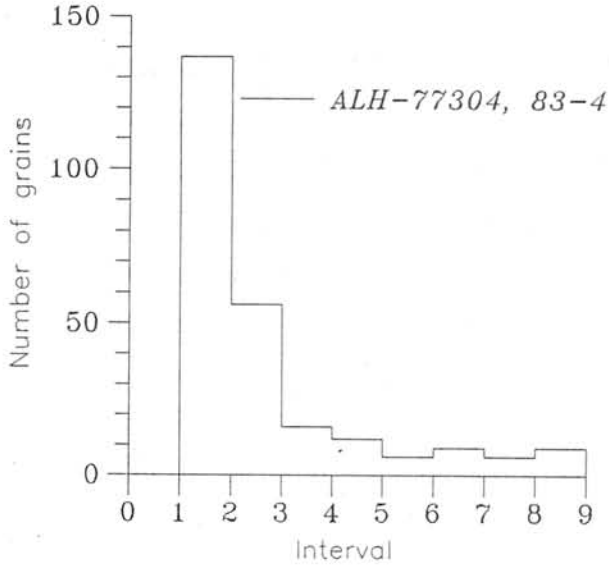

Fig. 1: Iron grain distribution in LL3

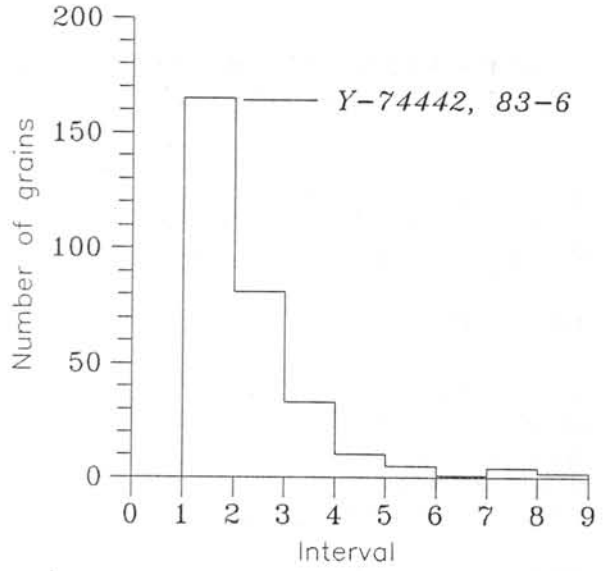

Fig. 2: Iron grain distribution in LL4

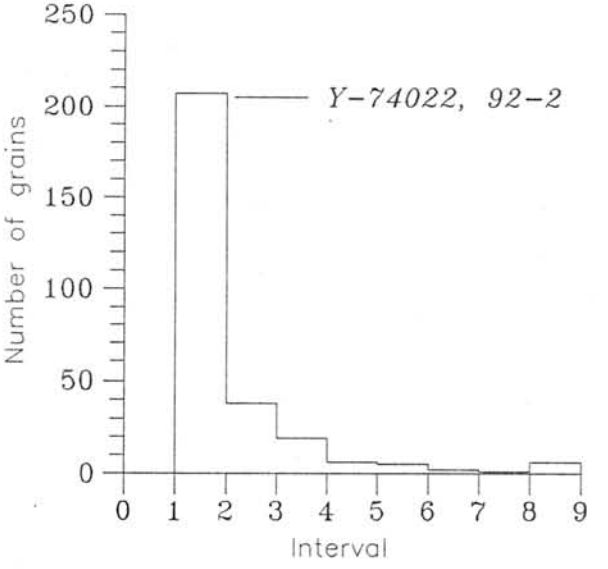

Fig. 3: Iron grain distribution in LL5

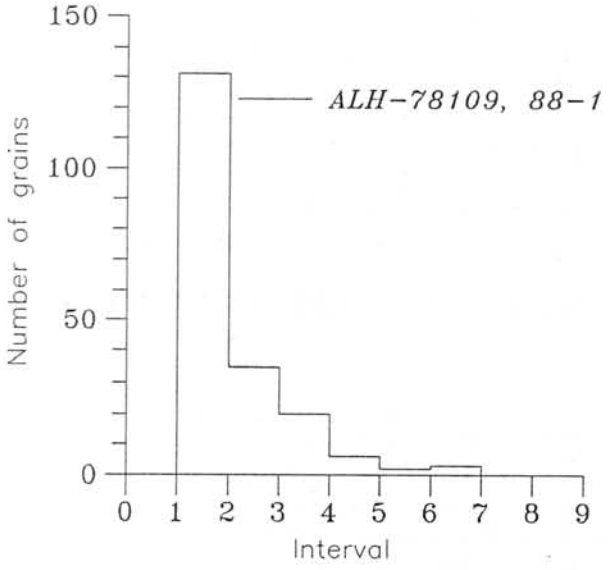

Fig. 4: Iron grain distribution in LL5

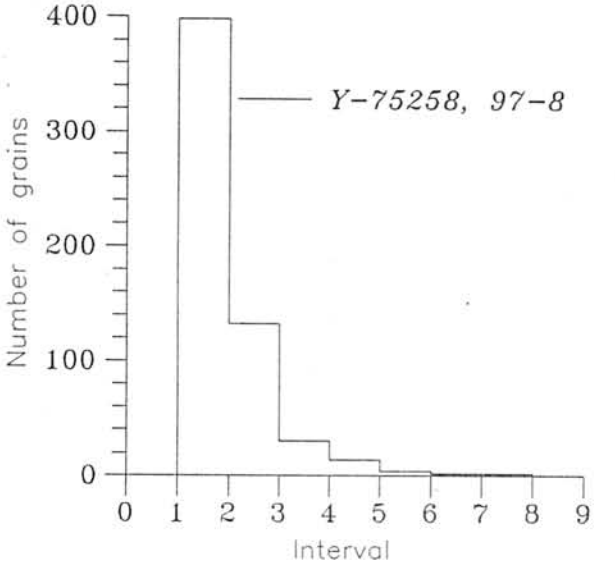

Fig. 5: Iron grain distribution in LL6

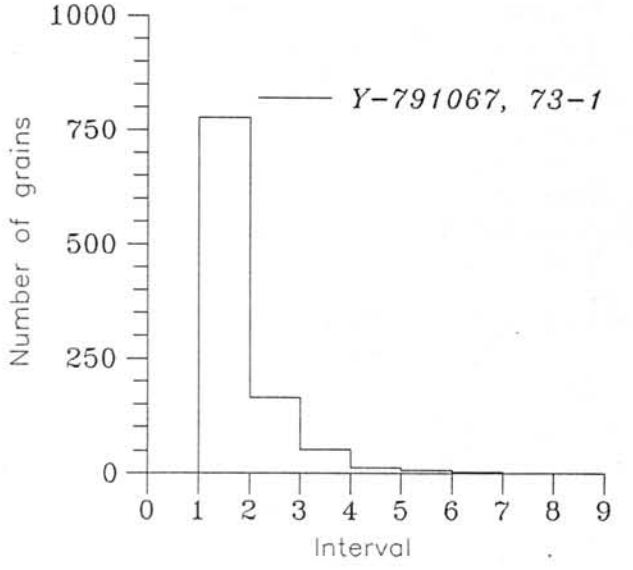

Fig. 6: Iron grain distribution in LL7

COMPARISON OF THE REDUCTION PROCESSES IN NATIVE-IRON BEARING BASALTS FROM DISKO ISLAND, AND IN CHONDRITES

Sz. Bérczi[1,2], Adrienn Kiss[2] & B. Lukács[3]
[1] Eötvös University, Dean's Office, H-1088 Budapest, Rákóczi 5.
[2] Eötvös University, Petrologic Dept., H-1088 Múzeum krt. 4/a
[3] CRIP RMKI H-1525 Bp. 114. Pf. 49. Budapest, Hungary

ABSTRACT

Disko Island is the only place on Earth where basalts with considerable amount of native iron occur. This native iron was produced by C-generated reduction of FeO-bearing silicates, when ascending magma crossed and partly assimilated a carbonaceous deposit, near to the surface. This process is compared in our paper to the reduction process of chondritic thermal evolution.

INTRODUCTION

Disko is a substantial island at the western shore of Greenland, at the 70° N and the 53° W (Fig. 1). The geological deposits of the Disko Island are famous. Its mesosoic layers originated in subtropical climate, so suggesting mesosoic warmth and shift of the continental platform. Its kainozoic deposits contain native-iron bearing basalts. Anthropologists refer that Disko Esquimaux manufacture tools (as e.g. fish hooks) from this native iron nuggets of the basalt (Birket-Smith, 1965). The metallic iron content of Disko basalts is known since the great Nordenskjöld expedition to West-Greenland, in 1870.

TERRESTRIAL AND ACHONDRITE BASALTS VERSUS DISKOS AND CHONDRITES

Achondritic and terrestrial basalts are extremely poor in metallic Fe, since at the complete disappearance of chondrules iron is already molten, and flows out. This process begins at cca. petrologic class 6. However, Disko basalts do contain metallic iron, visible for naked eye and going up to several weight % (Pedersen, 1978). The question is, how iron oxide reduced in the molten lava. The reducing conditions during basalt crystallisation are shown by the presence of armalcolite, first found on Moon, where it originated also in reducing conditions.

The usual answer (Steenstrup 1875) is that ascending lava crossed organic carbonaceous deposits, and carbon has reduced the iron oxide. There are opinions for the original lava source even down at the core, too (Bird & Weathers, 1977), Both ideas have analogies in meteoritics. Here we concentrate on the first one, since carboniferous layers are known there, the basalt contains cohenite as well, so C had the possibility to have reacted with basaltic FeO. Then Disko basalts are excellent counterparts in modelling chondritic reduction, mostly between the petrologic classes 3 and 4 in chondrites (Lux, Keil, & Taylor, 1980).

THE REDUCTION OF FeO BY CARBON IN CHONDRITES AND DISKO

The simplest mathematical model for reduction contains 3 differential equations. Consider FeO (mole concentration x), C (y) and Fe (z); the SiO_2 content is constant. Then

$$dx/dt \approx -2A(T)xy \quad (1)$$

$$dy/dt \approx -A(T)xy - R^{-1}B(T)y \quad (2)$$

$$dz/dt \approx -dx/dt \quad (3)$$

The 1/R term takes into account C evaporation through the surface. The temperature-dependent factors have the structure

$$A(T) \approx A_o \exp(-Q_A/T);\ B(T) \approx B_o \exp(-Q_B/T) \qquad (4)$$

These equations can be applied to chondrites at temperature T in the early Solar System for a time $t_o \sim 1$ My; but also to the Disko protobasalt at temperature T crossing the carboniferous layer for a time t_o. The solutions have the form

$$y_f = y_i - x_i + x_f + (B/2AR)\ln(x_f/x_i) \qquad (4)$$

$$z_f = z_i + x_i - x_f \qquad (5)$$

and x_f is the solution of the implicit equation

$$2At_o = \int_{x_f}^{x_i} w^{1} (y_i - x_i + w + (B/2AR)\ln(w/x_i))^{-1} dw \qquad (6)$$

In chondrites eqs. (1-6) establish a relation between degree of reduction and petrologic class through the T-dependences of reduction and chondrule diffusion. This relation cannot hold for Disko basalts in the lack of chondrules. However, grain sizes may correlate with degree of reduction, and indeed there is a substantial similarity in grain size distributions of our Disko sample (CM-D-1) and the LL7 NIPR sample (Y-791067, 73-1), studied elsewhere (Bérczi, Kiss, Lukács 1996). Here we will not solve equations for grain size growth: first measurements are needed for the temperature-dependent coefficients in the local minerals. But the analogy is clear, compare CM-D-1 and LL7 distribution in Fig. 2.

ON POSSIBILITY OF NEW TYPES OF METEORITES: IRON-BEARING ACHONDRITES?

By the force of the above analogy, can we expect iron-bearing achondrites? Such meteorites have never been reported, and the Disko iron was produced in a highly terrestrial situation. The reasons are the following:

- C deposits are locally differentiated only on Earth,
- carbonaceuos deposits are products of earlier life.

Still, the process is not exactly ruled out in the asteroid belt. Namely, the biggest asteroid, 1 Ceres, has a C chondritic surface. Now, 4 Vesta is basaltic; then how could the bigger asteroid have kept chondritic surface, if the smaller one produced strong volcanic activity?

An explanation is that 1 Ceres collected C chondritic components onto her surface. If this process had already started during the volcanic activity, then the fresh basalt met carbon-containing matter and some iron oxide had been reduced. Up to now no such meteorite has been seen, but they may exist.

HISTORICAL REMARKS ON THE POSSIBLE DISKO IRON METEORITES

There is another analogy between Disko basalts and some meteorites, but it is historical; both were used for toolmaking by Esquimaux. We mentioned this for the basalt; now, Thule Esquimaux manufactured some knives from the big Cape York iron meteorites (Birket-Smith, 1965), obviously by cold hammering. The problem is; how Disko Esquimaux without metallurgy recognised the iron in the basalt. Disko is some 600 km from Cape York. Maybe ancestors of Disko Esquimaux learnt the existence of iron from the Eystribyggd Vikings (at modern Julianehab). The Vestribyggd settlements (cca. Godthab, much nearer) became abandoned before 1361, while the Eystribyggd area was still populated beyond doubts in 1470 (Nörlund, 1924) and we do not know when and how it became depopulated. If Disco Esquimaux had been in contact with

them, it is not completely hopeless to solve the historical mystery, which is, however, irrelevant in meteoritics.

ACKNOWLEDGEMENTS

We thank to Ken Asger Pedersen for providing the CM-D-1 Disko basalt sample investigated here. Partly supported by OTKA T-014958, MÜI/TP.55/96, and OMFB-MEC/P-2113 & P-1330/95/96.

REFERENCES

Bérczi Sz., Kiss Adrienn & Lukács B. (1996): Subm. to NIPR **XXI**
Bird J. M. & Weathers M. S. (1977): J. Geol. **85**, 359
Birket-Smith K. (1965): The Paths of Culture. The University of Wisconsin Press, Madison
Lux G, Keil K, & Taylor G.J, (1980): Geochim. Cosmochim. Acta. 44. 841
Nörlund P. (1924): Meddelelser on Grönland **67**, 1
Pedersen A. K. (1978): Bull. Geol. Soc. Denmark **27**, 117
Steenstrup K. J. V. (1875): Videsk. Medd. Naturhist. Foren. Kφbenhavn **16-19**, 284

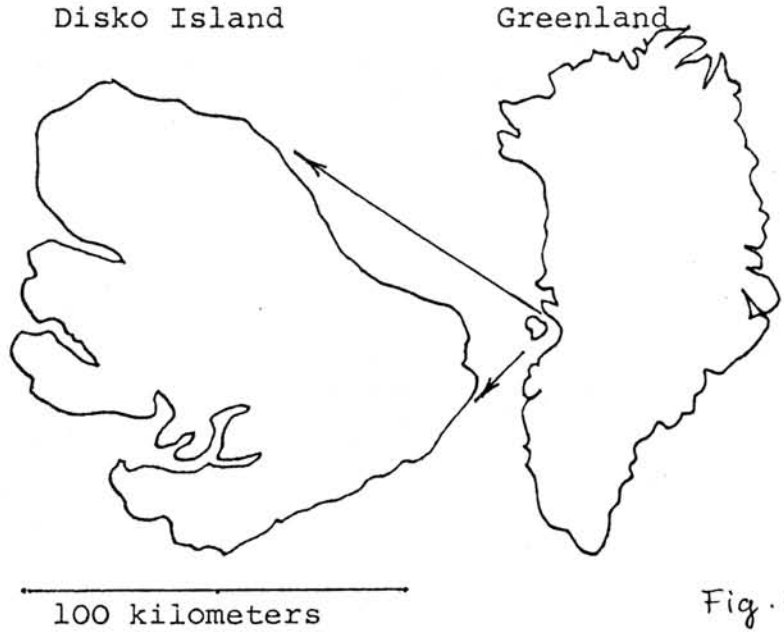

Fig. 1.

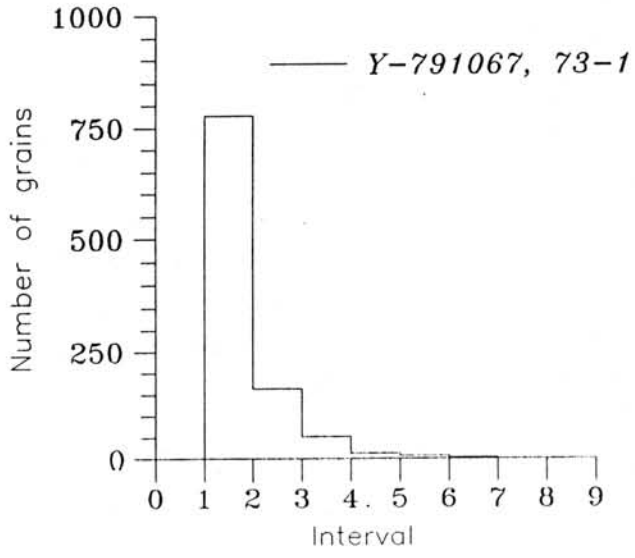

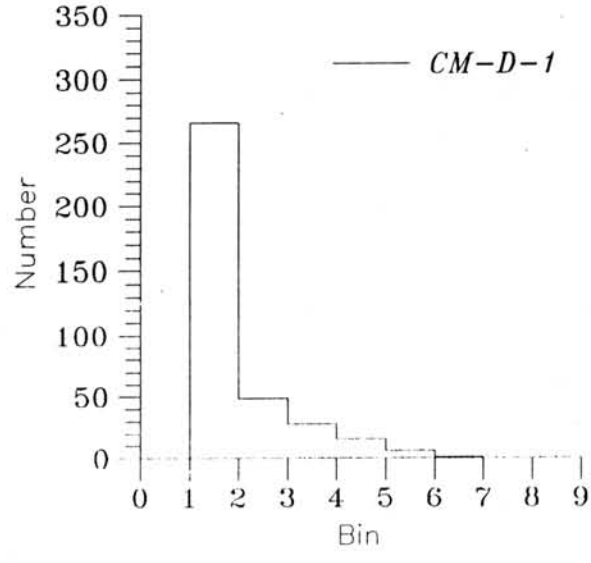

Fig. 2a: Iron grain distribution in LL7 Fig. 2b: As before, for a Disko basalt

ON DISCRIMINATING CHONDRITES ON THE BASIS OF STATISTICAL ANALYSIS OF IRON-BEARING COMPOUNDS: NIPR ANTARCTIC SAMPLES

Sz. Bérczi[1], Agnes Holba[2] & B. Lukács[2]
[1] R. Eötvös University, H-1088 Budapest, Rákóczi út 5, HUNGARY
[2] CRIP RMKI H-1525 Bp. 114. Pf. 49., Budapest, HUNGARY

ABSTRACT

The more than 550 chemical compositional data of the Catalog of Antarctic Meteorites (Yanai, Kojima, Haramura, NIPR 1995) made it possible to carry out statistical calculations in search of discriminating parameters for a few van Schmus-Wood petrologic types. (The H4 and L6 petrologic classes are the most populous.) We calculated the mean-deviation ellipse for the H4 chondrites and plotted it on the oxide-Fe versus non-oxide-Fe field. The distributions cannot be distinguished statistically from Gaussian, except for a few individuals.

INTRODUCTION

At the beginning of our century Hertzsprung and Russell plotted a great number of individual points of stellar parameters of surface temperature and luminosity field. These plot of great number of data helped theorists to find a model, and behind it a real mechanism about the working of stellar interiors. Now, this stage has been repeated for chondritic meteorites, when the 550 NIPR chemical compositional data were published.

Global iron content of chondrites is an important data in classification of chondrites. Early studies on chondrite compositions revealed that the global iron content scatter around two mean values (Wiik, 1956). Therefore first we looked for how this fact looks like in the light of the new NIPR data. But because of smaller-larger changes in the total mass of chondrites during chemical transformational processes (i.e. CO_2 loss during reduction and H_2O loss by evaporation, or H_2 loss from the oxidation of Fe by water molecules) we used Si normalized values of the total iron content data. Fe/Si ratio can be considered as initial condition parameter for chondrites.

The unified plot of all chondritic points of the 550 NIPR data shows the two dense regions in the vicinity of the Wiik values (Fig. 1). Separate plots of distribution of data for E, H, L, LL, and C chondrite types are shown on Fig.2. Statistical studies of the five chondrite types revealed clear discriminating parameters of the distribution of types.

THE GAUSSIAN DISTRIBUTION OF THE E, H, L, LL, AND C TOTAL IRON CONTENT: THEIR STATISTICAL PARAMETERS

Imagine a group of meteorites of common or similar origin, in which a quantity x of chemical components is influenced by a number of independent factors. Then, in a not too strict sense, the Central Theorem of Limiting Distributions suggests a more or less Gaussian or normal distribution. It has two independent parameters, the average $\langle x \rangle$ and the mean deviation σ_x. Let us see first this to the total Fe/Si content of chondrites. This ratio is conserved during the evolution for temperatures below the melting point of iron, so, maybe with the exception of extreme petrologic classes, it reflects the initial conditions.

Fig. 1 is the distribution of x for all NIPR chondrites chemically analysed, if at least the type was determined.

The curve is two-peaked, and clearly non-Gaussian at high significance level. This curve tells us that 2 different initial conditions are clearly distinguishable by their Fe content; in between which evolution seems rather rare.

Fig. 2 is the Fe/Si distribution individually for the types. Some distributions overlap, i.e. L & LL or C, H & E; however the averages differ within tolerance, since for the statistic error

$$\delta\langle x\rangle = \sigma/(N-1)^{1/2} \quad (1)$$

N being the number of chondrites of the given type.

A combination of third and second central moments $sk \equiv c3/\sigma^{3/2}$ measures the asymmetry; this number is in the general order of 1 for LL, L, H and E, while it is -0.174 for C.

Having measured $\langle x\rangle$ and σ one gets the best Gaussian fit, and the chi² test

$$chi^2 = \Sigma_i^k (n_i - n_{Gi})^2/n_{Gi};\ n_{Gi} = (2\pi\sigma^2)^{-1/2}\exp\{-(xi-\langle x\rangle)^2/2\sigma^2\} \quad (2)$$

where n_i is the number in the i^{th} bin, can be performed, giving

	LL	L	C	H	E
$\langle x\rangle$	1.154	1.289	1.683	1.735	1.896
σ	0.110	0.103	0.087	0.156	0.125
N	60	166	31	174	7
chi²	622	108	11.8	>>1	10.7
k	22	14	11	33	11

Since $\langle chi^2\rangle \approx k$, one can see that for C and E the distribution is statistically undistinguishable from Gaussian. However, by removing only the leftmost H, which is Y-790043 (clast), chi² drops to 34.8, conform with Gaussian. Similarly, L without the rightmost point, goes to 17.3, again fairly Gaussian. Clearly individual anomalies are present.

Deviation from an ideal composition can be visualized on a two-component plot, which we here choose to be the classical oxide-nonoxide Fe, however by normalizing to Si. If a van Schmus-Wood class has enough samples, averages and tolerance ellipses can be calculated and the 1σ ellipse shows the "expected" deviation *within* the group. In the available analyses only H4 and L6 are numerous enough, and here we consider H4. Fig. 3 shows that H4 does not separate from other H's on this plot. It would do it by using H_2O as a coordinate. However from other types H4 separates quite fairly, as shown on Fig. 4.

Always one H4 dot deviates far away. It turns to be notoriously Y-790043(clast). So either it is not H4 at all, or it is so highly weathered that the original composition changed beyond recognition. So indeed, statistical analyses are possible and seem useful on such a large set of meteorites as the chemically analysed part of the NIPR collection.

ACKNOWLEDGEMENTS

The authors highly acknowledge the use of the data set of the measurements of Drs. Yanai, Kojima & Haramura, published in NIPR, 1995. Partly supported by OTKA T/014958 & MÜI/TP.55/96.

REFERENCES

Yanai K., Kojima H. & Haramura H. 1995: Catalog of the Antarctic Meteorites. NIPR, Tokyo

Janossy L. 1965: Theory and Practice of the Evaluation of Measurements, Oxford University Press, Oxford

Wiik H. B. 1956: Geochim. Cosmochim. Acta **9**, 279

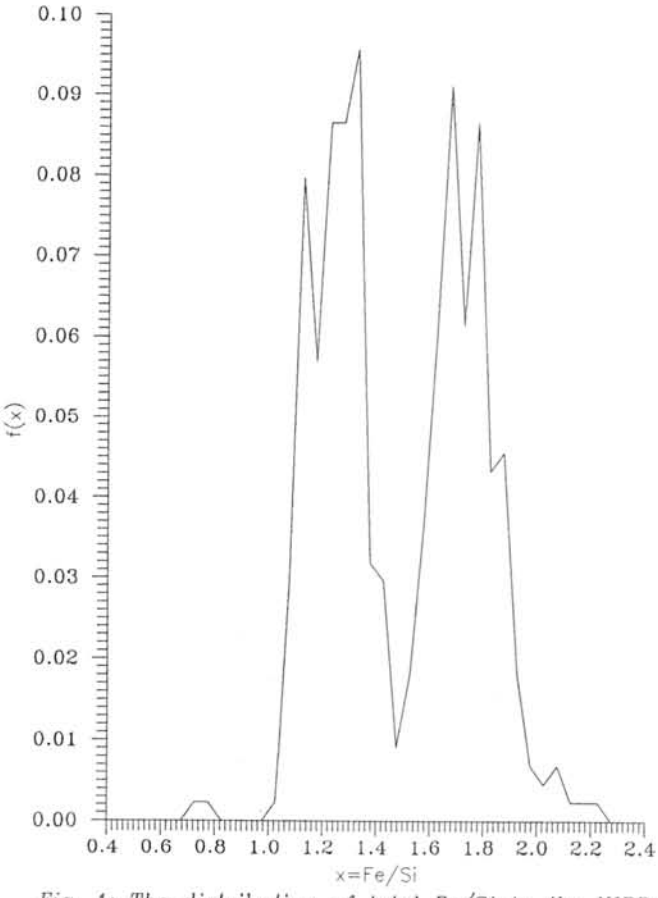

Fig. 1: The distribution of total Fe/Si in the NIPR chondrites analysed chemically.

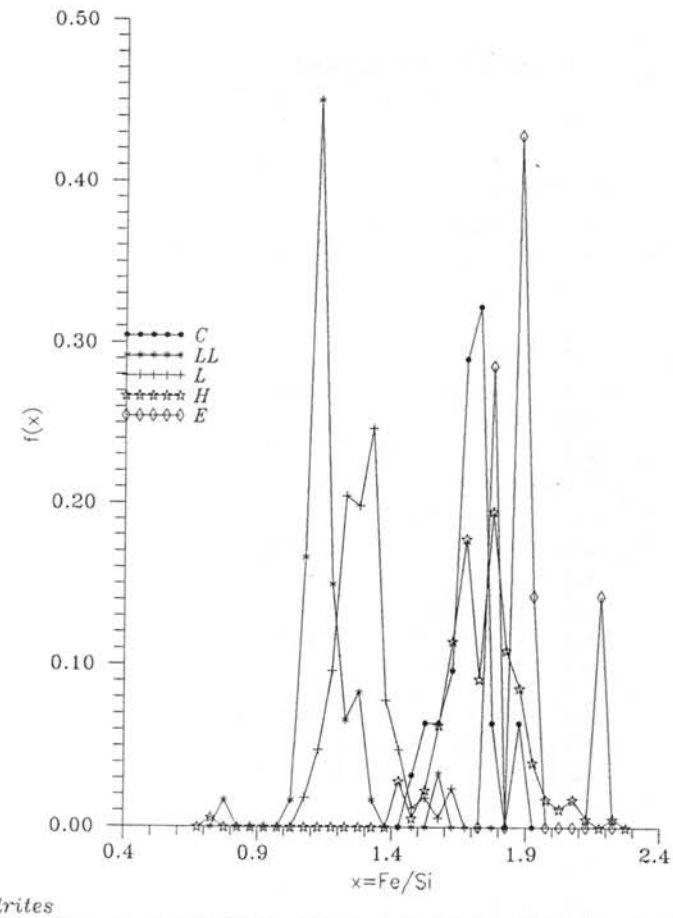

Fig. 2: Distribution of total Fe/Si in NIPR chondrites of various types.

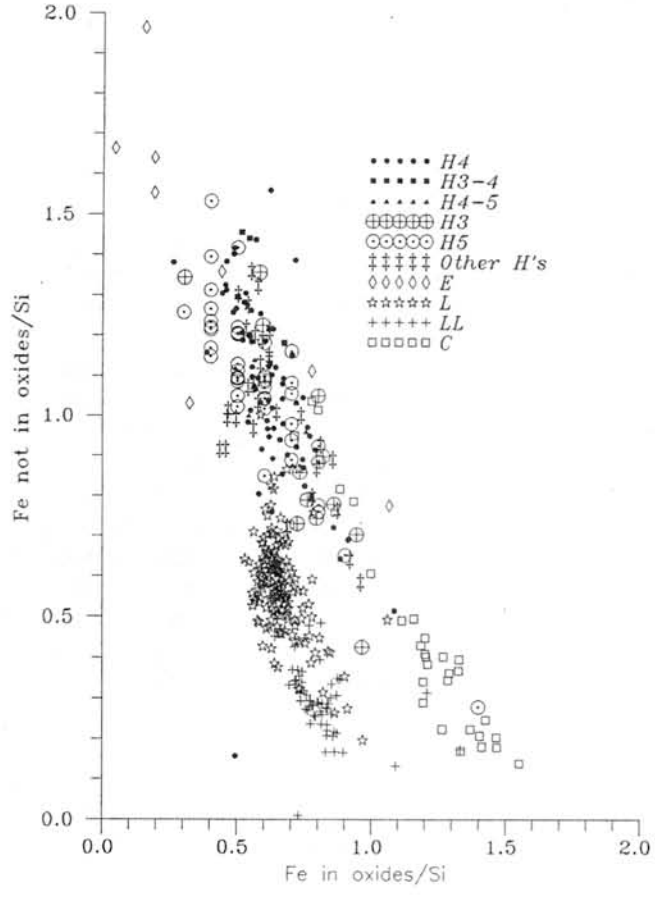

Fig. 3: The chondritic Hertzsprung-Russell diagram.

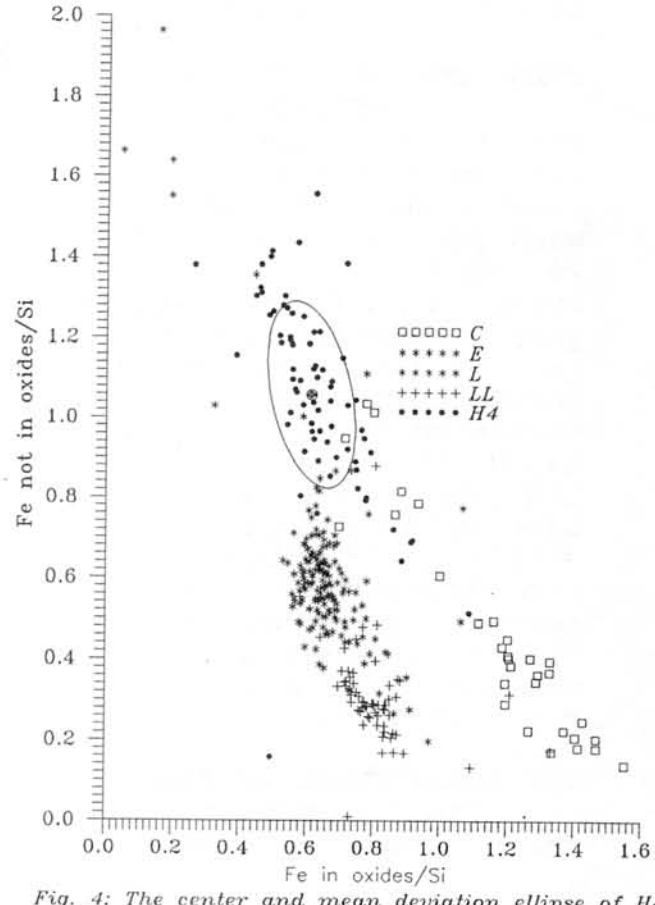

Fig. 4: The center and mean deviation ellipse of H4 chondrites with the individual non-H chondrites.

MEASURING WATER DROPLETS AS SPHERULES IN THE EJECTA CLOUD OF AN IMPACT EXPLOSION INTO ICE ON ANTARCTICA: A PROPOSAL

Bérczi Sz.[1], Lukács B.[2] & Földi T.[3]

[1] Dean's Office & Dept. of Petrology & Geochemistry, R. Eötvös University,H-1088 Rákóczi út 5, Budapest, Hungary
[2] CRIP RMKI, H-1525 Bp. 114. Pf. 49., Budapest, Hungary
[3] GEMINILUX, H-1117, Irinyi J. út 36/b, Budapest, Hungary

ABSTRACT

Impacts generate cloud of ejecta from the fragmented target material. This cloud contains molten droplets of the target material, solidifying before the end of the out-throwing process. Glassy spherule ejecta explain the famous ray system of fresh lunar craters, i.e. of Tycho, well visible on the full Moon. However the great majority of the fragmented material is expected to remain in crystalline form. Such an experiment would be rather difficult with rock target; after the impact it would be tedious to separate spherules from crystalls. However an analogous situation seems easily observable: impact on *icy* target, i.e. on Antarctica. If we observe *visually* an ejecta cloud made by an artificial impact on Antarctica, we can measure the ratio of the molten droplets of water to the crystalline ice grains by optical methods.

The measurements need two light sources. One for backscattering (for droplets) and one for forward-scattering (for crystalline ice particles). The backscattering will produce a rainbow; the forward scattering will give halos around the light source in front of the observer. One can then estimate the ratio of melt\solid particles in the ejecta cloud from the intensities of the two types of halos. This ratio is in intimate connection with the spherule production of impacts.

PHENOMENA USED IN THE EXPERIMENT

Project IGCP 384 focuses attention on terrestrial and extraterrestrial materials with spherulitic form. Their size range is from some tens of micrometers to some millimeters. Some of spherulites have got their spherical shape by friction heat melting when passing through the atmosphere. In the suggested experiment we concentrate on spherules originated in an impact explosion event. (Lunar soil samples collected by Apollo missions contain glassy spheruls from such impact melting events.)

If a soft explosion into a low melting temperature material should be tested by optical and scattering measurements, then the mechanism of spherule production could be experimentally investigated. The most available such crystalline material of low melting temperature is the ice in Antarctica. The melted ice can produce water droplets showing optical scattering phenomena: especially the rainbow from backscatering light source. At the same time forward scaterring by a light source in front of the observers can generate halos from different crystalline material clouds. The synchronous observation of the two types of clouds can give the possibility to estimate the crystal/water droplet ratio in different regions of the ejecta cloud.

THE ARRANGEMENT OF THE MEASUREMENTS

The two type of scattering optical phenomena need two different light sources. One of them may be Sun, low on the sky.

This may be the light source behind the observer. The inner reflection of sunlight gives the classical rainbow with average 42° cone angle. The forward scattering phenomenon needs an intensive light source in front of observer, on the side of the explosion event. For a simplicity of arguments consider hexagonal crystalls; then the cone angle is 22° for ice (Bérczi, 1993).

We would like to observe the spatial arrangement of spherule production, and the time sequence of the transmutations in the ejecta cloud. The phase transition from water to ice by freezing of droplets in air should be also observed. Therefore special main characteristics of the experimental arrangement are necessary, shown on Figs. 1 & 2. Observer locations are represented with cameras, able to make high speed photographs of the halo rings. 3 or 4 cameras form a sequence along a line, which pass by the explosion point by cca. 100 meters. The two or three light sources form another sequence, but on the opposite side of the explosion point, parallel to the camera line. The cameras turn toward the light sources and are synchronised to the explosion.

DESCRIPTION OF A HYPOTHETICAL EXPLOSION

Here we try to imagine some characteristical events from the complex phenomena during the explosion. The camera head on the explosion point would observe first some broken ice particles. Later the same camera would see the emerging and increasing rainbow from Sun (behind). For some moments both the halo from the broken ice (generated by the artificial light source in front of) and the rainbow (generated by Sun behind) will be prsent. Droplets thrown out mak the rainbow to appear for the camera looking at the the second light source (cca. 20 m from the first one). This line of sight is nearly parallel with the head on crater center line, but run about 20-30 meters by it.

This second camera can observe the phase transition of water droplets into ice crystals. According to the type of observation such a phase transformation may result in changes in the cone angle of halo: from that of 42° of the rainbow backscattering it may change to the one of the hexagonal crystal halos by the forward scattering light source. This may be a gradual transition, when first rainbow, then both of the halos, and finally only the forward-scattered halo can be seen (Fig. 2). According to this scenario the third camera, monitoring the outer region of the ejecta cloud, can observe only the frozen "droplets" of spherules, which may take the form of hexagonal crystals but spherulite shapes as well. Finally the experiment can show in what kind of final form the molten water will be frozen out in the ejecta blanket, and in what ratio.

The sampling of the ejecta blanket around the explosion crater will show the fate of the ejecta cloud particles. If the water droplets freeze into tiny ice crystals, then their regularity in size may be a characteristic parameter remembering their originally molten form. If water droplets remain molten till their final settling, their accumulated agglutinates will refer to this long term molten state. We think that, because of the complex nature of interactions during such a crater formation impact, theoretical predictions are rather uncertain. That is why we feel important to observe the fates of molten droplets.

REFERENCE

Bérczi Sz., 1993: 18th Symp. Ant. Met., NIPR, Tokyo, p. 71-1-3.

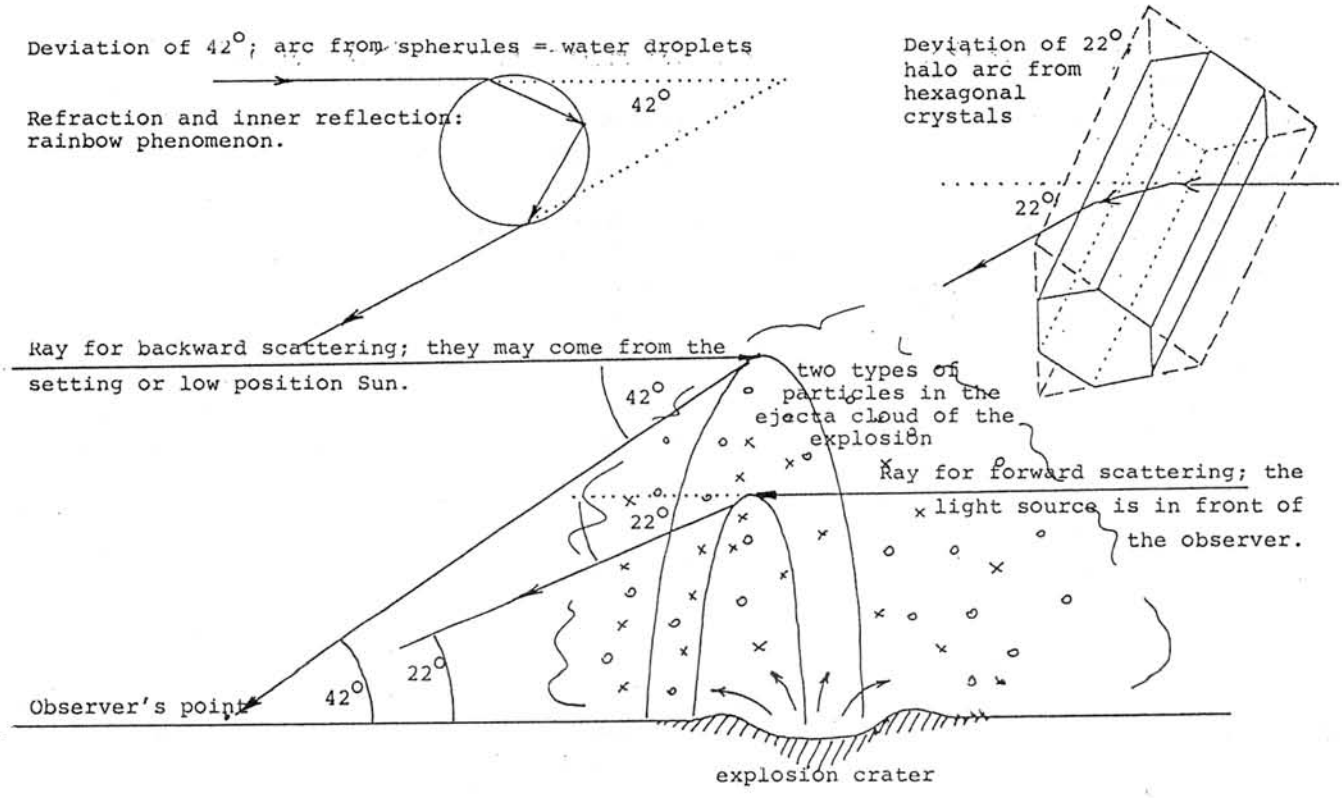

Fig. 1. Side view of the arrangement of our experiment projected. Far left is the low angle Sun /almost setting, behind the observer/. Sun's rays give backward scattering on spherules /droplets/ of the ejecta cloud. They sum up to exhibit a rainbow, which can be seen at 1. and 2. observers /see Fig.2./. Far right is an artificial light source. Its rays can couse forward scattering on crystal particles of the ejecta cloud. Here the hexagonal crystal deviation was shown, which give /sum up/ the 22° cone angle halo around the light source.

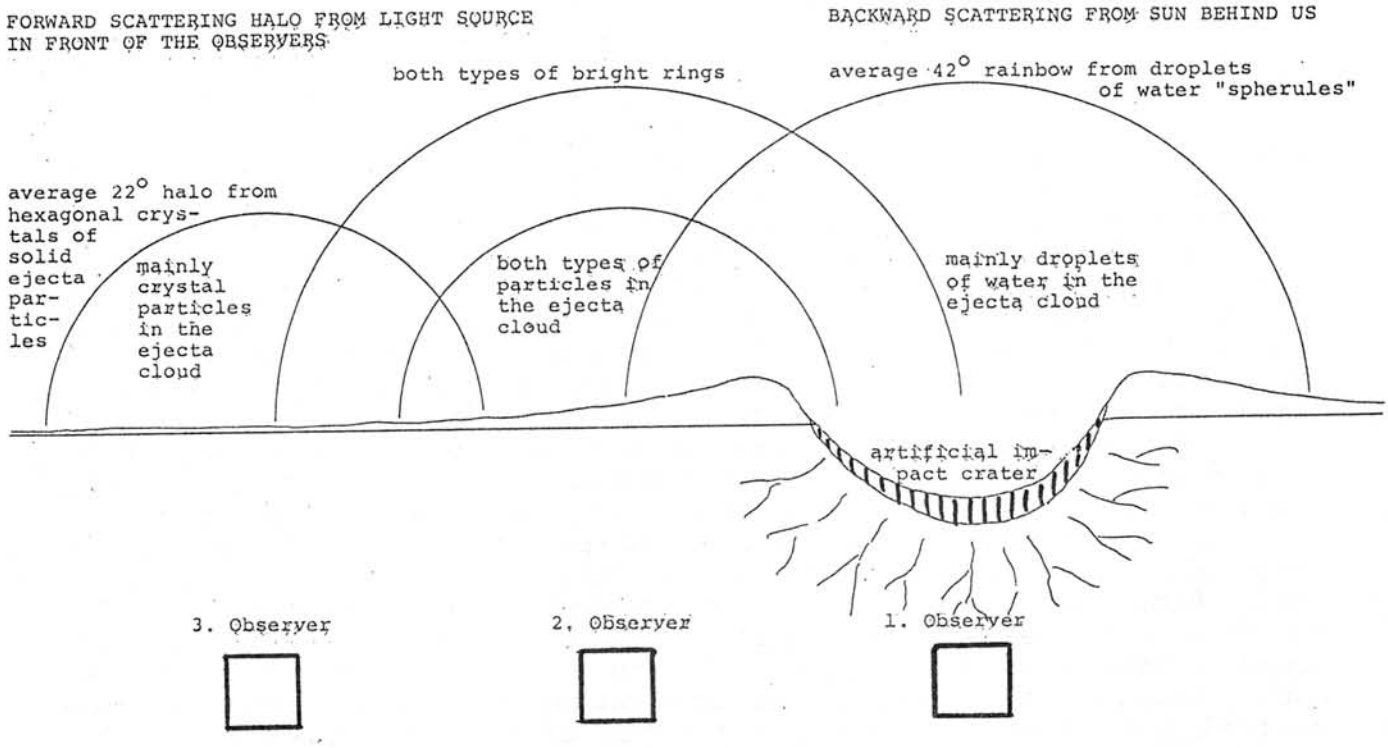

Fig. 2. The shematic representation of the impact ejecta cloud observation in Antarctica. The impact or explosion happens into the icefield, and the main constituent of the ejecta cloud is water and ice particles. Water droplets give backscatterred halo of rainbow from the Sun behind the observers, while hexagonal icy particles give a forward scatterred halo /on their hexagonal prism edge refraction/ from an artificial light source /or a great mirror to reflect setting Sun/. Ratio of water spherules to icy particles can be estimated on the basis of this experiment.

A COMPARISON OF THERMAL HISTORIES OF THE SHOCK VEINS IN TWO CHONDRITIC METEORITES

CHEN Ming[1], XIE Xiande[1] and CHEN Bichen[2]
1. Guangzhou Institute of Geochemistry, Academia Sinica, Guangzhou 510640, China
2. Guangdong Academy of Sciences, Guangzhou 510070, China

Introduction

The discrepancy between the shock levels of chondritic meteorites and the occurrence of high pressure phases in the shock veins has been a major point of discussion in the field of shock metamorphism of solid materials. Indeed, many severely impacted meteorites contain only a small amount of or no high pressure phases, whereas other contain abundant high pressure phases. It is our interest to investigate the causes which induce such discrepancy. Yanzhuang (H6) and Sixiangkou (L6) are two severely shocked and heavily reheated meteorites [1,2]. Both meteorites consist of unmelted chondritic materials and shock-produced melt veins ranging in widths from 0.1 to 10 mm. In this work, we make some comparisons of thermal histories of shock veins in the two meteorites based on the mineralogical and petrographic investigations of shock veins.

Mineralogical and petrographic characteristics of shock veins

(1) Shock-produced " melt " in the veins

The veins in Yanzhuang were nearly totally melted, and that those in Sixiangkou were only partially melted, during their shock events. More than 95 vol% of veins in Yanzhuang is composed of " melt " now mainly consisting of microcrystalline olivine and pyroxene, wadsleyite and majorite, metal-troilite spherule mixtures and silicate glass[1]. The veins in Sixiangkou are composed of "melt" matrix and "unmelted mineral fragments". The " melt " matrix composed of about 60 % volume of veins consists of microcrystalline majorite, Mg-wüstite, metal-troilite spherules, and plagioclase glass; The " unmelted mineral fragments " ranging in sizes from ten to several hundred micrometers consist of ringwoodite, majorite, olivine and pyroxene, diaplectic plagioclase glass[3,4].

(2) Mineral assemblages in the veins

Yanzhuang:

(a) Large amount of microcrystalline olivine and pyroxene
(b) Small amount of microcrystalline wadsleyite and majorite

Sixiangkou:

(a) microcrystalline majorite and Mg-wüstite occurred in melt matrix
(b) Polycrystalline ringwoodite and majorite grains

There are evident differences in shock-produced mineral assemblages in the shock veins of two meteorites. The assemblages of microcrystalline olivine and pyroxene in Yanzhuang should crystallize from melt at high temperatures or through retrograde transformations of their high-pressure polymorphs after pressure release. Small amount of wadsleyite and majorite are the remnants of high pressure phases. In the Sixingkou, two types of high-prssure assemblages are the major constituent components of veins, and they were formed at high temperatures and high pressures. Microcrystalline majorite and Mg-wüstite assemblage crystallized from melt, and polycrystalline ringwoodite and majorite assemblage was formed by solid transformations of olivine and low-Ca pyroxene.

(3) Metal-troilite nodules in the veins

Eutectic melting between Fe-Ni metal and troilite begins at about ~1000 °C [5,6]. When it cooled, eutectic crystallization of metal and troilite occurred. The veins of both Yanzhuang and Sixiangkou contain plenty of metal-troilite nodules.

Yanzhuang:

Metal-troilite nodules in the veins mostly have round outlines and contain troilite groundmass surrounding metal dendrites or metal cells (Fig. 1). It shows that the metal-troilite nodules were fully eutectic melting at high temperatures and well eutectic crystallization as cooling. The dendrites have central trunks (primary dendrites) and secondary arms perpendicular to central trunks. Secondary dendritic arm spacings or the cell widths are 12 - 19 μm. If using the methods of dendrite morphology by Flemings[7] to estimate the cooling history during solidification of dendrites, the cooling rates in the temperature interval of 950 - 1400 °C were 100 - 400 °C/sec [8].

Sixiangkou:

Metal-troilite nodules in the veins consists of two types of grains including eutectic melting and partially eutectic melting wherever metal and troilite were in contact.

(1) Eutectic melting of metal and troilite. These metal-troilite nodules contain well developed metal dendrite(Fig.2). It shows that the metal and troilite were eutectic melting and that eutectic crystallization took place subsequently. Spacings of secondary dendritic arms are 2 μm in average. To estimate the cooling history during the solidification of dendrites, the cooling rates was about 70000 °C/sec [3].

(2) Partially eutectic melting of metal and troilite. These metal-troilite nodules were not fully eutectic melting, and some nodules consist of several parts: (a) metal-troilite mixture containing metal dendrites or cells; (b) metal-troilite mixture with fine-grained metal spherules less than 1μm in diameter; (c) isolated troilite fragments with no contamination of metal.

Discussion

The shock veins of both Yanzhuang and Sixiangkou meteorites have experienced the peak temperatures more than 2000 °C since the chondritic materials in veins were melted and some high pressure phases were formed [1,4]. Based on the mineralogical and petrographic investigations of veins, we conclude that the cooling in veins of Yanzhuang should be much slower than that in Sixiangkou. The longer the time periods of high temperatures kept, the more melt would be produced. It is no doubt that the duration of shock-induced high temperatures in Yanzhuang was sufficient to melt majority of chondritic materials in the veins. In the Sixiangkou, shock-induced high temperatures above eutectic melting of chondrite were too short to induce total melt of vein materials thus remaining a lot of "meineral fragments".

It seems difficult to believe a mechanism that a cooling rate of 70000 °C/sec could occur in the shock veins surrounded by chondritic materials through heat radiation or heat conduction into adjacent cold materials. The method based on the dendritic morphology to estimate the cooling rates could remain question in applying to those naturally shocked meteorites. Based on the studies of mineral assemblages and microstructures, we indicated that the cooling rate in the shock veins of Sixiangkou was less than 1000 °C/sec [4]. The mechanism of heat dissipation from the veins relevant to such a fast cooling rate is still being studied. It is no doubt that the dendrite arm spacings or cell widths in the Sixiangkou could indicate an unusual fast cooling ever found in chondrites. The existence of partially eutectic melting of metal-troilite indicates that the duration of high pressures and temperatures were

very short. Even if the shock-induced peak temperature could be much higher than the melting points of metal and troilite, the cooling of veins was too fast to produce totally eutectic melting of metal and troilite. Therefore, we conclude that the cooling in Yanzhuang should be much slower than that in Sixiangkou. The difference in cooling rates of veins between Yanzhuang and Sixiangkou could be due to (1) average shocked level of meteorite, and (2) buried depth of samples in impacted fragments of meteorites. The average shocked level of Yanzhuang could be much higher than that of Sixiangkou. Shocked level of meteorites and buried depth of samples could be among the factors to affect heat radiation or heat conduction of shock veins.

The relative slow cooling of melt veins in Yanzhuang after high pressure release could result in widespread retrograde transformations of high pressure polymorphs to their normal phases. Quenching of melt veins in Sixiangkou took place under the pressure, thus resulting in preservation of most high pressure polymorphs. We think that other shocked meteorites with ringwoodite-majorite-bearing veins should also have experienced the same rapid cooling histories as the Sixiangkou.

References: [1] Xie Xiande et al. (1994) *Chinese J. Geochem.*, 13, 39-45.[2] Chen, M. and El Goresy, A. (1995) *Meteoritics*, 29, 456. [3]Xie X. and Chen M. (1995) *Antarctic Meteorites*, XX, NIPR, Tokyo, 265-268. [4] Chen, M. et al. (1996) *Science*,271, 1570-1573. [5] Wood J.A. (1967) *ICARUS*, 6, 1-49. [6] Smith, B. A. and Goldstein, J.I. (1977) *Geochim. Cosmochim. Acta*, 41, 1061-1072. [7] Flemings, M.C. et al. (1970) *J. Iron Steel Inst.*, 208, 371-381. [8] Chen et al. (1995) *Meteoritics*, 30, 28-32.

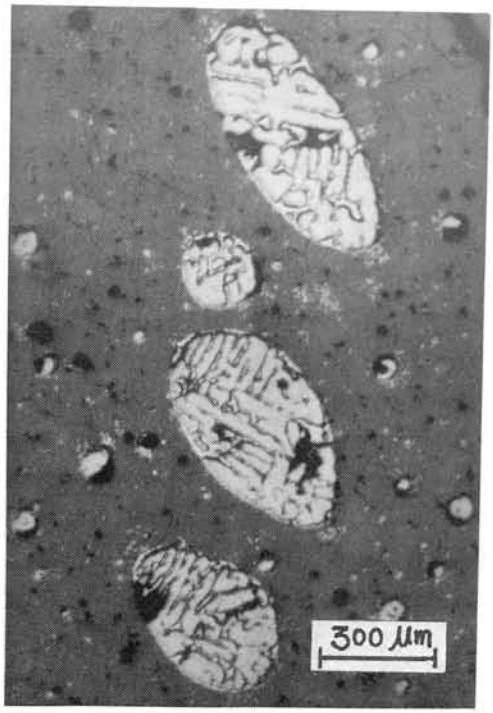

Fig.1 The metal-troilite eutectic nodules with metal dendrites in the shock vein of Yanzhuang .

Fig.2 A metal-troilite eutectic nodule with very metal dendrites in a shock vein of Sixiangkou

MINERALOGICAL COMPARISON OF HAMMADAH AL HAMRA 126 WITH OTHER UREILITES

J. Chikami[1], T. Mikouchi[1], M. Miyamoto[1] and H. Takeda[2]
[1]Mineralogical Institute, Graduate School of Science, University of Tokyo, Hongo, Tokyo 113
[2]Chiba Inst. of Technology, 2-17-1, Tsudanuma, Marashino City, Chiba 275

INTRODUCTION

39 ureilites are recovered from Antarctica and 13 ureilites are recovered from desert. Antarctic ureilites have given us many informations on the genesis of ureilites, because the range of the chemical composition in Antarctic ureilites is wider than those in non-Antarctic ureilites. In spite of recoveries of 52 ureilites, models for ureilite formation process are controversial because ureilites preserve chondritic texture such as O-isotope anomaly [1] and high noble gas content [2] in spite of its achondritic texture. Hammadah al Hamra 126 (HAH 126) is a new ureilite which was found in 1995 from the Libiyan part of Sahara [3]. This ureilite has several interesting points although it was found in the desert. Thus, in this study, we mineralogically studied HAH 126 comparing to Antarctic ureilites.

HAH 126 is fairly weathered probably due to severe weather in the desert. Sexton et al. [4] suggested that the composition of olivine core and the oxygen and carbon isotopic compositions of HAH 126 indicate that this meteorite is a Group 1 ureilite. They also suggested that HAH 126 is most closely related to Y74123 which has an almost identical oxygen isotopic composition to HAH 126. Chikami et al. [5] and Sexton et al. [4] found that reduction of olivine in HAH 126 is more extensive than those of other ureilites.

SAMPLE AND EXPERIMENTAL TECHNIQUES

A polished thin section (PTS) of HAH 126 was prepared at National Institute of Polar Research (NIPR). The PTS was examined petrographically by an optical microscope. Quantitative analysis of minerals was performed by elecron probe microanalyzers (JEOL EPMA JCXA-733 at the Ocean Research Institute, University of Tokyo and JEOL EPMA JCXA-733mk II at the Geological Institute, University of Tokyo). Elemental distribution maps were obtained using JXA-8900L at the Geological Institute, University of Tokyo. Beam current was 120nA.

RESULTS

HAH 126 is composed mainly of olivine and low-Ca pyroxene (Fig. 1). Grain sizes of olivine range from 0.4 mm to 1.8 mm in diameter. Most olivine grains have many veins. The grain boundaries of olivine are curved and they are not clear because of intense reduction and terrestrial weathering. Grain sizes of pyroxene range from 0.2 mm to 0.9 mm in diameter. The shape of pyroxene grains is elongated. Some olivine grains are surrounded by pyroxene grains. Interstice is filled with Fe-rich metal and carbonaceaous matrix. Modal abundances of minerals are: olivine 56 vol.%, low-Ca pyroxene 26 vol.%, others 18 vol.% by measureing an area of each mineral obtained by elemental distribution map. The rim of a low-Ca pyroxene shows a high Ca content. Several points along core-rim line analyses of low-Ca pyroxene gives chemical composition of pyroxene which were

identified as augite. The chemical composition of low-Ca pyroxene is $Wo_{11.0}En_{72.6}Fs_{16.4}$ and that of Ca-rich rim is $Wo_{25.5}En_{67.4}Fs_{7.1}$. Pyroxene crystals do not show so much reduction due to much slower atomic diffusion rate than olivine. Some pyroxene grains contain small patches of Fe-rich composition.

The core composition of olivine is fairly uniform and its Fa content is 20. Olivine crystals were intensely reduced and Mg contents show enrichment at rims (~70-100 μm) (Fa_3-Fa_5) (Fig. 2). The Mn content of olivine slightly increases (MnO: 0.3→0.4 wt%) as the Fa content deareases; that is, olivine crystals show Mn enrichment at rims (~70-100 μm). Intense reduction is also observed along the veins interior olivine crystals. According to a diagram to estimate the cooling rate from the initial temperature using diffusion calculation [6], the cooling rate of 0.1-0.7℃/hour gives the best fit for the observed zoning profiles of olivine reduction rims in HAH 126. This cooling rate is slightly slower than other ureilites.

DISCUSSION

Berkley et al., [7] indicated that olivine in ALH82106 shows complete reduction to pure forsterite at the rim of most grains, because ALH82106 crystallized from a high-T and highly reduced magma. We found that olivine crystals of ALH82106 shows Mg enrichment at rims (~20 μm). The range of ALH82106 reduction (~20 μm) is narrower than that of HAH 126 (~70-100 μm) although Fa content of ALH82106 olivine (Fa_3) is smaller than that of HAH 126. Chikami et al. (1996) suggested that cooling rates deduced from olivine reduction rims in ureilites show similar trends although the Fa components of olivine are variable in ureilites. Reduction rims and cooling rates of ureilites might not be supported by the model, in which ureilites are cumulates related by differentiation of a common magma.

Sexton et al. [4] indicated that oxygen isotopic composition of HAH 126 is most closely related to Y74123 because they have an almost identical isotopic composition. The Fa content of Y74123 (Fa_{19}) shows an almost identical value of HAH 126 (Fa_{20}). But over all abundance of pigeonite in Y74123 (3 vol.%) is small and is different from that of HAH 126 (26 vol.%). The Ca content of pigeonite in Y74123 ($Wo_5En_{77}Fs_{18}$) is a little different from that in HAH 126 ($Wo_{11}En_{72.6}Fs_{16.4}$). The Fe content of pigeonite in Y74123 is almost similar to that in HAH 126. Olivine crystals of Y74123 are coated by thin pigeonitic rims (3-20 μm) [8] as we oberved the similar one in pyroxene of HAH 126. We found that low-Ca pyroxene of HAH 126 contain augite-like rim and that olivines do not contain such as a Ca-rich portion. The composition of Ca-rich rim in Y74123 ($Wo_{25}En_{64}Fs_{10}$) is similar to that in HAH 126 ($Wo_{25.5}En_{67.4}Fs_{7.1}$). Bulk Ca content of pyroxene in Y74123 is lower than that in HAH 126 due to the composition of pigeonite. Ogata et al.[8] reported that the enrichment of Ca and Al in the Y74123 olivine is seen at the rims and that the Al-rich portion contains 6-7 wt% Al_2O_3 content. The augite-like rim in HAH 126 contains less Al_2O_3 content (1.0 wt%) than Ca-Al-rich rim in Y74123. Except for Al_2O_3 content, augite-like rim of low-Ca pyroxene in HAH 126 resembles that of Y74123. Ogata et al. [8] also indicated that ALH78019 and Y82100 contain such a pigeonitic rim materials. The Ca-rich rim materials of Y82100 are present at pyroxene-pyroxene boundaries. The augite-like rim materials in

HAH 126 can be formed by Ca-rich partial melt, which will be drained away from the grain boundaries when the vapor phases were escaped in the revised planetesimal collision model [9].

CONCLUSION

The mineral aseemblage of HAH 126 is common in ureilites. Olivine crystals were intensely reduced and the cooling rate deduced from the reduction rim of olivine is slightly slower than other ureilites. But this cooling rate is within those of other ureilites. Ca-rich rim of low-Ca pyroxene might be formed by Ca-rich partial melt produced by the planetesimal collision.

References

[1] Clayton R.N. and Mayeda T.K. (1988) Geochim. Cosmochim. Acta, 52, 1313. [2] Begemann F. and Otto U. (1983) Geochim. Cosmochim. Acta, 47, 975. [3] Weber D. and Bischoff A. (1996) LPSC, XXVII, 1393. [4] Sexton A., Franchi I.A. and Pillinger C.T. (1996) LPSC, XXVII, 1173. [5] Chikami J., Mikouchi T., Miyamoto M. and Takeda H. (1996) LPSC, XXVII, 221. [6] Miyamoto M. (1985) Proc. LPSC, 16, D116. [7] Berkley J.L., Goodrich C.A. and Keil K. (1985) Meteoritics, 20, 607. [8] Ogata H., Takeda, H. and Ishii T. (1987) LPSC, XVIII, 738. [9] Takeda H. (1989) Earth Planet. Sci. Lett., 93, 181.

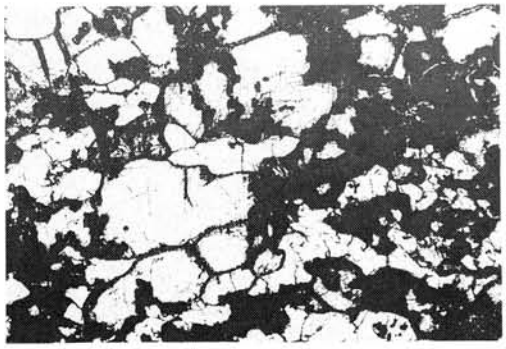

Fig. 1 Entire view of PTS of Hammadah al Hamra 126. The field of view is 11 mm.

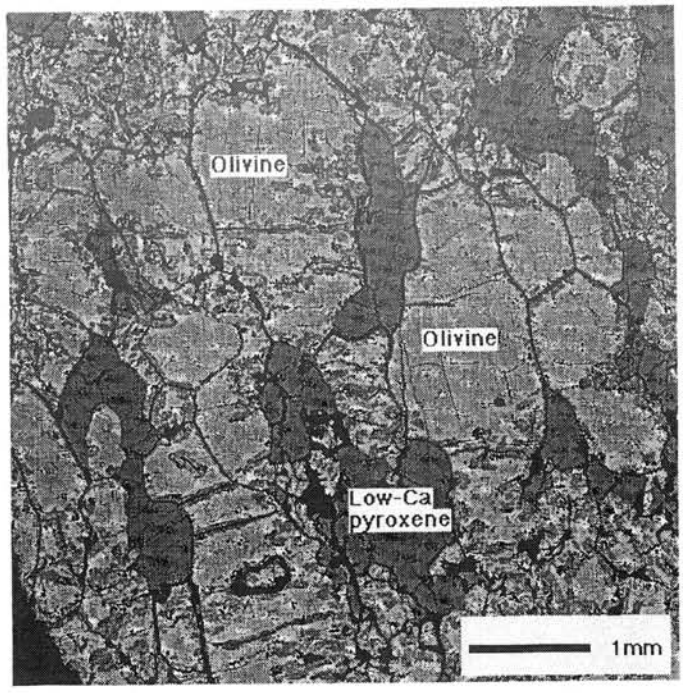

Fig. 2 Mg elemental dsitribution map of Hammadah al Hamra 126 analyzed with a JEOL JXA-8900L electron microprobe at Geological Institute, University of Tokyo. The areas of high Mg concentration (the bright grayish portion) are olivines. Olivine crystals are intensely reduced at their rims. The areas of the dark grayish portion are low-Ca pyroxenes.

^{40}Ar-^{39}Ar age of Y 81090 and Y 81095 chondrites.

M. M. Fugzan
Vernadsky Institute of Geochemistry and
Analytical Chemistry, RAS, Russia, Moscow.

The studying samples Y 81090 and Y 81095 was dated by ^{40}Ar-^{39}Ar method. They present ordinary chondrites L4 [1] from Japanese collection of the antarctic meteorites. We took two chips for analysis 0.4754 g (Y 81090) and 0.2230 g (Y 810950).

The sample was wrapped in high-purity Al foil and vacuum seald in qurtz tube. The samples was irradiated during 3 days in the reactor of UINR (Kurchatov United Institute of Nuclear Research). A neutron doze was 3 x 10^{18} nt/cm^2. The samples was shieled from thermal neutron fluency with Cd foil. The monitor Bt 70A (T=306 Ma) and the optical pure CaF_2 was irradiated with meteorites. After irradiation the samples removed from the qurtz tube and loaded into the extraction system in the same foil in which it were irradited. The 8 steps were applied for each sample. Isotope ratios were measured on MI-1201 mass spectrometer. The data have been corrected for extraction blank, mass discrimination, decay of ^{37}Ar and ^{39}Ar during the irradiation and between irradiation and analysis. Also the data were made correction on trapped and cosmogenic argon and intereference effects from neutron reaction on Ca and K: $(^{36}Ar/^{37}Ar)_{Ca}$ =1.15.10^{-3}; $(^{39}Ar/^{37}Ar)_{Ca}$ = 2.63.10^{-3}; $(^{40}Ar/^{39}Ar)_{K}$ = 0.01; $(^{40}Ar/^{36}Ar)_{trap.}$ = 1 ± 1; $(^{36}Ar/^{38}Ar)_{trap.}$ =5,32; $(^{40}Ar/^{36}Ar)_{cos.}$ = 0.15 ± 0.15. On the plotts apparant age vs cumulative ^{39}Ar releasd the low temperature fractions show the plateau ^{40}Ar-^{39}Ar ages (4,07 ± 6 Ga) Y 81095 and (4.02 ± 4 Ga) Y 81090 with about 80% and 50% of the integrated ^{39}Ar. At the time the higher temperature fractions have the yonger age. Isochron age are (4.00 ± 4 Ga) and (4.02 ± 4Ga) for Y 81090 and Y 81095, respectively.

Ref. [1] Photographic Catalogy of the Antarctic Meteorites 1995, NIPR, Tokyo.

Origin of metal-troilite clasts in seven ordinary chondrites, Y-794006(L4), Y-790126(L6), Y-793211(L6), Y-793213(L6), Y-791629(H4), Y-791686(H5), and Y-791555(H6).

[1]Takashi Fujita, [2]Hideyasu Kojima, and [3]Keizo Yanai
[1]Institute for Study of the Earth's Interior, Okayama University, Misasa, Tottori 682-01, Japan.
[2]National Institute of Polar Research, 9-10, Kaga 1chome, Itabashi-Ku, Tokyo 173.
[3]Department of Civil and Environmental Engineering, Iwate University, 3-5, Ueda 4chome, Morioka, Iwate 020, Japan.

Preface: Shock induced texture in ordinary chondrites has been studied in many samples (e.g., Scott, 1982; Horii et al.,1990; Stoffler et al.,1991). In some cases, a shock process causes a melting of metal-troilite grains in the host rock and forms a coarse metallic clast (e.g.,Scott, 1982). A thermal condition of the shock event can be estimated by a metallurgical study on such texture. In the present study, occurrences of coarse metallic clasts observed in seven Antarctic ordinary chondrite Y-794006(L4), Y-790126(L6), Y-793211(L6), Y-793213(L6), Y-791629(H4), Y-791686(H5), Y-791555(H6) are reported. Texture of the clasts and the host rocks in the polished thin sections were described using an optical microscope, scanning electron microscope and electron probe micro analyzer to clarify the formation process of the clasts.

Sample Description

1 Y-794006(L4) Fig.1

In this sample, a metallic clast (5X6 mm) is mainly composed of troilite and lesser amount of kamacite(Ni~6 wt%) forming a rim of the troilite portion. Both phases show an angular polycrystalline texture, and include silicate mineral fragments and chondrules. Metal in the host also show a polycrystalline texture. The composition of taenite ranges from Ni_{30} to Ni_{46}. Kamacite shows a nearly the same composition as the clast. Most of olivines in the host rock show undulatory or mosaic extinction. Many chondrules show ellipsoidal morphology, and some of them form a complex compound texture which indicates a compression after their accretion.

2 Y-790126(L6) Fig.2

In the metallic clast (2X1.5mm), metal globules are included in the troilite. The metals are richer in Ni in their edges (Ni~20) and include numerous phosphides of micron to submicron size. The texture form a metallic vein which shows a morphological continuity with oxide veins. The oxide contains P and Cl. The host rock shows a recrystallization of olivines, planer defects in pyroxenes, glassy groundmass. Discrete metal grains are rare in the host, but the silicate texture include numerous fine (<10 microns) grains composed of Fe,Ni,S, and P.

3 Y-793211(L6) Fig.3

In this sample, clast (2.5X3 mm) is mainly composed of kamacite. Troilite is observed in the rim of the metal region. The clast includes silicate fragments, fragments of silicate aggregates, and a fragment of host texture. Small fragments and aggregates of a few grains show clear extinction and rounded morphologies indicating the recrystallzation in the clast. Many olivines in the host rock show undulatory or mosaic extinctions. On the other hand, some olivine grains show normal extinction. In the host, taenite show a compositional range from Ni_{30} to Ni_{55}.

4 Y-793213(L6)

In this sample, clast (3X5 mm) is mainly composed of kamacite rimmed with lessor amount of troilite. Kamacite includes globules of a zoned taenite (Ni 22-46wt%) and troilites. Texture of silicate fragments observed in the clast resembles the inclusions in the Y-793211 clast. A silicate texture of the host rock is also similar to that of Y-793211. Most of olivines in the host rock show undulatory extinctions, and some show mosaic extinctions. In the host, zoned taenite (Ni30-50), and almost homogeneous tetrataenite (around Ni_{50}) are observed.

5 Y-791629(H4)

In this sample, clast (3X5 mm) is mainly composed of troilite rimmed with kamacite. The clast include fine silicate fragments. Two fragments of chondrule are observed in the edge of the clast. Many olivines in the host rock show undulatory or mosaic extinctions. Chondrules and metallic grains show a preferred orientation indicating a post accretional shock compression (Sneyd et al., 1988; Nakamura et al.,1992). Taenite in the host shows a composition range from Ni_{17} to Ni_{51}.

6 Y-791686(H5) Fig.4

In the clast (3X8mm), troilite is included in a kamacite. The clast include no or a little silicate inclusion: Silicate fragments is observed only in the rim of the clast. Olivines in the host rock show undulatory or mosaic extinctions. Taenite in the host show a composition range from Ni_{14} to Ni_{53}. Some taenite grains show a reverse zoning texture.

7 Y-791555(H6)

A texture of the metallic clast (3X3.5mm) resembles that observed in Y-791686. However, thick layers of oxides make the contact between metal and sulfide indistinct. In the same reason, texture of the host rock is indistinct. Silicate aggregates are observed in the oxide.

Origin of the clasts

In the metal-troilite clasts described above, the coarse morphologies and Ni poor composition of the metal indicates a different origin from the smaller grains in the host rock. On the other hand, host textures such as undulatory or mosaic extinction in olivine, preferred orientation of chondrules, show that the host rocks experienced shock metamorphism after their accretion. Compositions in the metal grains show the range of shocked chondrites (cf. Horii et al., 1990). It is plausible to interpret the clasts as products of shock event: They should be crystallized from the shock melts enriched in metal-sulfide component. The textural difference among the clasts reflects a difference of the shock condition, mainly heating condition and post shock cooling rate. For the melting of metal-troilite in the host, it requires a reheating temperature higher than eutectic temperature of Fe-Ni-S. In Y-794006 and Y-791629, the sulfide rich composition of the clasts resembles the eutectic composition. Inclusions in the clast remaining a host texture show that extensive melting of the silicate was not occurred. Therefore, the heating temperature of the two specimens should not depart so much from 1000°C. In Y-793211 and Y-793213, recrystallized grains in the clast show the melting of silicate. Therefore, the heating temperature should be higher than 1000°C. Clasts in Y-790126, Y-791686 and Y-791555 are less in inclusion. It should reflect the separation of silicate in immiscible melts. The texture of Y-790126 resembles the Ramsdorf (Begemann and Wlotzka, 1969) and Orvinio (Taylor and Heymann,1971) whose reheating temperatures were estimated as 1200°C(to1350°C in metal) (Begemann and Wlotzka1969; Taylor and Heymann,1971) . Fine phosphide observed in the metal may be formed by the reduction of phosphate in the host rock during the heating as reported by Taylor and Heymann., 1971. The compound texture, and zoning in the metal of the Y-790126 may be formed by a rapid cooling. In the other sample, distinct separation of the metal and sulfide reflects a slow cooling rate. On the other hand, it is shown by the description that a shock heating temperature is higher in type 5,6 than in type4 chondrite. The texture of the clast in the Y-794006(L4) resembles the troilite rich clast in Moorabie(L3) in which the parent body still retained a high temperature condition when a shock reheating occurred (Fujita and Kitamura, 1992). On the other hand, an artificial shock experiment on a hot chondritic material produces a deposit of metallic melt (Nakamura et al.,1993). The slow cooling process and correlation with the shock heating temperature and petrologic grade observed in the present samples implies a possibility that the shock processes also occurred during the earlier stage of metamorphism in the parent body still retaining a high temperature condition.

Acknowledgement: We thank National Institute of Polar Research for the loan of the polished thin sections used in the present study.

References

Begemann,F. and Wlotzka,F. (1969), Geochim. Cosmochim. Acta, **33**, 1351-1370.
Fujita,T. and Kitamura,M. (1992), Proc.NIPR.Symp.Antarct.Meteorites, **5**, 258-269.
Horii, Y., Fujii,N. and Takeda,H. (1990), Proc.NIPR.Symp.Antarct.Meteorites, **3**,254-263.
Nakamura,T.,Tomeoka,K. and Takeda,H. (1992), Earth Planet. Sci. Lett., **114**, 159-170.
Nakamura,T., Tomeoka,K., Sekine,T., and Takeda,H. (1993),Meteoritics, **28**.408 (abstract)
Scott,E.R.D.(1982), Geochim.Cosmochim.Acta,**46**,813-823.
Sneyd,D.S., McSween,H.Y.,Jr, Sugiura,N., Stragway,D.W. and Nord,G.L.,Jr. (1988), Meteoritics,**23**,139-149.
Stoffler,D., Keil,K., and Scott,E.R.D. (1991), Geochim.Cosmochim.Acta. ,**55**,3845-3867.
Taylor,G.J. and Heymann,D. (1971), J. Geophys. Res. ,**76**,1879-1893.

Fig.1 A back-scattered electron image of a metal-troilite clast in the Y-794006.

Fig.1 A back-scattered electron image of a metal-troilite clast in the Y-794006.
Troilite (right gray) region is rimmed with metal (white) region. Both phases of the clast include silicate fragments and chondrules (dark gray region).
Fig.2 A back-scattered electron image of a metal-troilite clast in the Y-790126. Metal globules are observed in the troilite. The texture is elongated to the vein in the host rock (left bottom of the figure).
Fig.3 A back-scattered electron image of a metal-troilite clast in the Y-793211. Metal region is rimmed with troilite. Silicate inclusions (dark gray regions) are mainly observed in the troilite.
Fig.4 A back-scattered electron image of a metal-troilite clast in the Y-791686. Troilite region is covered with metal region. Both phases show inclusion-less appearance.

Horizontal scale of the figures is 2mm.
tr: troilite, mt: metal

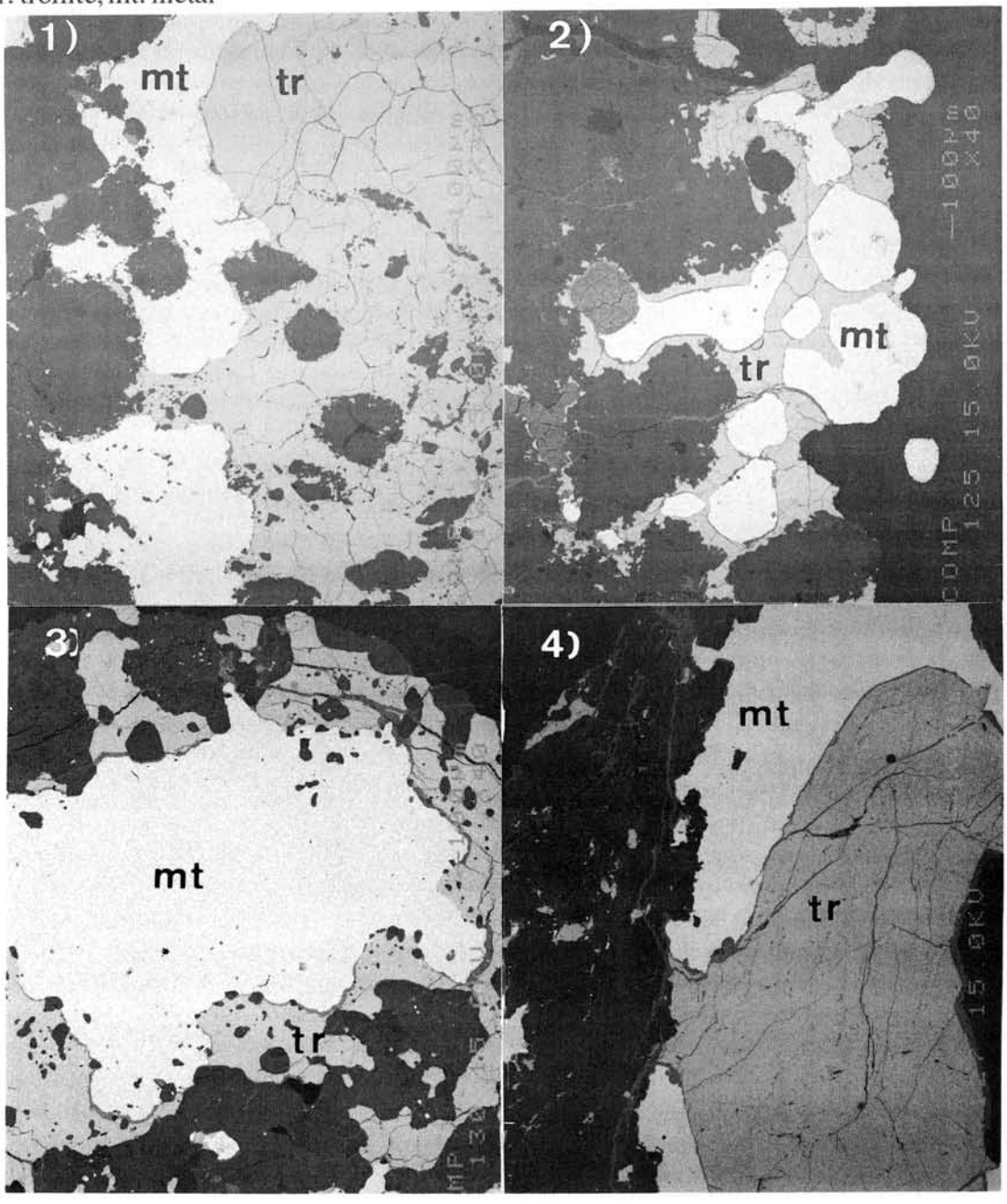

Instrumental neutron activation analysis for μg-size of cosmic spherules

T. Fukuoka[1] and Y. Tazawa[2]

1 Department of Chemistry, Gakushuin University, Mejiro, Toshima-ku, Tokyo 171.

2 Graduate School of Physics and Astrophysics, Kyoto University, Sakyo, Kyoto 606.

A large quantity of cosmic spherules will be collected from Antarctic ice within a few years by the Japanese Antarctic Research Expeditions. Chemical data of cosmic spherules are important to discuss nature and origin of spherules. Instrumental neutron activation analysis (INAA) is the most important analytical technique to obtain chemical data of cosmic spherules. Mineralogical, petrological data etc. can be obtained from same cosmic spherule after INAA, because INAA is a nondestructive technique. More than 10 elemental abundances can possibly be analyzed from μg size of spherule samples by INAA. However, because of tiny sample size, there are many problems (e.g. handling of samples, homogeneity of standard samples).

In this paper, we introduce a recently developed INAA technique for μg size of cosmic spherules. We discuss about a new alloy standard sample for siderophile elements such as Ni, Os, Ir, Au, etc. The INAA results for spherules in deep sea sediments are also shown as an example for 10-100 μg of spherule samples.

Sample spherules, JB-1 glass chip (standard for lithophiles) and alloy chip (recently produced standard for siderophiles) are heat sealed individually into ca 3 x 3 mm size of ultra pure polyethylene bag for easy handling, and they are activated with thermal neutron for 3 min at 20 MW (~2 x 10^{13}n/cm^{2}s) in the pneumatic tube of the JRR-3 reactor of the Japan Atomic Energy Research Institute (JAERI). The activated samples and standards with polyethylene bags are counted to determine Al, Ti, Mg, Ca, V, Na and Mn. After removal of polyethilene bag, the samples and standards are heat-sealed in ultra pure synthetic quartz vials, individually. They are activated again with thermal neutrons for 10-100 hrs at 20 MW (1 x 10^{14}n/cm^{2}s) in the JRR-3 reactor of the JAERI. The activated samples and standards without quartz vials are counted repeatedly to determine Na, Cr, Fe, Sc, REE, Ni, Co, Os, Ir, Au etc.

JB-1 glass standard was made by fusion of the GSJ standard rock powder JB-1. Chemical homogeneity of the JB-1 glass was checked on the chips of crushed glass standard. Alloy standard was provided from the Tanaka Kikinzoku Kogyo Co., Ltd. Chemical compositions of the alloy are shown in Table 1. Chemical homogeneity of the alloy was also checked on chips of the alloy. The homogeneity (standard deviation) for 10-100 μg chips of both standards were 3-4% which are similar to practical INAA precision (3-5%). It was difficult to obtain homogeneous samples for standard of siderophile elements so far. This was big problem for precise INAA of μg size cosmic spherules. The alloy is the best standard sample for siderophiles, at present.

Table 2 is examples of INAA results of cosmic spherules using the alloy chip and JB-1 glass chip. Spherule samples were collected from deep-sea sediments. These results show the spherules were cosmic origin with high precision, because they have high contents of siderophile elements.

Acknowledgements: We thank the Tanaka Kikinzoku Kogyo Co., Ltd. for providing of the alloy standard. The spherules analyzed in this study were supplied from late Prof. K. Yamakoshi and Prof. Nogami.

Table 1. Preliminary results of INAA for the alloy

Element	Row materials			Alloy	
	Purity (%)	Weight (g)	Content (%)	Content (%)	Error* (%)
Ni	99.99	3.9977	82.821	82.6	1
Os	99.99	0.1908	3.953	5.20	1
Ir	99.95	0.0105	0.218	0.192	1
Pt	99.992	0.214	4.433	4.26	5-15
Au	99.992	0.0368	0.762	0.741	1
Al	99.999	0.2091	4.332	4.11	0.5-1
Cu	99.990	0.168	3.480	3.86	1-3
Co	–	–	–	23.8 ppm	10

* Errors for INAA are due to counting statistics.

Table 2. Preliminary results of chemical abundances for spherules in deep-sea sediments by INAA

		Spherules in deep-sea sediments						Canyon Diablo	JB-1 glass	Alloy	Error* (%)
		A	B	C	D	E	F				
Wt	μg	90.7	152.1	18.9	8.9	12.1	17.1	158.6	31.5	39.8	
Al	%	0.705	0.25	0.034	0.46	0.29	0.64	–	=8.07		1-12
Fe[1]	%	9.84	66.0	67.6	20.1	67.0	25.0	90.3	=6.30	–	1-1.5
Mg	%	22.9	–	–	20.3	–	23.5	–	=4.67	–	3-13
Mn	%	0.326	–	0.15	0.10	–	0.18		=0.116		2-10
Cr	%	0.180	0.122	0.202	0.202	0.0052	0.197	–	=0.0414	–	1-9
V	ppm	77	55	96	89	15	96	–	=207	–	3-50
Sc	ppm	6.61	1.98	–	4.91	1.77	6.15	–	=28.9	–	1-5
Co	ppm	27.5	1810	1820	484	2360	257	3990	=39.1	23.8	2-13
Ni	%	0.05	5.16	4.50	1.27	1.59	0.38	11.2	–	=82.6	3-40
Os	ppm	0.30	1.1	–	1.9	–	–	4.7	–	=52,000	10-50
Ir	ppm	0.017	3.97	2.34	0.51	0.41	0.032	3.62	–	=1,920	1-28
Au	ppm	0.010	–	–	0.42	–	–	2.43	–	=7,410	2-20

* Errors for INAA are due to counting statistics.
1) Total iron as Fe.

PETROLOGY OF AN IMPACT-MELTED YAMATO-791088 H CHONDRITE FROM ANTARCTICA

Hiroyuki Fukushi[1,2], and Hirokazu Fujimaki[1]

[1]*Institute of Mineralogy, Petrology, and Economic Geology, Tohoku University, Aoba, Sendai, Miyagi 980-77, Japan*

[2]*Sendai Branch of Sumico Consultants Co., Ltd., Kokubun-cho 1-2-1, Aoba, Sendai, Miyagi 980, Japan*

Introduction

Yamato-791088 is an impact-melted high-iron chondrite (NIPR, 1987). Impact melting could cause vaporization of alkaline elements, and Rb losses from impact-melted chondrites were commonly reported (e. g., Okano et al., 1990; Fujimaki et al., 1992). In contrast, no Rb loss was discovered from severely impacted Yamato-791088 (Fujimaki et al., 1993). They concluded that when impacted, the meteorite seated in depth, and the alkaline element scarcely vaporized. We therefore tried to estimate how deep the meteorite seated when it was impacted in the parental body. Since a good barometer is not available, however, it would be difficult to measure the recorded pressure in the meteorite. Instead, we investigated the meteorite in detail by an electron microanalyzer, and somehow distinguish between pre-impact mineralogy and post-impact mineralogy to classify its petrologic type. The rock type classification should provide significant clue to estimate how deep Yamato-791088 seated.

Sample

The investigated polished thin section was provided by NIPR. The shapes of the chondrules are mostly unclear and deformed. Although the matrix cannot be distinguished from the chondrule, no opaque matrix is left; the matrix seems recrystallized. Mineral constituents are chiefly olivine, pyroxenes, plagioclase, troilite, and Ni-Fe metal. Irregular glass is abundant as well. Although some olivine, augite, pigeonite, and plagioclase appear in close association with glass, orthopyroxene hardly occurs with glass. Large crystals are anhedral, and appear neither in glass nor in close association with glass. In contrast, all of the euhedral crystals of olivine, pyroxenes, and plagioclase are very small (smaller than 40 μm in length), and associate with glass. Small and anhedral crystals are also abundant. The total mode of troilite and metal amounts to 16% .

Mineral compositions

Analytical results of olivine, and Ca-poor pyroxenes are shown in the frequency diagrams (Figs. 1 and 2). Both demonstrate exceedingly wide Mg/Fe variations. Olivines of $Fa_{15\text{-}20}$ are mostly anhedral crystals. Euhedral olivines coexisting with the glass are zoned and rather Fe-rich. The peak of the frequency distribution is around $Fa_{17\text{-}18}$; this is in the range of olivine in the equilibrated H chondrites. The peak of the distribution of Fe/Mg ratios of Ca-poor pyroxenes locates at a similar position to that of the equilibrated H chondrites. Although the

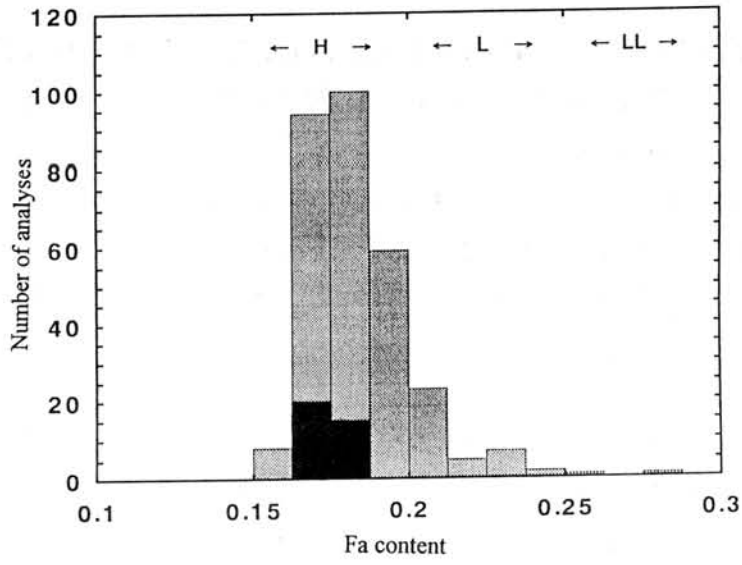

Fig. 1. Frequency distribution of olivine composition.
Solid bar: large and anhedral olivine

sharp peaks in the frequency diagram are common to the equilibrated chondrites, the wide variations are contrasted with the equilibrated chondrites. Most of the augite, and pigeonite coexist with glass. On the other hand, most of the orthopyroxene and some pigeonite do not coexist with glass. Equilibration temperature estimated from coexisting euhedral augite

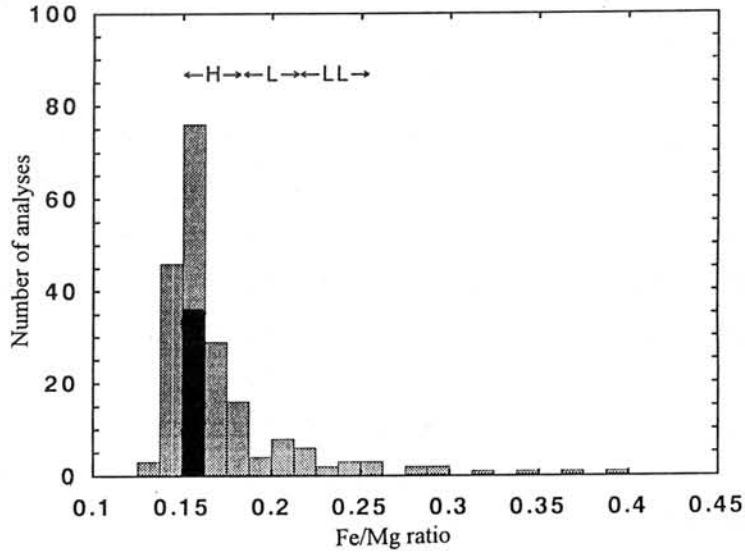

Fig. 2. Frequency distribution of Ca-poor pyroxene composition.
Solid bar: large and anhedral pyroxene

and orthopyroxene pair is approximately 1290℃ (Wells, 1977), and estimated temperatures from euhedral pigeonites are 1180-1200℃ (Ishii, 1975). The compositions of the central portion of large and anhedral crystals (larger than ca. 140 μm) are limited and indicated by the solid bars in the two figures. Compositional diversities of the large and anhedral olivine and pyroxene are as small as those of the equilibrated chondrites.

Plagioclase is euhedral and rich in An molecule comparing with those in the equilibrated

chondrites. All of the plagioclase crystals are euhedral and coexist with glass. The impact melt compositions vary wide. The glass compositions range from andesitic to rhyolitic, and coincide with the previous report (Fujimaki et al., 1993).

Some of large metallic phases show fine exsolution texture of taenite and kamacite. Those pairs seem to have recorded low equilibration temperature (ca. 500 - 700 ℃).

Discussion

Although pre-impact mineralogy cannot be sharply distinguished from post-impact mineralogy, small and euhedral olivine, pyroxenes, and plagioclase are post-impact products. The large and anhedral olivines are poor in Ca, and homogeneous in Fa content. Some of them are slightly zoned in their margins. The chemical features of the large and anhedral Ca-poor pyroxenes are similar to those of the olivine. Such characteristics can be easily accounted for if those large olivine and pyroxenes are equilibrated minerals in the parent body. We interpret the large and anhedral crystals were equilibrated in the parent body and their compositions were slightly disturbed by the impact. The low temperatures recorded in metal phases are consistent with our interpretation. The compositional deviation of the large and anhedral olivine is less than 1.2%, and the deviation of Fe/Mg ratios of the large and anhedral Ca-poor pyroxenes is less than 1.1%. The small deviations of the mineral compositions correspond to the highly equilibrated petrologic type. Although no albitic plagioclase was recognized, it might have melted by the impact. Therefore, Yamato-791088 have seated as deep as the mineral phases can be highly equilibrated.

References

Fujimaki, H., Ishikawa, K. and Aoki, K., (1992), Rb-Sr features of the impact-melted LL-chondrites from Antarctica: Yamato-790723 and Yamato-790528, Proc. NIPR Symp. Antarct. Meteorites, 5, 290-297.

Fujimaki, H., Ishikawa, K., Kojima, H., and Yanai, K., (1993), Rb-Sr age of an impact event recorded in Yamato-791088 H chondrite, Proc. NIPR Symp. Antarct. Meteorites, 6, 364-373.

Ishii, T., (1975), The relation between temperature and composition of pigeonite in some lavas and their application to geothermometry, Mineral. J., 8, 48-57.

NIPR (1987), Photographic catalog of the Antarctic meteorites, compiled by K. Yanai, and H. Kojima, pp. 298.

Okano, O., Nakamura, N., and Nagao, K., (1990), Thermal history of the shock-melted Antarctic LL-chondrites from the Yamato-79 collection, Geochem. Cosmochem. Acta, 54, 3509-3523.

Wells, P. R. A., (1977), Pyroxene thermometry in simple and complex systems, Contrib. Mineral. Petrol., 62, 129-139.

NRM Carrier Minerals of Allende (CV3) Carbonaceous Chondrite

M. Funaki[1] and P. Wasilewski[2]

1: National Institute of Polar Research, 9-10 Kaga 1 Itabashi Tokyo 173
2: Goddard Space Flight Center, Greenbelt Maryland 20771, USA

Many investigators studied remanent magnetization in the Allende (CV3) chondrite, but until Wasilewski (1981) and Wasilewski and Saralker (1981) and then Nagata and Funaki (1983) established that the stable component of NRM is carried by pyrrhotite and that the whole rock was remagnetized by a thermochemical event *i.e.* a sulfidation overprint, we did not have a clear understanding of the Allende magnetic record.

Though awaruite and magnetite are the main magnetic minerals (Banerjee and Hargraves, 1972), it was shown that 90% of the NRM is demagnetized by about 300°C appropriate to magnetic pyrrhotite (Wasilewski, 1981; Wasilewski and Saralker, 1981). Careful thermomagnetic analyses by Wasilewski (1981) shows however that other magnetic phases may contribute to the magnetic record. This paper concerns the search for the unidentified magnetic phases in Allende using magnetotactic bacteria.

The sulfide phase was extracted from Allende powder samples (less than 50μm mesh) using a floatation technic. The thermomagnetic (Js-T) curve of the sulfide phase was measured using an external steady magnetic of 1.0T under 10^{-4} Pa of atmospheric pressure. The curve of the 1st run cycle, as illustrated in Fig. 1, showed clearly defined Curie points at 330°C and 560°C and magnetic humps at around 150°, 310° and 480°C in the heating curve and only the Curie point at 560°C in the cooling curve. Intensity of magnetization decayed about 30% after heating.

Temperature dependence of coercivity (Hc-T) of the bulk sample (shown in Fig. 1) is obtained from hysteresis loops measured from +1.0 to -1.0T external field under 10^{-4}Pa pressure. Using coercivity instead of saturation magnetization, we identified Curie points at 110°, 320° and 560°C in the heating curve and 330° and 560°C in the cooling curve. The original coercivity of 36mT decayed to 11mT on heating to 320°C. The final coercivity after heating to 600°C and cooling to room temperature was 11mT.

Cultivated cocci type magnetotactic bacteria (north seeking) were applied to the polished surface of Allende. The bacteria should therefore migrate toward the S pole of mineral grains along the fields. The clusters were formed on the grains of pyrrhotite, awaruite, magnetite and FeNi sulfide. When the sample acquired a TRM (thermoremanent magnetization) on cooling from 700°C in the vacuum in an external field of 44μT, the clusters appeared on the FeNi sulfide, awaruite and magnetite grains. When the sample acquired a SIRM (saturation isothermal remanent magnetization), the densest clusters were observed on the aggregate of magnetite and FeNi sulfide.

Nagata and Funaki (1983) identified ferrimagnetic pyrrhotite from the chemical compositions, and we confirmed it by the bacterial method. Pentlandite is nonmagnetic, however, certain FeNi sulfides acquire NRM as observed by the bacterial method. This may

be one of the unidentified magnetic phases. This abnormal pentlandite should be studied in detail since it may prove to be important in carbonaceous chondrites. The Js-T curve shape of the sulfide phase is dissimilar to a typical pyrrhotite curve, although the Curie point is consistent. The low temperature component of NRM decayed before 300°C (Sugiura and Strangway, 1985) is likely carried by sulfide phases as pointed out by Wasilewski (1981). This component is considered to be anomalous pentlandite and pyrrhotite both of which formed by hydrothermal activity in the Allende parent body. However, a higher temperature component may be carried by not only the original magnetite and awaruite but also newly created magnetite due to sulfide decomposition during heat treatment. From these viewpoints, the higher temperature component, which was considered to be acquired before accretion of Allende (Sugiura and Strangway, 1985), should be reconsidered. Careful analysis is required since the sulfide phases appear highly reactive during heat treatment.

References

Banerjee, S.K. and Hargraves, R.B. (972): Earth Planet .Sci. Lett., 17,110-119.
Sugiura, N. and Strangway, D.W (1985): J. Geophys. Res., 90, Suppl., C729-C738.
Wasilewski, P. (1981): Phys. Earth Planet. Inter., 26, 134-148.
Wasilewski, P.J. and Saralker, C. (1981): Proc. Lunar Planet. Sci. 12B, 1217-1227.
Nagata, T. and Funaki, M. (1983): Proc. 8th Symp. Antarc. Meteorites, 403-434.

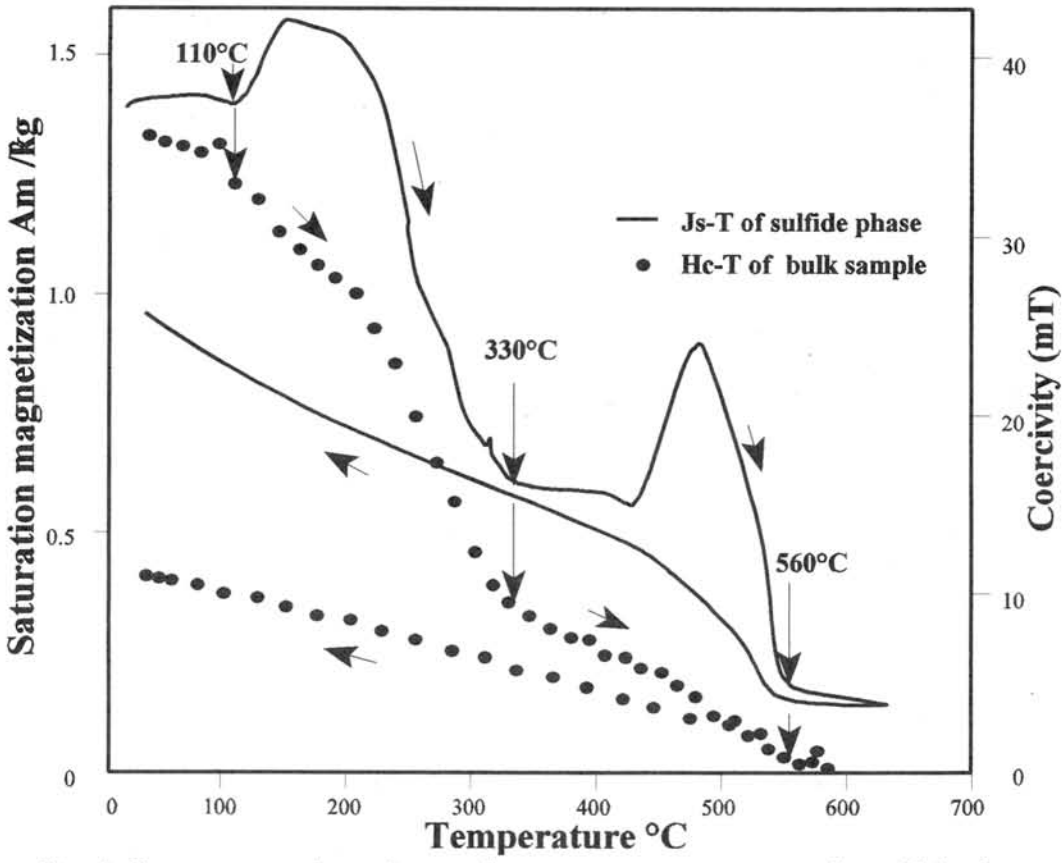

Fig. 1 Temperature dependence of saturation magnetization for sulfide phase and of coercivity for bulk sample

MAJOR ELEMENT CHEMICAL COMPOSITIONS OF ANTARCTIC CHONDRITES

H.Haramura[1], H.Kojima[1], N.Imae[1], M.S.Lee[2], T.Nobuyoshi[3], M.Kimura[3], and Y.Ikeda[3]

[1]Dept. of Meteorites, Nat. Inst. Polar Res.
[2]Dept. of Earth Sci., Seoul Univ.
[3]Dept. of Earth Sci., Ibaraki Univ.

The major element chemical compositions of 492 Antarctic meteorites were obtained by one of the authors (H.Haramura) with the wet chemical analysis method, and were presented in the "Catalog of The Antarctic Meteorites (1995)" [1]. Among them, chondrites are 402 in number, and we compared their major element chemical compositions with those of falls obtained by Jarosewich [2].

Antarctic ordinary chondrites have more or less experienced terrestrial weathering, and most of them contain various amounts of Fe_2O_3, up to 12 wt%. Their water (H_2O+) contents are also various, up to 3 wt%, and they are roughly in proportion to their Fe_2O_3 contents, suggesting that the water contents were added to Antarctic chondrites as limonites ($Fe_2O_3 \cdot 1\text{-}5H_2O$) during the weathering. The total Fe contents of Antarctic H and L chondrites slightly decrease with increasing Fe_2O_3 contents; for an example, total Fe contents of H chondrites with negligible Fe_2O_3 are about 28-29 wt% on average, and those with 10-12 Fe_2O_3 wt% are about 25-26 wt%. This decrease of total Fe contents may be explained by a "dilution" effect due to additional water and oxygen contents that formed limonites from metallic irons. This indicates that any iron contents of Antarctic ordinary chondrites were not lost during the weathering. Metallic Fe contents of H and L chondrites are clearly in inverse proportion to their Fe_2O_3 contents, although their metallaic Ni contents slightly decrease with increasing Fe_2O_3 contents. This suggests that kamacites in H and L chondrites have changed to Fe_2O_3 during the weathering, although most of taenites have not altered, being consistent with the conclusion obtained by Ikeda and Kojima [3] that kamacites were more easily altered to limonites than taenites. The other components such as Na_2O, K_2O, and FeS do not show any correlation with their Fe_2O_3 contents, and they seem to remain constant during the weathering. Therefore, we conclude that the Antarctic chondrites have experienced terrestiral weathering in a closed system except for water and oxygen to produce limonites insofar as concerning on the major element compositions.

The classification of Antarctic chondrites into chemical groups has been carried out on the basis of their petrographic characteristics. However, intense weathering of Antarctic ordinary chondrites obscured their original features, especially for unequilibrated chondrites. Among the Antarctic chondrites studied, Y-793408(L3) and Y-793567(L3) have higher total Fe contents than the normal L chondrites, and they should be classified as H3 chondrites. Y-790521(LL regolith) and ALH78015(LL3) have lower FeO contents than the

normal LL chondrites, and they may be L3 chondrites. A-881725(LL6) has low Na_2O and high total Fe contents in comparison to the normal LL chondrites, and includes a large amount of magnetites, indicating that it is a CK chondrite.

Antarctic chondrites have a wider compositional range than non-Antarctic falls. Especially, metallic Fe (or limonite) contents are highly variable among Antarctic chondrites studied. This may be caused by "sampling" effects; analysed samples of some chondrites are unusually enriched in metallic phases (or limonites) or sulfides, and they are plotted outside the compositional ranges of normal chondrites. Y-791563(H4) has the highest metallic Fe content among Antarctic ordinary chondrites studied and is plotted near Rose City(H5) or Netschaevo(anomalous IIE) in a U-C diagram.

Silicate components seem not to be affected by both the sampling effects and the terrestrial weathering except by the dilution effects. Therefore, the ratios of major element compositions such as Na/Si may be essential properties of the meteorites. The Na/Si ratios of L and LL chondrites studied seem to be slightly higher on average than those of H chondrites, supporting the conclusions obtained by Haramura et al. [4] that the Na_2O contents of Antarctic L and LL chondrites are higher than those of Antarctic H chondrites. The K/Si ratios of LL breccias (Y-74442 and Y-790527) are very high in comparison to other LL chondrites. They often include K-rich lithic fragments, indicating that the high-K contents of the LL breccias are their original property. The unusual C-chondrite trio (Y-82162(C1), Y-86720(CM2), and B-7904(CM2)) have high Na/Si ratios in comparison to normal CM chondrites, indicating that they are an intermediate type between CI and CM.

Several ordinary chondrites have unusual compositions; ALH-77015(L3) has a high Al/Si ratio and a high FeO content, Y-793408(H3), Y-793567(H3), and Y-82038(H3) have high Al/Si ratios, Y-74142(H3) has a high Ca/Si ratio, Y-790957(L5) has a low Mg/Si ratio, Y-793214(LL5) has a high Na/Si ratio, and Y-793465(L6) and Y-791315(H4) have low Na/Si ratios. These unusual ratios remain unsolved.

Reference: [1] Catalog of the Antarctic meteorites, published by Nat. Inst. Polar Res., Tokyo, 1995. [2] E.Jarosewich (1990) Meteoritics 25, pp323-337. [3] Y.Ikeda and H.Kojima (1991) Proc. NIPR Symp. Antarc. Meteor.., No.4, pp307-318. [4] H.Haramura, I.Kushiro, and K.Yanai (1983) Proc. 8th Symp. Antarc. Meteor., NIPR, pp109-121.

DO NEBULAR FRACTIONATIONS, EVAPORATIVE LOSSES, OR BOTH, INFLUENCE CHONDRULE COMPOSITIONS? Hewins, R.H.[1], Yu, Y.[1], Zanda, B[2]. and Bourot-Denise, M.[2]
[1]Department of Geological Sciences, Rutgers University, Piscataway, NJ 08855, USA [2]Museum National d'Histoire Naturelle, 61 rue Buffon, 75005 Paris, and Institut d'Astrophysique Spatiale, 91405 Orsay, France

Chondrules are very abundant in undifferentiated meteorites, and document a major melting event in the solar nebula. They may have been formed from undifferentiated, virtually solar composition solids or from material fractionated by nebular processes, e.g. high-medium temperature condensates. Chondrules occur as two major types, I and II (McSween, 1977a,b). Type I is FeO-poor, enriched in refractory elements and depleted in moderately volatile elements; type II is FeO-rich and approximately chondritic in composition. Chondrules then either represent two sets of nebular condensates formed at diffferent temperatures and subsequently melted as closed systems, or they formed from low temperature material melted under open system conditions, with volatiles much more extensively lost from type I than type II. The debate over which alternative is correct has been very heated, but we show here that both processes have been important.

We have made both observations and experiments relevant to the open/closed system problem. We systematically studied all the chondrules (300) in one thin section of Semarkona. Bulk chemical and mineral anlysis were obtained for all the finer-grained and a representative number of coarser grained. The finest grained type I chondrules, even finer-grained than typical dark-zoned (cryptoporphyritic) chondrules, have an intersertal texture with scattered patches of glass. Such finest grained type I chondrules have bulk compositions close to CI, with most of the Fe present as FeS. We determined number of olivines/unit area as a melting indicator, because it can be measured much more precisely than grain size, and converted it (inverse of square root) to a nominal grain size (more readily understood). The moderately volatile elements Na, K, Fe, Ni, P and S decrease systematically as grain size increases, i.e. degree of melting increases, (Hewins et al., 1996 and Figure 1). This suggests open system melting, because if compositions were acquired before melting it is not clear why the most volatile-rich ones should be the least melted (Hewins et al., 1996). However, large scale Mg/Si variations throughout the suite uncorrelated with grain size suggest that there were variations in precursor compositions, presumably due to condensation/agglomeration processes.

S is totally absent from the most melted type I chondrules (PO, BO) in Semarkona (and Renazzo). On the other hand it is concentrated in opaque veneers around chondrules (comprising about 1/2 of the meteorite's bulk S for Semarkona), suggesting condensation of S lost from chondrules onto the metal blebs decorating chondrule surfaces. S in veneers is present in troilite associated with pentlandite and awaruite resulting from the breakup of an initial Ni-bearing monosulfide condensate, in good agreement with experiments by Lauretta et al. (1995). The continuous negative correlation trend found in Semarkona between grain size and abundance of all the volatile elements (especially S), indicates a genetic continuity between all type I chondrules from the "orthodox" coarse ones to the finest ones, the only difference being in the melting intensity and the subsequent volatile loss. Thus the finest chondrules are closest to their precursors. In cryptoporphyritic chondrules, sulfide exhibits clear melt textures (droplets, and eutectic mixes when associated with metal). At even lower grain sizes (intersertal textures) the pentlandite assemblage of chondrule veneers is found, with very little kamacite. This suggests that Fe and Ni were present in the precursors dominantly as sulfide (Zanda et al., 1996) and sulfur loss contributes materially to the formation of metal in chondrules in ordinary chondrites.

We have made analyses of some of the type II chondrules in Semarkona. Again the coarser-grained (more melted) chondrules are volatile-depleted relative to the fine-grained ones. The finest-grained chondrules are close to CI and the finest grained type Is. However, a few have higher, superchondritic, levels of the more volatile elements (Figure 1). This, plus the difference in olivine composition on which the classification as type I or II is based, maintained down to the finest grain size, suggests that there were pre-chondrule differences as well as modifications during chondrule formation.

Various experiments have been performed to examine loss rates of moderately volatile elements from chondrule compositions. Na loss/retention was measured as a function of bulk composition, oxygen fugacity and cooling curve (Yu and Hewins, 1996). Naturally, it is much easier to retain Na with continuous cooling after very brief heating, than with the isothermal superheated liquids of earlier experiments (Tsuchiyama et al., 1981). Never-the-less, in order to retain chondritic levels of Na, as in type II chondrules, we require flash heating, peak temperature not much above the liquidus, initial cooling rates in the thousands of degrees per hour and, relative to the solar nebula, very high oxygen fugacity. Type I chondrule composition loses more Na than type IIAB chondrules under identical conditions because the melt is much less polymerized and the Na-O bond is weaker (Figure 2). In Semarkona chondrules, bulk Na concentrations correlate with oxygen fugacity (calculated from Fa) but also negatively with Mg/(Si+Al).

The bulk of prior chondrule experimentation has been done at 1 atm. pressure, much above canonical nebular pressures. Vacuum experiments have generated suggestions that chondrules could not have formed in

the nebula, because of heavy evaporative losses (Fredriksson et al., 1991). However, Na loss rates measured at low pressure are not greater than 1 atm. rates, provided that the effects of oxygen fugacity are considered (Shimaoka and Nakamura, 1991; Yu and Hewins, 1996). We therefore consider the 1 atm. experiments relevant to chondrule formation.

Chondrule formation in a nebular setting may lead to reduction as well as evaporation. For experiments with type I chondrule compositions, the typical result of gas reduction is the formation of "dusty olivines", $Fo_{\sim 90}$ when flash heated, up to Fo_{98-99} with longer heating time. Type IIAB chondrule materials seldom develop dusty olivines at similar conditions except with extremely low fO_2s. When flash heated, type IIAB charges are similar to those run at IW-0.5, with some Fe metal forming on the edge of the charge. Longer heating time or slower cooling rate always leads to growth of protopyroxene and poikilitic texture, with olivine Fo_{90} to Fo_{92}. Type IIAB starting material, with 5 to 15 minutes reduction and evaporation above liquidus, gradually becomes type IB in composition, c.f. Hashimoto (1983), but the Na loss is nearly 100%.

Reduction of chondrule materials by ambient gas could be as effective as the chondrule intrinsic fO_2s caused by graphite, etc. (Connolly et al., 1994). We used much shorter heating time than Danielson and Jones (1995) and Libourel (1995), but produced similar results. However it is uncertain how extensively reduction and evaporation actually affected chondrules. Dusty olivines occur only in a small portion of natural type I chondrules, and to reduce the relatively Fe-rich olivine into uniformly forsteritic olivine requires hours of heating in reduced gases. Virtually all the Na would have been lost under such conditions, requiring that a large portion of the evaporated Na later recondensed back to chondrules (Matsunami et al., 1993). Based on the same argument, forming type I chondrules from type II chondrule compositions through reduction and evaporation is an even more difficult process. Therefore though chondrules suffered some volatile loss during their formation (Yu et al., 1996), other characteristics were produced by pre-chondrule fractionations.

We conclude that precursors of type I and II chondrules were similar and near-chondritic, but with higher fayalite and troilite contents in the type IIs. This corresponds to small differences in the final temperature of condensation, or nebular segregation time. Both types of chondrules lost volatiles during melting, as a function of extent of heating. Type I chondrules lost more volatiles because of different oxygen fugacities and bulk composition effects on bond stregths. Type Is experienced a small amount of reduction of FeO, but breakdown of FeS followed by both evaporative and mechanical loss of Fe was more important. Both nebular fractionations and evaporative losses influenced chondrule compositions.

References

Connolly H. C., Jr., Hewins R. H., Ash R.D., Zanda B., Lofgren G. E., and Bourot-Denise M. (1994) Carbon and the formation of reduced chondrules: an experimental investigation. *Nature*, **371**, 136-139.

Danielson L. and Jones R. H. (1995) Experimental reduction of olivine... *Lunar Planet. Sci.* **26**, 309-310.

Fredriksson K Wlotzka F & Spettel B (1991) To make perhaps or not to make chondrules. *Meteoritics* **26**, 335.

Hashimoto A. (1983) Evaporation metamorphism in the early solar nebula... *Geochem. J.* **17**, 111-145.

Hewins, R.H., Zanda, B. and Bourot-Denise, M. (1996) Evaporative loss and degree of melting in Semarkona type I chondrules. *Lunar Planet. Sci.* **XXVII**, 537-538.

Lauretta D.S., Kremser D.T. and Fegley B.Jr. (1995) Nickel fractionation during troilite formation in the solar nebula. *Lunar Planet. Sci.* **XXVI**, 831-832.

Libourel G & Chaussidon M (1995) Experimental constraints on chondrule reduction. *Meteoritics* **30** 536-537.

Matsunami S. et al. (1993) Thermoluminescence and compositional zoning in the mesostasis of a Semarkona goup A1 chondrule... *Geochim. Cosmochim. Acta* **57**, 2101-2110.

McSween H. Y. (1977a) Chemical and petrographic constraints on the origin of chondrules and inclusions in carbonaceous chondrites. *Geochim. Cosmochim. Acta* **41**, 1843-1860.

McSween H.Y., Jr. (1977b) *Harvard/Smithsonian Center for Astrophysics Report* (Cambridge, Mass.) 19 pp.

Shimaoka T. and Nakamura N. (1991) The effect of total pressure on vvaporization of alkalis from partially molten chondritic material. In *Origin and Evolution of Interplanetary Dust* (eds. A.C. Levasseur-Regourd and H. Hasegawa), pp. 79-82. Kluwer Academic Publishers.

Tsuchiyama A, Nagahara H., and Kushiro I. (1981) Volatilization of sodium from silicate melt spheres and its application to the formation of chondrules. *Geochim. Cosmochim. Acta* **45**, 1357-1367.

Yu, Y., and Hewins, R.H. (1996) Transient heating and chondrule formation - evidence from Na loss in flash heating simulation experiments. *Geochim. Cosmochim. Acta*, submitted.

Yu Y., Hewins R.H., and Zanda B. (1996) Sodium and sulfur in chondrules: heating time and cooling curves. In *Chondrules and the Protoplanetary Disk* (eds. R.H. Hewins, R.H. Jones and E.R.D. Scott) Cambridge University Press, 213-219.

Zanda, B., Bourot-Denise, M., and Hewins, R.H. (1996) Chondrule precursors: the nature of the S- and Ni-bearing phase(s). *Lunar Planet. Sci.* **XXVII**, 1485-1486.

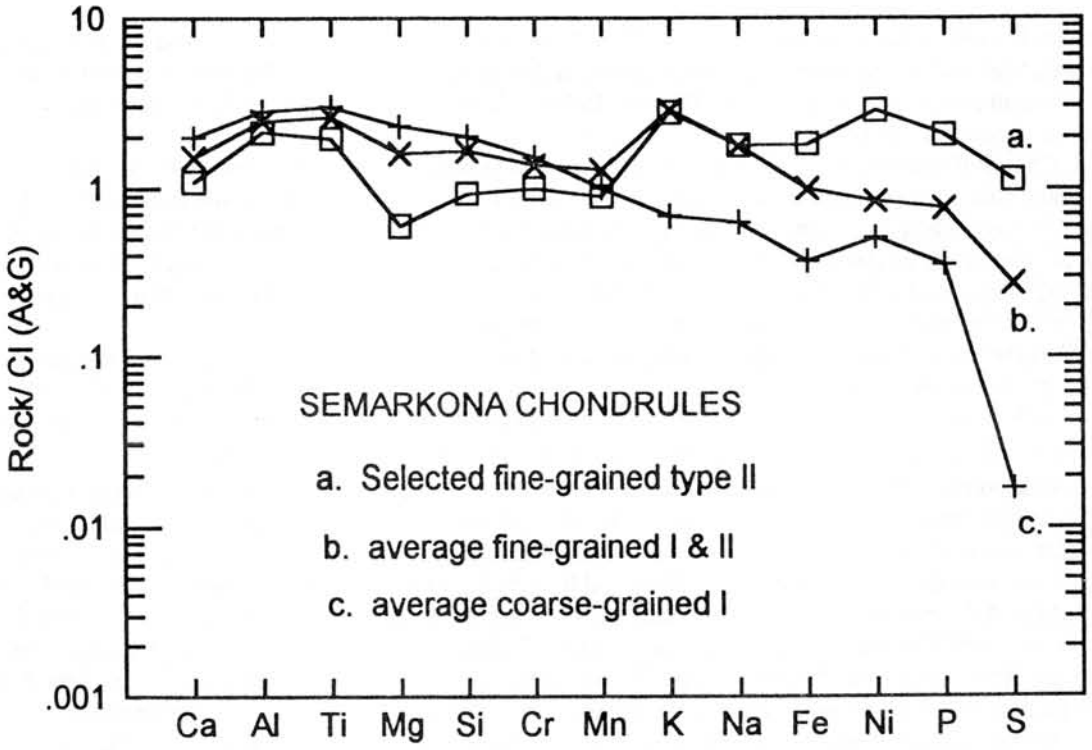

COMPOSITION EFFECT ON NA LOSS

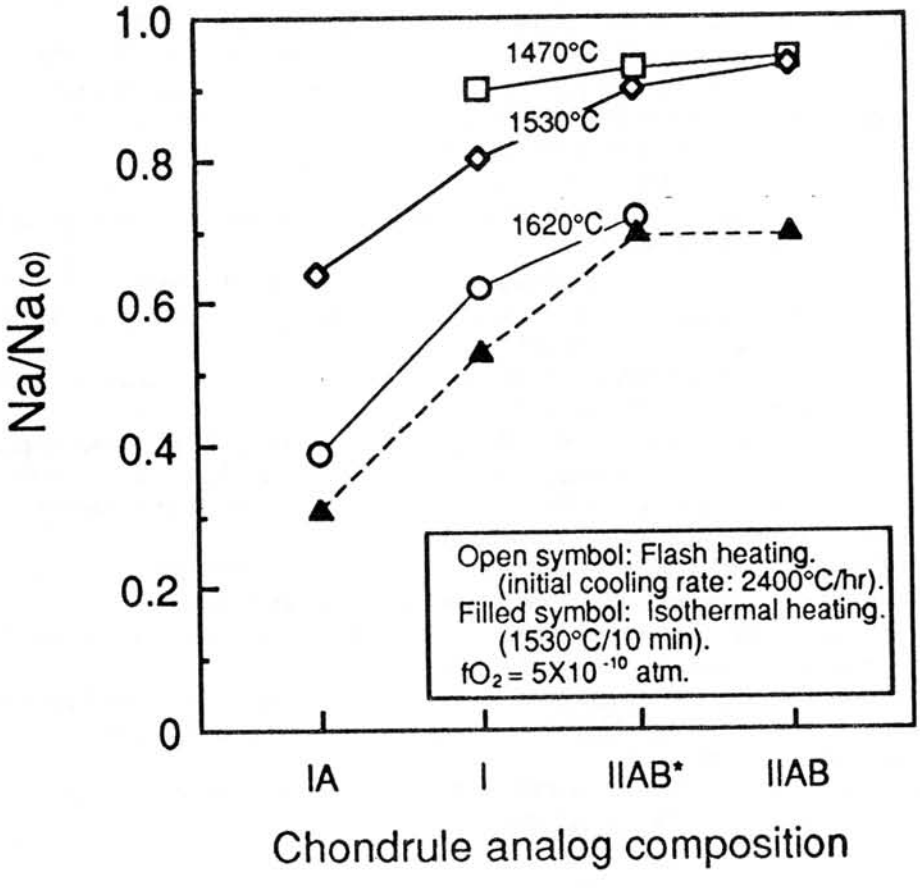

IN-SITU ANALYSIS OF OXYGEN ISOTOPES IN ALLENDE CHONDRULES USING A SIMS

Hajime HIYAGON

Department of Earth and Planetary Physics, University of Tokyo,
Yayoi 2-11-16, Bunkyo-ku, Tokyo 113, JAPAN

INTRODUCTION

Since the work of Clayton et al. [1], it has been revealed that meteorites and their constituents have variable oxygen isotopic compositions, suggesting the presence of several isotopically distinct reservoirs [2]. Most of the oxygen isotope analyses have been done using conventional mass spectrometry, which requires a sample of at least mg size, and hence the data represent averages of the >mm-sized areas. In this respect, secondary ion mass spectrometry (SIMS) has great importance for the analysis of much finer distribution of oxygen isotopic compositions. However, relatively few attempts have been made so far. Weinbruch et al. [3] separated individual olivine grains from Allende meteorite, pressed them into a gold foil to avoid charge-up, and analyzed them with a SIMS technique. They found that refractory (Mg-rich) forsterites and forsteritic cores of isolated olivine grains (IOGs) have relatively rich in ^{16}O ($\delta^{17}O$ down to -12‰ and $\delta^{18}O$ down to -9‰) but that fayalite-rich rims of IOGs and most of the matrix olivines have less enriched in ^{16}O ($\delta^{17}O$ ~-3‰ and $\delta^{18}O$ ~0‰). An *in-situ* analysis of oxygen isotopes using a SIMS technique was conducted by Hervig and Steel [4]. They analyzed oxygen isotopes in Allende olivines in thin-section by using an electron gun for charge compensation and by applying a high energy offset (300eV) to remove molecular ions, and obtained a similar result to that of Weinbruch et al.

I have been trying to develop a technique of *in-situ* analysis of oxygen isotopes in rock samples such as meteorites using a SIMS (CAMECA, ims-6f) which was installed at the University of Tokyo last March. In the present paper, I report some results of basic experiments and a preliminary result of *in-situ* analysis of oxygen isotopic compositions in olivine grains in Allende chondrules.

EXPERIMENTAL CONDITION

San Carlos olivine and Burma spinel were used in the present study as running standards for oxygen isotope analyses. San Carlos olivine was cut into a piece of ~1cm in diameter and ~1mm in thickness, surface polished, and gold coated (~500Å in thickness). Burma spinel was

prepared as a thin-section, surface polished, and gold-coated. A Cs^+ primary beam of 10kV energy was defocused to be a relatively homogeneous beam of ~50μm in diameter with a beam intensity of 0.6-0.9nA. The analyzed area was limited by a Field Aperture (FA) to be ~8μmϕ of the center of the sputtered area. This procedure was applied to avoid the edge effect and to minimize the interfering peak of $^{16}O^1H$ at mass 17. Oxygen isotopes (^{16}O, ^{17}O and ^{18}O) were analyzed as negative ions accelerated at -9.5kV. The mass resolving power (MRP) was set to be >5000 to separate ^{17}O and $^{16}O^1H$ peaks. A normal-incidence electron gun (NEG) was used for charge compensation. The size of the electron beam was ~150μm in diameter and carefully centered on the position of the primary beam. An ion counting system was used for detection of secondary beams. Dead time of the system was estimated to be ~25ns by Ti-isotope analysis and was used for the correction of the count rates.

REPEATED ANALYSES OF STANDARDS

In order to examine reproducibility of the measurements, oxygen isotope analyses were repeatedly conducted for San Carlos olivine and Burma spinel. For a typical analysis with a ~35 minutes integration time and with a typical count rate of $\sim 5 \times 10^5$ c/s for ^{16}O, the obtained statistical errors were ±3‰ for $^{17}O/^{16}O$ and ±1.5‰ for $^{18}O/^{16}O$ (1σ). However, the total variations of the obtained ratios were much larger: ±5‰ for both $^{17}O/^{16}O$ and $^{18}O/^{16}O$ (1σ). It was found that positioning of the observed area (limited by FA) in the sputtered area as well as homogeneity of the primary beam were important factors controlling the instrumental fractionation. The results for Burma spinel and San Carlos olivine were consistent with each other within analytical uncertainties.

PRELIMINARY RESULTS FOR ALLENDE OLIVINES

A thin-section of Allende meteorite was prepared, gold-coated, and used for a SIMS analysis. A chondrule was selected and oxygen isotopic compositions in olivine grains in the chondrule were *in-situ* analyzed with a SIMS. Burma spinel was analyzed at the same time for normalization of the oxygen isotope data. The analytical condition was the same as described above. The Fe/Mg ratios were also estimated using a Cs^+ primary beam at 10kV and by analyzing negative secondary ions of $^{24}Mg^{16}O^-$, $^{56}Fe^{16}O^-$ and $^{28}Si^-$ accelerated at -9.5kV at a MRP of about 3000. All the analyzed olivines were Mg-rich (Fo_{93}-Fo_{99}). The obtained $\delta^{17}O$ ranged from -19‰ to 0‰ and $\delta^{18}O$ from -16‰ to -2‰, which are similar to the results of Mg-rich olivines by Weinbruch et al [3] and those by Hervig and Steele [4]. There also seems to be heterogeneous distribution of oxygen isotopes within this particular chondrule, but this is not conclusive at present due to relatively large experimental uncertainties.

REFERENCES

[1] Clayton R. N., Grossman L. and Mayeda T. K. (1973) *Science* **182**, 485-488.

[2] Clayton R. N. (1993) *Ann. Rev. Earth Planet. Sci.* **21**, 115-149.

[3] Weinbruch S., Zinner E. K., Goresy A. El., Steele I. M. and Palme H. (1993) *Geochim. Cosmochim. Acta* **57**, 2649-2661.

[4] Hervig R. L. and Steele I. M. (1992) *Lunar Planet Sci.* **XVII**, 364-365 (abstr.).

COSMOGENIC PRODUCTS IN METAL PHASE OF THE BRENHAM PALLASITE.

M. Honda[1], H. Nagai[1], K.Nagao[2], and Y.N.Miura[3], [1] Nihon Univ.,Dept. of Chem., Setagaya, Tokyo 156. [2] Inst.for Study of the Earth's Interior, Okayama Univ., Misasa, Tottori 682-01. [3].Earthquake Res. Inst., Univ. of Tokyo, Bunkyo-ku,Tokyo 113.

Cosmogenic nuclides, stable noble gases and long-lived radioactivities, were determined in several fragments recovered from the Brenham pallasite. The metallic phase was separated mechanically and the surface was etched with dilute nitric acid. A sensitive noble gas mass-spectrometer was used to determine cosmogenic He, Ne, and Ar isotopes, separately in the metal samples. For radioactive products, Be-10 and Al-26, in metal, AMS method was applied. The facility is a remodeled 5 MV pellet type Tandem accelerator, at the Univ. of Tokyo. For Mn-53 in the metal the activation method was applied. Well thermalized neutron doses, higher than E18 n /cm2, were available at the JRR3 reactor, Japan Atomic Energy Inst, Tokai. Typical analytical data are tabulated in Table 1., comparing systematic model calculations for all products [1;2].

1). Under shielding inside the large meteoroid, stable and radioactive products are all distributed in the two phases. A single stage irradiation model can be applied for this meteorite. Throughout the long irradiation history, 200 my, the silicate has preserved a heavily shielded record as well as those in the metal samples. The data seem consistent with each other, except for radioactivities with larger errors in deep interior samples

2). Production of cosmogenic nuclides in stone and metal are equally influenced by observed model shielding factors, k_1' and k_2'. In general,

(Prod. rate) = f x k_1' x $(\Delta A')^{-k_2'}$ where, k_2' = 2.24log(He4/Ne21)m – 2.8.

Two parameters, f and $\Delta A'$, are characterized by products in a target. The productions in the metal phase are treated identically with those in irons [3]

3). It is rather surprizing that we can systematize products resulted by entirely different exitation functions employing common parameters for a wide range. Extremely extended range, however, causes slight variations in the parameters for other than typical spallation. Ar38m and Ne21m are typical by sharp thresholds in the excitation functions. (He3/Ar38)m are higher under both heavy and also light shielding conditions (Fig.1). These are common for He isotopes and multi-element target products (Fig.2), which are by continuously increasing cross-sections. It is reasonable considering shifts of cosmic-ray flux spectra inside meteorites. $1 + 0.2x(k_2' - 2.6)^2$ can be a correction factor to the parameter, " f ", for He3m. The factors seem in a sequence of, Be10m, He3s, He3m, and Ar38s, all relative to Ar38m.

Ref. [1].Honda M. (1985), EPSL, 75, 77-80; (1988), Meteoritics,23, 3-12. [2]. Nagai H. et al (1993), Geochim. 57, 3705-3723. [3]. Voshage H., Feldmann H.(1979), EPSL. 45 293-308. [4]. Schultz L. et al (1996), Compilation. [5]. Bhattacharia et al.(1980). EPSL51, 45-57.

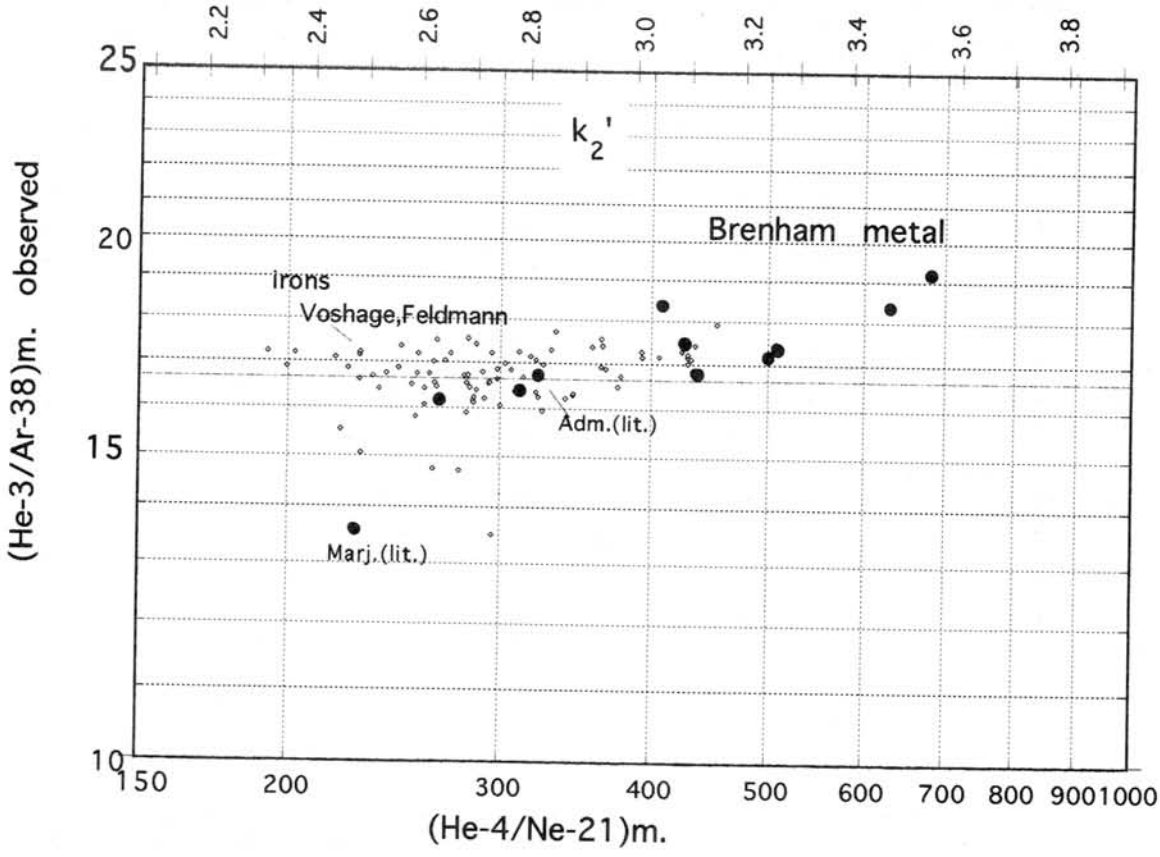

Fig. 1. He-3 /Ar-38 vs. shielding found in Brenham-metal and literature data in irons.

TABLE 1. Cosmogenic Products in Pallasites and Production Systematics.

Brenham	Noble gases, E-8cc/g					Radioactive Nuclides, dpm/kg				shield.factor		Texpos.
Sample ID	(metal, Fe-Ni)					(metal, Fe-Ni) '---(±error to last digit) ---						
model	He3m	He4m	Ne21m	Ar38m		Mn53m	Be10m	Al26m	Ref.	k2'	k1'	my
ΔA'	*22*	*14*	*39*	*22*	Ref.	*8*	*22*	*34*			atom/min.g	
f	*16.7*	*18.3*	*1*	*1*		*1.0*	*0.11*	*0.25*				
N.94	58.0	216	0.81	3.57			0.93±3	0.80±7				
model	*65.8*	*246*	*0.93*	*3.93*		*160*	*1.10*	*0.71*		*2.72*	*45*	*200*
N.91	45.6	173	0.56	2.78		137±4		0.62±4				
model	*50.4*	*195*	*0.68*	*3.00*		*132*	*0.84*	*0.52*		*2.8*	*44*	
UCSD 86						103±4						
model	*43.4*	*171*	*0.57*	*2.57*		*119*	*0.72*	*0.44*		*2.85*	*44*	
AMNH 880	7.24	30.1	0.074	0.39			0.09±1	0.050±6				
model	*7.73*	*33.9*	*0.081*	*0.44*		*28*	*0.12*	*0.07*		*3.15*	*19*	
Reed (av.)	6.07	25.5	0.060	0.346			0.10±2	0.055±8				
model	*5.99*	*26.7*	*0.061*	*0.34*		*22*	*0.09*	*0.05*		*3.2*	*17*	
H.J.91	4.15	18.8	0.038	0.24		16±1						
model	*4.93*	*22.0*	*0.040*	*0.28*		*18*	*0.08*	*0.04*		*3.2*	*14*	
H49.236	2.35	9.97	0.023	0.14		8.9±4	0.10±1	0.021±3				
model	*2.30*	*10.8*	*0.021*	*0.12*		*10*	*0.04*	*0.017*		*3.35*	*10*	
AMNH 881	0.205	1.09	0.0016	0.011								
model	*0.23*	*1.16*	*0.0016*	*0.012*						*3.6*	*2*	
LJ . Shima	0.177	0.81	0.0016	0.010		3.1±5	0.007±3	0.008±2				
model	*0.15*	*0.77*	*0.0010*	*0.007*		*0.77*	*0.0021*	*0.0009*		*3.65*	*1.5*	
Ward	0.127	0.63	0.0010	0.007		0.4±8	0.004±1	0.006±2				
model	*0.14*	*0.72*	*0.0009*	*0.007*		*0.72*	*0.0019*	*0.0008*		*3.65*	*1.4*	
Other pallasites (literature)												
Admire	62	270	0.78	3.85	Signer62		2.39±12	2.29±12	Nagai93			
model	*67*	*259*	*0.80*	*3.99*		*390*	*2.49*	*1.54*		*2.8*	*130*	*90*
Marjalhati,1902	204	718	3.16	15.00	Begem.76	522±28	5.91±35		Bhattacharya80			
model	*219*	*750*	*3.13*	*13.10*		*532*	*4.60*	*3.24*		*2.5*	*95*	*160*

*: Ne21/Ne22 = 1.000-1.004 in HJ91,H49.236 and Ward; 1.014-1.017 in N91 and UCSD.

Ref.: [2, 4, 5]

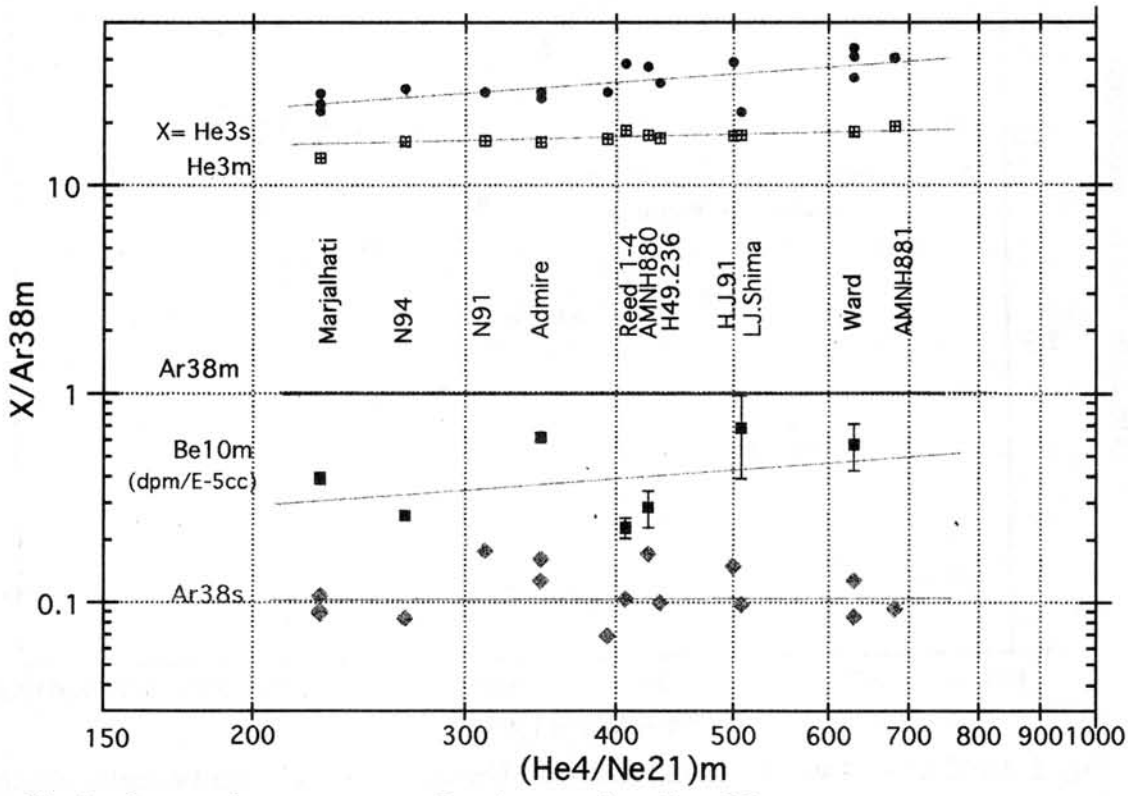

Fig.2. Comparisons among Products of ΔA' = 22.

THE FORMATION OF SILICA-RICH PHASE IN A CHONDRULE OF YAMATO-793495 CR CHONDRITE

Osamu ICHIKAWA[1] and Hideyasu KOJIMA[2]

[1]Department of Polar Science, The Graduate University for Advanced Studies, National Institute of Polar Research, 1-9-10 Kaga, Itabashi-ku, Tokyo 173

[2]National Institute of Polar Research, 1-9-10 Kaga, Itabashi-ku, Tokyo 173

Introduction It is known that olivine and pyroxene in a rim are generally smaller in size than those in a core in chondrules of the CR chondrites (Bischoff *et al.*, 1993; Weisberg *et al.*, 1993; Noguchi 1995; Ichikawa and Ikeda, 1995). PCA 91082 chondrite which was classified as a member of CR clan (Weisberg *et al.*, 1995) includes silica-bearing chondrules (Noguchi 1995). We found a chondrule in Yamato-793495 (Y-793495) having above two characters. Here we report the results of our petrographic studies on silica-rich phase bearing in a chondrule in Y-793495 using an electron microprobe analyzer (EPMA)

Petrography Y-793495, 93-2 is composed of chondrules, mineral fragments, and matrix. One large chondrule whose diameter is about 5.0 mm occupies most of the section. This chondrule is divided into three zones (I, II, and III). Zone-I is the chondrule core which consists of olivines, pyroxenes, and large Fe-Ni metals of which size up to several hundred μm with rare groundmass glass. Zone-II is the chondrule margin which consists of olivines, pyroxenes, Fe-Ni metals, troilite, groundmass glass, and silica phase. Silica phase occurs in the outermost parts of the second zone. Zone-III is the chondrule rim which consists of pyroxenes, Fe-Ni metals, troilite, and groundmass glass. Noguchi (1995) indicated that olivine phenocrysts concentrated in the chondrule cores and low-Ca pyroxene phenocrysts occupy the chondrule margins in PCA 91082. While zone-I and II in Y-793495, olivine phenocrysts concentrate in inner portion of each zone and low-Ca pyroxene phenocrysts occupy in the outer portion of each zone. Phyllosilicates occurs in both the matrix and chondrules. However, phyllosilicate in the chondrules is very rare. Matrix of this meteorite is composed of

olivine, pyroxene, opaque minerals, and fine-grained phyllosilicates less than several micrometers.

Mineralogy Olivines in zone-I and II are magnesian (Fa_{2-5}) and contain 0.6-0.8 wt. % Cr_2O_3 and 0.1-0.3 wt.% MnO. There is no obvious correlation between FeO and Cr_2O_3, and between FeO and MnO. The chemical compositions of olivine in zone-I is similar to those of zone-II. Although low-Ca pyroxene occurs in all zone, high-Ca pyroxene does not occur in zone-I. Cr_2O_3 content in low-Ca pyroxene in outer portion of zone-II is slightly higher than those in zone-I and inner portion of zone-II. On the other hand, Cr_2O_3 content in low-Ca pyroxene in zone-III is scattered ranges of both zone-I and II. Phyllosilicates in zone-I and II are richer in FeO and Al_2O_3 than phyllosilicates in zone-III. This is consistent with Weisberg *et al.* (1993). The grain size of the silica phase is up to 50 μm in a long diameter. They are mainly composed of SiO_2 (97.7-99.8 wt%) with minor amounts of Al_2O_3 (0.1-0.7 wt%), FeO (0.3-0.7 wt%), CaO (<0.05-0.2 wt%), and Na_2O (<0.05-0.14 wt%). The average chemical compositions of CaO in groundmass glass in zone-I, II, and III are 17.3 (wt%), 10.4 (wt%), and 9.0 (wt%), respectively, and the average chemical compositions of Na_2O in zone-I, II, and III are 0.41 (wt%), 2.2 (wt%), and 3.3 (wt%), respectively.

Discussion Silica pods are observed in the circumferences of the outermost parts of the zone-II and part of zone-III. Silica is associated with low-Ca pyroxene, high-Ca pyroxene, and groundmass glass. This texture and their mineral assemblages are similar to PCA 91082, although the outline of chondrule in PCA 91082 is sinuous (Noguchi 1995).

Noguchi (1995) argues possibility of four mechanisms to form of silica-bearing chondrules as follows, (1) crystallization from SiO_2-rich chondrule melt, (2) fractional crystallization of chondrules, (3) reduction of the outermost parts of chondrules, and (4) accretion of silica-rich materials on chondrules.

A unique feature of the chondrule is alternation of olivine and pyroxene concentrations through zone-I and II. It indicates that the chondrule have not simply crystallized from a core to rim in turn. Furthermore, chemical compositions of groundmass glass in zone-I and II are different each other. Therefore, it is difficult to form this chondrule only by the fractional crystallization or crystallization from SiO_2-rich chondrule melt.

The chemical composition of groundmass glass is different in zone-II and III. It is difficult to increase Na, and decrease Ca in groundmass glass in zone-II and III only by reduction. Therefore, the formation of silica phase by reduction is difficult.

In CR chondrites, large metal grains in chondrules occur in both interior and rim. Large metal grains (several hundred μm) occurs only in zone-I in this chondrule. Zone-I shows typical texture of CR chondrites which described by Weisberg *et al.* (1995). If zone-I is original chondrule portion, zone-II and III is produced by accretion of material. Difference of chemical composition of pyroxene and appearance of troilite in only zone-II and III may be indicate that silica phase in this chondrule was formed by accretion of silica-rich melt (material) on original chondrule (zone-I). This is consistent with Noguchi (1995).

References

Bischoff A., Palme H., Ash R.D., Clayton R.N., Schultz L., Herpers U., Stöffler D., Grady M.M., Pillinger C.T., Spettel B., Weber H., Grund T., Endreß M., and Weber D. (1993) Geochim. Cosmochim. Acta, 57, 1587-1603. Weisberg M.K., Prinz M., Clayton R.N., and Mayeda T.K. (1993) Geochim. Cosmochim. Acta, 57, 1567-1586. Noguchi T. (1995) Proc. NIPR Symp. Antarct. Meteorites 8, 33-62. Ichikawa O. and Ikeda Y. (1995) Proc. NIPR Symp. Antarct. Meteorites 8, 63-78. Weisberg M.K., Prinz M., Clayton R.N., Mayeda T.K., Grady M.M., and Pillinger C.T. (1995) Proc. NIPR Symp. Antarct. Meteorites 8, 11-32.

PETROLOGY AND CHEMISTRY OF SILICATE INCLUSIONS IN THE MILES IIE IRON

Yukio IKEDA[1], Mitsuru EBIHARA[2], and Martin PRINZ[3]

[1]Dept. of Earth Sciences, Ibaraki Univ.
[2]Dept. of Chemistry, Tokyo Metropolitan Univ.
[3]Dept. of Earth and Planetary Sciences, Amer. Mus. Nat. Hist.

The Miles IIE iron consists of a Fe-Ni metal host and many silicate inclusions, 5-10mm in size [1]. Forty nine silicate inclusions were petrologically studied, and among them nine inclusions and the metal host were analysed by instrumental neutron activation method.

PETROLOGY: Most of the Miles silicate inclusions show gabbroic textures, but a minor number of inclusions are cryptocrystalline. The gabbroic inclusions consist mainly of orthopyroxene, high-Ca pyroxene, and plagioclase with minor amounts of olivine, inverted pigeonite, anti-perthite, K-feldspar, tridymite, glass of granitic composition, chromite, rutile, armalcolite, ilmenite, whitlockite, chlorapatite, schreibersite, troilite, and Fe-Ni metal. Olivines and orthopyroxenes with mg ratios (MgO/MgO+FeO mole ratios) of 0.90-0.84 are surrounded by large orthopyroxenes with mg ratios of 0.83-0.76, and seem to be relic minerals. The gabbroic inclusions may have crystallized from silicate melts which were produced by partial melting of H-chondritic precursors [1].

Miles cryptocrystalline inclusions consist mainly of cryptocrystalline albite with variable amounts of orthopyroxene, high-Ca pyroxene, K-feldspar, anorthoclase, chromite, rutile, whitlockite, chlorapatite, P-bearing olivine, sodalite, schreibersite, troilite, and Fe-Ni metal. Sometimes they include large pyroxene phenocrysts similar to those in gabbroic inclusions. The MnO/FeO ratios of olivine, pyroxene, and chromite which crystallized directly in the cryptocrystalline inclusions are higher than those in the gabbroic inclusions, and the cryptocrystalline inclusions may have experienced reduction during their crystallization.

CHEMISTRY: The contents of the major and minor elements of the nine silicate inclusions and the host metal are shown in Table 1. The chemical composition of the host metal is very similar to that obtained by Wasson [2] and is in the compositional range of the host metal of the IIE irons. The Ir and Os contents of Miles are slightly lower than those of other IIE irons.

The nine silicate inclusions show a wide compositional range of lithophiles and siderophiles, by a factor of ten or more. The contents of the siderophiles of the silicate inclusions show compositional patterns similar to those of the host metal, and reflect the amounts of Fe-Ni metal trapped in the silicate inclusions.

Among the nine silicate inclusions studied, six are gabbroic and three are cryptocrystalline. The gabbroic inclusions show a narrower compositional range than it of the cryptocrystalline inclusions. The contents of Sc, Ca, Ti, REE's, V, Cr, and K are relatively less variable within a factor of 4, but the contents of Al, Mg, and Na are more variable, with a factor of 10. The latter reflect the differences in modal abundances of the main constituent minerals, pyroxene and plagioclase, in the gabbroic inclusions. The average contents of the REE's of the gabbroic inclusions are higher, by a factor of 4-5, than that of the H-chondrites [3]. This is consistent with our previous conclusion [1] that the gabbroic inclusions crystallized from silicate melts produced from H-chondritic precursors by 25% partial melting of the H-chondrite silicate portion. Cryptocrystalline inclusions are depleted in Sc, Ca, V, Cr, Mg, and Mn, in variable amounts, and enriched in Na and K, suggesting that they are either residual melts of late stage crystallization, or are partial melts with low degrees of melting of H-chondritic precursors. The average REE content of the cryptocrystalline inclusions is slightly higher, by a factor of 1.5-3.5, than that of the H-chondrites, but lower than that of the gabbroic inclusions. The low REE contents of the cryptocrystalline inclusions may be explained by a hypothesis that phosphate-predominant melts separated from silicate-predominant melts during in the crystallization of the cryptocrystalline inclsuions [1] and most of the REE's went into the phosphate-predominant melts, resulting in depletion of the REE's in the silicate-predominant cryptocrystalline inclusions.

REFERENCES: [1] Y.Ikeda and M.Prinz (1996), Proceedings of NIPR Symp. Antarc. Meteor., No.9, pp.144-174. [2] F.Wlotzka (1994), The Meteoritical Bulletin, No.77, Meteoritics, Vol.29, No.6, p.893. [3] G.W.Kallemeyn, A.E.Rubin, D.Wang, and J.T.Wasson (1989), Geochim. Cosmochim. Acta, Vol.53, pp.2747-2767.

Table 1. INAA results for nine silicate inclusions and the metal host in the Miles IIE iron (content in ppm, unless otherwise indicated).

Silicate inclusions	Al(%)	Sc	Ca(%)	Ti	La	Sm	Yb	Lu	V	Cr	Mg(%)	Mn	Na(%)	K	Fe(%)	Co	Ni(%)	As	Au(ppb)	Ir(ppb)
1B	1.68	19.5	3.39	2020	0.759	1.04	1.18	0.150	69.9	4140	5.08	2350	2.07	3050	11.4	378	0.796	0.545	49.3	53.2
1C	5.55	24.1	4.57		0.589	0.732	0.727	0.103	108	4070	4.20	1310	3.90		7.42	302	0.644		24.9	31.3
1D	7.90	10.0	2.50	3230		0.751	0.660	0.096	51.6	2060	0.97	620	5.37	33000	3.01	104	0.149		10	
1E	8.45	4.43	0.425	2350		0.084		0.058		427	0.84	378	6.34	6830	3.30	141	0.813		8.4	
1F	0.91	23.3	1.67	2130	1.06	1.07	1.61	0.257	131	5320	11.3	3830	0.529	2420	14.7	427	1.15	0.55	30	
1G	4.37	25.0	3.05	2730		0.200	0.289	0.064	113	5550	6.51	2070	3.23	5640	9.00	263	0.895		21.8	35.4
1H	6.02	6.13		3360	3.08	0.676	0.478	0.071	15.2	1770	0.45	283	5.10	12600	25.9	1310	2.50	2.34	251	298
1I	1.57	14.3	2.45	4320	1.39	0.497	0.423		413		10.0	4030	0.923		13.9	343	0.698	1.56	69.7	85.6
1J	6.67	8.47	2.69			0.326	0.31	0.036	51.1	1660	1.59	505	4.77		5.02	220	0.457		17.9	18.7

Metal host	Fe(%)	Co	Ni(%)	W	Mo	Re	Os	Ir	Pt	Rh	Pd	Au	Cu	As	Sb	Ga	Ge
	91.2	4580	7.55	0.818	5.95	0.102	1.24	0.894	7.06	1.47	2.99	0.976	172	10.4	0.384	29.8	70.8

YAMATO-791093, AN ANOMALOUS IIE IRON ?

Y.IKEDA[1], T.YAMAMOTO[1], H.KOJIMA[2], N.IMAE[2], P.KONG[3], and H.EBIHARA[3]

[1]Dept. of Earth Sciences, Ibaraki Univ.
[2]Dept. of Meteorites, Nat. Inst. Polar Res.
[3]Dept. of Chemistry, Tokyo Metropolitan Univ.

The Y-791093 meteorite is an unusual meteorite, weighing 4.12 g, and is an intermediate type between IIE irons and H-chondrites. It is similar in chemistry, mineralogy, and texture to the Netschaevo meteorite (anomalous IIE iron) [1,2], consisting of metal-predominant and silicate-predominant portions in roughly equal amounts.

The metal-predominant portions include many silicates, and looks like a IIE iron. The metals are mainly kamacite with Ni 5.3-6.3 wt%, and taenite is minor. Sulfides often occur as large subrounded grains, up to a few mm in length, and are surrounded by Fe-Ni metals. The amount of the sulfides may be about 1/5 of the metal, and is unusually large in comparison to normal IIE irons. The main sulfide is troilite or pyrrhotite, and minor sulfides are pentlandite, alabandite (MnS), and probably digenite (Cu_9S_5).

The metal-predominant portions include many silicates, 0.3-2.0 mm across, and they are chondrules and silicate mineral fragments with metals and sulfides. Chondrules are barred olivine or porphyritic olivine-pyroxene ones, consisting of olivine (Fo_{80-83}), orthopyroxene ($En_{80-84}Wo_{1-2}$), high-Ca pyroxene ($En_{45-50}Wo_{43-47}$), plagioclase ($An_{11-14}Or_{4-8}$), chromite, whitlockite, Fe-Ni metal, and sulfide. The chemical compositions of silicates and chromites are within the range of H6 chondrites. The two pyroxene geothermometer [3] gives equilibrium temperatures of 850-1020°C for orthopyroxene and high-Ca pyroxene pairs, and plagioclase grains are 10-100 micrometers in length, suggesting that the silicate inclusions in the metal-predominant portions are fragments of H6-chondrites.

The chemical compositions of metals and sulfides in the metal-predominant portions were obtained by instrumental neutron activation method, and the results are shown in Table 1. The metals are similar in chemical composition to IIE iron metals (Table 1), but the Os, Ir, and Ga contents of Y-791093 are lower in comparison to normal IIE iron metals. The sulfides are enriched in Mo, Ir, Cu, Sb, and Se in comparison to the coexisting metals.

The silicate-predominant portions are similar to H-chondrites. The chemical composition was obtained by INAA and is shown in Table 1. It is very similar in chemical composition to H-chondrites as shown in Fig. 1.

Although Y-791093 is similar in texture and composition to Netschaevo, the silicate portions are more abundant for Y-791093 than for Netschaevo (about 25 vol.%, [4]), and the Fo contents of olivines

in Y-791093 are lower than those in Netschaevo (Fo_{86}, [1]). Probably Y-791093 was originally an H6 breccia, and a metal-sulfide melt penetrated into the breccia to form Y-791093.

References: [1] E.Olsen and E.Jarosewich (1971), Science 174, pp.583-585. [2] R.W.Bild and J.T.Wasson (1977), Science 197, pp.58-62. [3] D.H.Lindsley and D.J.Andersen (1983), J. Geophys. Res., Vol.88 Supply., Proc. 13th Lunar Planet. Sci., Conf., Part 2, A887-A906, [4] V.F.Buckwald (1975), in "Handbook of Iron Meteorites".

Table 1. INAA results for silicates (coarse-grained, fine-grained), metal (big, small), and sulfide (magnetic, non-magnetic) in Y-791093 (content in ppm, unless otherwise indicated)

Silicates	Al(%)	Ca(%)	La	Yb	V	Mg(%)	Na	Fe(%)	Ni(%)	As	Ir(ppb)
	Sc	Ti	Sm	Lu(ppb)	Cr	Mn	Br	Co	Sb(ppb)	Au(ppb)	Os(ppb)
coarse	0.91	7.16	1.10	948	0.39	0.215	0.34	45	54.7	2760	12.2	2200	5450	1.82	24.8	786	1.36	86	2.86	193	519	589
fine	0.85	6.30	0.868		0.24	0.150	0.37	47	54.8	3180	10.9	1990	5380	1.91	27.9	979	1.65	114	4.05	286	547	496

Metal & Sulfide	Fe(%)	Co	Ni	Cr	W	Mo	Re	Os	Ir	Ru	Pt	Pd	Au	Cu	As	Sb	Ga	Se
Big metal	92.0	4950	6.97	269	0.946	5.09	0.140	0.719	0.615	4.09	3.02	2.97	1.05	134	13.1	0.362	11.8	
Small metal	92.0	4840	6.59		0.904	4.28	0.126	0.819	0.577		2.94	2.97	1.03	105	13.0	0.382	11.8	
Mag.sulfide	66.2	482	0.498	89.2					2.04				0.142	1840	0.932	0.676		252
non-mag.sulfide	61.4	98.1	0.124	78.6		12.1							0.067	3470	0.163	0.297		188

Fig. 1. Lithophile element contents of Y-791093.

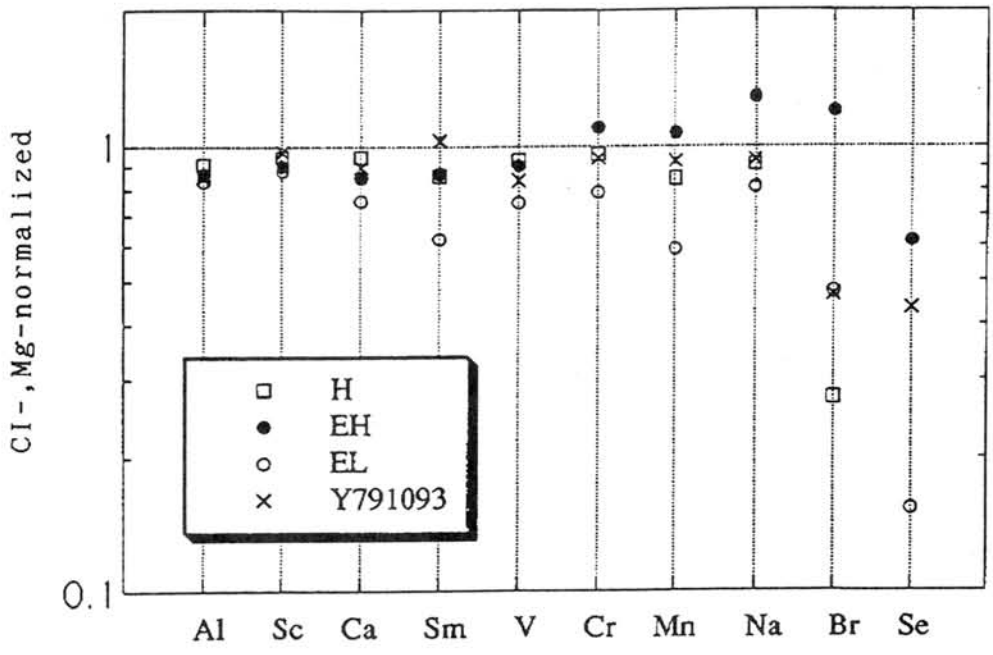

ALBA PATERA : A POSSIBLE BURIED CORONAL STRUCTURE ON MARS

E. Illés-Almár (Konkoly Observatory H-1525 Budapest P.O.B. 67, Hungary)

Alba Patera is an unique volcanic structure on Mars. Its singularity was already realised on Mariner 9 photos since it cannot be fitted into any of the three types of volcanism on Mars. Later surface features called "coronae" have been discovered on Venus by Venera space probes and have been morphologically investigated by the Magellan imagery. Based on morphological similarity we suggest that Alba Patera is also a coronal structure buried by volcanic flow material of several km thickness. The annulus belonging to Alba Patera may be the trench of the old corona projected on the new surface.

Sulfidation textures of Y-82094 (CO3) and its petrogenesis

N. Imae and H. Kojima
National Institute of Polar Research, Tokyo 173, Japan.

In unequilibrated chondrites, CO3 and LL3, a lot of textures that iron-sulfide (troilite) surrounds metal grain have been found. Imae (1994) has found the characteristic sulfidation texture of some metallic grains which has a fracture dividing sulfide layer into inner and outer in unequilibrated chondrites Y-791717 (CO3) and ALH-764 (LL3), and concluded that this texture can be formed by sulfidation of metal based on reproduction experiments. Lauretta et al. (1995) suggested that these assemblages were altered by post-heating events since no concentration gradients characteristic in solid-gas reaction layer could be observed in a sulfide layer in ALH-764.

In the present study, we found a lot of the sulfide textures with a metal core (about one hundred of grains) in Y-82094 (CO3), 91-1, PTS of 1.3 cm^2. We examined these textures using an optical microscope (OM) and a X-ray microanalyser (JXA-8800). Radius of metal in the core is the range of 20-100 μm accompanying stoichiometric troilite within an experimental error with the thickness of 10-50 μm. Generally, the grain is larger, the thickness of troilite is larger. These show the following characteristic sulfidation textures, which have not been observed in Y-791717 and ALH-764. Prominent features are summarized: (1) Small inclusions (1-2 μm) of iron-rich olivine (average Fa_{40}) and FeNi metals (average $Fe_{65}Ni_{35}$) are abundant in formed sulfide layer. (2) Phosphate inclusions (a few μm) are abundant in rim of core metal. (3) The interface between the core FeNi metal and the sulfide layer is irregular (Fig. 1). (4) For many grains, perfect coating of sulfide surrounding metal is not observed (Fig. 1). (5) Some metals with a sulfide layer are connected with another grain through sulfide vein. (6) Some grains have composite layers dividing sulfide layers. These features of (1) to (6) have not be seen in Y-791717 and ALH-764 chondrites.

Above mentioned characters of (4) and (5) can not be explained by sulfidation of metal in pre-accretionary events, but strongly suggest that sulfidation occurred after accumulation of grains including chondrules, perhaps, on a parent body.

As a petrogenesis of sulfidation after accretion of grains, thermal metamorphism and shock metamorphism can be raised. Since slight undulatory extinction can be observed in Y-82094 under an OM, the sulfidation of metal might be driven by a shock.

Now we can make a simple formation model of troilite in chondritic rocks such as CO3 and LL3. Wood (1967) experimentally showed a possibility of sulfidation of metal in a chondrite parent body. In the experiments, metal grains and FeS powder are included. The experiments show that metal grains reacted with sulfur in FeS powder to form sulfide surrounding metal grains. Sulfur vapor may be therefore supplied by incongruent evaporation of FeS powder. We assume that sulfidation of metal grains occurred under an equilibrium in a nearly closed system. The reaction proceeds by the following reactions,

$$FeS(s)+H_2(g)=Fe(s)+H_2S(g) \quad \text{(incongruent evaporation of FeS matrix)}$$
$$H_2S(g)=1/2S_2(g)+H_2(g) \quad \text{(equilibrium between gases)}$$
$$Fe(s)+1/2S_2(g)=FeS(s) \quad \text{(sulfidation of metal grain).} \qquad (1)$$

The net reaction can be thus summarized to be

$$Fe(s)+1/2S_2(g)=FeS(s), \qquad (2)$$

as an equilibrium reaction. Then $p(S_2)$ (atm) is determined by

$$\log p(S_2)=6.21-16300/T, \quad (3)$$

where $p(S_2)$ is the partial pressure of S_2 and T the absolute temperature. It is assumed that the rate determining step is diffusion in a formed sulfide layer of Fe^{2+} and S^{2-}. We can estimate the rate of the reaction using experiments by Fryt et al. (1979) carried out in the field of metallurgy. We consider that these data obtained by the thermogravimetric method are useful that we are now available, and also applicable to chondrite formation. This has been done using pure iron metal, being different from FeNi alloy in the case of metal in chondrites. We assume that the rate is not negligibly affected in the present case since Ni is not included into sulfide negligibly.

Hydrogen is expected to be significantly depleted compared with the solar nebula. Under the hydrogen-depleted condition and hydrogen-enriched condition, the relationship between δ and $p(S_2)$ is approximately distinguished by

$$\left(\frac{\log \delta}{\log p(S_2)}\right)_T \cong \frac{1}{8}, \quad (4)$$

and

$$\left(\frac{\log \delta}{\log p(S_2)}\right)_T \cong \frac{1}{2}, \quad (5)$$

respectively, dependent upon $p(S_2)$, where δ shows the nonstoichiometry of pyrrhotite ($Fe_{1-\delta}S$). We consider that δ could not be detected since it is expected that δ is negligibly small from data of Fryt et al. (1979). Even if δ should be large such as formation at large $p(S_2)$, equilibrium between residual FeNi metal and pyrrhotite would have occurred on a parent body. We note from eq.(3) that hydrogen-enriched case (eq. (5)) is adequate also in this case since we have already assumed that $p(S_2)$ is buffered by eq. (2). Then we use eq. (5) also in the case as similar with the case in the solar nebula.

The rate of sulfidation k (cm^2/s) is given by

$$k=p(S_2)^{1/2}0.06e^{-3830/T}. \quad (6)$$

Using eq. (3), the rate is only a function of T or $p(S_2)$. The reaction degree of sulfide formation ($x=(kt)^{1/2}$) under constant temperatures is determined (Fig. 2) as a simplest case.

Fig. 2 shows that it is capable to form observed thickness within the age of the solar system.

References:

Fryt E. M. et al. (1979) *J. Electrochem. Soc.*, **126**, 683-688.

Imae N. (1994) *Proc. Japan Acad.*, **70**, Ser. B, 133-137.

Lauretta D. S. et al. (1995) *Ant. Met.*, **20**, 134-137.

Wood J. A. (1967) *Icarus*, **6**, 1-49.

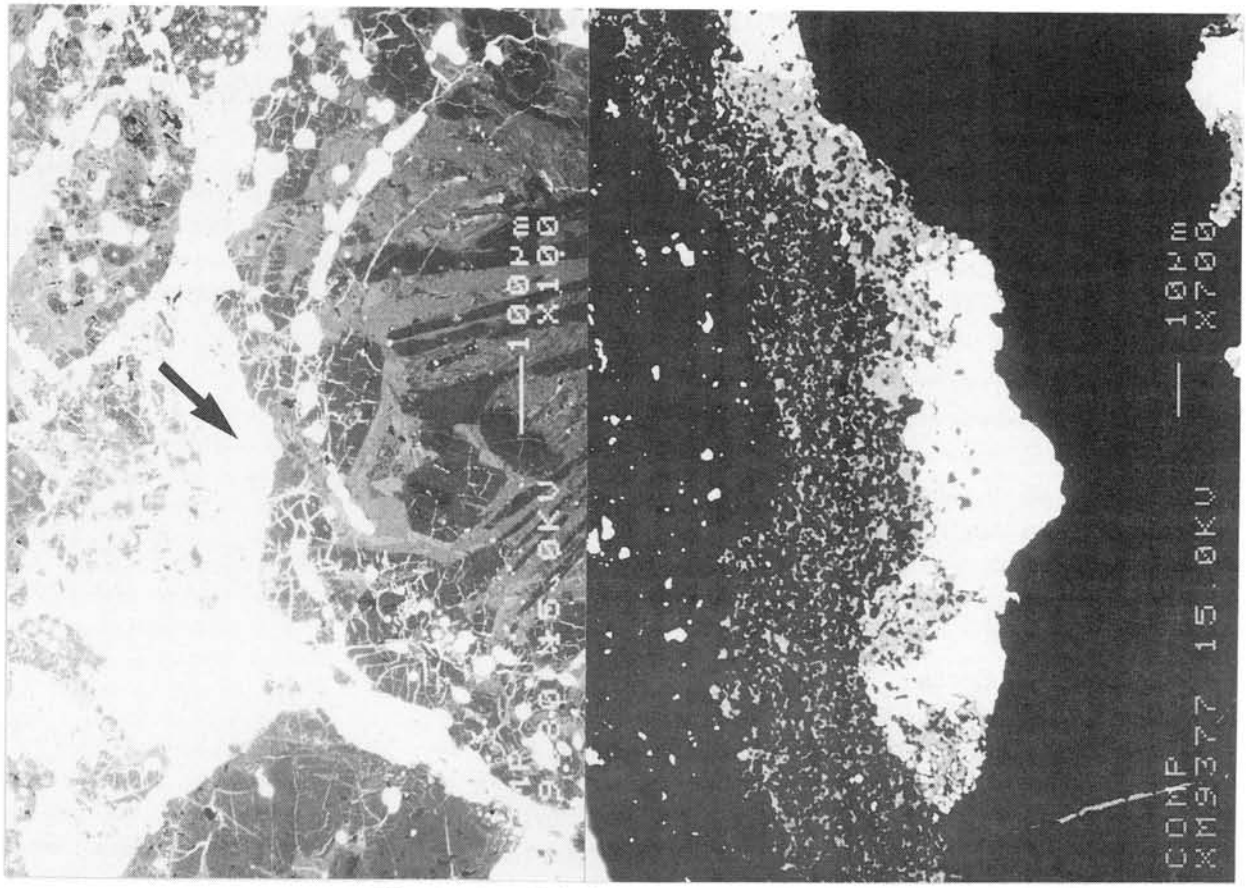

Fig. 1. A sulfidation texture in Y-82094.

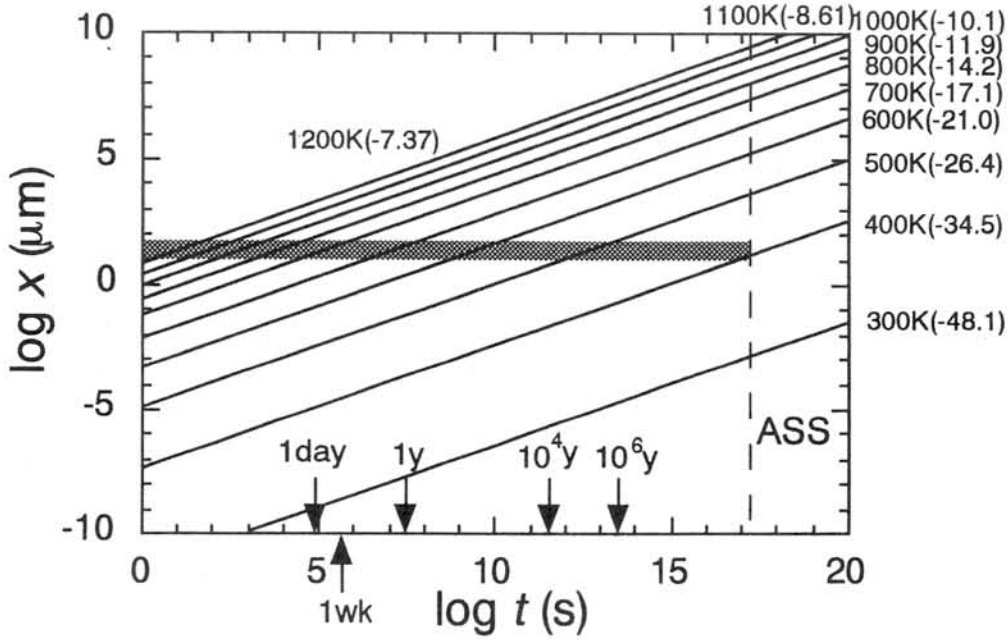

Fig. 2. Thickness of troilite (x) as a function of t and T (and $p(S_2)$ shown by parenthesis) to form by sulfidation after accretion of metal grains. Hatched area shows range of observed troilite thickness. Formation time is restricted by the dashed line (ASS=age of solar system).

Chemical Zoning of Olivines in CO3 and LL3 Chondrites

Hiroshi KAIDEN, Takashi MIKOUCHI, Koji NOMURA, and Masamichi MIYAMOTO
Mineralogical Institute, Graduate School of Science, University of Tokyo, Hongo, Tokyo 113, Japan.

Introduction

It has been shown that CO3 chondrites form a metamorphic sequence like type 3 ordinary chondrites [e.g., 1–3]. Allan Hills (ALH) A77307 and Semarkona are considered to be one of the least metamorphosed chondrites in CO3 and LL3 chondrite groups, respectively, mainly on the basis of their thermoluminescence (TL) properties. In this study, we have analyzed chemical zoning of two CO3 (Yamato- (Y-) 791717 and ALHA77307) and one LL3 (Semarkona) chondrites to explore their thermal history by applying alternative models: fractional crystallization and diffusive modification.

Samples and Analytical Techniques

The polished thin section of Y-791717 was supplied by the National Institute of Polar Research. Electron probe microanalysis was performed on a JEOL JCXA-733 microprobe at the Ocean Research Institute, University of Tokyo. The chemical zoning profiles of olivines from isolated grains and chondrules in Y-791717 were measured by line analyses at intervals of 1–2 μm. The acceleration voltage was 15 kV and beam current was 12 nA. We also employed the profiles of olivines in ALHA77307 [2,4] and Semarkona [5].

Calculation Procedures

Two models were assumed to analyze chemical zoning:

(1) *Fractional crystallization*: Rayleigh fractionation equation was employed for the fractional crystallization model. This equation was applied to the atomic Fe/Mg ratio and CaO wt% in olivines, assuming a closed system [5]. In order to fit the calculated profiles to the observed ones, the least-squares method has been used. The distribution coefficients (mineral/liquid) used in this calculation are 0.35 for Fe/Mg [6] and 0.05 for CaO [5].

(2) *Diffusive modification*: The diffusion equation was numerically solved using finite difference approximation. It was assumed that the compositional gradients of the Fa components and CaO contents of isolated and chondrule olivine grains were controlled by atomic diffusion and that initial profiles were uniform [7]. The diffusion coefficients employed in this study are taken from BUENING and BUSECK [8] for Fe and JUREWICZ and WATSON [9] for Ca. For Y-791717, cooling rates were calculated for four different temperature ranges (1500–1000 °C, 1200–500 °C, 800–300 °C, and 500–100 °C).

Results

Y-791717: Both the Fa component and CaO content in an isolated olivine increase from the core to the rim. In a chondrule olivine, the Fa component increases toward the rim, whereas the CaO content decreases from the core to the rim.

Fractional crystallization; The calculated zoning profile for the CaO content agrees with the observed one in an isolated olivine, whereas we could not obtain good agreement for the FeO/MgO ratio. In a chondrule olivine, we obtained poor agreement for both the FeO/MgO ratio and CaO content.

Diffusive modification; The calculated zoning profiles are in good agreement with the observed ones for both the Fa component and CaO content in isolated and chondrule olivines (Fig. 1). Among the four temperature ranges, the range of 800–300 °C gives the best fit between the calculated and observed zoning profiles. This range also gives a similar cooling rate between isolated and chondrule olivines.

ALHA77307: Chemical zoning profiles for several isolated and chondrule olivines are taken from SCOTT and JONES [2] and JONES [4]. All the olivines show an increase of the FeO content toward the rim, whereas the CaO content decreases in some olivines.

Fractional crystallization; We cannot use this model for the FeO/MgO ratio due to a lack of data on the MgO content in their papers. This model can be applied only to the CaO content that increases toward the rim, because the value of distribution coefficient for CaO is < 1.0. The observed and calculated

zoning profiles show little agreement.

Diffusive modification; The calculated zoning profiles are in good agreement with the observed ones in some olivines (Fig. 2).

Semarkona: Chemical zoning profiles of one chondrule olivine grain are given by JONES [5]. Both the FeO and CaO contents increase toward the rim.

Fractional crystallization; JONES [5] has concluded that Fig. 11 in her paper shows good agreement between the observed and calculated profiles. It appears, however, that there exists a little disagreement between the two.

Diffusive modification; Both the FeO and CaO contents show good agreement between the calculated and observed profiles (Fig. 3). Especially for CaO, the calculated profile fits better than that obtained by the fractional crystallization model.

Discussion

Y-791717 is classified as a CO3 chondrite [10]. SEARS et al. [3] subdivided several CO chondrites, including Y-791717, on the basis of TL, cathodoluminescence (CL), and other petrographic and compositional data. They classified Y-791717 as a subtype 3.3 carbonaceous chondrite, which means that this meteorite has been thermally metamorphosed to a certain extent. This assignment is substantiated by the fact that the observed zoning profiles are in accord with the calculated ones obtained by the diffusive modification model.

ALHA77307 has been considered to be one of the least metamorphosed CO3 chondrites [2]. SCOTT and JONES [2] assigned a petrologic subtype 3.0 to this chondrite in an analogous way that SEARS et al. [11] have used to subdivide the type 3 ordinary chondrites. On the other hand, SEARS et al. [3] recommended that ALHA77307 be classified as a subtype 3.1, which suggests that this chondrite was slightly metamorphosed. Their recommendation is supported by the fact that zoning characteristics of ALHA77307 is demonstrated by the diffusive modification model better than by the fractional crystallization model.

Semarkona is regarded as one of the least equilibrated ordinary chondrites, which is classified as a LL3.0 by SEARS et al. [11] mainly on the basis of its TL sensitivity. JONES [5] also supported this classification and concluded that type II (FeO-rich) chondrules may have been formed by closed-system fractional crystallization. In the present work, however, the diffusive modification model shows better agreement between the calculated and observed zoning profiles than the fractional crystallization model does. Our result suggests that olivines in Semarkona may have been thermally metamorphosed.

Conclusions

By investigating chemical zoning of olivines, we can demonstrate metamorphism of Y-791717 and ALHA77307. We also reached the tentative conclusion that olivines in Semarkona, which are not considered to have been thermally metamorphosed, are affected by diffusive modification. Further study on other unequilibrated chondrites is required to explore the possibility of their thermal metamorphism.

Acknowledgments

We thank the National Institute of Polar Research for the sample and the Ocean Research Institute, University of Tokyo for the use of a microprobe.

References

[1] MCSWEEN H. Y., JR. (1977) *Geochim. Cosmochim. Acta* **41**, 477–491. [2] SCOTT E. R. D. and JONES R. H. (1990) *Geochim. Cosmochim. Acta* **54**, 2485–2502. [3] SEARS D. W. et al. (1980) *Nature* **287**, 791–795. [4] JONES R. H. (1992) *Geochim. Cosmochim. Acta* **56**, 467–482. [5] JONES R. H. (1990) *Geochim. Cosmochim. Acta* **54**, 1785–1802. [6] STOLPER E. (1977) *Geochim. Cosmochim. Acta* **41**, 587–611. [7] MIYAMOTO M. et al. (1986) *J. Geophys. Res.* **91**, 12804–12816. [8] BUENING D. K. and BUSECK P. R. (1973) *J. Geophys. Res.* **78**, 6852–6862. [9] JUREWICZ A. J. G. and WATSON E. B. (1988) *Contrib. Mineral. Petrol.* **99**, 186–201. [10] KOJIMA H. et al. (1984) *Mem. Natl. Inst. Polar Res. Spec. Issue* **35**, 184–199. [11] SEARS D. W. G. et al. (1991) *Proc. NIPR Symp. Antarct. Meteorites* **4**, 319–343.

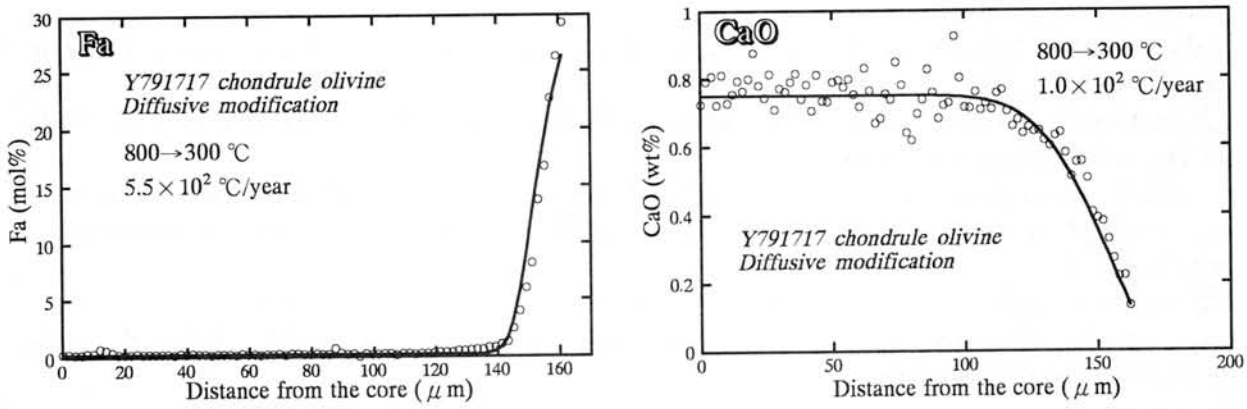

Fig. 1 Observed (circle) and calculated (solid line) chemical zoning profiles of the Fa component (left) and the CaO content (right) in a chondrule olivine from Y-791717. The calculated profiles are obtained by a diffusive modification model, assuming a temperature range from 800 to 300 °C.

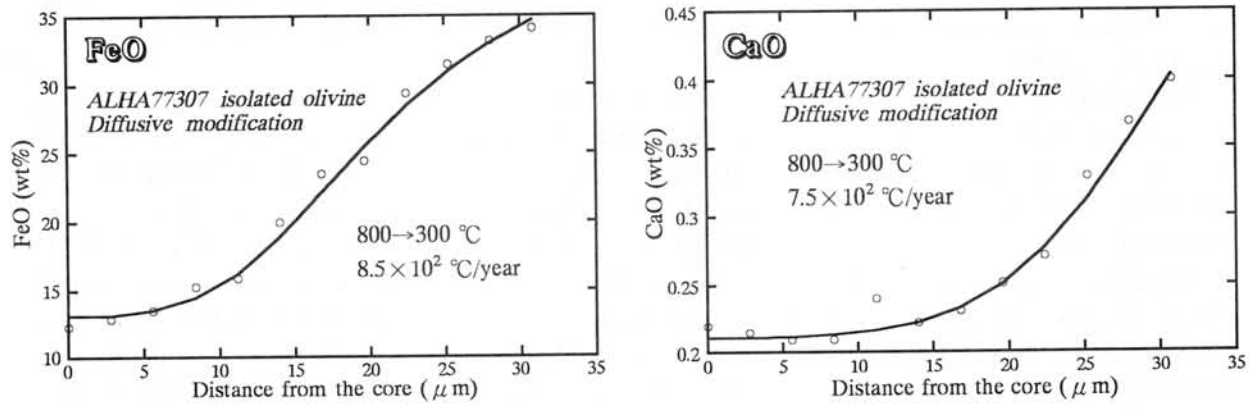

Fig. 2 Observed (circle) and calculated (solid line) chemical zoning profiles of the FeO (left) and CaO (right) contents in an isolated olivine from ALHA77307. The observed profiles are taken from JONES [4] and the calculated ones are obtained by a diffusive modification model, assuming a temperature range from 800 to 300 °C.

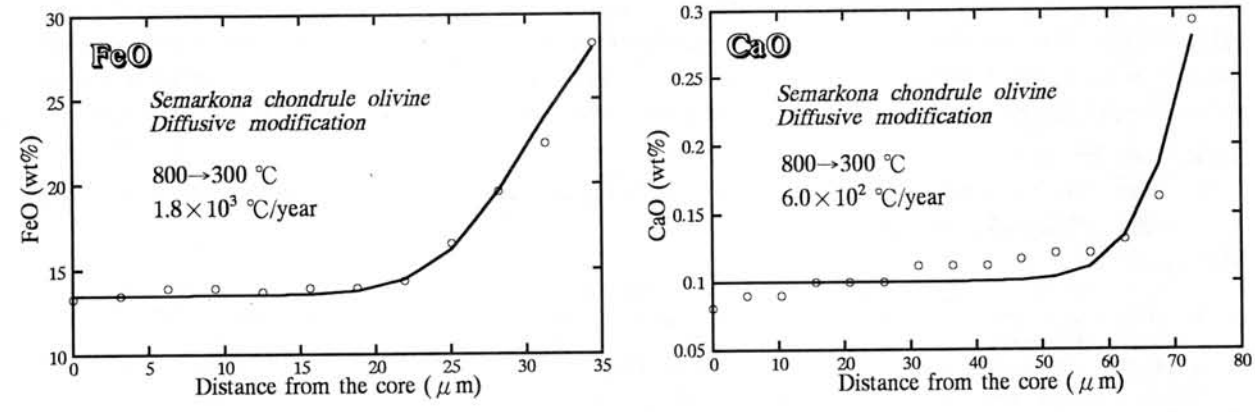

Fig. 3 Observed (circle) and calculated (solid line) chemical zoning profiles of the FeO (left) and CaO (right) contents in a chondrule olivine from Semarkona. The observed profiles are taken from JONES [5] and the calculated ones are obtained by a diffusive modification model, assuming a temperature range from 800 to 300 °C.

Volcanic Processes on Small Solar System Bodies, with Special Reference to the Asteroid 4 Vesta. Klaus Keil[1] and Lionel Wilson[1,2]. [1]Hawai'i Institute of Geophysics and Planetology, SOEST, University of Hawai'i at Manoa, Honolulu, Hawai'i, 96822, USA. [2]Environmental Science Division, Institute of Environmental and Biological Sciences, Lancaster University, Lancaster LA1 4YQ, U.K.

1. Introduction. The properties of many meteorite types, including the magmatic iron meteorites, pallasites, aubrites, HED meteorites, angrites, ureilites, lodranites, and acapulcoites suggest that these rocks have been affected by complex igneous, magmatic and volcanic processes that took place on their parent bodies (presumed to be asteroids) early in the history of the solar system [1]. We studied and modelled the physical processes that may have been important in the volcanic events that shaped the asteroidal-sized parent bodies of some of these meteorites, including pyroclastic volcanism and the formation and evolution of volcanic conduits (cracks growing to dikes) that enabled magma transport from internal zones of partial melting to the surface regions of these bodies [2-6]. Here, we summarize our results and apply these specifically to the asteroid 4 Vesta [3, 4], the presumed parent body of the HED meteorites [7].

2. Explosive (pyroclastic) volcanism and the missing enstatite-plagioclase basalts. [2] suggested that the missing enstatite-plagioclase basalts complementary to the aubrites may have been erupted at the asteroid surface explosively, as mixtures of pyroclastic fragments and released gas, at high enough speeds to exceed the escape velocities of the parent asteroids. Asteroids are likely candidates for explosive activity: the zero atmospheric pressure maximizes gas expansion, disrupting the melt and providing the source of the energy for the high eruption velocity. The smaller the asteroid, the smaller its escape velocity and the smaller the amount of gas needed to ensure that escape velocity is reached. [2] found that for asteroids $< \sim 100$ km in radius, even relatively low contents of volatiles in the partial melts [5] would eject these pyroclast-gas mixtures off the parent bodies early in the history of the solar system and, thus, these melts would have been lost and destroyed in space. Calculations by [3] show that the grain size range of pyroclastic droplets is small (~30 μm to ~4 mm), thus contributing to ready loss in space due to collisions and entrapment into the sun. Our calculations also show that pyroclast sizes are very insensitive to the sizes of asteroids and (except in the more gas-poor asteroids), the majority of droplets would have been lofted from the depth where the magma fragmented all the way to the surface. Since the work of [2], loss of basaltic partial melts by explosive, pyroclastic volcanism has also been suggested to explain the lack in the World's collection of basaltic meteorites complementary to the ureilites [8, 9] and the acapulcoites-lodranites [10].

3. Explosive (pyroclastic) volcanism and the compositions of cores of magmatic iron meteorite parent bodies. Eleven iron meteorite groups (the magmatic iron meteorites) show Ni/siderophile trace element correlations predictable by liquid metal/solid metal distribution coefficients. These meteorites are thought to be the fragments of fractionally crystallized cores of 11 differentiated parent bodies [11]. [6] proposed that the apparent S depletion of the magmas of many of these groups [12] resulted from removal of the first partial (Fe,Ni-FeS cotectic) melts by explosive, pyroclastic volcanism. Calculations show that even these dense, negatively buoyant melts can be driven to parent body surfaces due to excess pressure in the melt as a result of partial melting, and the presence of volatiles [13] that form buoyant gas bubbles which lower the melt density. Fe,Ni-FeS cotectic melts consist of ~85 wt.% FeS and 15 wt.% Fe,Ni and, hence, removal into space by explosive volcanism of even small amounts of this melt results in major loss of S but minor loss of Fe,Ni, leaving sufficient metal to form sizeable asteroid cores.

4. Formation of partial melts and migration to parent body surfaces. Partial melting leads to a volume increase and so melts are over-pressured and, thus, able to open cracks in the surrounding rocks as they move out of the partial-melting zone where only percolation is possible [3-5]. The earliest melts tend to sweep out any free gas which is trapped as bubbles in the melt-filled

cracks. The presence of gas can have a very large effect on the bulk density of melts, such as for the first melts in many differentiated bodies of chondritic precursor compositions, the Fe,Ni-FeS cotectics (see 3. above). Later basaltic partial melts forming in asteroidal mantles were both over-pressured and under-dense (i.e., buoyant); the presence of any gas would have lowered their densities even further. Liquid-filled cracks coalesced and eventually migrated upwards as dikes, reaching the surface to be erupted explosively if enough gas was present (see 2 above), or extruded as lavas if the gas content was low and/or the asteroid was > about 100 km in radius, such as on 4 Vesta (see 5. below). As the crust in such asteroids grew thicker it also became brecciated by impacts and, thus, less dense at and near the surface. When the crustal thickness became comparable with the vertical heights of dikes, many of them failed to reach the surface, being no longer buoyant in the crust, and cooled as intrusions at various depths, the most common being the base of the crust where the sudden decrease in density from mantle to crust acted as a trap. Larger asteroids underwent more compaction of the lower part of the crust by the weight of the overlying crust and so in these bodies dikes were less likely to be caught at the base of the crust [4].

5. Volcanic eruptions and intrusions on the asteroid 4 Vesta. We use the basic physical principles of volcanic fluid mechanics to predict the typical dimensions of dikes, sills and surface lave flows on 4 Vesta [4]. We assume that HED meteorites are from the asteroid 4 Vesta [7], and that 4 Vesta is ~260 km in radius, has a bulk density of 3,500 kg m^{-3} (resulting in a surface gravity of ~0.26 m s^{-2}), a mantle density of up to 3,400 kg m^{-3}, a crust density of 2,800 - 3,100 kg m^{-3}, a eucritic melt density of 2,800 kg m^{-3}, and a rock fracture toughness of 1 - 150 MPa $m^{1/2}$. Results and conclusions: **a**) Dikes carrying magma upwards from zones of partial melting at depth in the mantle had vertical extents of ~1 - 30 km and width of ~10 mm - 4 m. Corresponding driving pressures ranged from ~0.02 - 0.6 MPa. The low gravity causes the volumes of individual dikes migrating upwards from the partially molten mantle to be larger than on the Earth and Moon. **b**) Cooling would have prevented thinner dikes from penetrating to shallower depths unless the country rock apparent fracture toughness was > about 55 MPa $m^{1/2}$. Thus, dikes nearing the surface must have had vertical extents of ~16 - 30 km, widths of ~1 - 4 m, and internal excess pressures of ~1 - 2 MPa. **c**) Dikes reaching the surface will have erupted for ~ 8 - 60 hrs, with effusion rates of ~0.05 - > 3 m^3 s^{-1} per m of horizontal fissure outcrop (similar to basaltic eruptions on Earth). **d**) Erupted lava volumes ranged from negligibly small (with dike-like intrusions with widths < ~0.9 m and volumes up to ~250 x 10^6 m^3 forming very near the surface) to ~3 km^3 (whereby cooling of the shrinking dike at the eruption end will have trapped ~50 x 10^6 m^3 of magma as a shallow dike ~0.9 m wide). **e**) Dimensions of surface lava flows depended on effusion rates and mean surface slopes on which the flows were emplaced. Widths decreased with increasing slope and ranged from a few hundred m to a few km, whereas lengths increased with increasing slope and ranged from a few km to at least several tens of km. **f**) Thicknesses of surface lava flows were relatively insensitive to the controlling parameters and ranged from ~5 - 20 m. Essentially all flow units would have been volume-limited, i.e., would have been emplaced as single flow units extending from the vent (in contrast to cooling-limited flows, in which multiple break-out flow units form from earlier units of the same eruption). **g**) Time intervals between successive flows at the same location were ~1000 yrs, if a 20 km thick crust accumulated on 4 Vesta in ~1 Ma. **h**) Evolution of the density structure of the growing volcanic crust may have caused increased trapping with time of dikes as intrusions at levels where the buoyancy was neutral. These dikes or sills had long axis lengths of ~1 - 30 km, thicknesses of 0.01 - 3 m, and volumes of 10^4 m^3 - 3 km^3. Intervals between successive intrusions in the same region of at least ~100 years would have been much longer than the time required to cool a single intrusion (~1 year for a 3 m thick dike or sill) and so large, shallow magma reservoirs should not commonly have formed. **i**) The infrequent successive flow emplacement at the same location on the surface [see g) above], the relatively low temperature at the interface of successive flows of ~ 600 K, and the small sizes of the zones adjacent to

intrusions that were affected by thermal metamorphism (<~1 m) are too small to explain the prevalence of metamorphosed (equilibrated) vs. unmetamorphosed (unequilibrated) eucrites. This suggests, in agreement with the work of [14, 15], that heat diffusing from the interior during and following progressive brecciation and burial of surface eruptives was the metamorphic agent. **j)** Cooling rates deduced from the sizes of plagioclase crystals in eucrites suggest that they cooled as parts of rock bodies 5 - 10 m thick. These rates are consistent with the eucrites having formed as parts of surface lava flows, since our calculations predict that these have thicknesses of 5 - 20 m. They may also be consistent with some eucrites having formed parts of shallow dikes or sills, although such intrusions should generally have had thicknesses < 3 m. **k)** On small asteroids, explosively erupted pyroclast/gas mixtures would have been expelled at more than the escape velocity and, thus, be lost into space (see 2., 3., above). On larger asteroids such as 4 Vesta, one would intuitively expect massive pyroclastic deposits to be preserved on the surface of the asteroid. However, extensive searches for pyroclastic objects in HED meteorites by A. Yamaguchi (pers. comm.) have been largely unsuccessful. This could be due to 4 Vesta having had a negligible volatile content, and hence no explosive activity, or to early pyroclastic deposits having been buried and metamorphosed to the point of not being recognizable. It may also be the inherent result of the physical processes taking place during pyroclastic eruptions on asteroids. We have therefore investigated the dispersal patterns of pyroclastic droplets, with special emphasis on the accumulation rate at a given distance from the vent (which affects the cooling of material already landed before it is buried by new, hot material); the travel time (which affects the amount of cooling of liquid magma droplets in flight); and the mass flux leaving the vent and the median droplet size (which together determine the distance between droplets in flight, i.e., the optical density of the eruption cloud, and the ability of droplets to radiate freely to their surroundings and, thus, start to cool). We find that the small sizes of the magma droplets in lava fountains on asteroids causes the fountains to be very optically dense, so that virtually all of the pyroclasts coalesce on landing to form a lava pond around the vent which feeds lava flows. Unwelded pyroclasts should be rare in asteroidal volcanic deposits, unless released gas contents are more than several thousand ppm.

References

[1] TAYLOR G.J., KEIL K., McCOY T.J., HAACK H. and SCOTT E.R.D. (1993) Asteroid differentiation: Pyroclastic volcanism to magma oceans. *Meteoritics* 28, 34-52.

[2] WILSON L. and KEIL K. (1991) Consequences of explosive eruptions on small Solar System bodies: The case of the missing basalts on the aubrite parent body. *Earth Planet. Sci. Lett.* 104, 505-512.

[3] WILSON L. and KEIL K. (1996a) Clast sizes of basaltic ejecta from explosive eruptions on asteroids. *Earth Planet. Sci. Lett.* (in press)..

[4] WILSON L. and KEIL K. (1996b) Volcanic eruptions and intrusions on the asteroid 4 Vesta. *J. Geophys. Res.-Plan.* (in press)

[5] MUENOW D.M., KEIL K. and WILSON L. (1992) High-temperature mass spectrometric degassing of enstatite chondrites: Implications for pyroclastic volcanism on the aubrite parent body. *Geochim. Cosmochim. Acta* 56, 4267-4280.

[6] KEIL K. and WILSON L. (1993) Explosive volcanism and the compositions of cores of differentiated asteroids. *Earth Planet. Sci. Lett.* 117, 111-124.

[7] BINZEL R.P. and XU S. (1993) Chips off of asteroid 4 Vesta: evidence for the parent body of basaltic achondrite meteorites. *Science* 260, 186-191.

[8] WARREN P.H. and KALLEMEYN G.W. (1992) Explosive volcanism and the graphite-oxygen fugacity buffer on the parent asteroid(s) of the ureilite meteorites. *Icarus* 100, 110-126.

[9] SCOTT E.R.D., TAYLOR G.J. and KEIL K. (1993) Origin of ureilite meteorites and implications for planetary accretion. *Geophys. Res. Lett.* 20, No. 6, 415-418.

[10] McCOY T.J., KEIL K., MUENOW D.W. and WILSON L. (1996) Partial melting and explosive volcanism on the acapulcoite-lodranite parent body. *Geochim. Cosmochim. Acta* (submitted).

[11] MALVIN D.J., WANG D. and WASSON J.T. (1984) Chemical classification of iron meteorites - X. Multielement studies of 43 irons, resolution of group IIIE from IIIAB, and evaluation of Cu as a taxonomic parameter. *Geochim. Cosmochim. Acta* 48, 785-804.

[12] JONES J.H. and DRAKE M.J. (1983) Experimental investigations of trace element fractionation in iron meteorites II: The influence of sulfur, *Geochim. Cosmochim. Acta* 47, 1199-1209.

[13] MUENOW D.W., KEIL K. and McCOY T.J. (1995) Volatiles in unequilibrated ordinary chondrites: Abundances, sources and implications for explosive volcanism on differentiated asteroids. *Meteoritics* 30, 639-645.

[14] YAMAGUCHI A., TAYLOR G.J. and KEIL K. (1996a) Global crustal metamorphism of Vesta. *J. Geophys. Res.-Planets* (in press).

[15] YAMAGUCHI A., TAYLOR G.J. and KEIL K. (1996b) Metamorphic history of the eucritic crust of 4 Vesta. *Geophys. Res. Lett.* (submitted).

Alteration of chondrules in Allende, Efremovka, Leoville and Vigarano CV3 chondrites

Makoto KIMURA and Yukio IKEDA
Institute of Astrophysics and Planetary Science, Faculty of Science,
Ibaraki University, Mito 310

Almost all chondrules in Allende CV3 chondrite were secondarily subjected to anhydrous alteration reactions including 1) alkali-Ca reactions to form nepheline, sodalite, and Ca-Fe-silicates such as hedenbergite and andradite, 2) secondary zonation of olivine, and 3) replacement of enstatite by ferroan olivine [1,2]. Following our earlier works, we carried out a detailed mineralogical and petrological study of chondrules in the oxidized CV3 chondrite, Allende, and reduced CV3 chondrites, Efremovka, Leoville and Vigarano, in order to explore the alteration processes of chondrules in both of reduced and oxidized CV3 chondrites.

We found a Na-K-bearing micaceous phase in two barred-olivine chondrules among more than 200 chondrules in Allende. Both chondrules preserve their original spherical forms. The micaceous phase mainly occurs with diopside, nepheline, hedenbergite and andradite. These chondrules were also subjected to the anhydrous alteration reactions, although primary groundmass glass still remains unaltered in these chondrules. The Na-K-bearing micaceous phases seem to replace nepheline in the groundmasses, and partly forsterite phenocrysts. They contain 35.7-41.0 wt.% SiO_2, 13.8-16.6% Al_2O_3, 0.9-1.9% FeO, 22.1-29.5% MgO, 0.1-1.9% CaO, 1.6-3.4% Na_2O and 2.2-4.3% K_2O. The chemical composition resembles those of Na-rich phlogopites reported from Ca-Al-rich inclusions in Allende [3] and from chondrules in Mokoia CV3 chondrite [4]. However, the K_2O contents of the phases in Allende chondrules studied here are higher than those reported before, and they have just intermediate compositions between Na-phlogopite and K-phlogopite. At any rate, this is the first discovery of phyllosilicate in Allende chondrules. Some dark inclusions in Allende experienced aqueous alteration reactions, but followed by dehydration [5,6]. The discovery of phlogopite

evidently shows that rare Allende chondrules were also subjected to aqueous reactions. However, our observation of nepheline replaced by phlogopite suggests that the anhydrous alkali-Ca reactions were probably succeeded by the aqueous alteration.

Our study of more than 200 chondrules indicates that all Allende chondrules were subjected to the anhydrous alteration reactions in various degrees, which is consistent with our earlier conclusion [1,2]. Chondrules in Vigarano abundantly show the characteristic features of the anhydrous alteration reactions: nepheline and sodalite replacing primary groundmass, secondary hedenbergite occurring in the altered groundmass, ferroan olivine (Fo_{45-62}) replacing enstatite, and olivine phenocrysts secondarily zoned ranging from Fo_{99-62}. However, the other chondrules have their original textures and mineralogy. Most of chondrules in Efremovka also do not show the alteration textures, but a few chondrules have nepheline and sodalite replacing primary groundmass. On the other hand, all chondrules in Leoville do not show the alteration textures mentioned above. Chondrules in reduced CV3 chondrites were considered to have hardly experienced alteration reactions [7]. However, our observations suggest that the anhydrous alteration reactions took place in reduced CV3 chondrites as well as oxidized CV, although the degrees of the alteration for the reduced type are lower than that for the oxidized type.

We thank Dr. R. Hutchison and Dr. H. Kojima for loaning thin sections of Efremovka, Vigarano and Leoville.

References: [1] Ikeda Y. and Kimura M. (1995) Proc. NIPR Symp. Antarct. Meteorites, 8, 97-122. [2] Kimura M. and Ikeda Y. (1995) Proc. NIPR Symp. Antarct. Meteorites, 8, 123-138. [3] Hashimoto A. and Grossman L. (1987) GCA, 51, 1685-1704. [4] Tomeoka K. and Buseck P.R. (1990) GCA, 54, 1745-1754. [5] Kojima T. and Tomeoka K. (1995) Meteoritics, 30, 529. [6] Kort A.N. et al. (1996) Meteorit. Planet. Sci., submitted. [7] Kort A.N. et al. (1995) Meteoritics, 30, 748-775.

Size Effect of Aluminum Ultrafine Particles on Formation of Alumina Phase

°Seiji Kimura, Nobuyasu Tamura, Noritoshi Tsuda, Yoshio Saito[1], Chiyoe Koike[2] and Chihiro Kaito

Department of Physics, Ritsumeikan University, Kusatsu, Shiga 525, Japan.

[1]Department of Electronics and Information Science, Kyoto Institute of Technology, Sakyoku, Kyoto 606, Japan.

[2]Department of Physics, Kyoto Pharmaceutical University, Yamashina, Kyoto 607 Japan.

Introduction Corundum (Al_2O_3) grains have received considerable attention in the field of planetary science, since the possibility of the presence of corundum grains in space have been suggested from astronomical observations and theoritical calculations [1 $\sim$ 3]. However, spectral studies of alumina particles have not been performed thus far, except for spectral studies of γ-Al_2O_3 particles in our previous paper [4]. Therefore, those optical constants of alumina particles on various phases are not obtained. In a previous paper, it was shown experimentally that α-Al_2O_3 particles of different shape and size are produced under a different growth condition and those infrared spectra change by the difference of both shape and size. Although correlation among the effects on shape, size of particles and their spectra is a problem of very importance in spectroscopy, the definite experimental results on these problem is not found and not sufficient in agreement with theoretical consideration.

On the other hand, particles above 100nm can be easily produced by gas evaporation method. However, particles smaller than 10nm is very difficult to be produced by gas evaporation method because of influences of stationary convection flow and coalescence growth among particles. It is thought that surface effect of particles smaller than 10nm appear remarkably in specrtum. The problem of the size effects on spectrum is important. In this paper, new gas evaporation method to produce particles in very small size was developed. The structure of alumina particles produced by oxidation of both small Al particles and large particles have been studied by infrared spectroscopy and electron microscopy. The size dependence on absorption spectra have been elucidated.

Samples and experimental method An apparatus shown schematically in Fig.1 was used in order to prepare the small particles. After evaporation source was heated at 1200°C in Ar gas pressure of 13kPa, Al powder from a boat was dropped on evaporation source at regular intervals and at a fixed rate. In order to drop the powder into the evaporation source, a partition plate with a small hole was fixed in the boat as shown in Fig.1. By means of this method, small Al particles were produced and the collected particles were oxidized by heating in air at 400 $\sim$ 1100°C for 20 hours. The observation of the specimens was carried out by using Hitachi H-7100R electron microscope. The transmittance of KBr pellets embedded the particles was measured with a Fourier transform infrared spectrometer (FTIR) (Horiba Inc., FT-210).

Results and discussion Figure 2 shows electron microscopic (EM) image and electron diffraction (ED) pattern of small Al particles produced by means of the

apparatus shown in Fig.1. EM image inserted in Fig.2 shows Al particles produced by general gas evaporation method. Both EM images are shown in the same scale. The small Al particles is distributed in size ranging from 10 to 50nm. The size of Al particles was one order of magnitude smaller than that of Al particles produced by the usual gas evaporation method. Although ED pattern correspond to aluminum, diffraction spots due to (222) reflection of η-Al_2O_3 can be seen at the outside of (111) reflection of aluminum. In general, it is considered that alumina produced by the oxidation of metallic aluminum in air is amorphous and act as the protective layer [5]. However, in present particles, it was found that by taking out the particles into air the alumina phase becomes crystal. It is thought that this result is caused by the heat due to exothermic oxidation reaction on small Al particles. Figure 3 shows infrared spectra of (a) the small Al particles taking out the air, (b) small Al particles heated in air at 400°C for 20 hours and (c) small Al particles heated in air at 700°C for 20 hours. IR absorption peak of small Al particles appear at 11.2μm. With increasing of heating temperature, absorption peak shifted to long wavelength. By heating at 700°C, IR spectrum showed a broad peak at about 13μm as seen in that of γ-Al_2O_3 [4]. In this study, it was found that the phase transition temperature to γ-Al_2O_3 is 700°C, which is lower than that of large particles (900°C) [6]. This result indicates that the phase transition temperature become lower when particle size become small. Moreover, it was found from this experiment that IR spectrum of small particles become broad as compared to that of large particles. Size effect of particles on phase transition and correlation between infrared spectrum and particle size will be shown.

Acknowledgement This work is supported by a Research Fellowships of the Japan Society for the Promotion of Science for Young Scientist (Kimura).

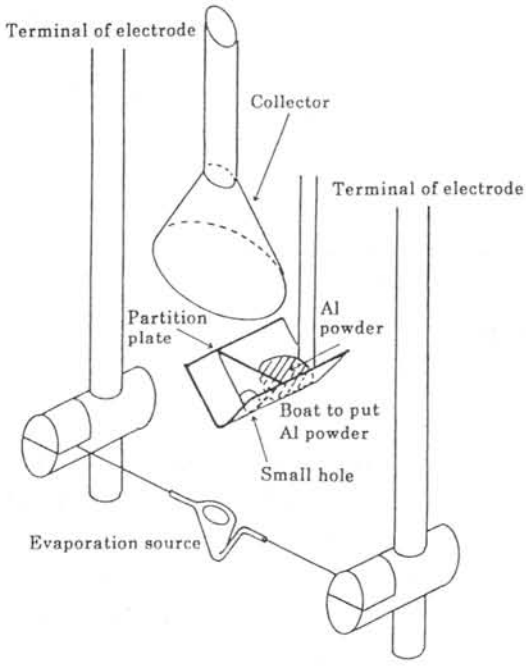

Fig.1 Schrmatic representation of apparatus used to produce small Al particles.

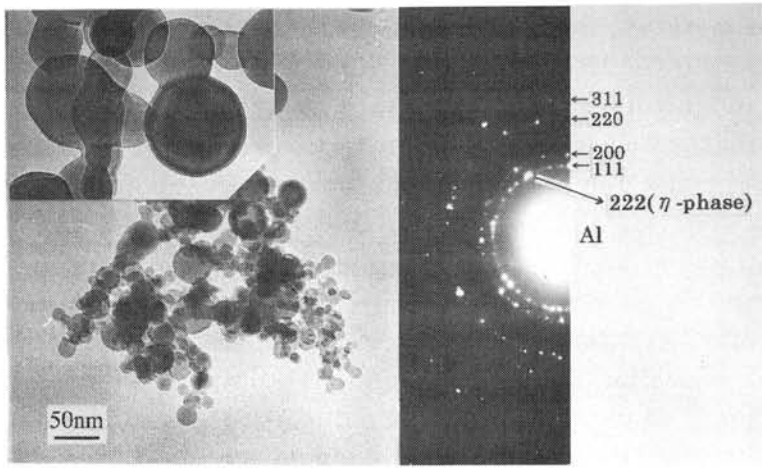

Fig.2 EM image and ED pattern of small Al particles produced by means of apparatus in Fig.1. EM image inserted shows large Al particles. Images are shown in the same scale.

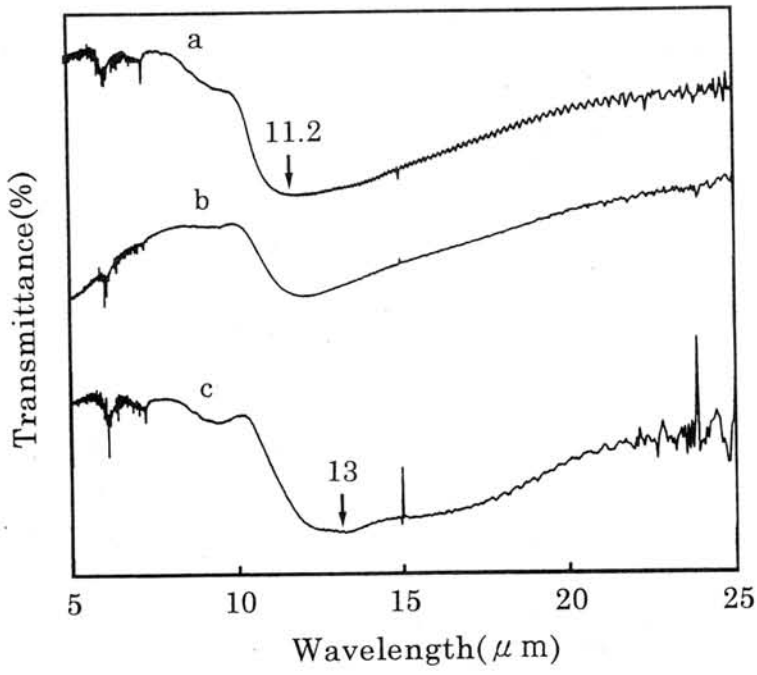

Fig.3 Infrared spectra of (a) small Al particles taking out the air, (b) small Al particles heated in air at 400°C and (c) small Al particles heated in air at 700°C.

References (1) E. Anders, A. Virag, E. Zinner and R.S. Lewis: Astrophys. J., 373, L77-80, 1991. (2) M.S. Vardya, T.De Jong and F.J. Willens: Appl. Phys. J., 304, 29-32, 1986. (3) T. Onaka, T.De Jong and F.J. Willens: Astron. Astrophys., 218, 169-179, 1989. (4) C. Koike, C. Kaito, S. Kimura, T. Yamamoto, H. Shibai and H. Suto: ICARUS, 114, 203-214, 1995. (5) E. Suito, M. Shiojiri and H. Morikawa: Jnp. J. Appl. Phys., 5, 1197-1203, 1966. (6) S. Kimura, K .Kamei, N. Tsuda, Y. Saito, C. Koike and C. Kaito: Proc. NIPR Symp. Antarct. Meteorites, 9, 240-246, 1996.

Veins in CM chondrites

Hideyasu Kojima1 and Keizo Yanai2 1: National Institute of Polar Research, 9-10, Kaga 1-chome, Itabashi-ku, Tokyo 173, 2: Dept. of Civil and Environmental Engineering, Faculty of Engineering, Iwate Univ., 3-5, Ueda 4-chome, Morioka 020, Japan

CM chondrite has suffered various degree of aqueous alteration. We do not have direct evidence weather the alteration occurs in the solar nebula or in the parent body. If the alteration progresses in water-rich interior of the parent body, we expect to find the vein filled with secondary minerals such as sulphates, carbonates and phillosilicates. These kinds of veins have been already reported in CI chondrites (e.g. Richerdson, 1978, Tomeoka, 1990). We found veins in two CM chondrites. One is Asuka-881594(A-881594). The other is Asuka-881280(A-881280).

A-881594 has suffered heavy alteration. All of high temperature components such as olivine and pyroxene have already altered into phyllosilicates. Several veins are observed in a PTS. The veins are up to several tens μm in width. The veins are clearly defined from phyllosilicates which compose matrix and pseudomorph of both chondrules and inclusions. EPMA analyses indicate that the veins consist of gypsum. Where have these gypsum veins been formed? Two candidates of the formation place are considered. One is in the parent body. The other is in the Antarctica. If the veins have been formed in the parent body, it is one of the evidence of the parent body alteration of CM chondrites. Microscopic observations under a microscope and an EPMA show no features to be judged where the veins formed. We try to find keys which indicate which places the vein has formed by another way. We observed the rock again by naked eye and under a stereoscopic microscope to know the relation between the vein and a fusion crust. If the vein cuts the fusion crust, it is the evidence of terrestrial formation of the gypsum vein. On the contrary, the fusion crust cuts the vein, it is the evidence of the extraterrestrial formation of the vein. This rock has many fractures. Thus the fracture index of this rock is C. The fusion crust is also fractured. We observed some fractures cutting the fusion crust are filled up by white material. The white material is not only observed near the surface, but also intrudes into the interior of the rock. These facts may indicate that the white material is the same as the gypsum filled the vein in the PTS and also indicate that the gypsum vein has been formed in the Antarctica.

We found this type of veins in another CM chondrite. However, minerals filled up the vein is not gypsum. EPMA analyses indicate they are dolomite and probably nesquehonite.

References; Richardson (1978) Meteoritics 13, 141-159., Tomeoka (1990) Nature, Vol. 345, 138-140.

AN UNUSUAL DARK INCLUSION IN THE VIGARANO CV3 CHONDRITE: POSSIBLE EVIDENCE FOR SEDIMENTARY PROCESS ON THE METEORITE PARENT BODY

Tomoko KOJIMA and Kazushige TOMEOKA

Department of Earth and Planetary Sciences, Faculty of Science, Kobe University, Nada, Kobe 657

Recent studies of dark inclusions (DIs) in CV3 carbonaceous chondrites have revealed evidence that they experienced aqueous alteration and subsequent thermal metamorphism on the meteorite parent body [1-4]. DIs widely range in texutre; one end-member contains chondrules embedded in a fine-grained matrix resembling the host CV3 meteorites, and the other end-member lacks chondrules but instead contains rounded to oval-shaped inclusions consisting of fine grains of Fe-rich olivine. All DIs that we have studied also show such petrographic variations, and we interpreted that they were once part of a chondrite parent body and that the chondrule-bearing DIs were affected by minor aqueous alteration, while the chondrule-lacking DIs were altered strongly so that chondrules were almost completely replaced by phyllosilicate [1-3]. They were subsequently heated, and phyllosilicate was dehydrated to form Fe-rich olivine. Although we are confident with the interpretation, it still remains uncertain whether all DIs can be explained by the same formation process.

Johnson et al. [5] reported two DIs, one from Allende and the other from Vigarano, which are not obviously related to the range of variations described above [5]. They consist almost exclusively of fine-grained dark matrix-like material and are devoid of chondrules and rounded inclusions. Among them, the DI from Vigarano (AMNH 2226-7) especially has unusual texture, *i. e.* crosscutting arcuate bands similar to fluvial sedimentary deposits [5]. By courtesy of Dr. M. Prinz, we were granted the opportunity to study this unusual DI. We here present the results of detailed mineralogical and petrographic study of DI AMNH 2226-7.

AMNH 2226-7, approximately 0.7 x 1.3 cm in size, is different from any of the DIs we have studied in that it is very dark and featureless under an optical microscope; it contains neither chondrules nor rounded inclusions. It consists predominantly of fine grains (<5 μm in diameter) of Fe-rich olivine (Fo_{49-65}). Most olivine grains are extremely fine (<1 μm), so it is difficult to resolve each grain by SEM. Relatively coarse grains (2-5 μm in diameter) show granular, equidimensional morphology. These characteristics of Fe-rich olivine are different from those in the major type of DIs which commonly contain olivine having acicular to fibrous morphologies. Relatively coarse, angular grains (10-20 μm in diameter) of Mg-rich olivine (Fo_{85-99}), Fe-rich olivine, Mg-rich pyroxene, Ca-rich pyroxene and spinel are dispersed throughout the DI; olivine commonly shows Fe-Mg zoning at their edges. These grains are apparently fragments of chondrules and CAIs.

A striking feature of AMNH 2226-7 is that it contains many arcuate bands (< 3 mm in length) and exhibits ripple-like texture. Several bands commonly occur roughly parallel to each other, forming a set of parallel bands. The width of bands and the spacing between bands are common in each set but differ greatly between sets; the width varies from 10 to 200 μm, and the spacing from 50 μm to 1mm. A more peculiar feature is that different sets of

parallel bands commonly crosscut one another. Each arcuate band is composed mostly of olivine grains which are similar in size and shape to those in other areas (matrix), but are more densely packed and slightly but distinctly richer in Fe (Fo_{49-52}). The boundary between band and matrix is sharp at the outer side of each arc but commonly gradated at the inner side; the gradation is particularly pronounced in the bands having relatively long intervals between parallel-oriented bands. The bands also contain fragments of chondrules and CAIs which show no differences in size and frequency from those in other areas. These textural features resemble those commonly seen in fluvial sedimentary deposits, as suggested by Johnson et al. [5].

It is clear that the texture and the mineralogy of AMNH 2226-7 are distinct from those of the major group of DIs containing chondrules or rounded inclusions. We believe that AMNH 2226-7 represents a clast that has an origin distinct from the major group of DIs. Our observations support the interpretation of Johnson et al. [5] that the bands in this DI reflect particle settling, possibly dust accumulation on a parent body surface. Because this DI contains abundant small fragments (<20 μm) of chondrules and CAIs, fragmentation and comminution probably occurred before accumulation. The predominant occurrence of extremely fine olivine grains appears to require that grain sorting process also predated the final accumulation. The equally spaced parallel bands and the gradation texture in each band may have resulted from cyclic deposition of particles; in each deposition cycle, Fe-rich particles deposited faster than Fe-poor particles, possibly due to gravitational difference, and formed base layers which are now seen as arcuate bands on the thin section. We are still uncertain what kind of actual events are responsible for the sequence of deposition process. But the process probably proceeded in the presence of fluid, possibly dense gas or water, on a surface of the parent body. Although more work is required to give a confident model for the origin of this unusual DI, we suggest this would potentially provide important insights into a previously unknown aspect of parent-body process, *i.e.* dust accumulation process on the meteorite parent body.

Acknowledgments - We thank Dr. M. Prinz for providing the AMNH 2226-7 sample. This work was supported by Grant-in-Aid of Japan Ministry of Education, Science and Culture (No. 06403001).

REFERENCES

[1] Kojima T. Tomeoka K. and Takeda H. (1993) *Meteoritics* 28, 649-658.
[2] Kojima T. and Tomeoka K. (1995) *Meteoritics* 30 (Abstr.), 529.
[3] Kojima T. and Tomeoka K. (1996) *Geochim. Cosmochim. Acta* 60, in press.
[4] Krot A., Scott E. R. D. and Zolensky M. E. (1995) *Meteoritics* 30, 748 -775.
[5] Johnson C.A., Prinz M., Weisberg M. K., Clayton R.N. and Mayeda T. K. (1989) *Geochim. Cosmochim. Acta* 54, 819-830.

Preliminary Reports on Cosmogenic Nuclides in Tsukuba Meteorite Fell on Jan. 7, 1996

K. Komura[1], S. Yamazaki[1], S. Yoneda[2] and M. Shima[2]

1) LLRL, Kanazawa University, Tatsunokuchi, Ishikawa 923-12, Japan.
2) National Science Museum, Shinjuku, Tokyo 169, Japan.

Cosmogenic nuclides in Tsukuba meteorite (H5-6) fell on Jan. 7, 1996, have been measured by non-destructive gamma-spectrometery using a 93% efficiency Ge detector installed in Ogoya Underground laboratory (270 mwe). Detection limit of most of cosmogenic nuclides is 0.001～0.002 cpm by 1 week measurement, which corresponds to 0.4 dpm/kg of ^{26}Al activity if 100g of sample is available. The fragments of the Tsukuba meteorite measured are No. 5 (30.5g), No. 13 (177.2g) and No. 19 (25.5g). Because ^{60}Co activity is considered to be extremely low, special effort was dedicated to detect ^{60}Co. Each sample was counted for more than 10 days (No. 5 : Jan. 20～Feb. 2, No. 13 : Mar. 15～28 and No. 19 : Feb. 28～Mar. 15).

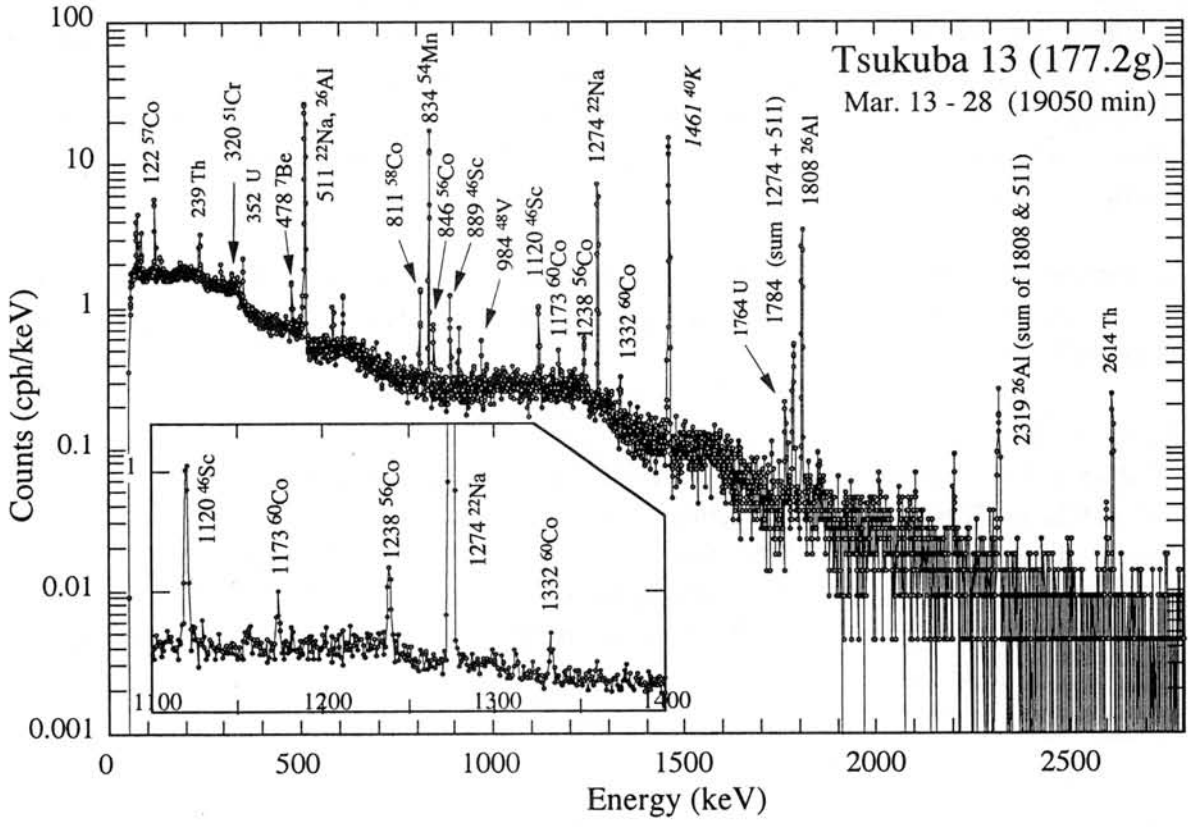

Fig. 1 Gamma-ray spectrum of No.13 fragment.

Example of gamma-ray spectrum obtained for No. 13 is shown in Fig. 1. Radionuclides recognized in the spectrum are ^{48}V(16 d), ^{51}Cr (27.7 d), ^{7}Be (53.3 d), ^{58}Co (70.9 d), ^{56}Co (77.3d), ^{48}Sc (83.8 d), ^{57}Co (272 d), ^{54}Mn (312 d), ^{22}Na (2.6 y), ^{60}Co (5.26 y) and ^{26}Al (7.2 x 10^5 y), ^{40}K and the nuclides belonging to the U and Th series. In the case of No. 5, which was measured 13 days after the fall, gamma-ray peaks due to ^{52}Mn (5.6 d, 744 keV, 935 keV) were clearly observed.

Detection efficiency was calibrated by using mock-ups (density : 3.3 g/cm^3) prepared from cupric oxide (Cu_2O) and potter's clay containing known amount of U, Th, K. Net activity of 1173 and 1332 keV gamma-rays from ^{60}Co was measured to be only 0.0053$\pm$ 0.0021 and 0.0037$\pm$0.0017 cpm, which are nearly the same as the system background (0.0045 and 0.0040 cpm, respectively), which corresponds to 1.4$\pm$0.5 dpm/kg. Correction for summing effect was made for ^{46}Sc, ^{60}Co, ^{22}Na and ^{26}Al by referring the summing effect observed for ^{214}Bi and ^{208}Tl gamma-rays of mock-ups.

Preliminary values of cosmogenic nuclides Tsukuba meteorite normalized to the date of fall are plotted in Fig. 2 and Fig. 3 Errors bars in these figures show only the statistical error of counting (1σ).

Fig. 2 shows the activities of ^{48}V, ^{54}Mn, ^{56}Co · ^{57}Co and ^{58}Co, which show rather lagely variation depending on fragments, and Fig. 3 show the activities of ^{7}Be, ^{22}Na, ^{26}Al, ^{46}Sc and ^{51}Cr, which show nearly same activity independent on the fragment. These differences may be explained either by heterogeneity of matrix and or depth effect of production in meteorite. Uranium, thorium and potassium contents determined by non-destructive gamma-spectrometry are ranging from 8.5 -14.1 ppb, 8.9 - 11.8 ppb and 0.07 - 0.089%, respectively.

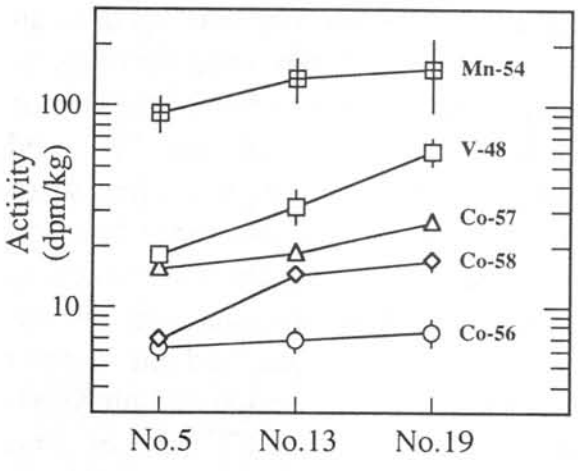

Fig. 2. Activities of ^{48}V, ^{54}Mn, ^{56}Co, ^{57}C,. and ^{58}Co.

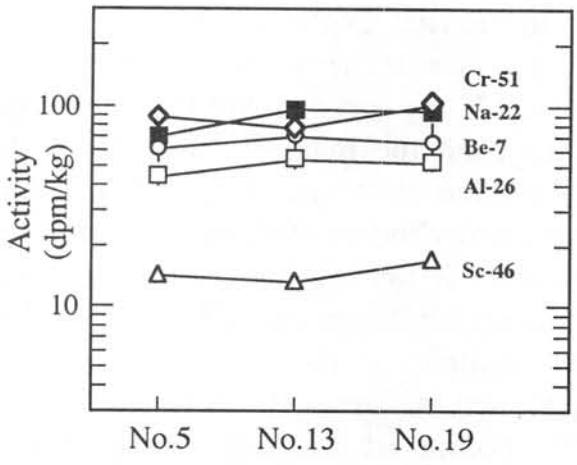

Fig 3 Activities of ^{7}Be, ^{22}Na, ^{26}Al, and ^{46}Sc and ^{51}Cr.

X-ray CT images of chondrites and chondrules

KONDO Masahiro[1], HASHIMOTO Hiroshi[1], TSUCHIYAMA Akira[1],
HIRAI Hidekazu[2], and KOISHIKAWA Atsushi[2]
[1]Department of Earth and Space Science, Osaka University,
Toyonaka 560, JAPAN.
[2]Nittetu Elex Co., Ltd, Sakai 590, JAPAN.

Introduction

Petrological studies on meteorites have been generally made by making thin sections so far. However, this method gives us only two dimensional informations on the textures of meteorites. Moreover, samples are broken when thin sections are made. An X-ray CT method gives textural informations on a sample without breaking the sample, and we can study three dimensional textures from successive images. In the present study, an X-ray CT method was applied to chondrites and chondrules to check the availability of this method.

Experiments

We used combined high resolution X-ray radiography and CT system (Nittetsu Elex Co., Ltd.) to take X-ray CT images. This system has a microfocus source of X-ray (the size of the focus is 3μm), thus we can take high resolution X-ray CT images. The target of an X-ray generator was tungsten. The accelerating voltage was ranging from 90 to 110 kV. Two types of experiments were done with different X-ray sensors.

(1) Line sensor

In the first experiments a line sensor made of 2048 sensors was used as an X-ray detector (Fig.1). The spacial resolution, which is determined by the size of the X-ray focus and/or the optical geometry, such as the number of the sensor array and the magnification of samples (8.0～11.0), is several μm. We used Moorabie meteorite (L3) and Allende meteorite (CV3) as samples. They were cut into cylinders of 8mm and 10mm in diameter, respectively, to remove halation of their X-ray CT images as long as possible. X-ray CT images were taken as slices with 20μm and 10μm thickness, respectively. After the imaging, we cut the samples at the same positions as their X-ray CT images, and made their polished thin sections for observation under an optical microscope and an SEM. We compared their microscope photographs with the X-ray CT images, and examined to what extent we can identify their textures and minerals in the X-ray CT images. A chondrule removed from Allende meteorite by frozen saw method was also used as a sample. X-ray CT images were taken as a slice with 50μm thickness. Polished thin section has not yet been prepared on this sample.

(2) Area sensor

When we used the line sensor, we could take only one X-ray CT image at one time. On the other hand, if we use an area sensor, we can take up to about 100 X-ray CT images at one time. Then, successive X-ray CT images for constructing three dimensional images can be obtained in a short duration. Therefore, in the second experiments an area sensor made of 512×512 sensors was used. We used Moorabie meteorite as a sample. We successively took 27 X-ray CT images of 15μm slice thickness at intervals of every 15μm. The spacial resolution determined from the optical geometry was about 15μm.

Results and Discussions

Fig.2a and b show X-ray CT images of Moorabie and Allende meteorites, respectively, taken by the system with the line sensor. The differences of the absorption of X-ray in each mineral appear as the differences of darkness in the X-ray CT images. When a mineral has larger absorption, the image is brighter. In Fig.2a, white and gray parts are Fe-Ni alloy and troilite, respectively, and dark parts are silicates. Then it is known that we can distinguish Fe-Ni alloy, troilite, and silicates clearly, and chondrules can be seen from Fe-rich rims. However, we cannot distinguish
minerals among silicates probably because (1) the difference in the X-ray absorption is not large, and/or (2) the magnification is not enough to identify small mineral grains (Fig.2a). In Fig.2b, we can distinguish matrix, chondrules, and CAI in Allende meteorite because this meteorite contains much matrix, in which the FeO contents are generally larger than those in chondrules and CAIs. However, each minerals cannot be distinguished as in the case of Moorabie.

Fig.2c shows an X-ray CT image of a chondrule removed from Allende meteorite. Because of the large magnification of the sample, the spacial resolution was several μm, and thus inner small structures can be seen. Probably, the surrounding white parts are Fe or FeS-rich rims.This chondrule has a porphyritic texture. Each crystal grain can be identified by bright rims probably enriched in FeO or CaO. These crystals may be olivine or pyroxene. Moreover, dark portions which may correspond to holes are seen inside of the chondrule although a possibility of carbon cannot be eliminated. If we observe holes in a thin section, we cannot distinguish real holes from artificial ones which are formed by thin sectioning without information from X-ray CT images. Holes were also observed in another chondrules of Allende meteorite (Fig.2b).

Fig.2d are X-ray CT images of Moorabie meteorite successively taken by the system with the area sensor. Chondrules can be recognized by distinguishing metal, troilite, and silicates although the S/N ratios of the images are slightly poorer than those with the line sensor. We can construct the three dimensional texture from these images by image treatment technique with a computer.

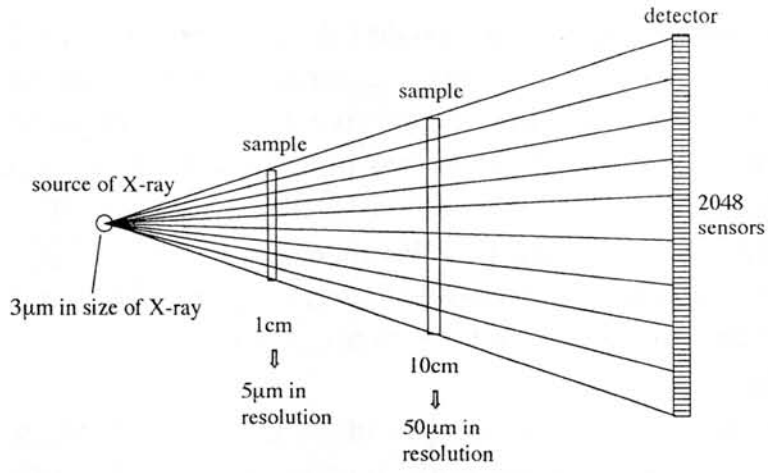

Fig.1 Schematic illustration of the system with a line sensor

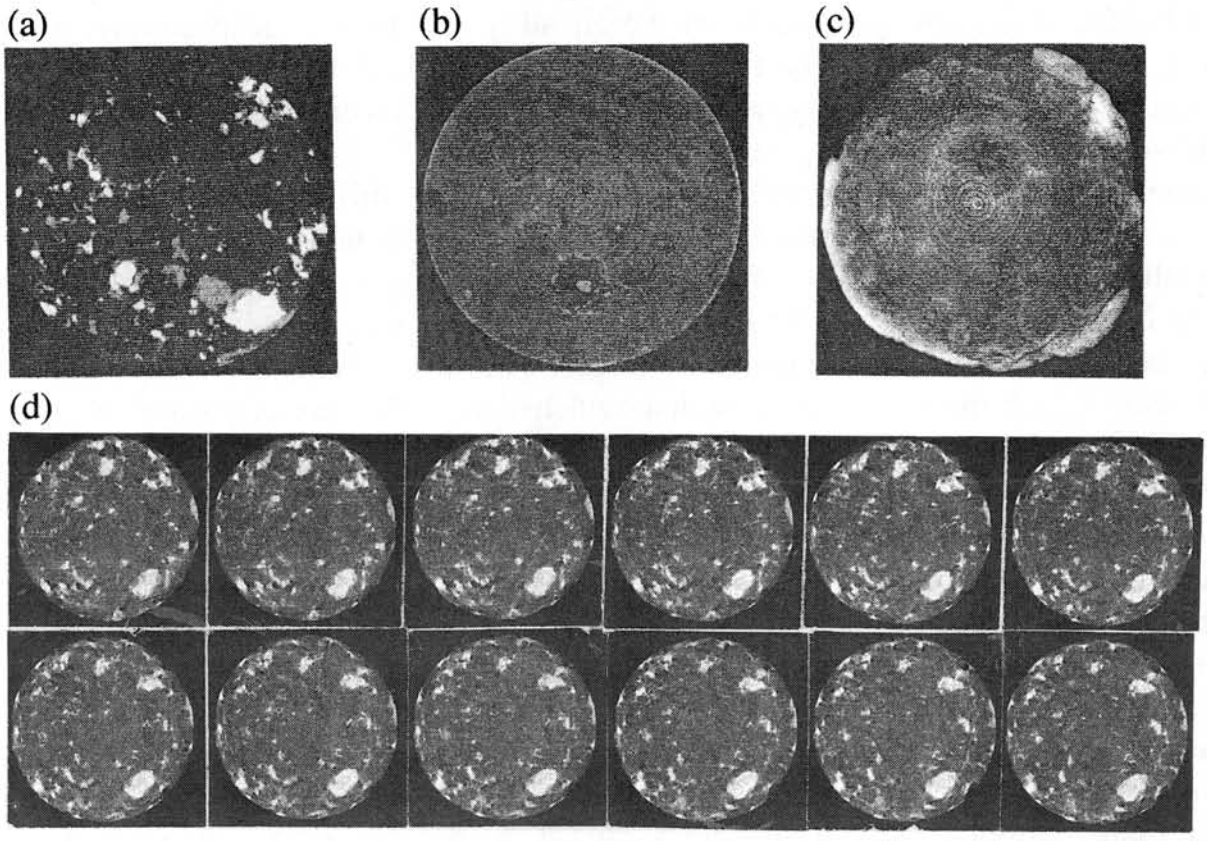

Fig.2 X-ray CT images. (a) Moorabie meteorite (8mm in diameter, 20μm in slice thickness). (b) Allende meteorite (10mm in diameter, 10μm in slice thickness). (c) Chondrule in Allende meteorite (2.5mm in diameter, 50μm in slice thickness). (d) X-ray CT images of Moorabie meteorite taken successively at intervals of 15 μm (8mm in diameter, 15μm in slice thickness).

Unique features of an anomalous enstatite chondrite LEW87223

Ping Kong and Mitsuru Ebihara

Department of Chemistry, Faculty of Science, Tokyo Metropolitan University, Hachioji, Tokyo 192-03, Japan

Introduction

LEW87223 contains abundant well-delineated chondrules and small amounts of olivine, indicating its classification as a type 3 enstatite chondrite [1]. Its oxygen isotopic property is also characteristic of E clan [2]. However, the bulk composition of LEW87223 and its mineral and petrologic features are unlike those of other E chondrites. Grossman et al. [2] suggested that LEW87223 represents a new group of E chondrites, a possible link between the ordinary and the enstatite chondrite clans. In contrast, Zhang et al. [1] insisted their previous suggestion [3] that this chondrite is a representative of EL3 which has gained metal and lost sulfide during a shock heating and brecciation event.

Chemical compositions of bulk LEW87223 and its mineral separates (bulk metal, taenite and non-magnetic fractions) were analyzed by instrumental neutron activation method in this study. We discuss the plausible classification of LEW87223 based on non-volatile elemental pattern and propose a mechanism for its volatile depletion. In addition, we notice the similarity of volatile depletion pattern and some other aspects between LEW87223 and EL chondrites and infer a possible process for loss of moderately volatile elements in EL chondrites. The unique feature of LEW87223 may provide a means of specifying where the mineral and textural properties of E chondrites were established, being either in the nebula or within a parent body.

Experimental

A chip of LEW87223 (about 1g) was crushed and ground in an agate mortar. A portion of the powdered sample was carefully taken with avoiding any sampling bias, from which an aliquot was sealed for bulk analysis. The remaining part was separated into magnetic and non-magnetic fractions by a hand magnet. An aliquot of the least magnetic fraction was sealed for INAA. The magnetic fraction was purified in conc. HF for 2 min for removal of attached silicates and sulfides. The leached residue was subjected to magnetic separation again and the metal was finally purified under an optical microscope. After taking a portion of the metal for INAA, the surplus was subsequently boiled in conc. HF for 20 min for obtaining taenite. Our previous studies showed that no fractionation of siderophile elements occurred during the chemical treatment [4].

Results and discussion

Enstatite chondrites are grouped as EH and EL based on their Fe and siderophile element abundances [5]. The high abundances of non-volatile siderophiles in LEW87223 suggest its classification as an EH. However, LEW87223 has many mineral features similar to those of EL3 but different from those of EH3. This makes Zhang et al. [1] classify it as an EL3. Zhang et al. [1] explained the high siderophile abundances of LEW87223 as an addition of ~15% of metal to this meteorite. Mineral chemistries and petrologic textures are controlled by thermal conditions meteorites have experienced. Unlike the case of ordinary chondrites, these features usually reflect different thermal histories of enstatite chondrites [1]. Therefore, before understanding where and when these features were established, it is better not to use them as a base for the classification of enstatite chondrites.

Among chondrite groups, EL is the sole one that has a fractionated refractory-lithophile pattern relative to the CI composition. This allows explicit classification of an

enstatite chondrite as either an EH or an EL. Even if a meteorite had gained metal, its lithophile elemental pattern would not change. In Fig. 1, abundance ratios of non-volatile elements to Mg for the bulk LEW87223 chondrite obtained both in this study and by Zhang et al. [1] are normalized to the corresponding CI values and compared with those of average EH and EL[6]. Both our results and those of Zhang et al. [1] set clearly LEW87223 to the EH group. A Ni content in the taenite of LEW87223 is similar to that of EH chondrites but significantly lower than that of EL chondrites, indicating that LEW87223 has also been placed in the EH location or the EH parent body.

Compared to EH chondrites, LEW87223 is obviously depleted in moderately volatile elements as shown in Fig. 2. The glossy depletion of volatile elements in association with their volatilities cannot be attributed to incomplete condensation, rather, the glossy depletion should be due to high temperature heating of LEW87223. Because the loss of volatiles in LEW87723 is regardless of affinities of the elements, the depletion could not result from loss of metal-sulfide fluid after shocking on a parent body. Furthermore, the shock-induced temperature necessary for the obvious loss of Au, Cu and As in LEW87223 is too high to allow the presence of well-delineated chondrules in LEW87223. Thus, it appears that the high temperature heating of LEW87223 occurred in the solar nebula, probably being associated with chondrule formation. If this is true, LEW87223 must have experienced a longer or a more intense chondrule formation process than other EH chondrites. In Fig. 2 are also shown depletion of volatile elements in EL chondrites. The similarity in volatile depletion pattern between LEW87223 and EL chondrites implies that the depletion of moderately volatile elements in EL chondrites compared to the EH chondrites could also be produced by vaporization of volatiles during the chondrule formation process.

LEW87223 has a nebular thermal history similar to that of EL chondrites while it has a metamorphic history similar to that of EH chondrites. This unique feature provides us a means of distinguishing where mineral compositions and petrologic textures of enstatite chondrites were established. The similarity in schreibersite composition between LEW87223 and EH chondrites [1] suggests that the composition of schreibersite of enstatite chondrites was determined in the parent body. Thus, a schreibersite composition could be used to distinguish an EH from an EL. The Si content in the metal and the Mn/Mg ratio in the Mg-Mn-Fe sulfide of LEW87223 are similar to those of EL chondrites [1], indicating that these mineral compositions were established in the solar nebula. The lower metal Si content for EL chondrites than that for EH chondrites suggests that melting of EL chondrules occurred at a more oxidizing environment.

References

[1] Y. Zhang, P.H. Benoit and D.W.G. Sears (1995) JGR 100, 9417-9438. [2] J.N. Grossman, G.J. MacPhenson and C. Crozaz (1993) Meteoritics 28, 358. [3] Y. Zhang, P. Benoit, and D.W.G. Sears (1993) LPS XXIV, 1571-1572. [4] P. Kong, M. Ebihara, H. Nakahara and K. Endo (1995) EPSL 136, 407-419. [5] D.W. Sears, G.W. Kallemeyn and J.T. Wasson (1982) GCA 46, 597-608. [6] J.T. Wasson and G.W. Kallemeyn (1988) Phil. Trans. R. Soc. Lond. 325A, 535-544.

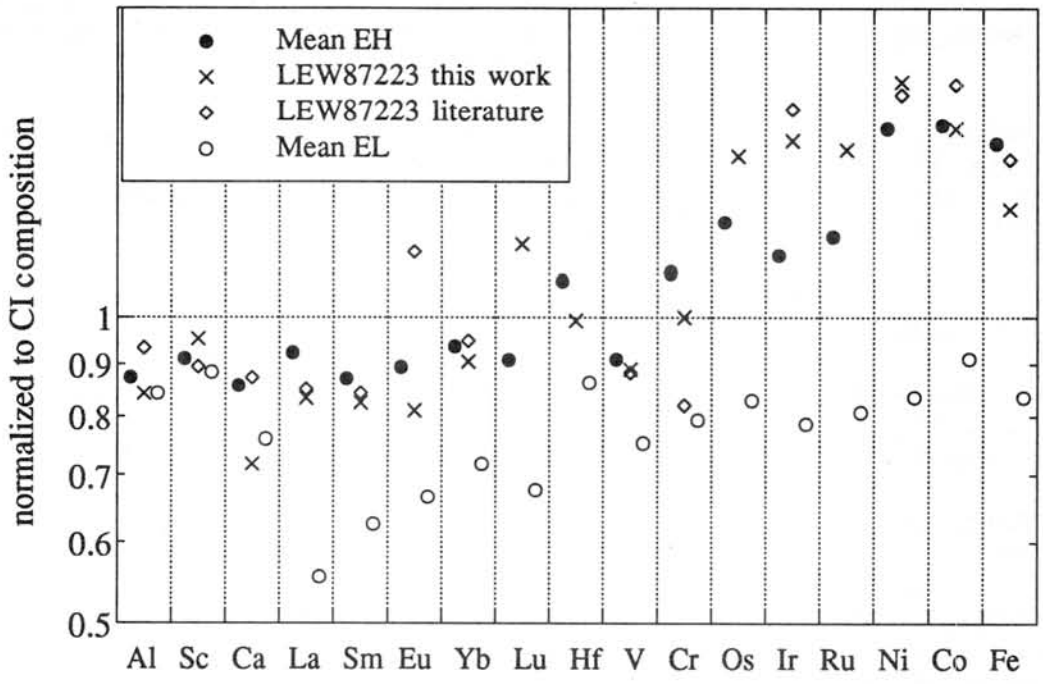

Fig. 1. CI- and Mg-normalized non-volatile elemental abundances for LEW87223 and for average EH and EL chondrites. Both our results and those of Zhang et al. [1] set LEW87223 to the EH group.

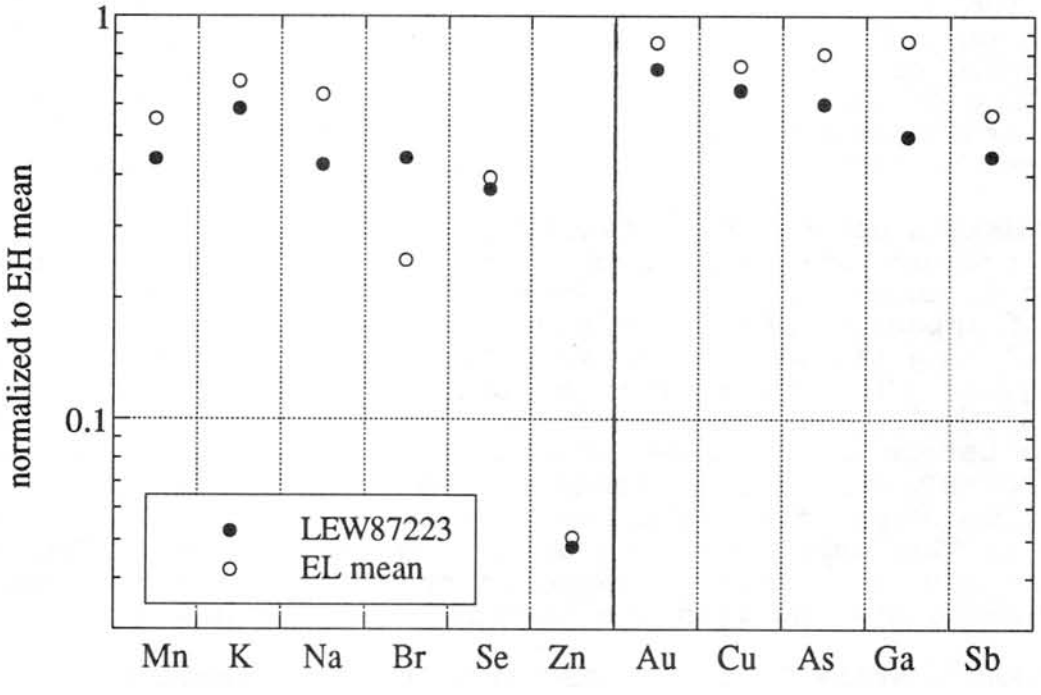

Fig. 2. EH-normalized volatile elemental abundances for LEW87223. Lithophile and chalcophile volatiles shown in the left are also normalized to Mg and siderophile volatiles shown in the right are normalized to Ni.

SCANDINAVIAN IMPACTITES: RAMSÖ SHARP PEBBLES FROM MIEN LAKE, SWEDEN - A NORTHERN EXAMPLE FOR A POSSIBLE ORIGIN OF THE TERRESTRIAL NIPR METEORITES

I. Kubovics[1], Sz. Bérczi[1,2], B. Lukács[3], Z. Puskás[1] & K. Török[1]
[1] R. Eötvös Univ., Dept. of Petrology, H-1088, Múzeum krt. 4/a.
[2] R. Eötvös Univ., Dean's Office, H-1088 Budapest, Rákóczi út 5.
[3] CRIP RMKI, H-1525 Bp. 114. Pf. 49., Budapest, Hungary

ABSTRACT

Sharp pebbles of the Ramsö Island in Mien Lake, Blekinge County, Sweden, originally were classified as rhyolites because of their similarity to Vlegyásza-Bihar rhyolites. But really they are impactites, which gives an example how terrestrial rocks can be transformed and trnsposed by extraterrestrial effects.

1. INTRODUCTION

Although the thick virgin ice layers of internal Antarctica are the best sites to collect meteorites without terrestrial rock background, a few NIPR Antarctic samples (some dozen of the investigated >3000) seem terrestrial. The number is small, still it should be understand how terrestrial rocks may appear on thick ice layers. Even rare extraterrestrials might hide among the "terrestrials". Note that Martian *basalts* are known (SNC), but feldspars are not; and the Shergotty meteorite was suspected to be terrestrial by many until the Zagami fall.

A possible mechanism to throw terrestrial fragments to thick icefields is an impact near but outside the icefield. But Antarctica is isolated and almost entirely icy. Intercontinental flight is known only for tectites and then fusion crust appears. So an impact would be needed on the icefree shore. We discuss first the possibility of such an impact, and then, for the better recognition of its fragments, we report analyses on fragments of an impact from the North, with long Hungarian scientific history.

2. THE THERMAL HISTORY OF ANTARCTICA

At present only some high mountains and oases are icefree. The largest oasis is Bunger, some 400 km², and it does not show traces of impact. However the present Antarctic climate is exceptional. During the whole kainozoic there was a continuous cooling (see Fig. 1). The Antarctic ice cupola started in the pliocene, cca. 5.5 My BP, and the ice cover might not be complete before Günz, so before cca. 1.5 BP. The penultimate interstadial was at cca. 65000 BP with a long tepid period, then the shore may have been icefree. This time is already on the C^{14} horizon.

So in the indeterminate past an impact on icefree Antarctic territory may have thrown fragments on the internal, higher ice fields whence now the ices are carrying them northward.

3. MIEN-RAMSÖ SHARP PEBBLES: DESCRIPTION OF OUR SAMPLES

Impact fragments are metamorphosed, which is a key to recognise them. So analogous fragmented rocks help us to recognise the impact origin of some "terrestrials". One well established astrobleme is the Mien Crater, whose fragments have been studied for more than a century, in Sweden and Hungary.

Mien Crater is the bed of the Mien Lake, in the Blekinge County, Sweden. Its center is the Ramsö Island. Holst (1890) found some rhyolite rocks around the lake, and sent samples to

Szádeczky (1888; 1904), who established similarity to the Hungarian rhyolites from the Vlegyásza-Bihar Mountain. Later it was found that the Mien-Ramsö rhyolites exhibit shock-metamorphosed quartz, so the crater and its central peak is of impact origin (Stanfors, 1969). The rhyolite layer is 20 m thick on Ramsö, some fragments are being carried southward glacially. The impact happened in the Cretaceous, on an original gneiss-granite bedrock.

Now let us see the samples from scattered Mien-Ramsö rocks. **Macroscopically** MRR samples are mainly "sharp-pebbles", rounded by water erosion. Surfaces frequently exhibit clear-cut cross section of the rock, showing the texture on visible scale. The texture consists of light pink and yellow fragments and larger inclusions, sometimes granitic, and vesiculas embedded into gray mesostasis, homogeneous on this scale. Larger samples may contain skeletal inclusions of some centimeter sized ones, too.

Microscopically 2 samples were chosen for observations. Both are complex "impactites" with variolitic texture, but parts with higher proportion of glass and smaller potash feldspar crystals with intersertal texture can also be seen and also parts with brecciated texture containing the mineral fragments of the preimpact rock. The rock is rich in small (<1mm) unfilled vesicles. Both contain potash feldspar, quartz, plagioclase, glass, opaque minerals (sometimes tiny grains of ilmenite), rutile, hematite, limonite. Potash feldspar (sanidine?) laths or fibers mostly show radiant or divergent arrangement which show quite rapid cooling of the molten material in the variolitic parts. The intersertal parts are characterized with unoriented potash feldspars with polygonal interstices occupied by glass (with composition close to that of the potash feldspar according to reconnaisance microprobe analyses), microcrystalline quartz and ilmenite. Quartz is mostly a relict phase, rounded polycrystalline aggregates with glass rim and clear indication of resorption on the edge of the aggregate. The composition of the glass rim is close to that of the potash feldspar as it was revealed during reconnaissance microprobing. The boundary between individual quartz grains is sutured. It seems that the quartz aggregates suffered some kind of recrystallization. The aggregates of quartz are full of tiny opaque minerals, possibly ilmenite and with reddish hematite. New quartz microcrystals crystallized from the melt, mainly in the intersertal parts in the interstices of the potash feldspar associated with glass of potash feldspar and ilmenite. Both quartz and potash feldspar are highly strained having undulose extinction. Relict plagioclases of the preimpact rock are rarely observable in the parts having intersertal texture and in the brecciated parts. The brecciated parts are bordered with plagioclase showing radiant arrangement and multiple twinning, glass and sometimes biotite. The breccias contain major strained quartz, plagioclase. microcline and accessory biotite, muscovite, amphibole, zoisite and zircon clasts in fine grained brownish groundmass.

4. CONCLUSIONS

The Mien-Ramsö fragments are rhyolitic; the impacting extraterrestrial body did not add more than a few %. The present shapes have been formed by subsequent eolic *and* aquatic erosion. The collected fragments remained rather near to the astrobleme, but this may be a selection effect, since present South Sweden is iceless. On an icefield they might stand out.

MR rhyolites are shock-metamorphosed terrestrial rocks, common with Lunar and Martian meteorites in the traces of impact, but without fusion crust and with terrestrial chemical composition. Long aquatic erosion, glacial transport and weathering may remove the fusion crust even from genuine meteorites, and then both they and astroblemic fragments might fall into a "doubtful" class; but microscopy may prove the impact and chemical analysis may check the terrestrial composition. Up to now composition of no "terrestrial" NIPR sample is known.

The possible mechanism behind *some* Antarctic "terrestrials" is then an astrobleme-forming impact on an icefree region of old Antarctica. Advancing glaciers later carried them northward. At the impact the site was icefree, so strong wind and liquid water was present, so eolic and aquatic erosions were as possible as at Mien. Therefore the shapes may be similar to the MRR samples.

ACKNOWLEDGEMENTS

Partly supported by OTKA T/014958, MÜI/TP.55/96 & OMFB-MEC/P-2113 & P-1333/95/96.

REFERENCES

Holst, N. O. (1890): Sver. Geol. Undersökning. Ser. C. No. 110.

Stanfors, R. (1969): Geol. Föreningens: Stockholm Förhandlingar, GFF. 91. pp.73-86. Lund

Szádeczky Gy. (1888): Rhyolithspuren in Schweden. Földtani Közlöny. Vol. 19. pp. 437-449

Szádeczky Gy. (1904): Beiträge zur Geologie des Vlegyásza-Bihargebirges. Földtani Közlöny. Vol. 34. pp. 115-184

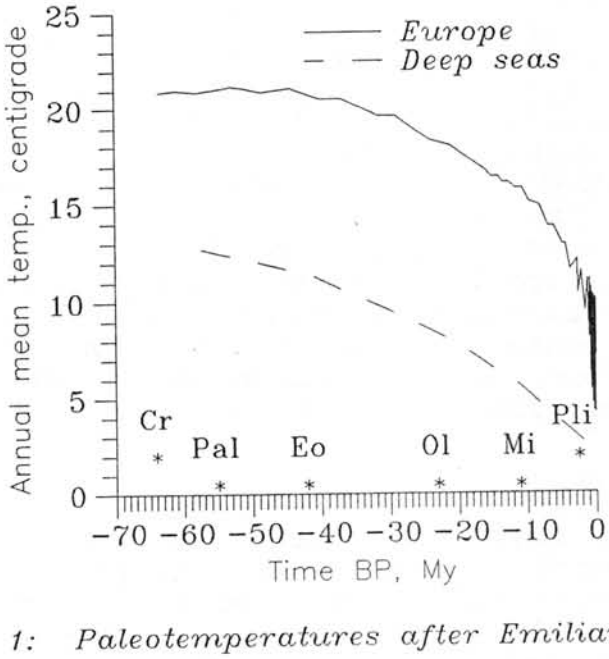

Fig. 1: Paleotemperatures after Emiliani

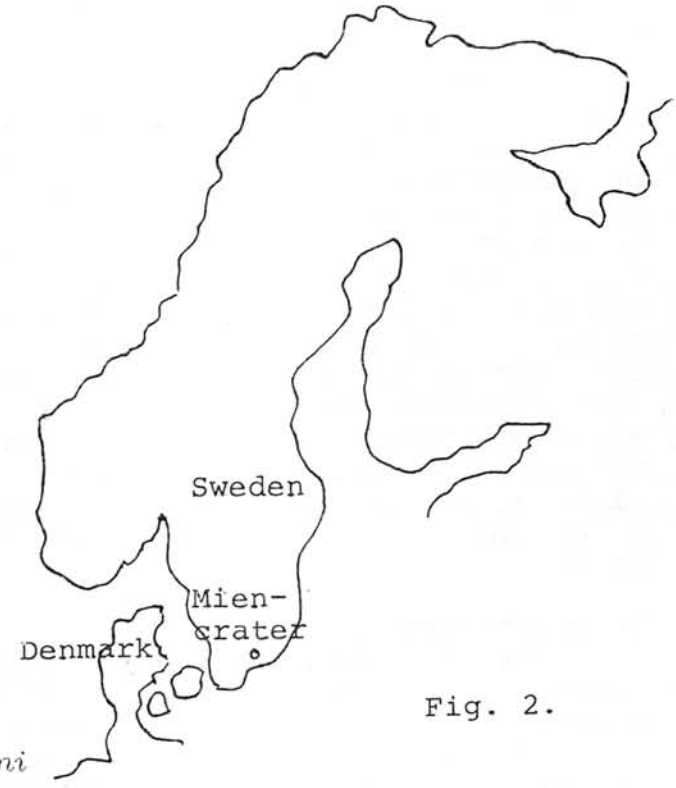

Fig. 2.

Refractory Inclusions in the Ningqiang Carbonaceous Chondrite

LIN Yangting[1,2], KIMURA Makoto[2], and WANG Daode[1]

[1]Institute of Geochemistry, Chinese Academy of Sciences, Guangzhou, P.R. China;
[2]Dept. of Earth Sciences, Ibaraki University, Mito 310, Japan

Introduction: The Ningqiang carbonaceous chondrite fell in China in 1983. It was first classified as anomalous CV3[1] but later reclassified as anomalous CK3[2]. In comparison with CV3 chondrites, the Ningqiang meteorite is clearly distinguished by the lower abundances of refractory elements (~0.82xCV3) and Ca-, Al-rich inclusions (hereafter CAIs) (0.5-1.5 vol%)[1]. The composition of Ningqiang does not fit into any of chondrite groups[3]. In spite of the anomalous nature, only a few of CAIs have been studied in the Ningqiang meteorite[1, 4]. Here we report our comprehensive study of the Ningqiang CAIs.

Petrography and mineral chemistry: We found 124 CAIs (a total area of 44.2 mm^2) by surveying 21 sections (a total surface of 1740 mm^2), suggestive of 2.5 vol% CAI in the Ningqiang meteorite. The half of CAIs are 150-450 μm in size and only 18 CAIs are mm-sized. Melilite-rich type (resembling Allende type A) is predominant (71 out of 124 CAIs). Spinel-pyroxene inclusions are the second abundant type (38). A new kind of anorthite-spinel-rich inclusions[5] are also encountered (9). In contrast, only two Type Bs, one Type C and two plagioclase-olivine-rich inclusions are found in the Ningqiang meteorite.

Melilite-rich type: Modal composition continuously varies from melilite predominant to spinel-rich or Ca-pyroxene-rich. Most of the melilite-rich CAIs are concentric objects or their complicated aggregates, which consist of melilite core, spinel mantle and diopside rim. Some CAIs of this type show the mineral sequence in order of spinel, melilite and diopside outwards. Accessory hibonite, usually as blades in spinel matrix, are found in 5 of them. Grossite, in contact with and/or enclosed in melilite, occurs only in cores of two hibonite-bearing CAIs. Rare fassaite are enclosed in melilite. Only 16 CAIs were significantly altered to replace melilite by nepheline. The other secondary phases are hedenbergite, ilmenite, wollastonite and sodalite. In CAIs of this type, melilite is gehlenite-rich (Geh_{100-70}, and Geh_{100-90} in the hibonite-bearing CAIs). V_2O_3-contents of spinel vary from under detection limit to 0.80 wt%. Fassaite is enriched in Al_2O_3 (19.5-26.8 %) and TiO_2 (15.5-26.8 %). A few fassaite grains contain up to 5.87 % V_2O_3 or 11.9-16.4 % Sc_2O_3. Hibonite contains 3.52-1.17 % MgO, 6.39-1.45 % TiO_2 and <0.60 % V_2O_3. Perovskite contains < 0.51% V_2O_3, <0.24 % Sc_2O_3 and <0.46 % ZrO_2.

Spinel-pyroxene inclusions: All are concentric objects or their complicated aggregates. They consist of spinel core and diopside rim, often with outermost layer of forsterite. Along boundary between spinel and diopside, there is a thin layer of melilite. Minor perovskite is

enclosed in spinel. Hibonite occurs only in 2 inclusions of this type and is embedded in spinel. Composition of melilite resembles those in melilite-rich type. Spinel contains up to 23.9 % FeO.

Anorthite-spinel-rich inclusions: There are "fluffy" subtype and "compact" subtype, both having similar modal compositions of 45-49 vol% spinel, 30-40 vol% anorthite, 8-12 vol% Ca-pyroxenes, 3-6 vol% melilite and minor phases (perovskite, nepheline, sodalite and hedenbergite). These inclusions are texturally zoned, having a coarse-grained spinel-predominant core, a thick but fine-grained spinel-anorthite-Ca-pyroxene mantle and a spinel-melilite crust covered by a thin diopside rim[5].

Type B: The largest CAI (3800×4500μm) studied here consists mainly of melilite, fassaite, spinel and anorthite with minor metallic Fe-Ni, perovskite and secondary phases (nepheline, hedenbergite and wollastonite). A continuous diopside rim surrounds its convoluted surface. Spinel occurs as framboids, palisades and individual inclusions in melilite, fassaite and anorthite. Both of fassaite and anorthite are enclosed in melilite, or as interstitial grains with plenty of spinel-inclusions. The other CAI of Type B contains a grossite-bearing nodule (Ø410 μm). The nodule consists of grossite (65×115μm in size), hibonite and perovskite in spinel matrix. The host shows brecciated texture around the nodule. Geh-content of melilite decreases from 90.0 mol% near the diopside rim to 7.6 mol% in center of the largest CAI. Spinel shows no relationship between composition and occurrence, except V_2O_3-poor in the grossite-bearing nodule (<0.15 %) in comparison with grains in the host (0.28-0.49 %). Ca-pyroxene is heterogeneous in Al_2O_3 (6.15-22.6 %) and TiO_2 (1.0-18.1 %). Plagioclase is nearly pure anorthite with minor MgO (<0.53 %) and Na_2O (<0.29 %). In the nodule, grossite is stoichiometric $CaAl_2O_7$ and hibonite contains 2.96-3.66 % MgO and 5.52-6.92 % TiO_2.

Type C: A inclusion (Ø770 μm) of this type consists of anorthite lathes in fassaite matrix. Abundance of anorthite lathes tend to increase toward its rim, while spinel and a few small grains of melilite concentrate in the center. Minor hedenbergite and nepheline occur along boundaries of anorthite and fassaite. Composition of anorthite is similar to that of Type B. Fassaite contains 9.26-20.8 % Al_2O_3, 1.17-4.55 % TiO_2 and <1.26 % Cr_2O_3. Spinel is heterogeneous (1.47-14.1 % FeO, 0.19-0.79 % V_2O_3, and 0.29-2.72 % Cr_2O_3). Melilite is Åk-rich (80 mol%).

POIs (plagioclase-olivine-rich inclusions): There are only two inclusions of this type. Different from the previously reported one of them[6], the other POI shows radial texture with anorthite lathes enclosing numerous fine blades of enstatite, and contains less abundance of spinel. In addition, plagioclase contains less An-content (81.4±3.96 mol%), and spinel contains lower V_2O_3 (0.31-0.38 %), Cr_2O_3 (1.98-4.29 %) and TiO_2 (0.16-0.20 %) than those in the POI reported before[6].

Discussion: In comparison with CAIs in CV chondrites, one of the most remarkable features of Ningqiang CAIs is the distinctly high abundance of non-molten fraction. Most of Ningqiang CAIs do not show textures of once melting. In addition to their irregular or convoluted

shapes, mineral sequence in order of hibonite ± grossite, perovskite, melilite, spinel, Ca-pyroxenes and forsterite is well consistent with condensation sequence[7]. Type B, Type C and POIs are common in Allende and the other CV3 chondrites, but scarce in the Ningqiang meteorite. Our observations probably indicate different thermal histories between reservoirs of Ningqiang and CV chondrites. However, since the average size of Ningqiang CAIs is significantly smaller than that of CAIs in Allende and the other CV chondrites, a size-based sorting mechanism in the nebula might be also related to the difference of CAIs in the Ningqiang meteorite and others.

Most of CAIs in the Ningqiang meteorite contain little feldspathoids, hedenbergite and wollastonite, which are abundant in Allende CAIs[8, 9]. It is evident that the secondary alteration of CAIs hardly prevailed in Ningqiang in comparison with Allende, although high abundances of magnetite indicate oxidizing conditions of both meteorites. Furthermore, no grossular is found in Ningqiang CAIs, which is a common alteration product of CAIs in CV chondrites[9] and becomes stable under ~1000K[10, 11]. These observations suggest that most of Ningqiang CAIs escaped alteration reaction at low temperatures in comparison with Allende CAIs. On the other hand, the spinel-anorthite-rich inclusions experienced a reaction between melilite, spinel and vapor producing anorthite and part of Ca-pyroxene at high temperature, probably ~1410-1000K[5].

Although both of the two Type Bs were once molten from their texture, one of them contains the grossite-bearing nodule. The grossite-bearing nodule distinctly shows different modal composition and mineral chemistry in comparison with the host. This nodule can not crystallize from host melt based on crystallization experiment[12]. It represents a much more refractory object and is similar with an unusual grossite-bearing spherule in Murchison in mineralogy[13]. The nodule may have incorporated with the host by impact process, as indicated by the brecciated texture of the host around the nodule.

Acknowledgments: This study is supported by the Japan Society for Promotion of Sciences.

References: [1] Rubin A. E., et al. (1988) **Meteoritics 23**, 13-23. [2] Kallemeyn G. W., et al. (1991) **GCA 55**, 881-892. [3] Kallemeyn G. W. (1996) **LPS XXVII**, 635-636. [4] Lin Y. T., et al. (1991) **Meteoritics 26**, 364-365. [5] Lin Y. T. and Kimura M. (1996a) **LPS XXVII**, 755-756. [6] Lin Y. T. and Kimura M. (1996b) **LPS XXVII**, 753-754. [7] Yoneda S. and Grossman L. (1995) **GCA 59**, 3413-3444. [8] MacPherson G. J. and Grossman L. (1984) **GCA 48**, 29-46. [9] MacPherson G. J., et al. (1988) **Meteorites and the early solar system** (ed. Kerridge J. F. and Matthews M. S.), 746-807. [10] Fuchs L. H. (1974) **Meteoritics 9**, 11. [11] Hutcheon I. D. and Newton R. C. (1981) **LPS XII**, 491-493. [12] Scolper E. (1982) **GCA 46**, 2159-2180. [13] Simon S. B., et al. (1994) **GCA 58**, 1937-1949.

COMPETITION OF C AND H_2O FOR FE IN E, H, AND C CHONDRITES

B. Lukács[1] and Sz. Bérczi[2]
[1] CRIP RMKI, H-1525 Bp. 114. Pf. 49., Budapest, Hungary
[2] R. Eötvös Univ., Dept. of Petrology, H-1088 Múzeum krt. 4/a.

ABSTRACT

During thermal evolution of chondrites Fe may change its carrier mineral by reduction and oxidation. Reducing agent is C, oxidizing agent is H_2O. However, their activities start at different temperatures. This C vs. H_2O competition may cause a trifurcate evolution of the initial source material (of which only C1 survived). Differences in the initial C/H_2O ratio may lead to trifurcation at petrologic class 3 into E, H and C.

1. INTRODUCTION

For Fe content chondrites fall into 2 separate groups Wiik (1956): higher, ≈27% (E, H, C) & lower, ≈21% (LL, L). Statistical calculations on the new NIPR Antarctic Meteorite Compositional Data Set (NAMCOD) showed that the distributions of E, H and C chondrites overlap. The more than 550 "points" of NAMCOD makes it possible to reopen the question of the common origin of these three chondrite types, because other distinctive parameters of the types might have been the consequences of the bulk compositional trifurcation, which step by step distinguished E, H and C till they reached petrologic class (PC) 3. We include *all* analysed NIPR E, H and C chondrites into our discussion.

Fe/Si ratio may be selected as a parameter characterizing initial conditions, because both elements are surviving any thermal transformations inside the parent body. First we plotted the "Chondritic Hertzsprung-Russell Diagram" (C-HRD) for the oxide Fe\non-oxide Fe content (Si normalized) of E, H, L, LL, and C types of chondrites from NAMCOD (Bérczi, Holba, Lukács, 1995). From averages for all petrologic classes of each types (E, H, L, LL, C) we have got a bulk path of chemical evolution of these meteorite types. These plots focused our attention to the competition of C and H_2O for Fe during the thermal evolution, because there was a common trend. In all cases except E first reduction, then oxidation was the dominating change for Fe containing components. This showed that reduction could start at lower temperatures, while oxidation switched on later.

2. POSSIBILITY OF TRIFURCATION

Imagine an ancesral material similar to present C1-2's. Short-living radioisotopes or contraction may have heated up them for the first 1-100 My. Then some volatiles left and chemical transmutations went on. 4 major components might change in chondrites in 3 main reactions as

A) $2FeO + C \leftrightarrow 2Fe + CO_2 \rightarrow 2Fe$
B) $Fe + H_2O \leftrightarrow FeO + H_2 \rightarrow Fe$
C) $C + 2H_2O \leftrightarrow CO_2 + 2H_2 \rightarrow \phi$

Total Fe content is constant until Fe melting point and SiO_2 and MgO practically remain unreduced in chondrites.

We do not perform detailed calculations here for the processes because all reaction rate coefficients are T-dependent and some are poorly known at the relevant temperatures. Data are just being collected; however all 3 reactions, or analogons, are known

from industry. A) is in iron industry, B) from an old method of producing rustfree knives and C) from city gas factories.

In C1's the C content is 3-5 weight %, while H_2O is some 12-20 weight %.; but 1 % C can balance 3 % H_2O. One expects final reduction for $H_2O/C>3$ and final oxidation for <3, while for ≈ 3 oscillation may be expected. (The T-dependence of rates may cause some complications.) NIPR composition data show the first behaviour for E3-4 (and we know that reduction goes on for E5-6 too), the second beyond C3 ant the third for H3-6.

3. COMPOSITIONS

As an almost balanced group, early C's seem hopeful ancestors for a trifurcate evolution. We cannot directly prove the trifurcation on the NIPR composition data because they do not contain carbon data, but indirect conclusions can be made.

Fig. 1 shows Fe vs. Mg, both normalised Si as anywhere henceforth. As seen, E, H and C overlap for Fe, but not for Mg. It seems *as if* later C's had evolved from the high Mg tail of the ancestral distribution, and E's of the low Mg tail. True, the gap is seen between enstatite and bronzite, which we cannot explain and therefore ignore henceforth.

It is strange that the fate of a meteorite depend on *Mg* content, since Mg does not enter into the chemical transmutations; but Fig. 2 shows that in PC 3 the H_2O content correlates positively with Mg. Let us use the working hypothesis that silicates with high Mg content keep H_2O better than ferrous ones; if mineralogic experiments confirm this, then one may expect that oxidation balances better the reduction at higher Mg contents (see Procs. A-C)).

Indeed, Fig. 3 show that *oxidized* Fe correlates *positively* with Mg in PC 3, while there *total* Fe correlates *negatively* with Mg (cf. Fig. 1).

Fig. 4 is H_2O vs. reduction at PC 3; the correlation is indeed negative (the same is true for all PC's, not shown here); although the E line seems separate. The simplest explanation is a larger E parent body.

4. CONCLUSIONS

According to Figs. 1-4, NIPR data do not contradict a trifurcate evolution from early C's to late C's, H's & E's as:

I: For higher than average H_2O/C and/or MgO/FeO the reduction starts, but FeO and H_2O uses up C at some stage, while H_2O is retained. When the thermal impact carries the body to PC 3 by thermal chondrule diffusion, H_2O already strongly dominates C, so reduction stops and reoxidation will come as for C4-6.

II: For most initial conditions (average H_2O/C and MgO/FeO, or high H_2O/C but low MgO/FeO or low H_2O/C but high MgO/FeO) most C *and* H_2O are used up or diffuses away before the stage PC 3. Therefore if the thermal impact is sufficient to reach later stages of higher PC's, the possibilities for reduction or oxidation are moderate and balanced. This resembles H3-6.

III: For lower than average H_2O/C and/or MgO/FeO some C is used up, but at PC 3 C still dominates H_2O, so Proc. A) does not have competitors, and reduction keeps going. This resembles E3-6.

We admit that detailed calculations for chemical reaction rates (in preparation) are needed and that E's still seem to stand somewhat apart. Even then, the scheme is not impossible.

ACKNOWLEDGEMENTS

Partly supported by OTKA T/014958, MÜI/TP.55/96 & OMFB-MEC/P-2113 & P-1330/95/96. funds. NIPR Databasis is acknowledged.

REFERENCES

Bérczi Sz. & al. 1995: Acta Mineral. Petrog. Szeged **36**, 143

Wiik H. B. 1956: Geochim. Cosmochim. Acta **9**, 279

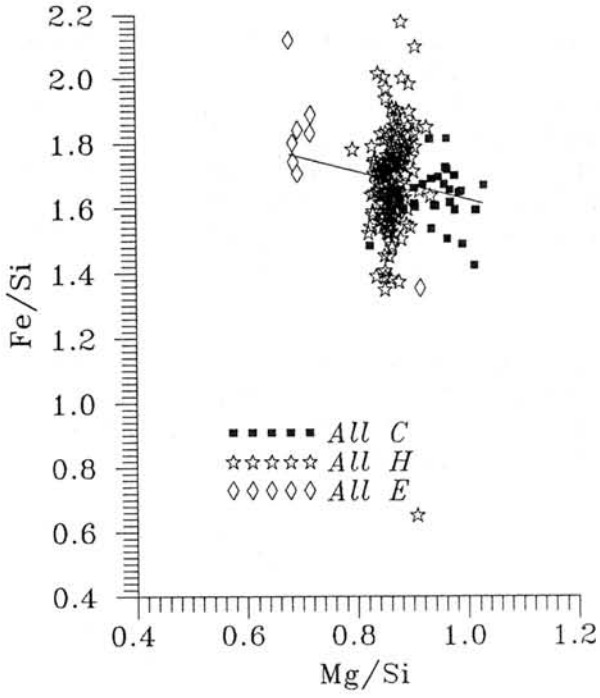

Fig. 1

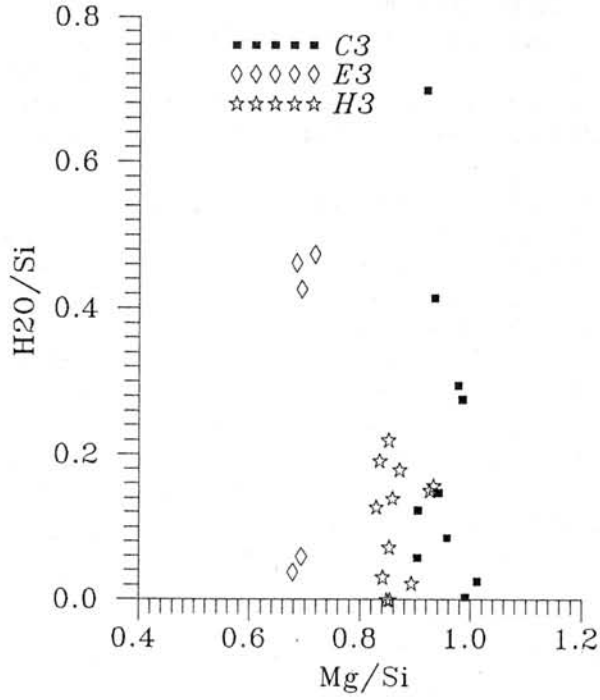

Fig. 2

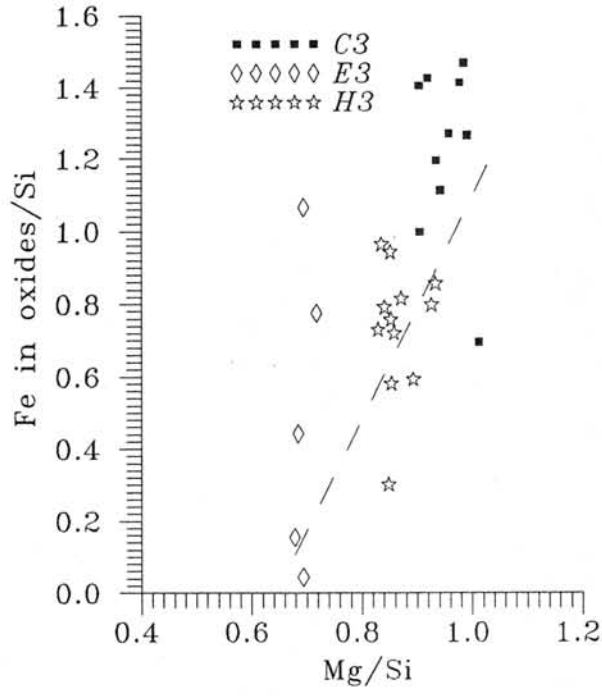

Fig. 3

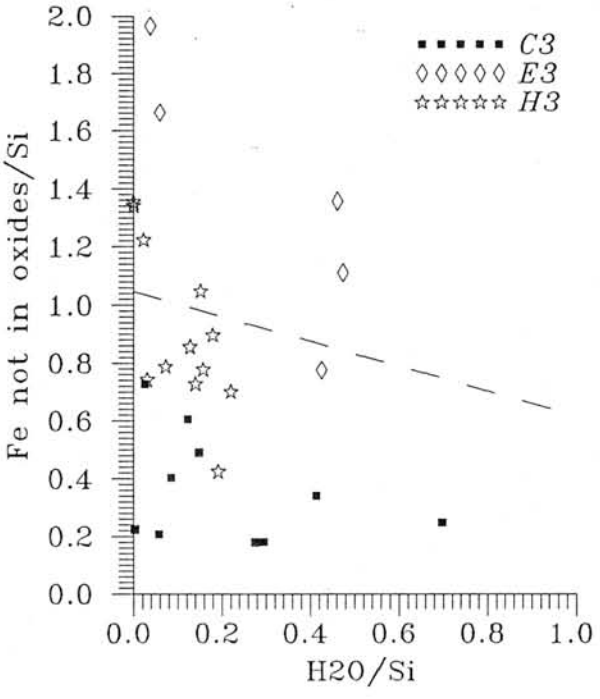

Fig. 4

FACTORS OF OXYGEN ISOTOPIC VARIATIONS IN METEORITES

A.A.Marakushev

Institute of Experimental Mineralogy, Russian Academy of Sciences, Chernogolovka, Moscow region, 142432 Russia

The data of Clayton and Mayeda (1992, 1978, and 1983) and some other scientists (Clayton et al., 1976, 1977, and 1983; Grossman and Larimer, 1974; Robert et al., 1992; etc.) are summarized on the $\delta^{17}O$-$\delta^{18}O$ diagram (Fig.) to demonstrate the principal features of oxygen isotopic composition in meteorites. The trends follov two directions plotted in the diagram by solid and dashed lines. The solid lines correspond to the variations of the oxygen isotopic composition of chondrites and primitive achondrites-ureilites (Ure) and lodranites (Lod). The three trends presented in the diagram correspond to three genetic groups of chondrites: ordinary chondrites (H-L), forsterite, forsterite-enstatite, enstatite chondrites, and lodranites (F-E), and carbonaceous chondrites and ureilites (C3-Ure). In the plot, the respective lines (H-L, F-E, and C3-Ure) are set at an angle of 45^{O}, which characterizes these trends as anomalous, i.e., distinct from the common trends of the normal massfractionation of oxygen isotopes. In the diagram, the latter are represented by dashed lines with gentler slopes. These lines portray the normal isotope fractionation ($\delta^{17}O$ is half as large as $\delta^{18}O$) typical of achondrites (diogenites-howardites-eucrites-meso- siderites, chassignytes-naklites-shergottites, etc.), lunar and terrestrial rocks, and some minerals (olivine-pyroxene- plagioclase) from chondrites of the main types. This clearly determines the genetic groups of chondrites.

The diamondiferrous mineralization of meteorites is best pronounced in the family of carbonaceous chondrites and ureilites (C3-Ure), which is illustrated by the Allende (C3) meteorite. It contains magnesian chondrules with barred and porphyric textures, which are described by two anomalous trends of their oxygen isotope compositions. The trend for barred chondrules reflects genetic links between the carbona-

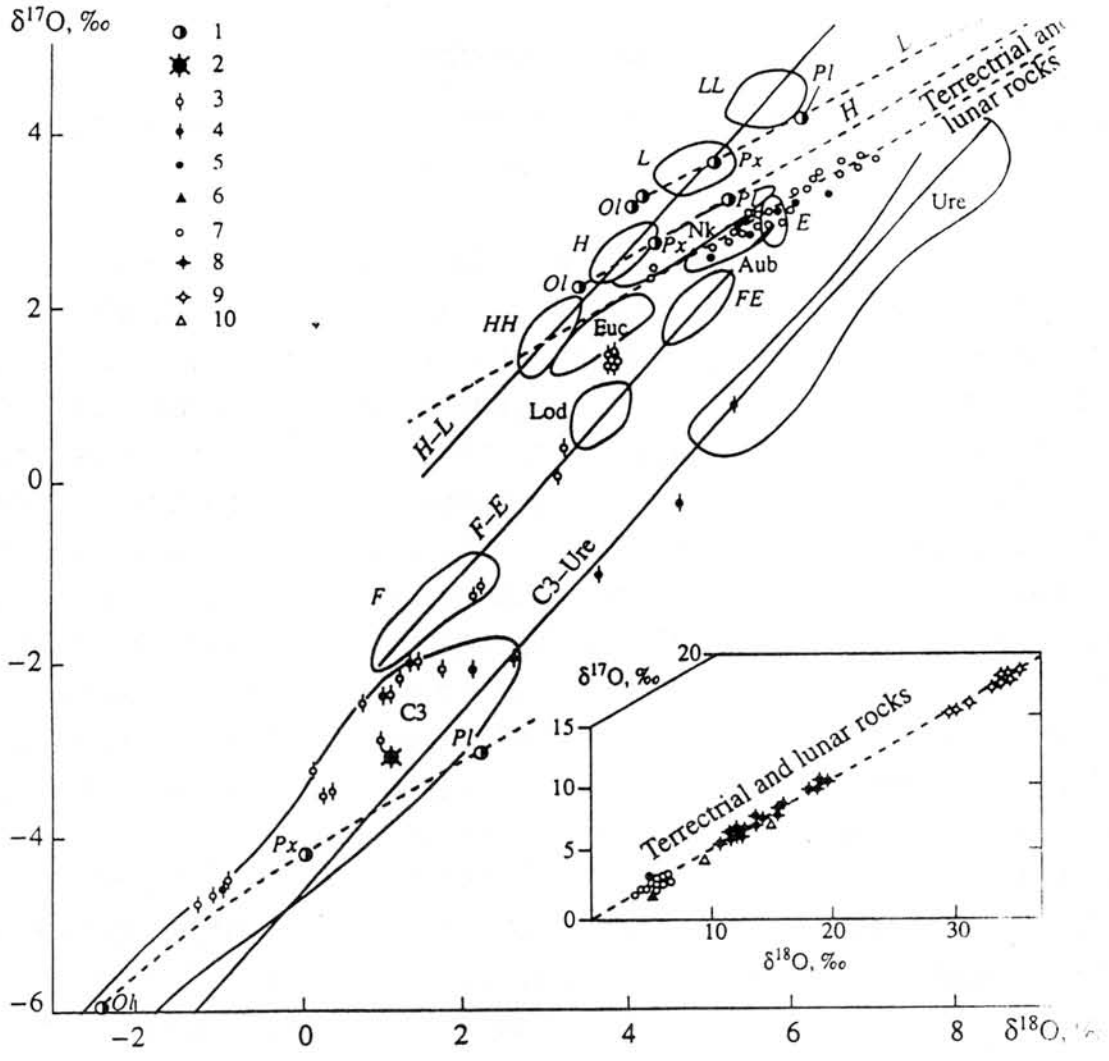

Position of diamondiferous meteorites in the general system of the genetic groups of meteorites in terms of oxygen isotope composition ($\delta^{17}O$-$\delta^{18}O$). Solid lines show anomalous variation trend of the oxygen isotope composition typical of families of diamondiferous meteorites: C3-Ure- carbonaceous chondrites and ureilites, F-E- forsterite.enstatite (FE) chondrites and lodranites (Lod), H-L- ordinary chondrites. Dashed lines indicate normal oxygen isotope massfractionation trends, which can be traced using minerals in each chemical group of chondrites [olivine(Ol)-pyroxene(Px)-plagioclase(Pl)], achondrites [diogenite-howardite-eucrite (Euc), chassignite-shergothite-naklite(Nk), aubrite(Aub), and in terrestrial and lunar rocks. 1-chondrite minerals (Ol, Px, Pl); 2-4- Allende chondrite: 2-average composition, 3-barred chondrules, 4-porphyritic chondrules and dark inclusions, which reflect genetic links between C3 chondrites, forsterite chondrites, ordinary chondrites, and ureilites; 5-10- lunar and terrestrial rocks in the diagram and inset: 5- lunar volcanic rocks (basalts and microanorthosites), 6-9- terrestrial rocks: 6- peridotites, 7-basalts, 8-9- metapelite schists (8- Precambrian, 9- Phanerosoic), 10-granites

ceous (C3) and ordinary chondrites and intermediate values of both the isotopic compositions of the barred chondrules and the iron mole fractions of the silicates (numbers in parentheses): LL(27)-L(24)-H(16)-Allende barred chondrules (12-0)-C3).

This sequence reflects the progressively more reduced conditions under which chondrite magmatism evolved. These conditions predetermined the diverse "maturity" of chondritic magmas, caused by the pressure of the hydrogen envelopes of their parental planets. The average oxygen isotope compositions vary as follows (o/oo): $\delta^{17}O$= 3.8(LL), 2.7(H), and -4.4(C3) and $\delta^{18}O$= 5.0(LL), 4.9(L), 4.3(H), and -0.1(C3). These values determine the genetic sequence of the parental chondritic planets.

The parental planets of carbonaceous chondrites (C3), which are the last in the sequence, are differentiated into meteoritic compositions whose isotopic variations determine the respective trend of the C3-Ure genetic group. This anomalous trend is most clearly pronounced in the porphyry chondrules and melanocratic inclusions of the Allende meteorite. The relative richness of the inclusions in heavy oxygen isotopes makes them similar to ureilites and principally different from leucocratic calcic inclusions in carbonaceous chondrites. These inclusions contain minerals that are particularly poor in heavy oxygen isotopes (o/oo): olivine ($\delta^{17}O$= -23.0 and $\delta^{18}O$= -28.5), fassaite ($\delta^{17}O$= -16.3 and $\delta^{18}O$= -21.7), spinel ($\delta^{17}O$= -39.3 and $\delta^{18}O$= -38.0), etc.

The respective calcic melts formed the outer silicate layers of C3-planets and were, thus, most actively affected by hydrogen envelopes. This fact predetermined their anomalously high contents of isotopically light oxygen. In contrast, ureilites originated in the planetary interiors together with sich iron meteorites and pallasites as Eagle Station, which composed the cores of the planets. This follows from the oxygen isotope compositions of pallasites, for example, Eagle Station (whose olivine has $\delta^{17}O$= -6.3 and $\delta^{18}O$= -2.9 o/oo) and ureilites ($\delta^{17}O$= 2.8 and $\delta^{18}O$= 7.7 o/oo). These features

clearly determine the affiliation of such meteorites to the C3-Ure trend. This trend was controlled by differentiation processes in planets of the C3 type, whose liquid cores were compositionally approximated by very high-iron meteorites (Eagle Station), and the "mantles" corresponded to ultrabasic olivine meteorites (ureilites). The interaction occurred under the high pressure of the hydrogen envelopes (evidence of this phenomenon is shown by ureilites) and provided the conditions required for their diamondiferous mineralization.

The high hydrogen pressure predetermined the diamondiferous mineral assemblages, for example, the parageneses of diamond and moissanite (SiC), which persistently occurs in chondrites. This mineral, like the native silicon of diamondiferous meteorites, is related to the origin of isotopically anomalous silicon-oxygen compounds under high hydrogen pressure: $SiO_2+H_2=SiO+H_2O$. That the light oxygen isotope can concentrate in such compounds (SiO) is evident from the isotope composition of meteoritic water, which participated in these reactions. The water of the Ranazzo chondrite has the following specific isotope composition of oxygen: $\delta^{17}O=$ 13.2 and $\delta^{18}O=$ 26.2 o/oo (Clayton et al.,1976). The participation of such anomalous compounds as SiO, SiH_2, etc. in the processes of silicate crystallization may have been accompanied by the origin of diamond: $2MgO+2SiO+CH_2+CO= Mg_2SiO_4+SiC+C+H_2O$.

Such reaction can explain the pervasive coexistence of diamond and moissanite in carbonaceous chondrites. The moissanite associates with silicates that are anomalously depleted in heavy oxygen isotopes.

References. Clayton,R.N.,Mayeda,T.K. Earth Planet.Sci. Lett.,1978,**40**,168-178; Earth Planet.Sci.Lett.,1983,**62**,1-6; Seventeenth Symp.Antarctic Meteorites. Tokyo,1992, 160-163. **Clayton et al.** Earth Planet.Sci.Lett.,1976,**30**,1607-1608; Earth Planet.Sci.Lett.,1977,**34**,209-224; Chondrules and their Origins,1983,**18**,37-43. **Grossman et al.** Rev.Geophys.Space Phys.,1974,**12**,71-101. **Onuma et al.** Eighth Symp.on Meteorites, 1983,306-314. **Robert et al.** Earth Planet.Sci.Lett.,1992. **108**.1-9.

THERMAL EFFECTS ON NOBLE GAS ABUNDANCES OF DEHYDRATED CARBONACEOUS CHONDRITE YAMATO-86789

K. Matsuoka [1], T. Nakamura [1], N. Takaoka [1] and K. Nagao [2]

1) Department of Earth and Planetary Sciences, Faculty of Science, Kyushu University, Fukuoka 812-81.

2) Institute for Study of the Earth's Interior, Okayama University, Misasa, Tottori 682-01.

Introduction: CI and CM chondrites are primitive meteorites but are affected by secondary aqueous alteration on their parent bodies. Recently, some carbonaceous chondrites with CI-CM affinities were found to have experienced thermal metamorphism after aqueous alteration. They are Belgica(B)-7904, Yamato(Y)-82162 and Y-86720 [1]. They can carry information on evolution processes of primitive metorites. Because primordial noble gases can provide information on formation conditions of meteorites and their parent bodies, it is important to know correlation between noble gas data and degree of thermal metamorphism which can be given by mineralogical studies. Our recent mineralogical study indicates that Y-86789 is a new member of thermally metamorphosed carbonaceous chondrites with CI-CM affinities [2]. A small chip (59.5 mg) of Y-86789 has been analyzed for noble gases with a modified VG5400 mass spectrometer of Okayama University [3]. The sample was heated stepwise at 600, 800, 1000, 1200, 1500 and 1850℃ in a Ta-furnace.

Results and discussion: Concentrations of trapped gases are very low, compared with the Orgueil CI carbonaceous chondrite [4], e.g., x1/70 and x1/5 for trapped Ne and trapped heavy gases, respectively. The amount of trapped Xe is significantly low, even compared with B-7904 [2], which is a metamorphosed, dehydrated meteorite. As shown in Fig. 1, the maximum release of trapped Xe is found at 1200℃, which is in clear contrast with the peak temperatures (e.g., 800℃ for Orgueil) for the release of trapped Xe from the Orguel CI and Murchison CM chondrites. These suggest heavy loss of trapped gases from low retentive sites for Y-86789. Particularly trapped gases released at 600 and 800℃ are very low, suggesting metamorphic heating up to 800℃.

On the other hand, radiogenic ^{40}Ar, amounting to 2.7×10^{-6} cm^3 /g, .was released mostly at 800℃. This indicates enrichment of K in low temperature minerals and a possibility to date the last heating event. K content is not available for Y-86789. With a K content (K=432ppm [5]) of Y-86720 that is paired with Y-86789 [2], we have 1.1 Ga for K-Ar age. The young age trend is also found for other dehydrated carbonaceous chondrites: 1.2, 1.2 and 0.77 Ga are calculated using data on ^{40}Ar and K contents for B-7904 [5-7], Y-82162 [5,7] and Y-86720 [5,7], respectively. They are similar in the K-Ar age to CI chondrites(: 1.1 to 1.5 Ga) but considerably shorter than CM chondrites (: around 3.4 Ga), as calculated from literature data on ^{40}Ar [8] and K

[9]. Similarities in K-Ar ages as well as in oxygen isotopic ratios [10] between CI and dehydrated chondrites indicate that dehydrated carbonaceous chondrites are more intimate to CI than to CM carbonaceous chondrites.

Ne isotopic ratios for all temperature fractions except at 600℃ are plotted below a mixing line between trapped and cosmogenic components in a three-isotope plot of Ne (Fig. 2). With Ne-A2 for trapped Ne [11], Ne-E amounts to 1.8×10^{-9} cm^3 /g, while trapped ^{22}Ne and cosmogenic ^{22}Ne are 1.3×10^{-9} and 1.5×10^{-9} cm^3 /g, respectively. In calculation, we assumed no Ne-E in the 600℃ fraction and $(^{20}Ne/^{22}Ne)_{cos} = 0.80$. This indicates that most of trapped Ne was lost from carbonaceous trapping sites, but Ne-E was retained in SiC and/or graphite [12] during metamorphic heating after aqueous alteration. Cosmogenic $^{22}Ne/^{21}Ne$ is calculated to be 1.226 from the 600℃ fraction. With this ratio for shielding correction and 1.23×10^{-9} cm^3 /g for cosmogenic ^{21}Ne, we have 0.8 Ma for a cosmic-ray irradiation age.

Xe isotopic ratio indicates that Xe released at 1200 and 1500℃ contains Xe-S and Xe-HL [12]. (Fig. 3) It is supposed that loss of Xe-Q [13] during metamorphic heating made Xe-S and Xe-HL visible, implying that the dehydration event destroyed trapping sites of Xe-Q but not the host phases for Xe-S (SiC) and Xe-HL(diamond). This is consistent with the existence of Ne-E.

The degree of metamorphic heating has been given as follows: B-7904 (>750℃) > Y-86720 (700-750℃) > Y-82162 (600-700℃), and Y-86720 (>700℃) > Y-82162 > B-7904 (>600℃), based on transformation of phyllosilicates into olivine [14] and contents of labile trace elements [15], respectively. The order of B-7904 is quite opposite: Maximum heating based on the minaralogical study but minimum heating from the chemical study. The noble gas concentrations for Y-86789, a paired meteorite with Y-86720 [2], are much lower than those for B-7904, e.g., x1/3 for ^{132}Xe and the release patterns for Y-86789 always sift to the high temperature side, compared to B-7904. These results indicate that Y-86789 was heated at higher temperature than B-7904. Hence the present result is consistent with the order of metamorphic heating deduced from the chemical study [15]. Our X-ray diffraction analysis has revealed that phyllosilicates of Y-86789 are dehydrated and transformed to olivine [2]. However, no data are available on X-ray diffraction of matrix phillosilicates for others. We need such data to check the degree of metamorphic heating.

References : [1] Ikeda (1992): Proc. NIPR Symp. Antarct. Meteorites, **5**, 49-73. [2] Matsuoka et al. (1995): Proc. NIPR Symp. Antarct. Meteorites. **9** (in press). [3] Miura et al. (1995): Geochim. Cosmochim. Acta, **59**, 2105-2113. [4] Bogard et al. (1971): J. Geophy. Res. **76**, 4076-4083. [5] Yamamoto and Nakamura (1990): Proc. NIPR Symp. Antarct. Meteorites, **3**, 69-79. [6] Nagao et al. (1984): Mem.Nat. Inst. Polar Res., Spec. Issue **35**, 257-266. [7] Weber and Schultz (1991): Meteoritics **26**, 406. [8] Mazor et al. (1970): Geochim. Cosmo-chim. Acta, **34**,

781-824. [9] Kallemeyn and Wasson (1981): Geochim. Cosmochim. Acta, **45**, 1217-1230. [10] Mayeda et al. (1987): Mem. Nat. Inst. Polar Res., Spec. Issue **46**, 144-150; Clayton and Mayeda (1989): Lunar Planet. Sci., **XX**, 169-170. [11] Alaerts et al. (1980): Geochim. Cosmochim. Acta, 44, 189-209. [12] Tang and Anders (1988): Geochim. Cosmochim. Acta, **52**, 1235-1244. [13] Wieler et al. (1992): Geochim. Cosmochim. Acta, **56**, 2907-2921. [14] Akai (1992): Proc. NIPR Symp. Antarct. meteorites, **5**, 120-135. [15] Paul and Lipschutz (1990): Proc. NIPR Symp. Antarct. Meteorites, **3**, 80-95.

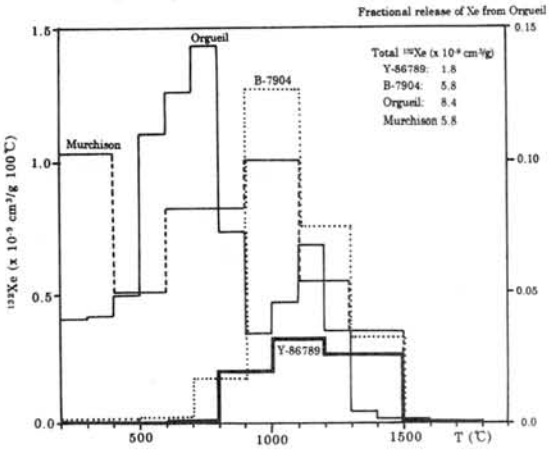

Fig. 1 Xe release pattern. Data source: Orgueil [4], Murchison (Kuroda et al., 1975) and B-7904 [6].

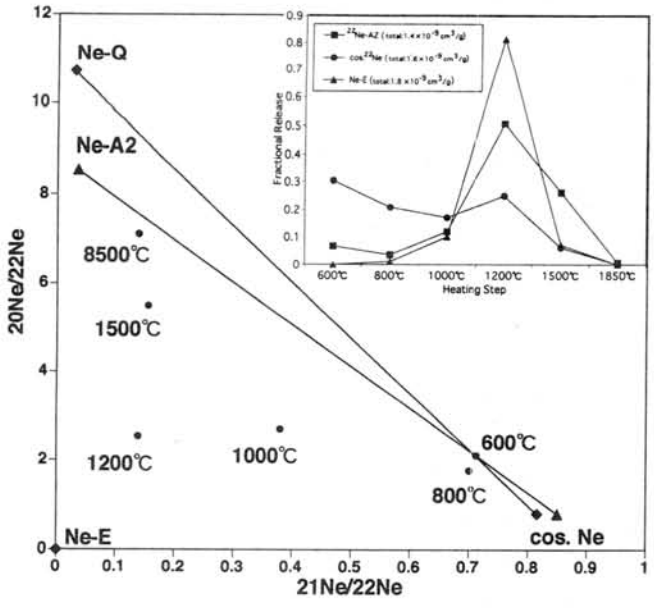

Fig. 2 Three-isotope plot of Ne and releases of Ne components.

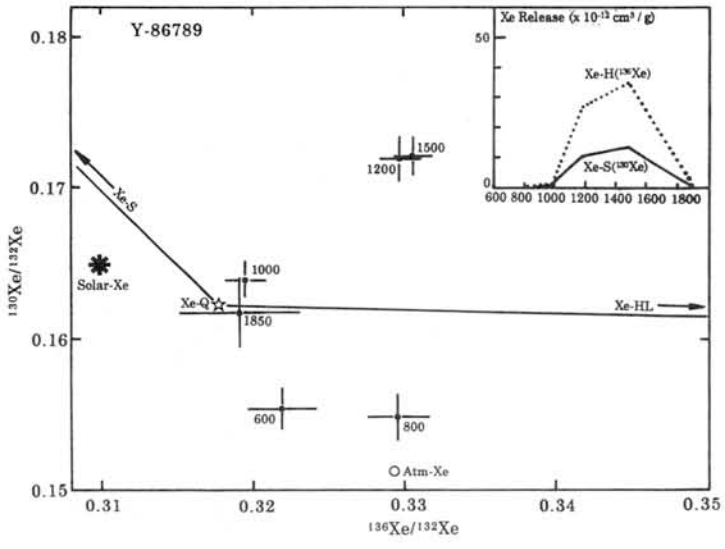

Fig. 3 Plot of $^{130}Xe/^{132}Xe$ against $^{136}Xe/^{132}Xe$, and releases of Xe-S and Xe-HL.

AMS measurement of ^{10}Be and ^{26}Al in deep sea spherules

Hiroyuki Matsuzaki[a], Ugo Zoppi[a], Koichi Kobayashi[a], Satoshi Hatori[a], Mineo Imamura[b] and Hisao Nagai[c]

[a] *Research Center for Nuclear Science and Technology, University of Tokyo, 2-11-16 Yayoi, Bunkyo-ku, Tokyo 113, Japan*
[b] *Institute for Nuclear Study, University of Tokyo, 3-2-1 Midori-cho, Tanashi, Tokyo 188, Japan*
[c] *College of Humanities and Sciences, Nihon University, 3-25-40 Sakurajosui, Setagaya-ku, Tokyo 156, Japan*

Introduction

AMS(Accelerator Mass Spectrometry) is useful for the measurement of cosmogenic nuclides such as ^{10}Be or ^{26}Al in the deep sea spherule because of its small mass(~50μgr). Present status of AMS measurement of the deep sea spherule using 5MV tandem accelerator at RCNST(Research Center for Nuclear Science and Technology), university of Tokyo is reported below.

Sample treatment

Deep sea spherule is a small sphere with 100μm~500μm size found in deep sea sediment. Sizes and weights of collected spherules were first measured. Then buried in acrylic resin, they were polished to make small flat surface. This surface was made mirror surface by using diamond paste for the elemental analysis by EPMA. Fig.1 is the composite image of the section of a typical spherule obtained by SEM. The size, weight and elemental composition of samples are shown in Table.

After EPMA measurement, samples were picked up again from the resin and washed in the supersonic bath with acetone, then put into Teflon beaker added few drops of HF for resolving silicate, HNO_3 and HCl for resolving metal. Finally $HClO_4$ was added for oxidizing remaining HF and Be and Al carrier of proper amount was added. Present status of the measurement limit of AMS system of tandem accelerator of RCNST is $5*10^{-14}$ for ^{10}Be/^{9}Be and $1*10^{-13}$ for ^{26}Al/^{27}Al, which makes the carrier amount kept ~50μgr for Be and ~150μgr for Al. This amount is around 1/5~1/10 of one of usual measurement(Nishiizumi et al., 1991). About 1cc quarts column was used for the cation ion exchange in order to make elemental separation for such a small amount of sample. Be comes out at around the 5th column using 1N HCl. Fe comes out at around the 9th and Al at around 11th if 2N HCl is used from the 8th column.

Separated Be and Al was purified by making precipitation with few drops of NH_4OH. Purified Be and Al was then dropped on the Pt plate, and then ignited at 1000 °C after preliminary heating at 200 °C. For the case of Al, we have still a problem in the purification process. For some samples enough precipitation could not gotten and AMS measurement

was not performed. After ignition, the oxide powder was picked off the Pt plate and pressed with Ag powder into the Cu cathode which is designed to fit the ion source of the accelerator.

Apparatus and basis of AMS measurement

Fig.2 shows the beam line of the AMS measurement system. Oxide of Be and Al pressed into the cathode is sputtered by Cs ion at the ion source to be 1 valency minus ion. At this stage our desirable isotope is in the form of $^{10}Be^{16}O^-$ for the Be case and $^{26}Al^-$ for the Al case, which mass is 26 in both case. While most abundant molecular ion is $^{9}Be^{16}O^-$ and $^{27}Al^-$, mass is 25 and 27 respectively. After accelerated with about 70kV injection voltage, mass 26 is selected by the analyzer magnet 1. For the Al case, the sequencer selects mass 26 and mass 27 sequently by changing the injection voltage with μsec order period. This operation is called as "jumping". The ion selected by the analyzer magnet 1 is accelerated with 5MV at most and injected to the stripper gas(Ar). Changed to atomic plus ion of multiple valence in the stripper gas, the ion accelerated with 5MV at most again. Desired valency ion is then selected by the analyzer magnet 2. In this study 3+ is selected in both Be and Al case. In Be case, ^{9}Be is monitored by collecting $^{17}O^{5+}$ current at the faraday cup set outside the line. In Al case, $^{27}Al^{3+}$ is monitored directly at this faraday cup. Then, the isobar separation is performed with foil(carbon, harver) and N_2 gas layer, i.e., eliminating $^{10}B^{3+}$ from $^{10}Be^{3+}$ and $^{26}Mg^{3+}$ from $^{26}Al^{3+}$. Finally, $^{10}Be^{3+}$ and $^{26}Al^{3+}$ is counted by the solid state detector.

Present status of AMS measurement

Present status of the measurement limit is $5*10^{-14}$ for 10Be/9Be and $1*10^{-13}$ for $^{26}Al/^{27}Al$, which makes the carrier amount kept ~50μgr for Be and ~150μgr for Al. For such small amount of carrier, enough current is not produced so that the statistical precision of the data has not been obtained. Especially for the Al case, there is much space for improvement of the chemical treatment. It is one way to perform more precise measurement to improve the chemical treatment. On the other hand, if the improvement of the measurement limit of the AMS occurs, much more carrier can be used, which will be the great advantage for the chemical treatment. Now, development of the gas ionization detector which has high precision is proceeding.

Measurement data are summarized in Table.

Acknowledgment

We thank very much N. Imae and H. Kojima of NIPR for precious advises for the elemental analyses with EPMA.

References

Nishiizumi, K. et al. (1991) EPSL, 104, 315-324

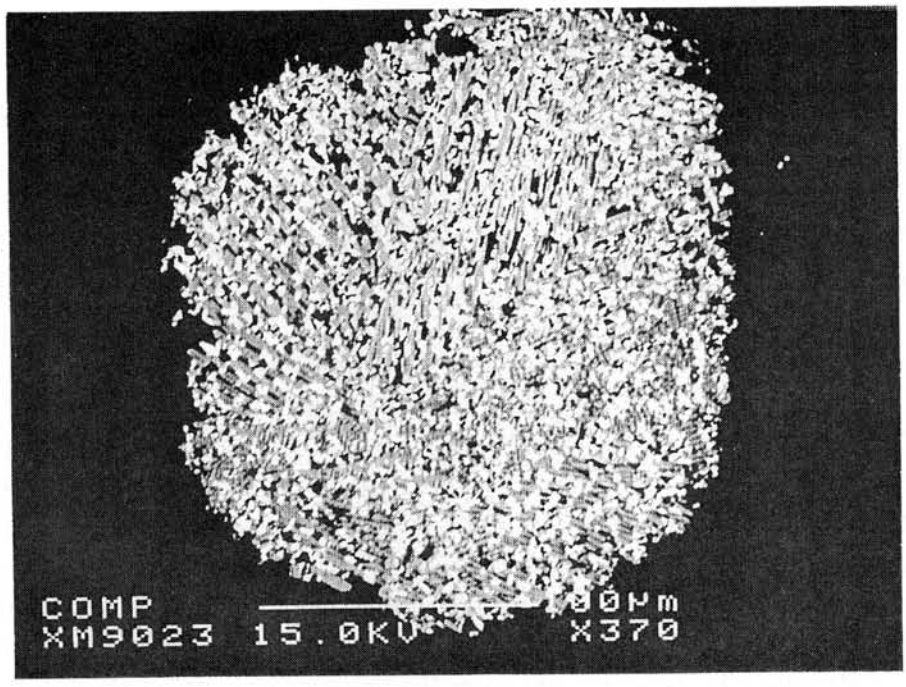

Fig.1 Composite image of the section of a typical spherule

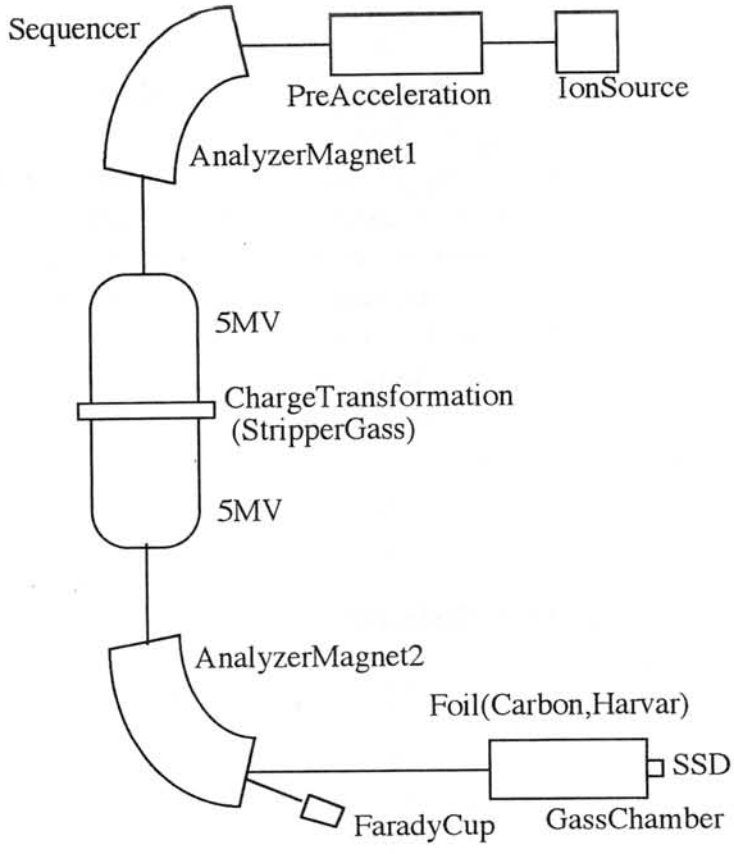

Fig.2 AMS beam line

Table Summary of measurement

Sample Code	Weight (μgr)	Size1 (μm)	Size2 (μm)	Density	Chemical composition(wt.%) Mg	Al	Si	Ca	Mn	Fe	Co	Ni	O	Weight after Polish(μgr)	Be carrier (μgr)	Al carrier (μgr)	10Be (dpm/kgr)
2	125.7	398	385	4.07	2.3	3.39	0.1	0.02	0.02	68.5	0.02	0.01	25.6	125.8	41.9	172.3	7.3 ± 3.9
3	59.6	435	410	1.56	16.5	0.74	25.3	0.68	0.31	10.3	0.02	0.00	46.1	45.9	48.4	145.0	30.7 ± 9.3
4	101.2	435	435	2.35	28.1	0.10	18.4	0.11	0.09	9.8	0.06	0.00	43.3	90.5	49.4	152.6	16.3 ± 4.2
5	139.5	398	373	4.83	0.0	0.30	0.1	0.00	0.04	76.3	0.17	0.04	23.0	119.7	49.8	194.1	11.7 ± 2.9
6	71.5	410	373	2.40	17.8	0.60	14.5	0.26	0.17	26.0	0.06	0.04	40.6	59.8	50.8	146.2	18.0 ± 8.9
7	74.7	410	385	2.35	18.7	0.66	14.6	0.17	0.18	26.2	0.05	0.06	39.4	73.2	47.2	144.0	12.3 ± 7.5
8	56.2	360	348	2.46	25.7	0.13	18.4	0.12	0.07	13.2	0.02	0.06	42.3	50.2	48.3	146.2	19.4 ± 8.5
9	77.2	385	360	2.95	16.4	0.11	23.9	0.12	1.48	14.7	0.04	0.00	43.3	78.3	49.1	145.9	3.4 ± 2.3
10	154.9	398	398	4.71	0.0	0.03	0.0	0.00	0.00	71.3	0.36	5.98	22.4	133.0	42.7	145.2	8.0 ± 2.2
12	72.9	373	373	2.69	20.2	0.20	16.2	0.15	0.20	23.2	0.05	0.41	39.4	66.2	38.5	132.3	1.9 ± 2.4
17	111.1	373	360	4.39	0.0	0.52	0.1	0.01	0.01	75.4	0.50	0.01	23.5	99.5	39.5	184.1	16.1 ± 6.0
18	64.5	360	323	3.28	17.3	0.11	19.0	0.01	0.26	22.3	0.01	0.02	41.0	60.0	42.7	138.9	46.6 ± 13.3
20	40.6	348	298	2.51	18.9	0.38	13.2	0.17	0.16	25.6	0.06	0.04	41.5	26.5	46.1	98.9	26.1 ± 12.2
21	61.6	348	311	3.51	5.3	0.71	6.8	0.25	0.01	56.8	0.60	0.07	29.4	59.8	44.9	139.5	14.4 ± 5.7
23	38.7	410	273	2.41	20.3	0.35	23.2	0.31	0.43	10.6	0.06	0.03	44.7	38.2	50.0	93.4	32.1 ± 9.2
24	35.2	323	311	2.16	13.7	0.84	13.4	0.24	0.20	33.8	0.04	0.04	37.8	35.5	50.1	99.3	33.1 ± 9.9
25	30.9	323	273	2.45	4.5	0.73	12.3	0.16	0.22	27.8	0.10	0.05	54.1	27.1	47.3	95.1	23.8 ± 8.7
26	34.3	335	335	1.74	16.3	0.16	16.8	0.09	0.22	21.1	0.06	0.02	45.3	31.4	40.9	140.3	21.5 ± 7.7
27	94.8	335	323	5.17	0.0	0.25	0.1	0.08	0.01	75.8	0.57	0.09	23.2	90.7	44.3	136.9	11.2 ± 5.4
28	50.9	335	323	2.78	16.2	1.63	17.9	2.43	0.18	21.5	0.04	0.02	40.1	49.9	39.1	95.8	7.8 ± 5.3
29	38.9	323	298	2.59	19.8	0.83	16.7	0.60	0.19	21.4	0.04	0.72	39.7	38.7	44.2	98.3	7.5 ± 5.5
30	42.8	323	298	2.85	17.4	1.18	15.1	0.22	0.16	26.8	0.07	0.96	38.1	42.1	46.6	98.9	2.6 ± 3.9
31	44.6	335	323	2.43	25.9	0.07	18.7	0.10	0.21	10.9	0.03	0.06	44.0	32.9	45.0	99.6	39.8 ± 10.4
33	35.8	348	311	2.04	23.1	0.41	16.4	0.17	0.07	19.1	0.03	0.00	40.8	34.6	47.4	97.2	23.0 ± 9.6
35	25.6	360	298	1.53	18.9	0.96	21.4	1.65	0.26	14.0	0.00	0.01	42.8	24.7	47.8	97.4	19.8 ± 13.6
36	28.9	335	323	1.58	19.9	0.52	16.7	0.41	0.33	22.0	0.08	0.07	40.0	24.3	48.1	96.5	30.8 ± 16.2
37	51.4	379	318	2.55	16.8	0.60	12.6	0.15	0.19	27.8	0.09	1.11	40.6	51.7	34.9	97	1.7 ± 3.0
38	23.0	294	282	1.89	23.7	0.21	15.8	0.13	0.16	19.1	0.00	0.12	40.8	16.5	43.2	68	14.7 ± 12.0
40	22.9	269	245	2.71	18.2	0.30	17.0	0.26	0.23	24.9	0.05	0.00	39.1	20.1	43.5	81	2.5 ± 6.7
54	23.4	306	282	1.84	25.7	0.05	18.1	0.08	0.21	13.9	0.02	0.05	41.9	21.3	36.0	76	17.4 ± 10.4
64	30.1	453	355	1.01	2.9	0.37	7.2	0.21	0.16	46.4	0.16	0.04	42.6	17.1	32.6	77	13.0 ± 12.8

A New Member of Lherzolitic Shergottite from Japanese Antarctic Meteorite Collection: Mineralogy and Petrology of Yamato-793605.

Takashi Mikouchi and Masamichi Miyamoto
Mineralogical Institute, Graduate School of Science, University of Tokyo, Hongo, Tokyo 113, Japan.

Introduction.

SNC (shergottites, nakhlites, and chassignite) meteorites are widely believed to have originated from the planet Mars and so that they have offered valuable information on martian igneous processes [1]. The 18 g small meteorite Yamato-793605 that recently described as a new member of SNC meteorites [2,3] shows a close relationship to lherzolitic shergottites. Shergottites can be divided into two sub-groups, basaltic shergottites and lherzolitic shergottites [1]. Basaltic shergottites consist of Shergotty, Zagami, EET79001, and QUE94201, and while lherzolitic shergottites are ALH-77005, LEW88516, and now Yamato-793605. Discovery of Yamato-793605 has a potential to give us another aspect on petrology of lherzolitic shergottites. Here, we present the preliminary results of our mineralogical and petrological study of Yamato-793605 as a part of the consortium investigation organized by National Institute of Polar Research (NIPR), Tokyo and suggest a petrogenesis of this meteorite.

Samples and Analytical Technique.

Petrographic observations and chemical analyses were made on a polished thin section (PTS) of Yamato-793605 (Y-793605,51-2) supplied by NIPR. Several single pyroxene grains were also supplied, and they were analyzed by a single crystal X-ray diffraction technique (precession method).

Backscattered electron images were taken with a JEOL JXA840 scanning electron microscope with an energy dispersive spectrometer (EDS) (Mineralogical Inst., Univ. of Tokyo). Quantitative wavelength dispersive analyses were performed on a JEOL 733 electron probe (Ocean Research Inst., Univ. of Tokyo) and a JEOL JCM 733 mk II microprobe (Geological Inst., Univ. of Tokyo). Microprobes were operated at 15 kV accelerating voltage, and beam current was 12 nA. In analysis of maskelynite and glass, broad beam of 10 μm in diameter were employed to minimize loss of volatile elements.

Petrography.

The PTS of Y-793605 that we studied is about 9 x 6 mm in size, and it is composed of pigeonite, olivine, augite, maskelynite, chromite and several other accessory minerals (Fig. 1). No Ca-phosphate grain has been identified. Y-793605 is principally poikilitic in texture, but partly contains a non-poikilitic (interstitial) area (Fig. 1). The boundary between them is continuous, but not straight.

In the poikilitic area, a large oikocryst of pigeonite that is larger than 7 mm across encloses rounded olivines and aggregates of chromite. The oikocryst has wide twin bands (~1.5 mm in width) that are partially faulted by intense shock. Irregular extinction of the oikocryst will be caused by a shock effect. The pigeonite oikocryst contains the patches of augite usually around its edge. The patches are irregular in shape and do not follow the specific crystallographic orientations. Olivines in the oikocryst are brown in color and their sizes reach up to 1 mm. They are extensively altered along their rims and interior cracks. Olivine also exhibits undulatory extinction. Chromites are euhedral in texture ($\leq$ 100 μm) and they are scattered in the oikocryst. Maskelynites are rarely observed in the poikilitic area, but small maskelynite grains (up to a few hundreds μm across) are present usually in the augite patches. Some olivines contain rounded magmatic inclusions up to a few μm in size. The inclusion has several unique phases such as Al-Ti-rich pyroxene (both low and high-Ca pyroxenes), K-Si-rich glass, and spinel.

The non-poikilitic area is formed by almost same sizes (~1 mm across) of olivine, interstitial maskelynite and pigeonite. Olivine and maskelynite are more abundant than pigeonite in the non-poikilitic area. Unlike poikilitic area, almost all pyroxenes are pigeonite, and augite is rarely observed. Pigeonite is colorless and usually has well developed two sets of cleavage. Maskelynite in the non-poikilitic area often contains inclusions of pyroxene and several other phases. Maskelynite is distributed mainly near the boundary between the poikilitic and non-poikilitic area. Fe-P-rich phase is also included in the non-poikilitic area. A shock induced melt vein which is about 100 μm in width is cutting the PTS. The vein contains lithic fragments of pyroxenes, olivine, and chromite.

Although Y-793605 is reported to be brecciated [2,3], our PTS does not show such a texture possibly due to a sample heterogeneity.

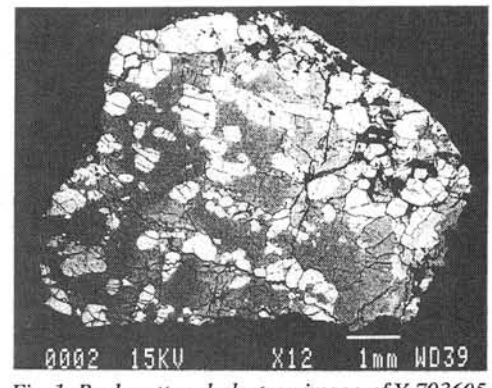

Fig. 1. Backscattered electron image of Y-793605. Note that a poikilitic texture is dominant in the PTS. A non-poikilitic area is observed in the upper right. Whilte: olivine, gray: pyroxene, black: maskelynite.

Mineral Compositions.

Representative chemical compositions of several major and minor phases in Y-793605 are listed in Table 1.

Pyroxenes: The oikocryst of pigeonite is zoned from a Ca-poor composition ($Ca_3Mg_{76}Fe_{21}$) to a little Ca-Fe-rich composition ($Ca_{11}Mg_{66}Fe_{23}$) (Fig. 2). The zoning is coherent and there is little scattering in both Ca and Fe. The structural state of the lowest-Ca pyroxene is unknown. Augite patches in the poikilitic area are also zoned from $Ca_{32}Mg_{52}Fe_{16}$ to $Ca_{37}Mg_{49}Fe_{14}$ (Fig. 2). The equilibration temperature using two pyroxene thermometer [4] gives *ca*. 1150 °C. Pigeonite in the non-poikilitic area is more Ca-Fe-rich than that in the poikilitic area. The composition is scattered in both Ca and Fe comparing with that in the poikilitic area. In many cases it ranges from $Ca_7Mg_{65}Fe_{28}$ to $Ca_{13}Mg_{60}Fe_{27}$ (Fig. 2). It is noted that pigeonite in the non-poikilitic area clearly has higher Ca and Fe composition than that in the poikilitic area. Minor elements further exhibit the difference between the two. TiO_2 in the pigeonite in the non-poikilitic area has higher concentration (0.4~0.9 wt%) than that in the poikilitic area (0.05~0.3 wt%) (Fig. 3). Low-Ti pyroxene from the non-poikilitic area (TiO_2: 0.2~0.3 wt%; Al_2O_3: 0.9~1.1 wt%) is observed (Fig. 3), but there is a possibility that these pyroxenes are from another poikilitic area because they are located near the edge of the PTS and are difficult to identify the textural pattern. Indeed, olivine in this pigeonite has lower Fa content (Fa_{29}) than that in the typical non-poikilitic area. Except for these plots, Al is positively correlated with Ti in pigeonites from both textures. However, there is another trend from high-Ti and medium-Al composition (TiO_2: 0.7 wt%; Al_2O_3: 0.6 wt%) to medium-Ti and medium-Al composition (TiO_2: 0.4 wt%; Al_2O_3: 0.6 wt%) in the pigeonite from the non-poikilitic area. This is because some pigeonite shows unique zoning in Ti. In such pigeonite, TiO_2 once decreases from 0.7 wt% to 0.5 wt%, and again increases to 0.6 wt% from the core to the rim, while Al monotonously increases towards the rim. Cr also shows similar two-trend zoning as Al.

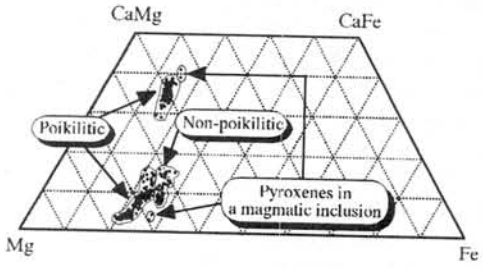

Fig. 2. Pyroxene quadrilateral of Y-793605.

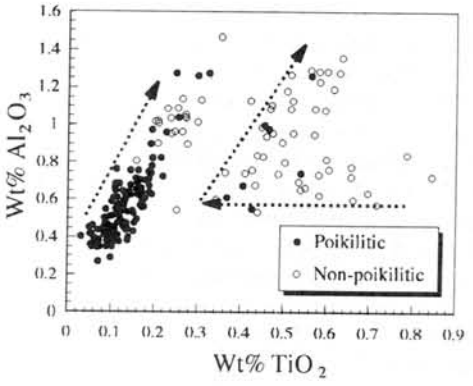

Fig. 3. Al vs. Ti contents of pigeonite in Y-793605.

Olivine: Olivine shows a weak compositional variation from Fa_{26} to Fa_{35}. Olivines in the non-poikilitic area is slightly more Fe-rich (average: Fa_{34}) than those in the poikilitic area (average: Fa_{31}) (Fig. 4). Minor elements show little difference between the poikilitic and non-poikilitic area. CaO contents are nearly homogeneous or show slight decrease from the core (0.3 wt%) to the rim (0.1 wt%). Unlike other achondrites, olivine has up to 0.1 wt% NiO. Olivine is altered around the edge and the crack. Altered portion is rich in Si, K and P, while poor in Fe and Mg. The total sum is generally low (83-89 wt%) presumably due to unanalyzed phases like S.

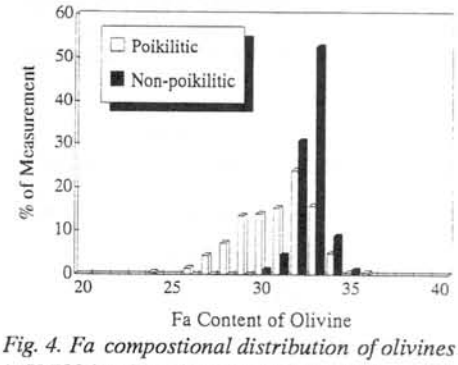

Fig. 4. Fa compostional distribution of olivines in Y-793605 from 300 points of analysis.

Maskelynite: Maskelynite is weakly zoned and it typically ranges from $An_{55}Ab_{44}Or_1$ to $An_{45}Ab_{52}Or_3$. However, the real composition will be more albite-rich due to Na loss during microprobe analysis. FeO and MgO is contained 0.4 wt% and 0.15 wt%, respectively. K increases as Ab content increases.

Chromite: Chromites are up to a few μm in size in both textures and they are euhedral in texture. They also show chemical zoning towards the rim of ulvöspinel-rich component.

Accessory Phases: Ilmenite is a minor constituent, but contains up to 5 wt% MgO and 1 wt% Cr_2O_3. In the non-poikilitic area, the void filled with very fine-grains less than 1 μm is present. Microprobe analyses show enrichment of Fe and P, but the beam must be overlapped. The total sum is extremely low (40~70 wt%). Similar compositional phases are also observed as an isolated lass.

Magmatic Inclusion: The pyroxene in the magmatic inclusion in olivine has high Al (Al_2O_3: ~15 wt%) and Ti (TiO_2: ~3.5 wt%). The low and high Ca pyroxene pair in the magmatic inclusion (Fig. 2) suggests an equilibration temperature of *ca*. 950 °C [4]. However, this temperature is somewhat uncertain due to high Al and Ti contents. Several kinds of Si-rich glass are observed in the inclusions. Some glasses contain about 65~80 wt% SiO_2, 3.5~5.5 wt% CaO, and 3~6 wt% Na_2O, but these have usually less than 0.1 wt% K_2O. Another glass rich in K_2O (>5 wt%) and another whose total is low (~77 wt%) are also observed. Chromite in the inclusion contains ~10 wt% Al_2O_3.

X-ray diffraction study of pyroxene.

An X-ray diffraction photo of a pyroxene single crystal shows diffuse streak of reflections due to a strong shock effect. The photos indicate that this crystal belongs to a monoclinic crystal system. The cell dimensions deduced from reflections on (*hk0*) and (*h0l*) planes give a: 9.4 ±0.2Å, b: 8.88 ±0.15Å, c: 5.28 ±0.1Å, β=107 ±0.5°. Although cell dimensions have large errors due to obscure reflections, these values indicate that this pyroxene is pigeonite.

Implications for Petrogenesis.

It is very interesting that Y-793605 has two distinct textural patterns and shows strong affinities to previously known lherzolitic shergottites ALH-77005 (ALH) and LEW88516 (LEW) in mineralogy and petrology [5,6,7]. Rounded olivines and euhedral chromites are cumulus phases like ALH and LEW. The non-poikilitic area has clearly more Fe-rich pyroxene and olivine. The distinct chemical composition of pigeonite between the poikilitic and non-poikilitic area is also obvious for minor elements. Coherent zoning of Al and Ti in the large pigeonite oikocryst suggests a fractional crystallization in a closed system (Fig. 3) [5]. The volume of the system must be relatively large. Unlike ALH and LEW, Y-793605 rarely contain augite in the non-poikilitic area. This can be explained by onset of plagioclase crystallization instead of augite in the non-poikilitic area. Another possibility is that the poikilitic and non-poikilitic pyroxenes have formed from different magma or by different igneous processes because there is little overlap of chemical composition of both major and minor elements between the poikilitic and non-poikilitic pigeonite. The drop of Ti in the core of pigeonite from the non-poikilitic area (Fig. 3) will reflect co-crystallization of ilmenite, while increase of Ti at the rim will be due to stop of ilmenite precipitation or a larger effect of a small volume of the interstitial liquid. The narrower distribution of Fa content and more Fe-rich content of olivines in the non-poikilitic area (Fig. 4) indicate near-solidus or subsolidus re-equilibration because olivines in the non-poikilitic area would have contact with Fe-rich interstitial melt as proposed for LEW olivines [5]. Olivines surrounded by a pigeonite oikocryst could not have a chance to be highly re-equilibrated.

From many lines of evidence, all three meteorites would follow a similar crystallization history as proposed by [5]. This model can apply to Y-793605. That is, at the first stage cumulus olivine and chromite crystallized. Then, a large oikocryst of pigeonite formed surrounding them. After that, accumulation of these phases occurred. Plagioclase crystallized from an interstitial liquid instead of augite, and formed a non-poikilitic portion. Re-equilibration of cumulus olivine occurred and accessory phases crystallized. The only difference of crystallization sequence from ALH and LEW is that augite did not crystallize in the non-poikilitic area of Y-793605. Augite now observed in the PTS would be exsolved from the host pigeonite in the late stage of the crystallization.

It is difficult to conclude that Y-793605 is paired with ALH and LEW because Yamato-793605 is slightly distinct from ALH and LEW in mineral chemistry. Fe-rich olivine of Y-793605 shows a closer relationship to LEW than ALH [5], while pyroxene composition of Y-793605 almost corresponds to both of them [5,6,7]. Pyroxene equilibration temperature in the poikilitic area is nearly identical to those of ALH and LEW pyroxenes [5,8]. However, Y-793605 has no whitlockite and rare augite in the non-poikilitic area unlike ALH and LEW, and the location of Yamato Mountains is more than 2500 km apart from Lewis Cliff and 3000 km from Allan Hills. Nevertheless, it seems likely that Y-793605 has originated from the same igneous body or rock as ALH and LEW.

Acknowledgment.

We thank Dr. H. Kojima of NIPR for the sample and Mr. O. Tachikawa and H. Yoshida for technical assistance. Discussion with Prof. Takeda of Chiba Inst. Tech. was very much helpful. This work was partially supported by Ito Science Foundation.

References.

[1] McSween H. Y. Jr. (1994) *Meteoritics 29*, 757-779. [2]Mayeda T. K. *et al.* (1995) *LPSC XXVI*, 917-918. [3]Yanai K. (1995) *LPSC XXVI*, 1533-1534. [4] Lindsley D. H. and Anderson D. J. (1984) *Proc. 13th LPSC, JGR, 88*, A887-A906. [5] Harvey R. P. *et al.* (1993) *GCA 57*, 4769-4783. [6]Treiman A. H. *et al.* (1994) *Meteoritics 29*, 581-592. [7]Ikeda Y. (1994) *Proc. NIPR Symp. on Antarctic Meteorites 7*, 9-29. [8] Ishii T. *et al.* (1975) Mineral J. 9, 460-481.

Table 1: Representative electron microprobe analyses (wt%) of major and minor phases in Y-793605

	1	2	3	4	5	6	7	8	9	10	11	12
SiO_2	56.0	54.7	52.0	38.6	54.4	54.0	53.2	36.9	54.7	0.1	44.1	45.6
Al_2O_3	0.3	0.8	1.9	0.0	27.9	0.6	1.1	0.0	27.4	6.6	4.9	9.6
TiO_2	0.1	0.2	0.5	0.0	0.0	0.7	0.6	0.0	0.1	1.1	0.5	3.3
FeO	13.4	14.4	8.9	26.7	0.4	17.0	14.9	29.5	0.5	26.2	18.2	8.8
MnO	0.4	0.5	0.4	0.5		0.8	0.5	0.6		0.4	0.5	0.4
MgO	28.0	23.6	16.7	33.7	0.1	22.9	21.3	32.5	0.2	5.4	23.1	14.0
CaO	1.4	5.6	17.6	0.2	11.7	3.7	7.1	0.2	11.2	0.1	5.3	16.7
Na_2O		0.0	0.2	0.0	5.2	0.1	0.1		5.4	0.1	1.0	0.4
K_2O	0.0		0.0		0.2	0.0	0.0	0.0	0.2	0.0	0.1	0.0
Cr_2O_3	0.4	0.5	0.8	0.1		0.2	0.5	0.0	0.0	58.5	0.6	0.0
V_2O_3	0.0	0.0	0.1	0.0	0.0		0.0			0.5	0.2	
NiO	0.0			0.1		0.0		0.1	0.0	0.0	0.0	
P_2O_5		0.1	0.4	0.1							0.7	0.4
Total	100.0	100.3	99.6	100.0	99.9	100.0	99.3	99.9	99.6	98.9	98.9	99.1
Ca	*2.8*	*11.2*	*36.9*			*7.6*	*14.7*					*38.9*
Mg	*76.6*	*66.2*	*48.7*	*69.2*		*65.2*	*61.3*	*66.3*				*45.2*
Fe	*20.5*	*22.6*	*14.4*	*30.8*		*27.2*	*24.0*	*33.7*				*15.9*
An					*55.0*				*52.9*			
Ab					*44.0*				*45.8*			
Or					*1.0*				*1.3*			

1: Low-Ca pyroxene in the poikilitic area. 2: Pigeonite in the poikilitic area. 3: Augite in the poikilitic area. 4: Olivine in the poikilitic area. 5: Maskelynite in the poikilitic area (core). 6: Pigeonite (Ca-poor) in the non-poikilitic area. 7: Pigeonite (Ca-rich) in the non-poikilitic area. 8. Olivine in the non-poikilitic area. 9: Maskelynite in the non-poikilitic area (core). 10: Chromite in the non-poikilitic area (core). 11. Impact melt vein. 12: Ca-rich pyroxene in a magmatic inclusion.

SHOCKED METAMORPHOSED MATERIALS FROM LIMESTONE BY IMPACTS

Y. Miura and M.Okamoto

Institute of Earth Sciences, Faculty of Science, Yamaguchi University, Yamaguchi, 753, Japan

1. INTRODUCTION

There are two major reported shock metamorphosed minerals of shocked quartz silica and graphite carbon. Both shocked minerals are characterized by existence of high-pressure phases. The detailed characteristics of original shocked minerals reported [1,2,3,4,5,6,7,8] are (a) mixing with crystalline and amorphous grains (i.e. low crystallinity with low X-ray intensity), (b) quenched and rapid-depressed phases from high-pressure phase (i.e. high X ray-density with high Bragg angle, and multiple crystalline structures with major average structure), and (c) mixed textures of vapor-fluid-solid (VLS) wormy bubble or micro-fine structures.

First shocked graphites and calcites are found in the Barringer and Ries impact craters from the ejected shocked materials [3,4,5,6,7,8], though main source of carbon element should be checked as follows:

(a) Main source from meteorite or projectile (i.e. mixed by impact), or

(b) Main source from limestone target-rock (i.e. evaporation by the VLS reaction).

Therefore, shocked graphite carbon should be checked by artificial impact experiment. In order to check carefully, queching material of ice block is used in this impact experiment on limestone target-rock.

2. SAMPLES AND EXPERIMENTAL

Calcite samples from Akiyoshi-dai, Yamaguchi, Japan were used for impact experiment, where ice block of 10x 20x30cm as used to collect fine ejecta with the VLS reaction, and projectile of 1.1 gram poly-carbonate resin (PCR) with Fe-Cu metallic support was used due to make ultra high velocity of impact, 6.59km/sec. The following four samples are collected from impact chamber with ice block (Table 1 and Fig.1).

1) Sample No. 1 : Fine-grained particles formed by impact without hitting to ice-block, designated as 1fp.
2) Sample No. 2 : Quecheed fine ejecta formed by hitting direct to ice block, which were collected by filter papers from carbon with ice or liquid after impact, designated as 2fi.
3) Sample No. 3 : Medium-grained ejecta within the chamber, designated as 3m.
4) Sample No. 4 : Coarse-grained limestone with simple cracking, designated as 4c.

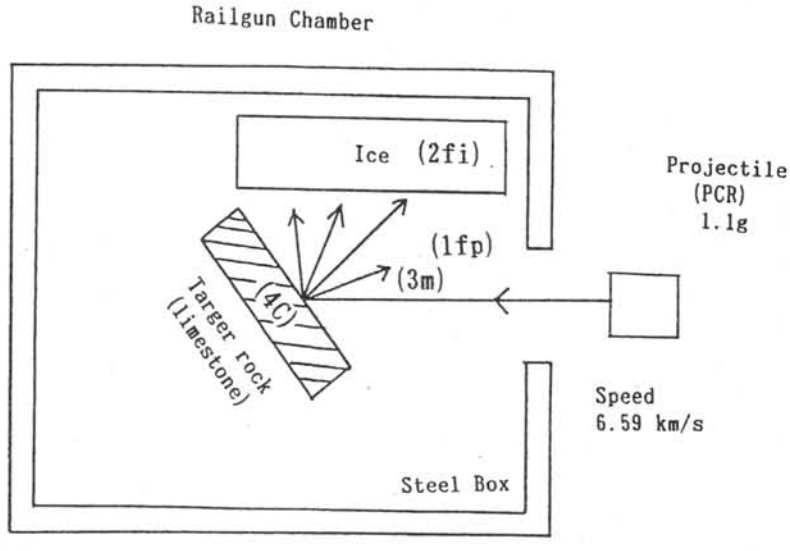

Fig.1. Sample chamber of railgun with ice block for collecting quecheed ejecta (2fi).

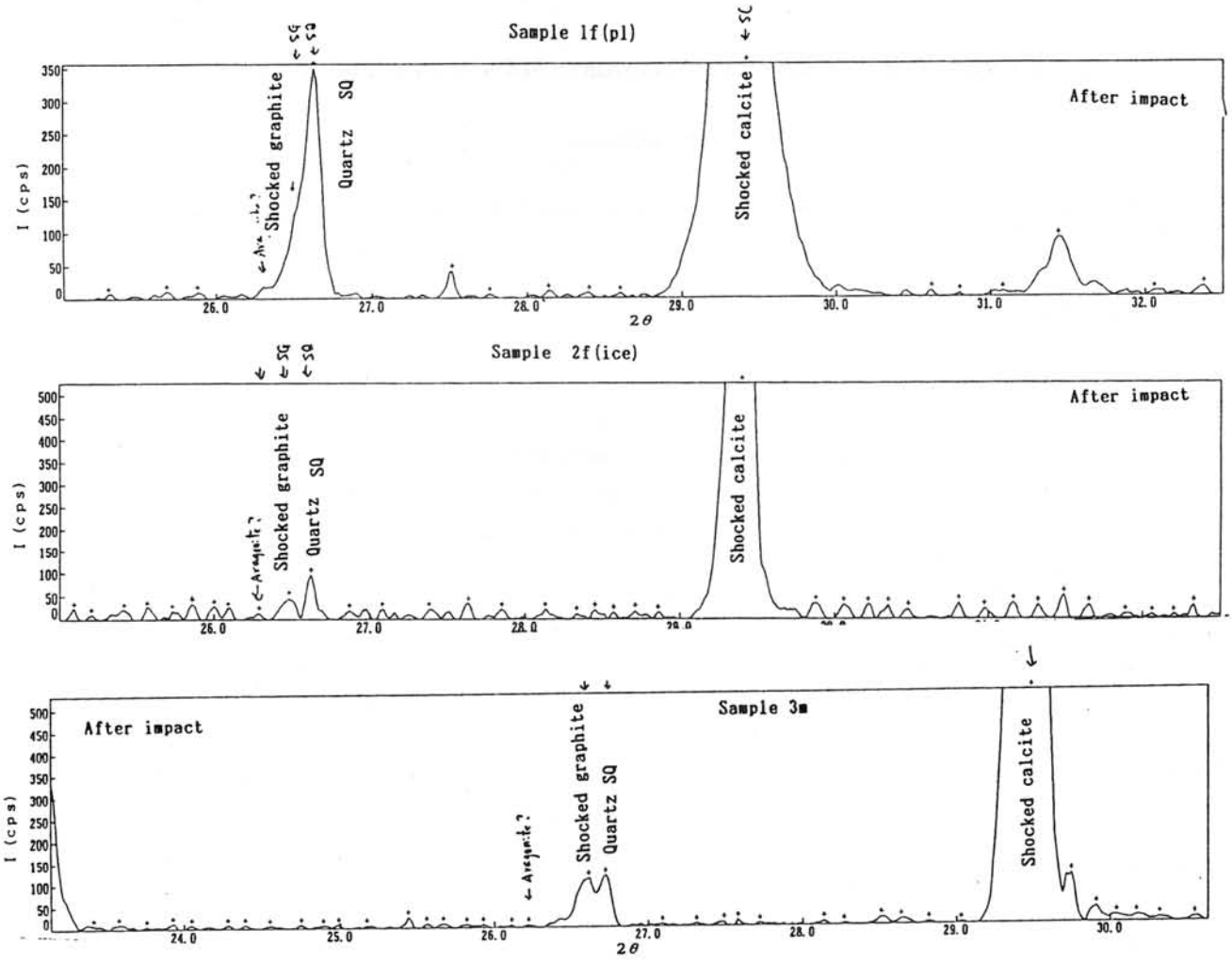

Fig.2. X-ray powder diffraction diagram of samples 1,2,3 and 4 in this impact experiments.

3. RESULTS AND DISCUSSIONS

3.1 Artificial shocked calcite with ice block

From X-ray diffraction data, the following data of calcites are obtained (Table 1):

(1) Sample 3m shows slightly glassy and high X-ray density of shocked calcite.

(2) Fine grains (2fi) collected by ice block show the largest degrees of glass and low-density.

(3) Fine grains (2fp) reveal low density but crystalline.

Table 1. X-ray powder diffraction data of shocked calcites by artificial impacts.

Samples	a (A)	c (A)	V (A^3)	ρ (g/cm^3)	$\Delta\rho$ (%)	I (104)	Remarks
4c (std)	4.991 (1)	16.994 (5)	366.6 (2)	2.720 (1)	----	11772 (I/I_0)	-
3m	4.976 (2)	17.058 (15)	365.8 (5)	2.726 (3)	+0.20 (10)	7396 (63%)	High P
2f (ice)	4.987 (1)	17.044 (4)	367.2 (1)	2.715 (1)	-0.17 (4)	2437 (21%)	High P
1f (pl)	4.988 (1)	17.049 (2)	367.4 (1)	2.714 (1)	-0.23 (2)	4912 (42%)	High T

3.2 SHOCKED GRAPHITE CARBONS AFTER IMPACT

Graphite carbons are confirmed also in this experiment after impact by the following method of confirmation.

(1) Carbon materials from the projectile PCR are found uniformly on all the samples (Nos.1,2,3,4) in closed sample chamber.

(2) Graphite carbons from the PCR and limestone targets can be distinguished from the following equation (cf. Table 2):

(Total graphite carbon from limestone target rock by impact) =
(All carbon content from ejecta) − (Carbon content 1.1 % from the PCR on sample 4c)

(3) Two types of graphite carbons can be checked by the following methods:
(a) Graphite carbon from target rock of limestone contains Ca element by mixing.
(b) Graphite carbon from the PCR projectile contains Cu−Fe metallic elements by impact mixing.

Table 2. Abundances (%) of crystalline shocked materials after impact.

Sample	Calcite (shocked)	Graphite (from ls)	Aragonite	Quartz (inclusion)	Dia./Lonsd.	Chaoite
1f(pl)	90.9%	2.6%(1.5%)	-	6.5%	-	-
2f(ice)	92.7%	1.7%(0.6%)	0.5%	3.6%	0.6	0.9
3m	97.0%	1.4%(0.3%)	-	1.6%	-	-
4c(*)	98.6%	1.1%(0.0%) PCR	-	0.3	-	- [std]

* Calcite of sample 4c is not shocked calcite (i.e. the same as standard calcite).

3.3 DISTINGUISHMENT OF GRAPHITE FROM QUARTZ AND FORMATION OF SHOCKED MATERIALS

Powder X−ray diffractometer data shows two similar X−ray Bragg angles which can be distinguished when quartz silica contains in all the samples to identify X−ray peak of graphite (cf. Fig.2). This method suggests that all impact samples in this experiments contain graphite carbons as follows (Table 3):

(1) The sample 1fp contains the largest content of graphite carbon, which indicates high−temperature condition (without formation of high−pressure type carbons) of reduction state inside of the vapor plume.
(2) The sample 2fi contains high−pressure carbons of diamond/lonsdaleite/chaoite, which indicates high−pressure condition of oxidation state in jetting stream.
(3) The sample 3m contains shocked calcite of high X−ray density with less amount of shocked carbon.

Table 3. Formation condition of shocked graphites by impact materials [4, 7].

Sample	Condition	Remarks
1f(pl)	High temperature (in vapor plume)	Reduction (evaporated carbon)
2f(ice)	High pressure (in jetting stream)	Oxidation (Aragonite, Dia/Lonsd)
3m	Less high pressure (in shocked wall)	Oxidation (High density calcite)
4c	(standard calcite)	No change (Carbon from PCR)

3.4 FORMATION PROCESSES OF IMPACT

The previous interpretation on impact process are only on solid−state reaction as follows:

Solid → (impact) → Solid (by high pressure, or glassy)

The present impact experiments suggest that there are at least three reactions by imapct processes as follows, though these distinct boundaries of three reactions are progressive those.

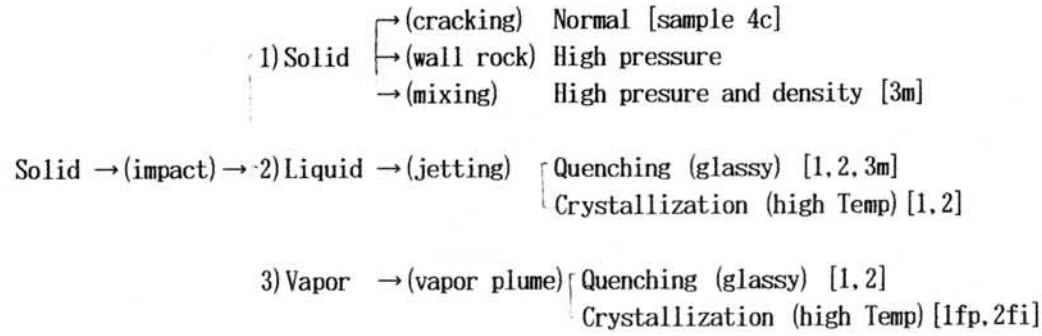

The VLS reaction of impact indicates that solid - states after impact are formed through various states of vapor (to form glassy solid materix after cooling) or liquid (to form glassy or crystalline matrix after cooling). These VLS reaction by impact can be checked by compositional mixing from projectile and target rock after impact [2,3,4,5,6,7,8].

4. SUMMARY

The present results are summarized as follows:

(1) New shocked calcites and graphite carbons after impact on limestone target rock can be confirmed in this impact experiments.

(2) Shocked graphite can be formed by evaporating from the target rock of limestone after impact.

(3) The largest amount of shocked graphites can be obtained in fine sample 1fp, which is reduction and high-temperature condition of vapor plume.

(4) Shocked high-pressure type carbons of diamond-lonsdaleite-chaoite can be formed on quenched icy sample 2fi, which suggests high-pressure and oxidation condition of jetting stream by impact.

(5) Amount of carbons from the PCR projectile can be estimated from carbon amount deposited on original target-rock of limestone. The largest amount of graphite carbon is ca.2% in sample 1fp.

References:

[1] Miura Y.(1991): Shock Waves (Springer-Verlag), 1, 35-41.

[2] Miura Y.(1993): Proc. ISAS Lunar and Planet. Sci.(ISAS, Tokyo), 26, 98-101.

[3] Miura Y. et al.(1994): Proc. ISAS Lunar & Planet. Sci. (ISAS, Japan), 27, 204-207.

[4] Miura Y. (1994): Antarctic Meteorites XX (NIPR), 20, 166-171.

[5] Miura Y. (1995): Proc. 28th ISAS Lunar and Planet.Symp. (ISAS,Tokyo), 28, 53-56.

[6] Miura Y. et al. (1995): Proc. Shock Waves (Springer), 19, 399-410.

[7] Miura Y. (1995): Meteoritics, 30, 550-551.

[8] Miura Y. et al.(1995) : Shock Wave Handbook (Springer-Verlag, Tokyo, 1256pp.), 1073-1176.

[9] Melosh H.(1989): Impact cratering (Oxford University Press, 245pp), 75.

COMPLEX FORMATION OF TAKAMATSU CRATER BY IMPACT

Yasunori MIURA [1] and Takamatsu Crater Investigation Group
1 Faculty of Science, Yamaguchi University, Yoshida, Yamaguchi, 753, Japan

1.INTRODUCTION

Takamatsu crater is recently found as a buried circular structure on wide Rhyoke granitic region of the southern part of Takamatsu City, Kagawa Prefecture, northeast Shikoku, Japan [1,2,3]. Anomalously low value of Bouguer gravity anomaly in systematic gravimetric survey of the Japanese islands is incidentally found in the southern part of Takamatsu City (Fig.1). Kono et al. [1] showed that the crater is ca. 4km in diameter with −10 mgal of gravity anomaly from surrounding Rhyoke granitic region. The sizes and relations of gravity and magnetic anomalies are similar to the previous relations for known terrestrial impact craters [4]. Model calculation of density difference with 250kg/m^3 showed that the depth of crater is ca. 1.4km.

Two shallow boring cores of 160m and 300m deep near small mountains inside the crater for the purpose of undergrandwater projects could not reach the granitic bottom of the crater so far, though 18 shallow drilled cores (up to ca. 160m deep) outside the crater have been reached the granitic basement without any volcanic tuffs. Miura et al. [3,4,5] have been reported that impact−induced materials of Fe, Ni−bearing particles and shocked materials of silica and feldspar are found from xenoliths in Miocene glassy breccias in zeolite rocks around small intruded andesitic rocks inside of the crater.

Recently, CSA·MT (Controlled Source Audio−frequency Magneto−Telluric) method was used to search the structure of the Takamatsu crater [6], which suggests as follows:

(1) low−resistivity layers (10 ～ 100 ohm·m) of "water−bearing materials" are found up to ca.700m,
(2) high−resistivity materials (>1000 ohm·m) are found from the depth of 700m,
(3) there are cracks of the wall rock which are induced by the CSA·MT method.

The purposes of the scientific drilling on the Takamatsu crater planned by the Takamatsu Crater Investigation Group (TIG) are summarized as follows:

(1) The nature of crater structure (depth and size) and filled crater−sediments (volcanic or shock metamorphism) to elucidate meteoritic impact crater by material research.
(2) Transportation process of shock−induced fragments and rhyolitic tuff breccias inside and outside the crater to estimate the origin of meteoritic crater, which is applied to new conception of an impact crater on active Japanese islands as a "time capsule of crustal activity" in the period of formation of the crater.
(3) The nature of materials in the bottom of the crater to explain the magnetic anomaly.
(4) The geological and chemical evidences of Rhyoke granite from xenolith fragments of the crater−sediments and intruded andesitic magma to reveal detailed process of the rhyoke granitization during formation of the present Japanese islands.
(5) Identification of water−bearing materials found by the CSA·MT method.
(6) Collection of old water inside the crater to estimate terrestrial environments including geochemical and biochemical researches.

2. GEOLOGY OF TAKAMATSU CRATER

The surface area of the Takamatsu crater structure is partly covered by Mitoyo−Group sediments of Plio−Pleistocene Epoch (up to 150m deep) to form southern part of the Takamatsu plain, which is intruded by the Sanuki−Group rocks of biotite−quartz andesites of Miocene Epoch (Hiyama and Jissoji−yama) including brecciated rocks of zeolitic rock, andesite, basaltic rocks, volcanic glasses, and glassy gneiss (cf. Table 1). Although the Takamatsu crater is covered by the Quaternary sediments, two types of zeolitic rocks (from volcanic tuff or impact glass) are found around small intrusions of andesites as (a) zeolitic rocks (two types of mordenite, cristobalite, montmorillonite, opal, plagioclases and quartz) with shock−induced materials of silica with halite evaporite in the Hiyama region, and (b) zeolitic rocks of heulandite zeolite and glasses with Fe,Ni−bearing particles and weakly shock−induced silica in the Jissojiyama region (Table 1) [2,3,4,5,7,8].

3. ORIGIN OF TAKAMATSU CRATER

The circular structure in active volcanic islands is considered to be formed by fault−depression, volcanic caldera or cauldron, pipe−like intrusion from the upper mantle magma, or meteoritic impact crater. From surface investigation of the Takamatsu crater, the major model of origin of the Takamatsu crater is volcanic caldera or meteoritic impact crater. The small volcanic intrusions inside the crater are not direct related with cause for large circular structure, because zeolitic rocks around small volcanic mountains of Hiyama and Jissojiyama inside the crater are formed by the same volcanic activities of the Goshikidai andesitic intrusions outside the crater. There are no large pyroclastic flow deposits from the large crater (even in remained rocks or topography) around the surrounding granites out of the crater[2]. There are no high plateau topography and active fault near the crater to be explained by volcanic caldera

Table 1. Geology of the Takamatsu crater, Takamatsu, Kagawa, Shikoku, Japan [5,6,7,8].

Quaternary Period		
Pleistocene Epoch	**Mitoyo-Group**(~ 1.7Ma)	Upper (sediments of clay, sand etc.)
Miocene Epoch	**Sanuki-Group**(11 ~ 14Ma)	Within the crater
	1)Intrusion: B.andesite	1)Biotite-andesite: Hiyama etc.
	2)Quenched glasses near bottom:Jissojiyama(13Ma)	2)Glasses with F,Ni-bearing grain diaplectic minerals. Heulandite.
	3)Filling: Mixed breccias (14.2Ma)	3)Halite, various glasses, mordenite and Fe grains as xenolith.
	Takamatsu crater (>14.2Ma)	Shock materials (Fe-Ni,silica,Feld.)
Cretaceous Period	**Rhyoke Granite** (83 ~ 87Ma)	Balled granite (Basement target-rock)

or cauldron. On the other hand, shock-induced materials of quartz silica and Fe-Ni bearing grains are found around small andesitic intrusions which are transported from deep interior of the impact crater.

4. SHOCKED AND WATER-BEARING MATERIALS IN THE CRATER

The detailed examinations of the anomalous minerals of the brecciated flow mixed rocks which are found at the surrounding rim of andesitic intrusions, are clue to origin of the Takamatsu crater. Anomalous shock-induced fragmental materials are recently found only at the rim of small volcanic mountains (Hiyama: Sample Nos.2,3,6; Jissojiyama: No.15) by examined by polarized and reflected microscopes, powder and single-crystal X-ray diffractometers, analytical scanning electron microscope (AEM) [4,5,7,8] as follows.

(1) ***Fe,Ni-bearing grains*** Black volcanic glassy rocks as xenolith of andesitic intrusion at the Jissojiyama (No.15) contain irregularly Fe,Ni-bearing grains of 10 to 100 μ m in diameter (Fig.1). Chemical composition of the small grains of Fe+Ni varies from ca. 18 ~ 90 atom.% mixed with Si and Al from the major granitic components. Atomic ratios of Fe/Ni are 3.4 to 68.7 which are the similar those of kamacite in meteorite, but differ from those of awaruite (Fe/Ni<0.5) from the deep seated rock of the interior of the Earth [9]. The same tiny Fe-Ni grains can be obtained in the Barringer(U.S.A.), Ries (Germany) and Wolf Creek (Australia) meteoritic craters. The same Fe,Ni-bearing grains could not find in the other volcanic glassy rocks of the Goshikidai or Yashima intrusions outside the Takamatsu crater, though "iron sulfide (FeS)" can be found on the two plateau outside of the crater. Various iron grains are obtained within the crater as follows:

(a) Fe-Ni particles, Fe-Ni rich mixtures of Si-Al-Na-Ca components (in No.15, Jissoujiyama),
(b) Fe-grains (in No.6A, Hiyama), and (c) Fe-Mn particles (in 300m boring core, Funaokayama).

(2) ***Shocked quartz with high-density and/or shock lamellae*** Anomalous quartz grains with high density and shock lamellae are found at Hiyama (Nos.2,3,6 in zeolitic breccias) and Jissojiyama (No.15 in brecciated glasses) as xenolith fragments from the crater sediments. There are two types of shocked quartz as follows:

(a) glassy lamellar fragment of crystalline quartz and glassy silica checked by the AEM which is probably formed during brecciation (followed by volcanic intrusion) after impact.
(b) the other is shocked quartz grains with undulatory anomalous extinction and with a few shock lamellar texture along (102) which is selected for X-ray single diffraction analysis to obtain high X-ray calculated density (density deviation $\triangle \rho = +0.9 \pm 0.3\%$) and lower values (ca.- 0.4%) of each plane-distance of all shock-generated plane deformation features (PDFs). These structural data of high density are the same of shocked quartz grains in the terrestrial impact craters [10,11,12,13].

Materials with low resistivity are considered to be water-bearing minerals of zeolites by the following reasons (cf.Table 2):

(a) Zeolitic rocks are found as mordenite (in Hiyama) and heulandite (in Jissoujiyama) on the outcropes around small intrusions in the crater.
(b) The 300m drilling core contains mordenite zeolites.

Water-bearing minerals of zeolites in the Takamatsu crater are formed by zeolitization from glassy materials of the interior sediments. The same secondary zeolites are also reported from impact melt rock of suevite, Polisinger, Ries impact crater, where water molecules are considered to be taken during formation of lake inside the crater[14]. In fact, water contents of the zeolite are the same both in the Takamatasu and Ries craters, as listed in Table 2. These analytical data of water-bearing minerals indicate that the Takamatsu crater has water lake (or shallow sea water) to form zeolitization after excavating the crater structure.

Table 2. Water contents of zeolite minerals in Ries and Takamatsu craters.

Crater	Sample No.	Water content	Remarks
1) Takamatsu, Japan	a)No.6A(lower,Hiyama)	16.2 wt.%	Glasses+mordenites
	No.6B(upper,Hiyama)	9.4 wt.%	Glasses(+mordenite)
	b)No.15(Jissoujiyama)	18.2 wt.%	Glasses+heulandite
	No.15(Jissoujiyama)	7.7 wt.%	Brecciated glasses
2) Ries, Germany (Oettingen)	a)No.5 (black part)	16.8 wt.%	Suevite glasses
	(white part)	25.4 wt.%	Suevite breccias

5. PROPOSED FORMATION PROCESS

Fine-grained xenolith breccias of Hiyama (No.3) show 14.2 ± 0.7 Ma by K-Ar dating, which are the major crater sediment of middle to upper regions from the CSA·MT method and are slightly "older than age of the Goshikidai activities" outside of the crater. The other glassy breccias with numerous inclusions at the Jissojiyama (No.15) reveal 12.8 ± 4 Ma by K-Ar dating, which the similar age of the Goshikidai activity. The various fragments with anorthite compositions (from An_{0-60} mol.%) are found in the shallow crater sediments. The present results indicate that crater basin structure is considered to be "time capsule" of geological products which consist of balled granite, glassy gneiss and CPX-feldspar-bearing rock transported from different sources outside the crater, and of dacite and Al(61-84)Gr(11-25) andradite-bearing glassy andesite formed after impact event (Table 1).

The present model of the Takamatsu crater from the surface materials, the CSA·MT data and shallow drilling core data indicates as follows:

(1) Meteoritic impact on the Rhyoke granite (before ca. 14.2 Ma). Impact site is probably within or closed to shallow inland sea, which is confirmed by dating data and inclusion of halite grains.

(2) Filling of the crater by transported outside the original crater. Transportation process is supported by balled blocks of various rocks and basement granite without any large volcanic activity (including sulfides), and at least five different orientation and rocks from outcrops within the crater. The crater sediments are time-capsule to keep various products on that period.

(3) Weathering and covering the surface of original crater. The covered layer is confirmed by the Mitoyo-group with ca.180m depth within and around the crater.

(4) Secondary crystallization of crater sediments within the crater. The secondary zeolitization of the crater sediments are formed at "stable buried condition" (without active and progressive volcanism within the crater) as listed in Table 3.

Table 3. Zeolitization of buried crater sediments covered Mitoyo-group in the Takamatsu crater[10,11,12]. Shocked minerals are included to original and altered grains.

Sample No.	Minerals	Remarks
1)Surface exposed samples:		
a)TK-6A-2	a)Mordenite zeolites(37 vol.%)	Altered from brecciated glasses
(lower,Hiyama)	b)Plagioclase feldspar(22 vol.%)	Original and altered products
(lake sample)	c)Quartz (13 vol.%)	Original and altered products
	d)Cristobalite (13 vol.%)	Zeolitization product
	e)Opal (12 vol.%)	Zeolitization product
	f)Montmorillonite (3 vol.%)	Zeolitization product
2)Drilled core samples:		
a)TK-300BC-2	a)Quartz (43 vol.%)	Original and altered products
(Funaokayama)	b)Plagioclase feldspar(23 vol.%)	Original and altered products
	c)Cristobalite (27 vol.%)	Zeolitization product
	d)Mordenite zeolites (7 vol.%)	Zeolitizationproduct

(5) Small intrusions from the bottom of the crater: Small biotite andesitic magma veins are penetrated through cracks of the bottom of the crater (ca.13Ma ago). Various fragments from the crater interior of balled granite, glassy gneiss and anomalous altered glasses with shock-induced materials are found around the small intrusions. Zeolite minerlas of heulandite (or clinoptilolite) found near the Jissoujiyama are different from the buried zeolitization products of the crater interior, which are formed by hyrothermal alteration of small volcanic intrusions (Table 1) [4,5,7,8].

6. SIGNIFICANCE OF TAKAMATSU CRATER

Among 22 buried impact craters from 141 reported impact craters reported on the large and stable continents of the Earth [4,12,13], four impact craters of the Manson, Vredefort, Sythylemenkat Lake and Sudbury are intruded by volcanic or plutonic rocks along the cracks after impact, which are used to be checked by deep drilling cores finally.

However, there are few meteoritic impact craters on active volcanic islands or coasts, because original meteoritic impact craters are completely broken or buried by crustal evolution of subduction, volcanism or earthquake. Only survived case for impact crater in active islands is considered to be formed on wide and rigid basement rock of granite (ca. 100km widein the Takamatsu crater). Due to drilling project of the Takamatsu crater in future, the following scientific affairs are significant for the earth science field:

(1) To make clear the first impact crater in active orogenic area of the world.
(2) To study size and formation age of the crater is determined finally by detailed projects of the CSA·MT method and deep drilled cores.
(3) Source and transportation process of the crater sediments can be discussed in detail on the buried crater.
(4) From proposed mixed crater sediments of shock-induced breccias, glassy gneiss, andesite, basaltic rock, zeolitic breccias, gabbroic glassy rocks, foreign granitic rock, sanukite-like rock and cpx-feldspar-bearing, geological environments of the filling the crater sediments with various xenoliths and secondary minerals can be discussed in detail.
(5) Zeolitization from impact melt glasses can be confirmed by craters and laboratory experiments.
(6) Crater sediments in the bottom to explain magnetic anomaly are obtained and determined finally.
(7) Impact craters found on extraterrestrial bodies of the Moon and the Earth-type planets can be investigated for development of the Earth and Planetary Science at near active orogenic area of Japan on the Earth.

7. CONCLUSIONS

The main results of the complex formation of the Takamatsu crater can be summarized as follows:

(1) Anomalously low values of Bouguer gravity gravity anomaly (-10mgal) showing circular basin structure with ca. 4km in diameter(designated as Takamatsu crater) are confirmed by the CSA·MT method with low resistivity layer (water-bearing materials of zeolites) and granitic basement. The calculated structure of the Takamatsu crater is considered to be an impact crater.
(2) Meteoritic impact of Takamatsu crater is confirmed by existence of tiny of Fe,Ni-bearing grains and shocked quartz with high X-ray density as xenolith or brecciated fragments in altered sediments or glassy intrusions within the crater.
(3) Meteoritic impact site on the Rhyoke granite (before ca. 14.2 Ma) is probably within or closed to shallow inland sea, which is confirmed by dating data and inclusion of halite grains.
(4) Transportation and filling processes of the original crater are supported by balled blocks of various rocks and basement-granite without any large volcanic activity. The crater sediments as time-capsule consist of various geological products on that period.
(5) Secondary crystallization of crater sediments within the crater are formed at stable buried condition (without active and progressive volcanism within the crater) of buried metamorphism in mordenite zeolites, which suggests stable buried crater of impact origin.
(6) Small intrusions of andesite from cracks of the crater have various-source fragments as xenolith from the interior of the crater, together with hydrothermal product of heulandite zeolite.

REFERENCES

[1] Kono, Y.et al.(1994): ISAS Lunar and Planetary Symp., 67-70.
[2] Sato, H. (1982): Sci. Rep. Kanazawa Univ.,Japan, 27, 13-70.
[3] Miura,Y. et al.(1994): Seismol. Soc. Japan-1994, 73. Volcano. Soc. Japan.
[4] Hodge,P.(1994): Meteorite Craters & Impact craters of the Earth (Cambridge Univ. Press), 124 pp.
[5] Miura,Y. et al.(1995): Lunar. Planet. Sci. XXVI (LPI, Houston), 987-988.
[6] Takamatsu City Publication (1996): Report on grandwater in Takamatsu crater(Japanese). 71pp.
[7] Miura,Y. et al.(1995): Antarctic Meteorites XX (Japan), 20, 163-165.
[8] Miura,Y. et al.(1995): Meteoritics (U.S.A.), 30(5), 551-552.
[9] Miura,Y. et al.(1981): Contrib. Mineral. Petrol., 76, 17-23.
[10]Miura,Y.(1991): Shock Waves (Springer-Verlag, Heidelberg), 1, 35-41.
[11]Miura,Y. et al.(1992): Shock Wave Proc.(Springer-Verlag), 18, 403-407.
[12]Miura,Y. et al.(1995): Shock Waves (Springer-Verlag), 19, 399-404.
[13]Grieve,R.A.F. et al.(1988): Lunar Planet.Inst. Technical Report (LPI, Houston), No.88-03, 89 pp.
[14]Chao,E.C.T.et al.(1978):Principal exposures of the Ries meteorite crater in Soutjern Germany (Muenchen, 84pp.), p.62.

FORMATION OF QUASICRYSTALLINE AND NEW-TYPE MATERIALS BY IMPACTS

Yasunori MIURA, Makoto OKAMOTO, Hiroyuki KOBAYASHI, Gabor KONDOROSI, and Seijiro FUKUYAMA

Institute of Earth Sciences, Faculty of Science, Yamaguchi University
Yamaguchi 753, Japan

1. Introduction

The main projects of planetary and material sciences are divided into three items:
(1) to find new materials,
(2) to check the interior structure of planets, and
(3) to develop expedition technology.
Among these projects, new materials on the Moon and Astroids are classified into three types of materials:
(1) New minerals on the extraterrestrial Moon and Asteroids without atmosphere.
(2) Shocked materials formed by mixing with planetary target-rocks and projectile of meteoroids.
(3) Completely new materials of quasicrystals [1,2].
The main purpose of the present paper is to discuss new materials of quasicrystals on the Moon and Asteroids expected in the next sample researches.

2. Shocked crystalline-materials

There are three types of shocked materials as follows [3]:

(1) Shocked graphite (carbon element) found near impact craters of carbon-bearing target rocks,
(2) Shocked quartz (silica molecule) found also at impact crater of silica-bearing target rocks,
(3) Shocked calcite (calcium carbonates) found at impact crater of limestone,
(4) Shocked iron (iron element with Ni, Co) found at impact crater hitted by iron meteoroids.

Among them, shocked iron and quartz silica will be found on the Moon and Asteroids, though shocked graphite and calcite materials are difficult to find them because target rocks of limestone- and carbon-bearing rocks are minor or trace on the Moon and Asteroids. Compared with air planets of the Earth, Mars and Venus, airless planetary bodies of the Moon, asteroids, and Mercury are expected to find more shocked materials on these surfaces.

3. New-type minerals on the Moon

New minerals on the Moon are included new (terrestrial) minerals and newly-found mineral on the Moon. Only 21 kinds of minerals are reported previously on the Moon as major and reliable minerals. This suggests that the Moon is completely waterless environments without thick atmosphere. This interpretation does not accept the presence of water-, OH-, volatile-bearing minerals on outcrops of the Moon, though there are many reports or suggestions of these anomalous minerals on lunar rocks.

However additional 40 kinds of new-type minerals will be found on next expedition of the Moon (cf.Table 1), where the following anomalous minerals are included [4]:

(1) lawrencite ($FeCl_2$) and goethite (FeOOH) of rusty rock 66065 (impact melt rock).
(2) iron-nickel (with trace Si, Ti, Cr) of 10058, 12021, 10085.
(3) Recrystallized minerals of amphibole, biotite and muscovite (OH-bearing those on the Earth) of 10058, 12021, 14163, where OH-molecules can be replaced by Cl- or F-elements.
(4) Carbides of cohenite (in 14003, 68501, 66095), and Al-C (no name; in thin section 863,Luna 20).
(5) Carbonates of basalt 10058, and soil 66081.
(6) Composite metals of Cr-Fe (norite 62295), Cu-Ni-Zn (basalt 10045, 12040, 14053), Cu-Zn-Sn (breccia 12013), Sn-Ni (soil 10084), Ni-Fe-Co (basalts 12022, 12004, soil 12003), Cu-Ni-Zn-Fe metal (basalts 12022, 12004), and indium metal (basalt 12040).
(7) Graphite C (in soil 10085).
(8) Various sulfides of mackinawite 812018, 12063), pentlandite (basalt 10072, breccia 14315), chalcopyrite (basalts 12021, 15475), cubanite (basalt 12021), bornite (soil 68841), talnakhite (basalt 12018), sphalerite (basalt 12018, breccia 66095), and niningrite (soil 15602).

Although these minerals are considered to be formed on the Earth as terrestrial contaminations, these anomalous minerals with volatile elements are considered in this study to be formed by vapor-liquid-solid (VLS) reaction or relic compositions from meteoritic minerals in impact process on the Moon.

Numbers and kinds of the reported lunar minerals are significant to check origin and evolution of the Moon: In fact, oxides of the lunar rocks (26%) are much more than those of high meteoritic minerals (18%), compared with silicates (on the crust of the Earth). The fact that variety of minerals suggests origin and evolution of planetary surfaces suggests that the Moon is not largely evolved as following interpretations (Table 1):

(1) lunar bulk composition is caused by giant impact processes between bulk materials of mantle region (i.e. oxides-rich region) and Mars-sized parent-body (i.e. mantle-rich region).

(2) lunar bulk data are secondary bulk those formed by multi-stage impacts with vapor-liquid-solid (VSL) reaction [5,6].

Origin and evolution of the present Moon should be analyzed by the consideration of compositional changes after impact processes (by the VLS reaction) [5,6].

4. OH- or volatile-bearing minerals on the Moon

The main reason why lunar rocks from the waterless Moon do contain OH- or volatile-bearing minerals is summarized as follows:

(1) Relic compositions from meteoritic origin: It is considered that carbon, carbites, carbonates and OH-, or volatile-bearing new-type minerals are mainly supplied from carbonaceous chondrites or comets on the airless Moon. Metallic and sulfides are also relic minerals of chondritic or iron meteoroids (cf. No name of meteorites on the Moon because there are no original stone and no effects by atmosphere to make fusion crust. Term of meteoroids or meteoroids can be used on the Moon).

(2) Reaction products of the impact VLS or solar-wind reactions:

(a) Composite metals, chlorides, phosphates and carbites might be formed by the VLS reaction of impact processes on the Moon.

(b) OH-bearing minerals of goethite, amphiboles and micas might be complex reaction processes of oxygen and volatile vapors from the VLS reaction, or oxide-reduction by the solar wind, and hydrogens from solar winds.

(c) The interior of lunar basalts might contain the impact products of new-type minerals due to its mixing during uplift process from the bottom to form the lunar maria.

These three processes are difficult to find on the Earth, mainly because The Earth has thick atmosphere to cut the solar-wind flow and OH- or volatile-bearing meteoroids as projectiles to make fresh meteoritic impact craters on the Earth. This is the main reason why we can collect new-type minerals (esp. impact VSL products by meteoroids and solar-wind) on the Moon.

Numbers and kinds of meteoroids (or meteorites) are similar to those of the Earth (from total data of many and various fragments of the meteoroids), but are diffrent from those of the Moon.important to check the Moon evolution (cf. Table 1). This indicates that meteoroids of collision fragments from planetesimals are originally from asteroids belt formed by various planetesimals with various evolution processes.

5. New minerals on Asteroids

Although numbers and variety of the present lunar minerals are limited in the previous sample collection (cf. Table 1), variety of meteoritic minerals, 149 kinds, is 2.5 times of lunar minerals [4,5]. This suggests that meteoroids are various fragments of various evolved planetesimals, which are proved by various types of real samples of meteorites on the Earth, and of reflectance spectroscopy from the Earth.

The following new-type minerals on various asteroids are expected to collect in the next sample expeditions:

(1) Composite metals including quasicrystals (formed by metallic impacts on the surface),

(2) New-type metals of transition and Pt-group elements,

(3) Carbons, carbites, carbonates, hydrates, OH-or volatile-bearing minerals, phosphates and sulfide minerals.

6. Quasicrystals

Quasicrystalline materials are considered that the first idea was designed by astrophysian (Professor Staeinhard) in 1984 [4], and thst those are one of the greatest founding in this century in material science fields expalined as follows [4,7]:

(1) Third materials (not crystal or amorphous glass).

(2) Anomalous rotation symmetry (5-fold axis) forbittened in crystalline materials.

(3) Giant molecular structure with high-order dimensions structure (not twin or glass).

(4) New physical properties (esp. strong and hard, variety, low thermal electric conductivity and high thermal escape ratio).

Although new materials of quasicrystals are artificial inorganic materials so far, but there are many connection with natural planetary materials because of similar formation conditions with between artificial (CVD) and impact process (including the VLS condition).

Table 1. Materials on the Moon and Asteroids of various type minerals [4,5].

Minerals	Major lunar minerals (reported)	New-type lunar minerals (reported or expected)	Minerals on Asteroids
Silicates	7 (33%)	11 (Amphibole, mica etc.) 30%	52 (35%)
Oxides	10 (48%)	6 (Ti-oxides and others) 26%	27 (18%)
Sulfides	*1	*8 (Many metallic sulfides)15%*	25 (17%)
Metals	1	*5 (Alloy, quasicrystals)	5
Carbonates	0	*2 (Calcite, dolomite)	5
Carbites	0	*3 (Cohenite, Al_4C_3)	2
Hydrates	0	*1 (Goethite)	1
Phosphates	2 (10%)	*3 (Whitlockite,monazite)	13
Chlorides	0	*1 (lawrencite)	1
Others	0	0	18
Total	21	40	149

* Minerals formed by impact processes of meteoroids or solar-winds. These impact materials are secondary those which are different from original bulk compositional data on the Moon.

7. Relation of shock formation of quasicrystals on the Earth, Moon and Asteroids

There are many similarity with quasicrystals and shocked materials as follows:

(1) Plasma arc spraying synthesis:
Synthesis of vapor-liquid condition (CVD) is similar to the formation methods of quasicrystal. The same The CVD condition has been **firstly** indicated on the CVD diamond-shaped carbon-Fe metallic materials found at the Barringer meteorite crater, U.S.A. [8]. Thus same vapor-mixing VLS process is really existed on iron-meteorite impact crater. Quasicrystal coatings are artificially applied by plasma arc spraying method.

(2)Fine-grained materials: Fine-grains of 10 μ m order are characteristics of impact processes with ejection.

(3)Multi-phase mixture: Multi-phase mixtures are found on impact processes with short time and vapor-VLS condition.

(4)Siderophile elements: These elements are contained in iron-meteorites and found near meteorite impact craters on the Earth and the Moon.

(5)Airless parent bodies: there are much more chances of impact mixing and shock metamorphism with large scale, especially on the Moon and Asteroids.

Metallic mixtures are not found clearly on Astroids so far. However, airless Moon with much more various impact craters should have anomalous mixture of matallic materials (including quasicrystalline materials, QC). In fact, the following metallic mixtures reported by the NASA Apollo projects are really found, though these data are only on composition (by EPMA) and/or structure (by X-ray diffraction). Electron microscopic (TEM) data should be expect-ed to check whether these are quasicrystals or not, though it is very difficult to pick up only the QC grains coated by other metallic matrix.

In fact, unknown new-type materials (mainly metallic compounds so far) are reported on the Apollo-mission projects as follows [4]:

(1)Cu-Zn-Sn metals: on 10044, 10017, and 12013 lunar samples.
(2)Cu-Ni-Zn-Fe metals: on 12004, 12022, and 14053 (mainly Cu-Fe).
(3)Fe-Ni metals: on 14001, 14161, 14262, and 14258.
(4)Cr-Fe metals: on 62295.
(5)Ni metals: on 12022, 12004, and 12003.
(6)Sn metals: on 10084.
(7)Vapor-mobilized elements: on 66095.

These metallic composite samples are required to check whether these are the QC or not.

8. Giant molecules in the Solar System bodies

The following giant (or multi-) molecules are considered to be existed in the parent bodies of the Solar System including on the Earth:

(1) Water (on the Earth, Mars, some icy satellites and the Asteroids),
(2) silica 3-D framework (on the Earth-type planets and the Asteroids),
(3) zeolite (on the Earth),
(4) quasi-crystals (by artificial products sor far),
(5) fularen (on the Earth and Asteroids),
(6) mixture of organic and inorganic compounds (on the Earth and Asteroids), and
(7) Ring (and oligomer-polymer) organic compounds (on the Earth and Meteoroids)[8].

These giant molecules are significant to various fields of planetary science, biosciences, advanced material sciences, and resource sciences in future.

9. Summary

The followings are summary in this study:

(1) On airless Moon and asteroids, new tyep materials of new minerals, shocked materials and quasicrystals are expected to find.
(2) Shocked materials are simple compounds of carbon, silica, iron and calcite which have high-pressure phases and dynamic formation of the Vapor-Liquid-Solid (VSL) reactions.
The CVD condition has been **firstly** indicated on the CVD diamond-shaped carbon-Fe metallic materials found at the Barringer meteorite crater, U.S.A. [8]. Thus same vapor-mixing VLS process is really existed on iron-meteorite impact crater.
(3) New types of minerals are considered to be carbon-bearing compounds, Ti-bearing oxides, Fe-bearing compounds, and Ca-Si-Fe-bearing compounds.
(4) Quasicrystals (QC) are expected to exist largely in the fine-grained ejecta near meteorite impact craters. Thus one of the purposes to return to the Moon and to go to the Asteroids is to collect quasicrystalline materials.

Acknowledgments

Authors thank the NASA-JSC for preparing Apollo project documents, and Professor H.-U.Nissen, ETH, Switzerland for discussion on quasicrystals in our laboratory as invited lecture.

References

[1] D.Shechtman et al. (1984): Phys. Rev. Lett., 53, 1951-1953.
[2] T.Ishimaru, H.-U.Nissen and Y.Fukao (1985): Phys. Rev. Lett., 55, 511-513.
[3] Y.Miura (1991): Shock Waves, 1, 35-41.
[4] J.W.Frondel (1975): Lunar Mineralogy (J.Wiley & Sons), 1, 18-40.
[5] Y.Miura (1995): Proc. ISAS Solar System Symp. (ISAS), 17, 4pp. (in press).
Y. Miura et al. (1995): Shock Waves Proc.(Springer),19, 399-410.
G.Gevay (1995): Antarctic Meteorites XX (NIPR), 20, 69-71.
[6] Y.Miura et al.(1996): Proc. Shock Waves (Caltec,U.S.A.), 21, 6pp. (in press).
[7] J.F.Kerridge and M.S.Matthews (1988): Meteorites and Early Solar System (U.Arizona Press), 1, 1189-1190.
[8] Y. Miura (1993): Proc.ISAS Solar System Symp.(ISAS), 15, 48-51.
Y. Miura et al.(1993): Shock Waves Japan-1993, 193-196.
Y. Miura (1994): Antarctic Meteorites (NIPR), 19, 122-125.

Noble gas elemental and isotopic studies on pallasites

Yayoi N. Miura[1], Keisuke Nagao[2] and Naoji Sugiura[3]

[1] Earthquake Research Institute, University of Tokyo, Bunkyo-ku, Tokyo 113, Japan.

[2] Institute for study of the Earth's Interior, Okayama University, Misasa, Tottori 682-01, Japan.

[3] Department of Earth and Planetary Physics, University of Tokyo, Bunkyo-ku, Tokyo 113, Japan.

Introduction Although noble gases including Kr and Xe in the pallasite Brenham have been studied in detail (*e.g.*, [1, 2]), only a small number of data has been reported for the other pallasites. Trapped noble gas component as well as production rates of cosmogenic noble gases in pallasites are still one of questions to be clarified. Our previous studies on the Brenham [1] showed that silicate phases might contain primordial Xe with isotopic ratios similar to those of U-Xe and that they have wide variation in cosmogenic noble gas concentrations more than two orders of magnitude. In order to investigate relationship between the Brenham and other pallasites, we carried out noble gas analyses for some other pallasites as well as the Brenham employing total fusion and stepwise heating for noble gas extraction.

Samples and experiments The analyzed pallasite samples and number of analyses are Brahin (5 analyses), Brenham (2), Esquel (2), Huckitta (1), Imilac (1), Mt. Vernon (2) and Somervel County (1). One analysis of Brahin was for metallic phase, and the others for silicate phases. Sample weight used in each analysis was from 0.2 g to 1.7 g. Silicate and metallic phases were mechanically separated from bulk samples. Magnetic fractions in silicate phases were removed by hand magnet. Some of the silicate samples were treated with HCl or HNO_3, and the metal sample was with HF. Noble gases have been analyzed at ISEI, Okayama University using the typical way applied to meteorite analyses (*c.f.*, [3, 4]). The silicate samples wrapped with Al-foil were heated in a Mo crucible and an alumina crucible was used for the metallic phase (*c.f.* [2]). Extracted noble gases were purified by Ti, Zr getters, and were separated into four fractions; He-Ne, Ar, Kr and Xe, which were analyzed on a modified-VG5400 mass spectrometer. Typical blank levels at 1850°C throughout the analyses are $(2\text{-}3)\times10^{-10}$, $(1\text{-}8)\times10^{-12}$, $(1\text{-}10)\times10^{-9}$, $(3\text{-}10)\times10^{-14}$, $(5\text{-}20)\times10^{-15}$ cm^3STP/g for ^4He, ^{20}Ne, ^{40}Ar, ^{84}Kr and ^{132}Xe, respectively.

Results and discussion Isotopic compositions of He and Ne indicate that they are mostly composed of cosmogenic He and Ne. On the other hand, Ar is a mixture of cosmogenic and terrestrial atmosphere-like Ar. Small excesses in radiogenic ^{40}Ar are, however, observed in lower temperature fractions of the Brahin, Brenham and Somervel County, which is shown as the data points plotted above the mixing line in Fig. 1.

For Kr and Xe, trapped noble gas components are dominant, and a small amount of cosmogenic noble gas component was observed. Enhancement by the cosmogenic products is noticeable in only the light isotopes, ^{78}Kr, ^{80}Kr, ^{124}Xe, ^{126}Xe and ^{128}Xe. No significant contribution of cosmogenic or fissiogenic components was found in heavy isotopes. A plot of $^{134}Xe/^{132}Xe$ versus $^{136}Xe/^{132}Xe$ for the measured pallasites is given in Fig. 2. Because most of the data are plotted around the terrestrial atmospheric Xe, the Xe could be originated from adsorbed terrestrial atmosphere. This is supported by the elemental compositions of trapped Ar, Kr and Xe, which range within a trend for elemental fractionation of the atmospheric gases. On the other hand, some data points of Brahin and Brenham are plotted away from the terrestrial atmospheric Xe beyond experimental errors. Similar isotopic ratios have been found in the previous analyses of several specimens from the Brenham [1]. Xenon isotopic compositions of them are rather similar to those of Solar Xe or U-Xe. The elemental compositions of Ar, Kr and Xe, however, fall near the Earth-Mars trend on a plot of $^{36}Ar/^{132}Xe$ versus $^{84}Kr/^{132}Xe$ [5], implying no significant contribution of solar noble gases if heavy elemental fractionation did not occur. In any case, our Xe data indicate a presence of some Xe component in addition to the atmospheric Xe, though it is difficult at present to clarify the component.

Acknowledgments: This work was supported by Grant-in-Aid for Scientific Research of the Ministry of Education, Science and Culture of Japan.

References: [1] Nagao K. and Miura Y.N. (1995) *20th Symp. Antarct. Meteorites*, 174-175 (Abstr.). [2] Nagao K. *et al.* (1996) *21th Symp. Antarct. Meteorites* (Abstr.), this volume; Honda M. *et al.* (1996) *21th Symp. Antarct. Meteorites* (Abstr.), this volume. [3] Nagao K. *et al.* (1995) *Proc. NIPR Symp. Antarct. Meteorites* **8**, 297-303. [4] Miura Y.N. *et al.* (1995) *GCA* **59**, 2105-2113. [5] Nagao K. (1994) *Proc. NIPR Symp. Antarct. Meteorites* **7**, 197-216.

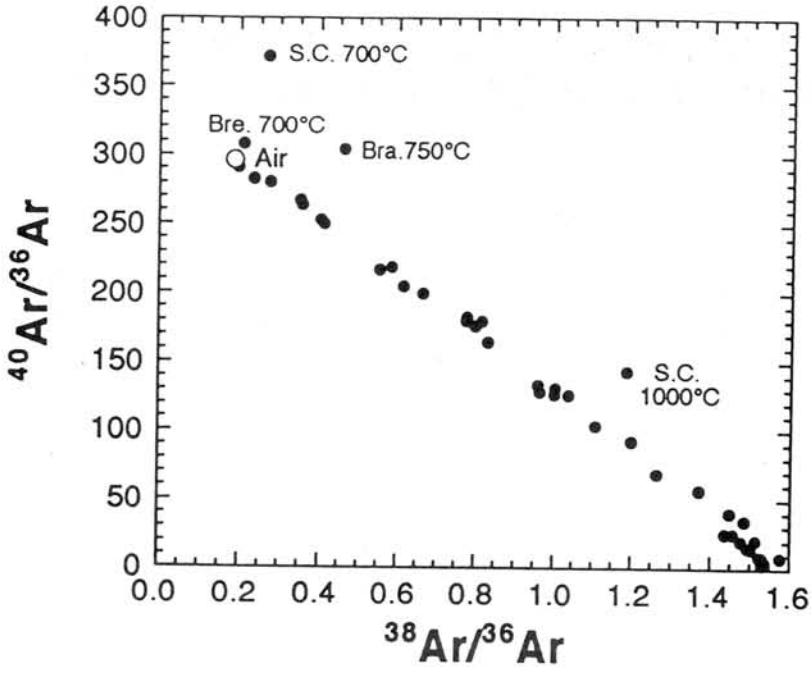

Fig. 1. Plot of $^{38}Ar/^{36}Ar$ versus $^{40}Ar/^{36}Ar$ for the measured pallasites. Argon in the pallasites are mixtures of cosmogenic and terrestrial atmosphere - like components partly accompanying with radiogenic ^{40}Ar.

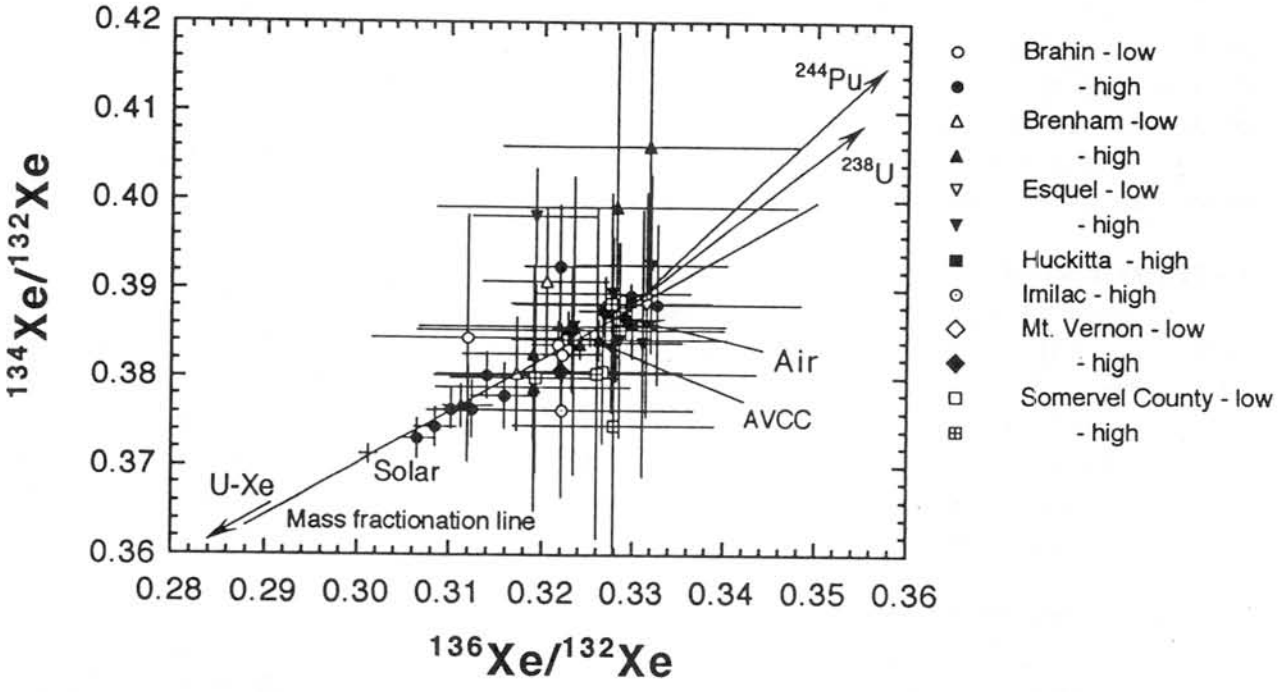

Fig. 2. Plot of $^{134}Xe/^{132}Xe$ versus $^{136}Xe/^{132}Xe$ for the measured pallasites. "low" and "high" mean extraction temperatures of 700-750 °C and > 700-750 °C, respectively.

Effect of structure on IR spectra of synthetic amorphous silicon oxide films

Tomonari Morioka[1], Seiji Kimura[1], Noritoshi Tsuda[1], Chihiro Kaito[1], Yoshio Saito[2], and Chiyoe Koike[3]

[1] Department of Physics, Ritsumeikan University, Noji, Kusatsu-shi, Shiga 525-77, Japan
[2] Kyoto Institute of Technology, Matsugasaki, Sakyo-ku, Kyoto 606, Japan
[3] Kyoto Pharmaceutical University, Yamashina-ku, Kyoto 607, Japan

INTRODUCTION

On the basis of absorption peaks from infrared objects [1], oxygen-rich stars [2] and the galactic center [3], it is recognized that the 10 and 20 μm bands are due to silicate minerals. Siliceous dust is also thought to exist in the interstellar space. Infrared Astronomical Satellite, IRAS, provided a few thousand spectra from infrared sources, most of which exhibited a single broad absorption band at 10 μm and an 18 μm absorption band. Both 10 and 18 μm bands are attributed to the silicon-oxygen bond. The broadness of the 10 μm absorption band is attributed to siliceous dust with an amorphous structure. IR spectra of some amorphous silicates have been measured by one of the present authors [4,5,6]. Some materials were synthesized by evaporation of olivine, pyroxene and quartz. All the materials produced in the laboratory were amorphous [7,8]. Therefore, it is difficult to discuss the relationship between the spectra and structure of the produced materials. Refractory materials do not always have the same structure as the evaporant [9,10]. It has been believed that the most important compounds from interstellar dusts were carbonaceous and siliceous materials. Sakata and Wada reported the IR spectra of SiO condensates and discussed the feature of H_2O trapped on them [11].

The purpose of the present study is to identify the peak corresponding to SiO condensates, taking into consideration the structural change due to heating.

EXPERIMENTAL

A tungsten V-boat was used as the evaporation source for the production of SiO films and particles. SiO films were prepared by evaporating SiO powder in a vacuum of ~ 10^{-6} Torr onto KBr pellets, and SiO particles were prepared in Ar gas pressure of 100 Torr. Some of the collected samples were oxidized by furnace heating at 300 or 500℃ in air. The spectra of these samples were measured using a Horiba Fourier transform infrared spectrometer FT-210 in the wavelength region from 2.5 to 25 μm, and these samples were examined using Hitachi H-7100R and H-800 electron microscopes.

RESULTS AND DISCUSSION

The IR spectrum of commercial SiO showed four peaks at 9.2, 12.5, 15.3 and 21.3 μm. X-ray diffraction pattern of the starting material obtained using the Debye diffraction technique showed that about 1% of the starting material consists of silicon and quartz crystals. The crystal structure of silicon dioxide has many interstices which may be occupied by some other atoms.

The peak at 15.3 μm may be due to O–interstitial Si stretching vibrations. Silicon crystal shows no absorptionin peak in the IR region. Since pure quartz powder is white and commercial SiO silver gray, the SiO powder was a mixture of Silicon and quartz.

A SiO film was yellow. As shown in Figure 1a, the IR spectrum shows a strong absorption peak at 10.2 μm and three weak peaks, which are different from those of quartz, indicating that the structure of the as–deposited film differs from that of commercial SiO. We previously showed by high–resolution electron microscopy that SiO film is composed of microcrystallites of silicon and α–cristobalite with size of ~ 2 nm [12]. Thus, it was concluded that the present SiO film is composed of silicon and α–cristobalite.

The SiO film was oxidized by heating for 30 hours in air. The film heated at 300℃ was still yellow, and that at 500℃ became nearly transparent. As shown in Figures 1b and 1c, the IR spectra of these films showed changes through the heat treatment. Even if the film which has been heated at 300℃ is reheated at 500℃, the IR spectrum of the film is the same as that shown in Figure 1c. As the phase transition from α–cristobalite to β–cristobalite occurs at about 250℃, the α–cristobalite film transforms to the β–cristobalite film by heating at 300℃. By the phase transformation, the peaks corresponding to Si–O stretching vibrations and O–Si–O bending vibrations shifted, but the only peak due to Si–Si stretching vibrations split into two peaks. Since the color of the film hardly charged with the heat treatment at 300℃, elemental silicon may remain in the film, and the weak peak at 15.0 μm may be due to interstitial silicon in β–cristobalite. On the other hand, the IR spectrum of the film heat–treated at 500℃ corresponds to that of quartz. Since the color of the film changed, most of silicon atoms might be oxidized. The heat produced by the exothermic reaction accelerated the phase transition of β–cristobalite to α–quartz. As all electron diffraction (ED) patterns of the as–deposited SiO and the heat–treated films showed halo rings, which hardly change through the heat treatments, these films were amorphous. In the present experiment, the phase transition of the film took place by heating in air for 1 hour. Therefore, it can be concluded that difference in the peak position depends on the crystal structure of the film.

SiO particles were brown. As shown in Figure 2a, the IR spectrum is similar to the IR spectrum of the film heated at 300℃ as shown in Figure 1b. Thus, it was concluded that SiO particles are composed of silicon and β–cristobalite. In the production of particles, because vapor near the heat source cooled rapidly due to collision with inert gas, the nucleation and growth stopped within a few mm around the heater. Therefore, β–cristobalite, which is a high–temperature phase, is produced near the heater in high–temperature regions. The absorption peaks from the IR spectrum of the particles also shifted toward the short–wavelength region in comparison with those of the film. This is due to the pressure exerted on microcrystallites, which the samples are composed of, during the pellet preparation process. In fact, a pressure of about 5800 atm is added in order to prepare transparent KBr pellets. Figures 2b and 2c show IR spectra of the particles heated at 300 and 500℃ for 30 hours in air, respectively. The IR spectrum of the particles heated at 300℃ hardly changed because SiO particles were β–cristobalite. On the other hand, a comparison of Figures 2a with 2c indicates that the characteristic peak at 11.4 μm due to Si–Si stretching vibrations in β–cristobalite disappeared. This suggests that β–cristobalite might have fully transformed into quartz as well as in the case of as–deposited film.

Astronomical spectra seen in the mid-IR are characteristic of silicate materials. It has been discussed that the silicate spectral position, strength and shape depend on the amorphous, crystallinity and degree of hydration. But in the present study, it became evident that the peak shift due to the heat treatment of SiO film or grains correspond to the change of crystallite structure. Spectral studies on mixtures of Mg and SiO are now under experiment.

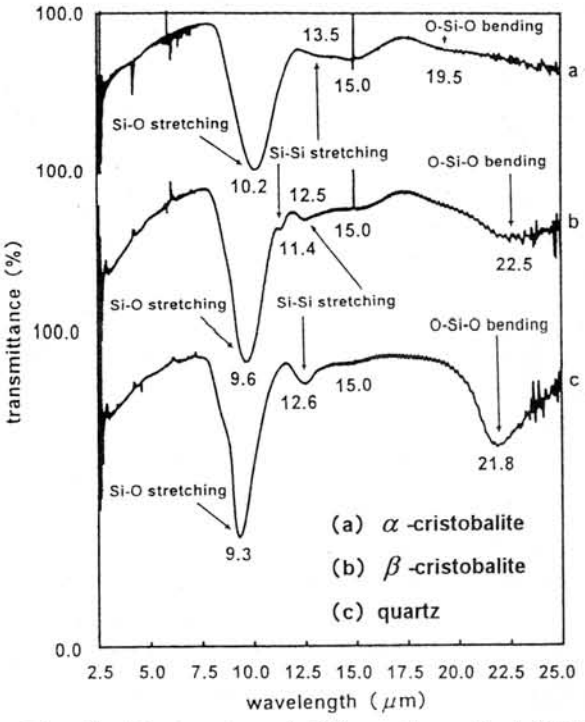

Fig. 1. IR spectra of, (a) as-deposited SiO film, (b) the film heated at 300℃ for 30 hours, and (c) that at 500℃ for 30 hours.

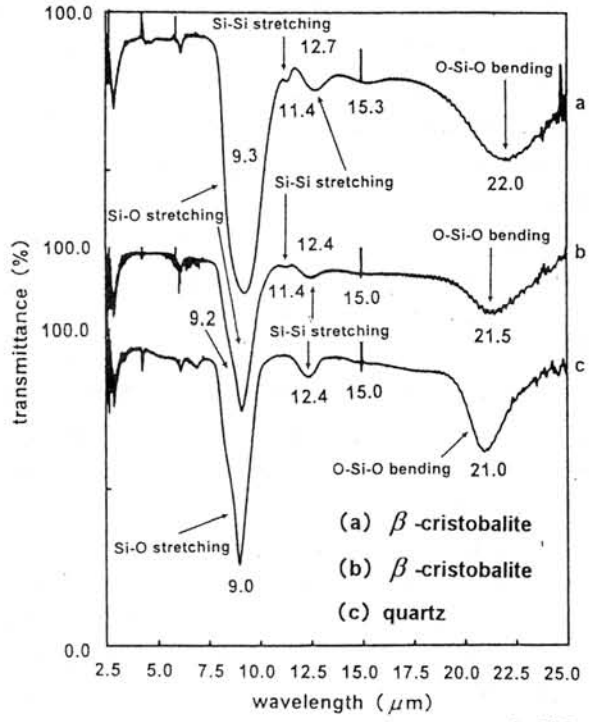

Fig. 2. IR spectra of, (a) as-prepared SiO particles, (b) particles heated at 300℃ for 30 hours, and (c) those at 500℃ for 30 hours.

References

[1] Woolf, N. J., and Ney, E. P. (1969) ApJ, 155, L181. [2] Forrest, W. J., McCarthy, J. F., and Houck, J. R. (1979) ApJ, 233, 611. [3] McCarthy, J. F., Forrest, W. J., Briotta, D. A., Jr., and Houck, J. R. (1980) ApJ, 242, 965. [4] Koike, C., and Hasegawa, H. (1987) Ap&SS, 134, 361. [5] Koike, C., Hasegawa, H., and Hattori, T. (1987) Ap&SS, 134, 95. [6] Koike, C., and Tsuchiyama, A. (1992) MNRAS, 255, 248. [7] Day, K. L., and Donn, B. (1978) ApJ, 222, L45. [8] Nuth, J. A., and Donn, B. (1982) ApJ, 257, L103. [9] Saito, Y., Kaito, C., Nishio, K., and Naiki, T. (1985) Appl. Surf. Sci., 22/23, 613. [10] Kaito, C., Watanabe, T., Ohtsuka, K., and Saito, Y. (1992) Proc. NIPR Symp. Antarct. Meteorites, 5, 310. [11] Sakata, A., and Wada, S. (1993) Primitive Solar Nebula & Origin of Planets, ed. H. Oya (Tokyo: Terra Scientific Publishing Company), 113. [12] Kaito, C., and Shimizu, T. (1984) Jpn. J. Appl. Phys., 23, L7.

EVAPORATION OF SILICATE MELT IN THE SYSTEM Mg_2SiO_4-SiO_2

H. NAGAHARA and K. OZAWA
(Geol. Inst., Univ. Tokyo, Hongo, Tokyo 113, Japan)

Evaporation is one of the most important phase changes in the nebula where total pressure is considerably low. Evaporation rates of minerals and rarely silicate melt affect degree of chemical evolution of the nebula and we can estimate the time scale of processes on the basis of chemical fractionation induced by evaporation which is recorded in chondrites. Nagahara and Ozawa [1] made isothermal heating experiments for melts with four different compositions along the MgO-SiO2 join in an open system, and showed that the melts crystallized forsterite isothermally due to bulk compositional change by evaporation and that a product of long heating consists of barred olivine and minor amount of interstitial melt. The evaporation rate decreases with time and becomes almost constant after a considerable time for the four different starting materials. In order to apply the results to estimation of time dependent processes, equilibrium vapor pressure of silicate melts in the Mg2SiO4-SiO2 system was calculated and evaporation coefficient was estimated.

Evaporation rate is related to the equilibrium vapor pressure of the substance by the Hertz-Knudsen equation, $j=\alpha P_{eq}/(2\pi mkT)^{1/2}$, where j is the evaporation rate, α is the evaporation coefficient which is the kinetic factor for the surface reaction, P_{eq} is the equilibrium vapor pressure, and m is the weight of a gas molecule. Because the experimentally obtained evaporation rate, j, is related to two parameters, P_{eq} and α, it is necessary to evaluate P_{eq} and α for understanding the mechanism of evaporation. Therefore, the experimentally obtained evaporation rate is calculated into evaporation flux. Because the gas coexisting in equilibrium with silicate melt does not have a stoichiometric composition, the flux is shown for Mg and Si (Fig. 1). The evaporation flux of Si is much larger than that of Mg at the beginning of evaporation, decreases quickly with time, and the difference between the flux of Mg and Si becomes very small after a considerable time. This indicates that the gas composition is very rich in Si at the beginning of evaporation and tends to be not so much with progress of evaporation. The total evaporation flux from melt is larger than that from solid forsteirte by more than an order of magnitude at the beginning to about one order of magnitude after a considerable time (Fig. 2). In the present experiments, because forsterite crystallized after about 1 hour due to bulk compositional change by progress of evaporation, the obtained evaporation rate for experiments longer than 1 hour has contribution from melt and solid forsterite.

The low pressure phase diagram of the silica-rich portion of the binary Mg2SiO4-SiO2 system at temperatures 1700°C and 1600°C was constructed by using the thermodynamic data set by [2] (Fig. 3). The phase diagram shows that forsterite is the vaporous phase in a wide range of composition and coexists with gas in a wide compositional range. On the contrary, the gas coexisting with the melt has a very limited composition and it is extremely rich in Si. The calculated vapor pressure of the gas in equilibrium with the melt was converted into the evaporation flux along the vaporous, which is the theoretically maximum value for the system (Fig. 4). The flux of Si has a strong dependence on pressure; it is larger at higher pressures and is smaller at lower pressures, and the flux of Si is much larger than that of Mg and the difference is larger at higher total pressurse. This is different from the flux from solid forsterite, which are shown by arrows in Fig. 4. Because forsterite evaporates congruently, the flux of Mg is twice of Si.

By comparing the experimentally obtained flux and that calculated from the experiments, the condensation coefficient for Si and Mg can be obtained. The coefficient was obtained for the melt before crystallization of forsterite (for 20 minutes data) and evaporation flux for the averaged pressure for stability of melt (about 9×10^{-6} bar). The obtained condensation coefficient of Si for the melt is about 0.08 and that of Mg is 0.12. This indicates that the kinetic barrier for evaporation is larger in Mg than in Si. These values are a little higher than that of forsterite (0.06 [3]); in the case of forsteirte the coefficient is the same for Mg and Si due to congruent evaporation. The present result that the evaporation coefficient

for the melt in the Mg2SiO4-SiO2 system is close to that of forsteirte is consistent with previous work that forsterite melt at temperatures not so far from the liquidus temperature has similar coefficient to solid forsterite [4]. In summary, the equilibrium vapor pressure of Si is much higher than that of Mg, but the barrier for evaporation is smaller for Mg, which may be due to nature of silicate melt where the Si-O bond is much stronger than Mg-bearing bonds. The present results predict that forsterite is the final product of evaporation of chondritic materials having SiO2 and MgO because forsterite has the lowest vapor pressure among species that contain MgO and SiO2 except for extremely MgO-rich portion of the system. Therefore, the lifetime of silicates and silicate minerals in the solar nebula is roughly estimated from the evaporation rate of forsterite

References: [1] Nagahara, H. and Ozawa, K. (1996) *LPSC* XXVII, 927-928, [2] Berman, R. G. (1985) Ph. D. thesis, Univ. British Columbia, [3] Nagahara, H. and Ozawa, K. (1996) *GCA* (in press). [4] Hashmoto, A. (1990) *Nature* 347, 53-55.

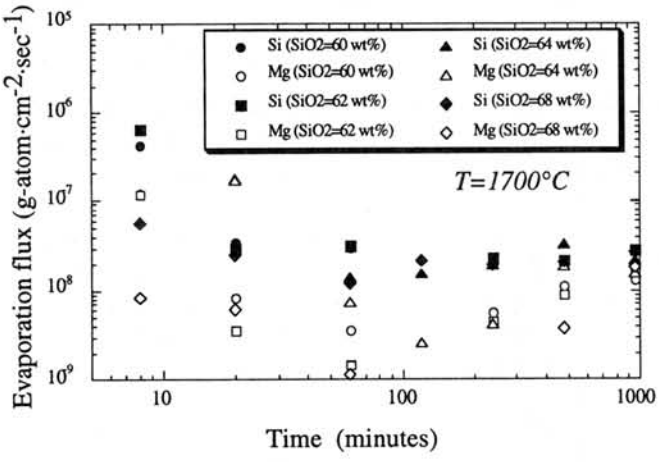

Fig. 1 Evaporation flux of Mg and Si from melt in the system Mg2SiO4-SiO2 at 1700°C. The flux is shown for Mg and Si separately because the melt evaporates incongruently and that the relative flux varies with time. Difference in symbols is difference in the chemical composition of the starting materials. The experimental charges made for shorter than 1 hour consists essentially of melt, but those longer than 1 hour contain both melt and forsterite, and the relative amount of forsterite increases with time.

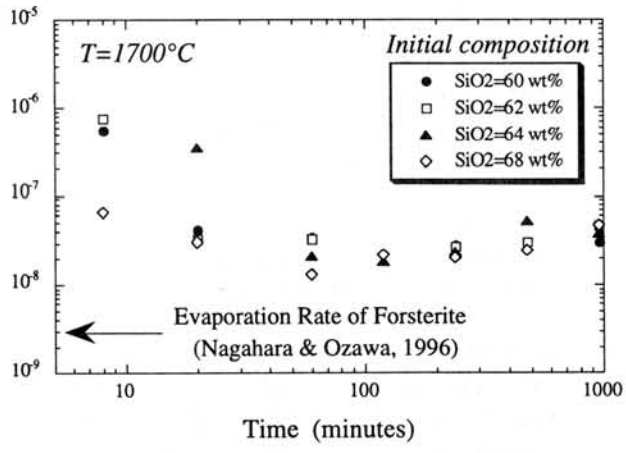

Fig. 2 Total evaporation flux from the silicate melt in the Mg2SiO4-SiO2 system at 1700°C. Data from Fig. 1.

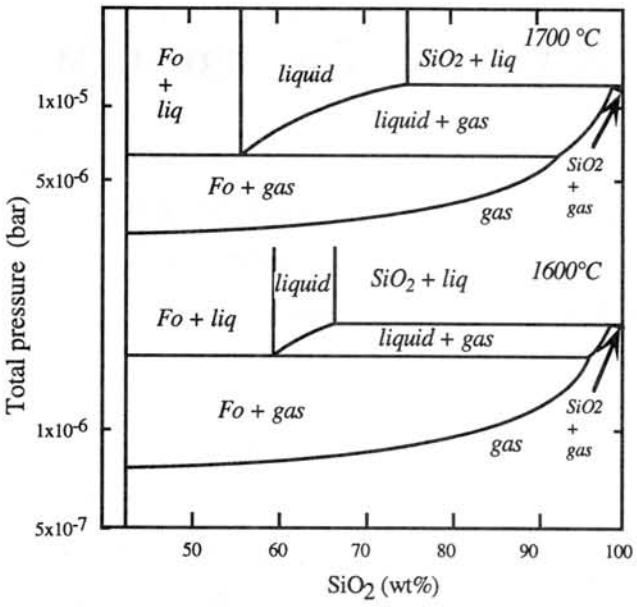

Fig. 3 The phase diagram of the SiO2-rich portion of the MgO-SiO2 system at low pressures at 1700°C and 1600°C. Thermochemical data were taken from [2].

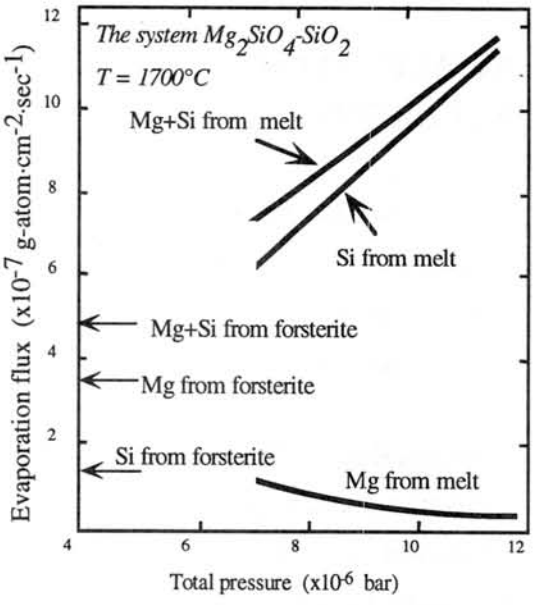

Fig. 4 The evaporation flux of the melt along the vaporous of the MgO-SiO2 melt at 1700°C calculated from Fig. 3. The flux shown gives the theoretically maximum values for evaporation of silicate melt at the present experimental conditions. Data for solid forsteirte are from [3].

NOBLE GASES IN METAL PHASE OF THE BRENHAM PALLASITE

Keisuke NAGAO[1], Yayoi N. Miura[2], Masatake HONDA[3], and Hisao NAGAI[3]

1) Institute for Study of the Earth's Interior, Okayama University, Misasa, Tottori-ken 682-01, Japan.

2) Earthquake Research Institute, University of Tokyo, Bunkyo-ku, Tokyo 113, Japan.

3) Nihon University, Department of Chemistry, Setagaya, Tokyo 156, Japan.

Introduction Noble gases in metallic phase of meteorites are generally difficult to be measured accurately because of difficulties in noble gas extraction by melting and of interaction with metal crucible (e.g. molybdenum) resulting in damage of vacuum of extraction furnace. Slow diffusion rate in melted metal phase might be a reason for the difficulty in noble gas extraction. Previously, we measured noble gases by carrying out several re-extractions to perform complete degassing from the metal sample heated at 1700-1800°C (1), and then sum up the results to obtain total abundance of noble gases in it. Alumina (Al_2O_3) crucible was used to avoid attacking the metal crucible.

We present noble gas data for 10 metal samples from 9 Brenham pallasite fragments. In the present experiment we vaporized metals at high temperature of about 1900°C, resulted in perfect degassing from the metal phase.

Experimental method Metal phases separated from the Brenham pallasite were mechanically polished on their surface and etched with dilute nitric acid repeatedly in ultrasonic bath. Non metallic materials visible on the surface were carefully removed mechanically again and rinsed in distilled water and acetone. Samples weighing 600-1200 mg ware loaded in a glass sample holder connected to a noble gas extraction furnace, then baked out at 200°C for more than 2 days. Blank levels of alumina crucible after degassing at about 1950°C for several hours were $(7\text{-}10)\times10^{-10}$, $(3\text{-}7)\times10^{-11}$, $(3\text{-}4)\times10^{-8}$, $(2\text{-}3)\times10^{-12}$, $(1\text{-}2)\times10^{-13}$ cm^3STP, for ^4He, ^{20}Ne, ^{40}Ar, ^{84}Kr, and ^{132}Xe, respectively. They were still an order of magnitude higher than those with Mo crucible. The high blank level was not sufficient to detect trapped noble gases if they are in the metals. For noble gas extraction the metal samples were heated at high temperature of 1900°C for 30 min. The metal in the crucible was evaporated and deposited on cooler part above the crucible. Extraction efficiency of noble gases was examined by re-extraction under the same heating condition, which indicated almost complete extraction. Noble gases were purified and separated into 4 fractions, He-Ne, Ar, Kr, and Xe, and analyzed on a modified VG5400 mass spectrometer using two ion detectors, Daly-multiplier and ion counting (2,3). Detection limit of the mass spectrometer for Kr and

Xe isotopes with the ion counting mode is $<1\times10^{-16}cm^3STP$.

Results and discussion Blank levels for measured ^4He signals were at most 14 %. On the other hand, atmospheric gases were not negligible in the Ne and Ar analyses, and the isotopic ratios are plotted on a mixing line between cosmogenic and atmospheric components (Figs. 1 and 2). This enabled us to calculate the concentrations of cosmogenic ^{21}Ne and ^{38}Ar based on the two component mixing. Though blank Kr and Xe were significant, up to several ten per cent, in Kr and Xe analyses, considerable amounts of Kr ($^{84}Kr>1\times10^{-11}ccSTP$) and Xe ($^{132}Xe> 5\times10^{-13}ccSTP$) were released probably from the metals. As the isotopic ratios of Kr and Xe are atmospheric with small excesses in cosmogenic isotopes, the gases would not be indigenous but be an atmospheric contamination trapped in the samples. Another possible source for the Kr and Xe is the alumina crucible itself which might be attacked during high temperature by non-metallic impurity remained in the metallic phase.

Cosmogenic ^3He, ^{21}Ne and ^{38}Ar concentrations observed for the samples show wide variations, more than two orders of magnitude (Fig. 3), corresponding to shielding depths against cosmic-ray irradiation. The data are consistent with those observed for coexisted silicate phases. The cosmogenic gases will be discussed by Honda et al. (in this abstract volume).

Slight shifts of data points upward from the mixing line in the plot $^{40}Ar/^{36}Ar$ vs. $^{38}Ar/^{36}Ar$ (Fig. 2) are probably due to radiogenic ^{40}Ar in the samples, whose concentrations are in the range of 0.15×10^{-8} (Ward) and 9.4×10^{-8} (N91) cm^3STP/g. Assuming 4.55 Ga retention age for the samples, we can calculate K concentrations of 0.019 and 1.17 ppm for Ward and N91, respectively. We tried to measure cosmogenic ^{81}Kr for three samples with different concentrations of cosmogenic light noble gases, and the obtained concentrations were very small: 3.0 ± 1.3, 1.4 ± 0.4 and 0.7 ± 0.8 $\times10^{-16}cm^3STP/g$ for Reed, H49.236 and LJ.Shima, respectively. The results are, however, consistent with those of cosmogenic light noble gases. The presence of ^{81}Kr indicates a presence of heavy elements such as Sr, Rb, Zr and Y etc., which are the target elements for ^{81}Kr production. Trace impurities are still present in the metal phases used in this study.

Acknowledgments: This work was partly supported by a Grant for Basic Science Research Project of the Sumitomo Foundation and a Grant-in-Aid for Science Research (No. 07454141) from the Ministry of Education, Science and Culture of Japan.

References: (1) Matsuda et al. (1996) Meteoritics Planet. Sci. 31, 227-233. (2) Nagao, K. et al. (1995) Proc. NIPR Symp. Antarct. Meteorites 8, 297-303. (3) Miura, Y.N. et al. (1995) Geochim. Cosmochim. Acta 59, 2105-2113.

Fig.1

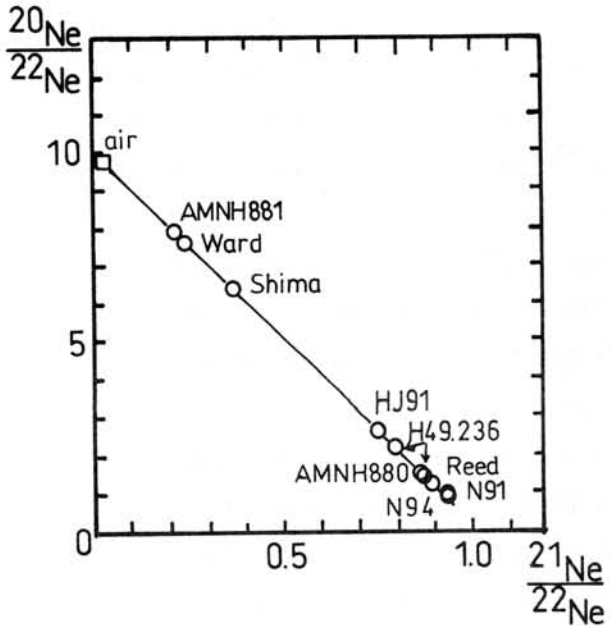

Fig. 2

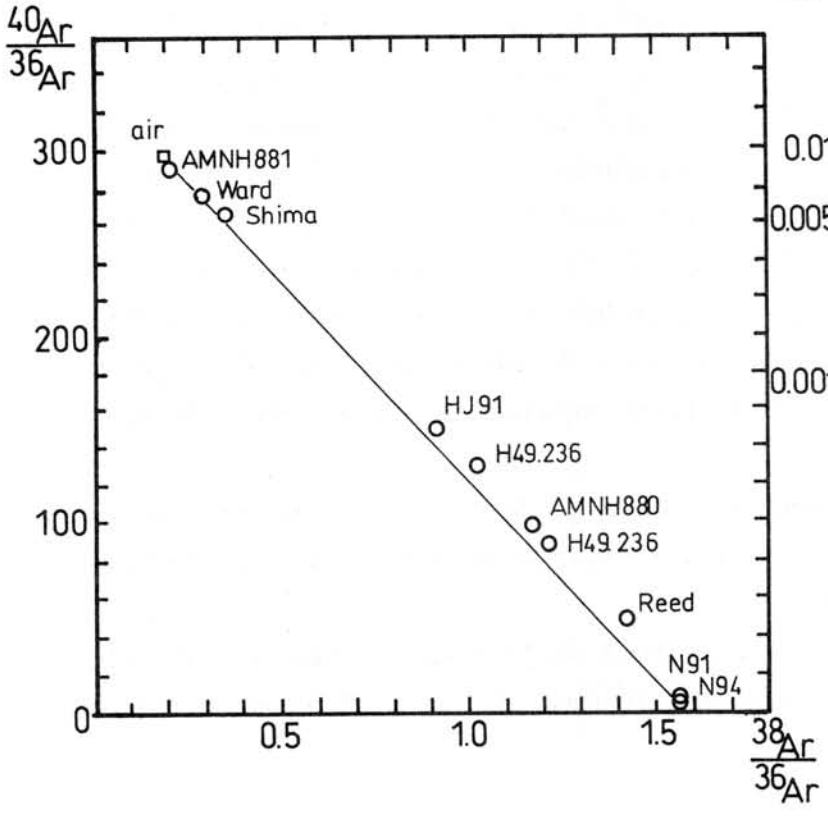

Fig. 3

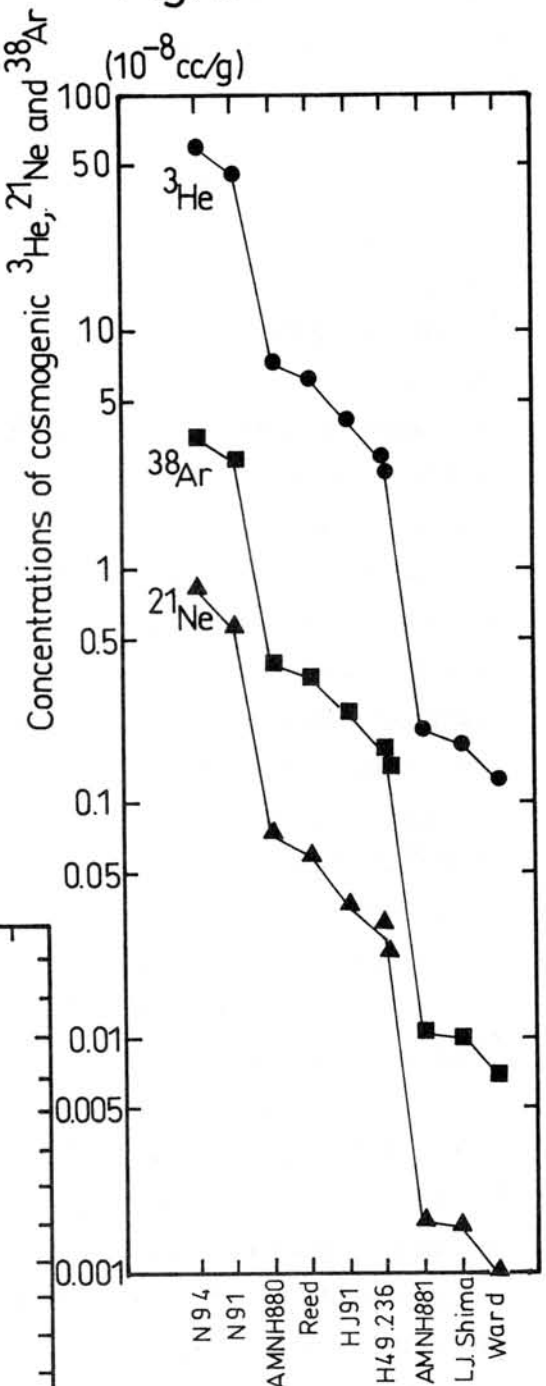

REE abundances in the "most pure" matrix materials from the Allende (CV) meteorite

Noboru Nakamura[1,2], Mutsuo Inoue[2*] and Makoto Kimura[3]

[1]Department of Earth and Planetary Sciences, and [2]Graduate School of Science and Technology, Kobe University, Nada, Kobe 657, Japan

[3]Ibaraki University, Bunkyo 2-1-1, Mito 310, Japan

Introduction: Matrix in primitive chondrites represents surviving pristine nebular material but individual components of matrix were subjected more or less to secondary processing. Matrix is among the most abundant constituents of chondrites and contains many silicate debris as well as oxides and metal/sulfides. Definition of matrix is not well established [1]. It seems likely that many bulk chemical analyses for matrix reported so far could not be free from effects of contaminants of CAIs and chondrules, particularly for refractory trace elements which are enriched in CAIs and some chondrules. It must be careful that refractory trace element data are most sensitive to contamination of CAIs and chondrules. Previous matrix data [e.g. 2,3] should be re-evaluated. In this work, We spent our best effort to obtain the "most pure" matrix materials and then to carry out precise REE determination by direct-loading isotope dilution mass spectrometry [4].

Experimental: Thick (~150 μm) sections of the Allende meteorite were prepared for petrographic examination by EPMA and for excavation of matrix materials for isotope dilution. In order to avoid possible contamination of chondrules, CAIs and mineral fragments, etc., careful searches for sampling locations were made using EPMA and optical microscopes attached with a microdrill. Under optical microprobe observation, one series of matrix materials (each sample=~100 μg in size) were excavated from two sections (M2 and M3) prepared with petropoxy resin. They were analyzed for trace elements (REE, Sr, Ba, K, Rb) and major elements (Mg, Fe, Ca) by isotope dilution. It turned out that significant amounts (20-30 wt%) of resin were contaminated in the drilled samples. After correction of effects of resin, REE patterns of matrix materials were obtained.

Results and Discussion: As shown in Table 1, the compositions of matrix materials are typical for Allende matrix [5], but it turned out that abundances of Ca (and Al) are more variable among samples for EPMA data but less for isotope dilution data. It is

*Present address: Low Level Radioactivity Laboratory, Faculty of Science, Kanazawa University, Wake, Tatsunokuchi, Ishikawa 923-12

suggested that some refractory elements rich materials such as CAIs and/or Ca-rich pyroxene were heterogeneously distributed in sampled matrix areas. Isotope dilution data suggest that M2 contained least amounts of such components. Results of trace element analyses are presented in Fig. 1. The results for two samples from the same sections are consistent each other. The alkali metals (K and Rb) in matrix are systematically depleted. All the matrix materials indicate grossly unfractionated REE abundances in CI-chondritic level. However, if we look more careful the REE patterns, the M3 matrix materials are slightly enriched in Ca, Sr, Ba and light REE. On the other hand, the general REE patterns have no recognizable sizes of anomalies at Ce, Eu nor Yb. Hence, the positive Eu anomaly expected for counterpart of Allende chondrules [6] is not identified here. If matrix is residual material after removal of CAIs and/or chondrules from common refractory precursor, then we might expect some kinds of REE fractionations in the matrix materials. The flat REE patterns in Fig. 1 do not resemble those of many Allende CAIs and chondrules which tend to have anomalous REE patterns, nor their possible counterparts. Therefore, in terms of REE abundances, no direct relationship is considered between matrix and CAIs or chondrules.

Because present results were obtained after significant correction of effects of contaminant resin, we have been carrying out further more precise trace element analyses for the second series of matrix materials prepared with P-resin.

References; [1] Scott, E.R.D. et al. (1988) In Meteorites and the Early Solar System, 718-745. [2] Tanaka, T. and Masuda, A. (1973) Icarus 19,523-530. [3] Rubin, A.E. and Wasson J.T. (1987) Geochim. Cosmochim. Acta 51, 1923-1937. [4] Nakamura, N. et al. (1989), Analyt. Chem. 61, 755-762. [5] McSween, H.Y.Jr and Richardson, S.M. (1977) Geochim. Cosmochim. Acta 41,1145-1161. [6] Misawa, K. and Nakamura, N. (1988) Geochim. Cosmochim. Acta 52, 1699-1710.

Table 1. Average values of bulk chemical compositions (wt. %) in matrix materials excavated from five different sections of Allende (CV) chondrite (M2, M3, M4, M5 and M6).

	Allende matrix					
	M2 (2)	M3 (2)	M4 (4)	M5 (2)	M6 (4)	previous* data
Na_2O	0.18	0.19	0.24	0.18	0.31	0.22
MgO	18.60	19.25	18.56	18.14	20.36	20.20
Al_2O_3	2.25	1.63	1.95	2.00	2.39	2.30
SiO_2	28.56	27.37	30.55	28.88	29.62	28.00
P_2O_5	0.20	0.12	0.19	0.22	0.23	---
SO_3	2.07	2.05	2.46	2.57	2.09	2.82
K_2O	0.01	0.01	0.01	0.02	0.01	0.01
CaO	2.36	1.18	2.50	2.10	1.54	2.37
TiO_2	0.02	0.01	0.02	0.02	0.05	0.09
Cr_2O_3	0.43	0.34	0.35	0.47	0.57	0.38
MnO	0.21	0.22	0.19	0.14	0.17	0.21
FeO	35.78	36.36	34.43	35.06	34.13	31.90
NiO	1.60	1.62	1.67	1.75	1.42	1.83
Total	92.27	90.35	93.12	91.55	92.89	90.33

* McSween and Richardson (1977)
M2 and M3 were prepared with petropoxy resin, and M4, M5, M6 were P-resin.

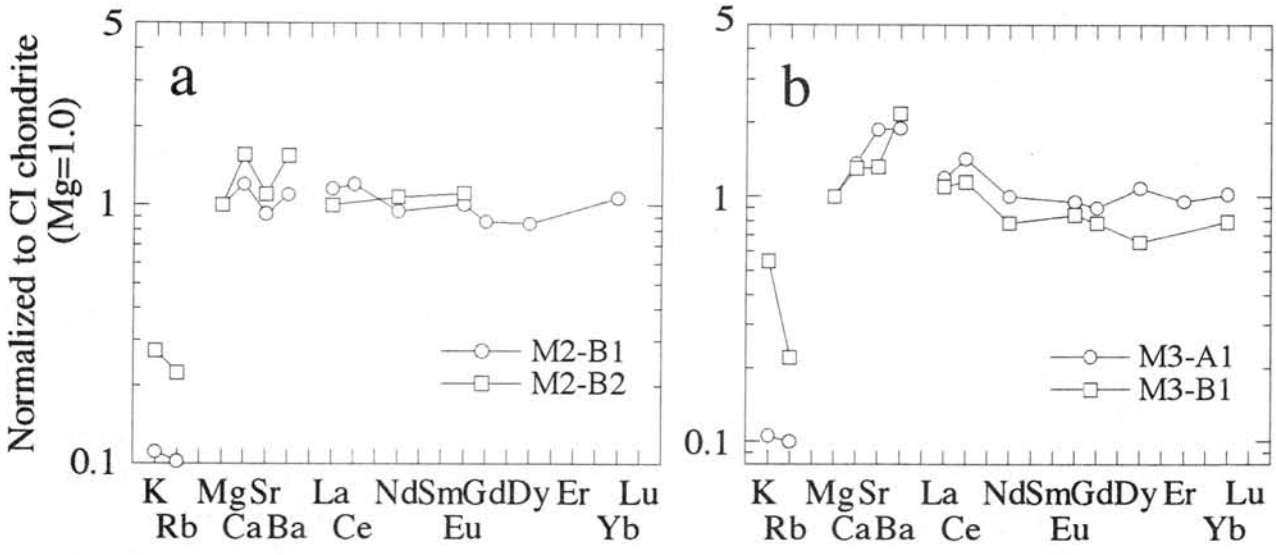

Fig. 1. CI normalized lithophile element abundances in matrix materials of the Allende chondrite. (a) B1 and B2 samples from the section M2. (b) A1 and B1 samples from the section M3.

AN APPLICATION OF X-RAY POWDER DIFFRACTION ANALYSIS TO METEORITES BY USING A GANDOLFI CAMERA: METAMORPHIC TEMPERATURE ESTIMATION OF ORDINARY CHONDRITES

Y. Nakamuta and Y. Motomura
Dept. Earth and Planetary Sciences, Faculty of Science, Kyushu University, Fukuoka 812, Japan.

X-ray analysis of a very small mineral

X-ray powder diffraction analysis has been rarely applied to meteorites, because it is very difficult to obtain enough amounts of a mineral from meteorite for the x-ray powder analysis by using a widely used diffractometer. A Gandolfi camera is a kind of Debye-Scherrer camera and has a special attachment devised to obtain a powder pattern directly from a single crystal of down to 20 μm in size. The authors used a Gandolfi camera in order to obtain an x-ray powder pattern of a very small mineral from meteorite. The powder diffraction data recorded on a film by a Gandolfi camera were analyzed precisely by reading it with a microdensitometer and applying a profile-fitting technique to the read data. The x-ray powder pattern of plagioclase of about 50 μm in size and profile-fitting results of a part of the pattern are shown in Figs. 1 and 2, respectively. In Fig. 2, dots are the experimental data obtained by a Gandolfi camera, and solid

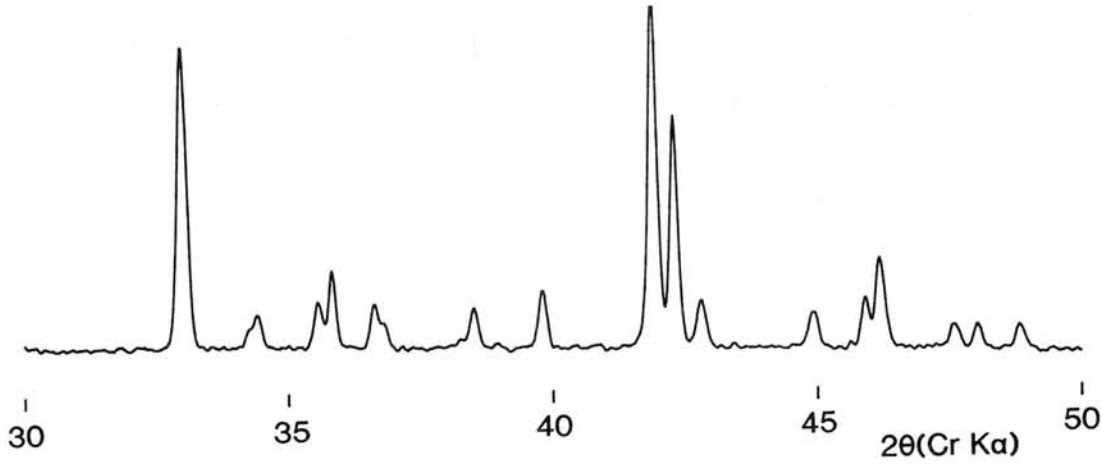

Fig. 1. X-ray pattern of plagioclase.

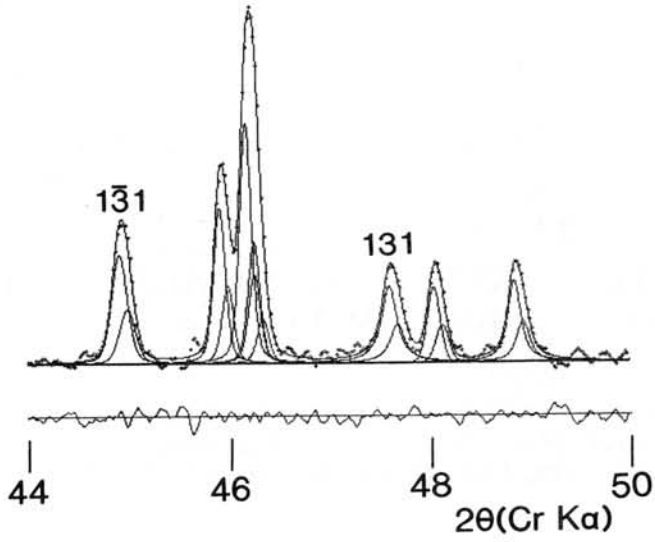

lines are the calculated profile and its $K\alpha_1$ and $K\alpha_2$ components. Differences between observed and calculated intensities are also shown at the bottom of the figure. Figs. 1 and 2 show that the precise x-ray powder analysis can be performed even by using a very small particle of mineral as in meteorites.

Fig. 2. Results of profile-fitting.

Metamorphic temperature estimation by a plagioclase thermometer

Plagioclase which has been formed from glass through metamorphic processes in parent bodies is a subdominant constituent mineral of equilibrated ordinary chondrites. The structural states of Na-rich plagioclase, e.g. the degree of Al/Si order in the four symmetrically non-equivalent tetrahedral sites in the framework structure, correlate to its equilibration temperatures. The structural state of plagioclase can be estimated by measuring the distance between the 1-31 and 131 reflections in the x-ray powder pattern of plagioclase.

The x-ray powder patterns of individual plagioclase grains, about 50μm in size, from H5 (Faucett), H6 (Mulga north), L6 (Holbrook) and LL6 (Dhurmsala) chondrites were obtained by a Gandolfi camera after the analysis of chemical compositions by an electron probe microanalyzer. The distance between 1-31 and 131 reflections in an x-ray powder pattern was determined precisely, with an error less than 0.01 degree (2θ), by applying a profile-fitting technique. The measured distance between 1-31 and 131 reflections was corrected for the influence of Or content by using the correction diagram proposed by Kroll and Ribbe(1980).

All the analyzed plagioclases are plotted in Fig. 3. The plagioclases from each chondrite disperse widely along the [2θ(131)-2θ(1-31)] axis on Fig. 3, indicating variable equilibration temperatures. Even the plagioclases taken from the same chondrule also have different [2θ(131)-2θ(1-31)] values. These results reveal that the structural states of plagioclase are not in equilibrium, maybe due to the sluggishness of order-disorder reactions in plagioclase in a dry environment. Therefore, the temperatures estimated from Fig. 3 may correspond to the temperatures at which plagioclase crystallized from pre-existing glass during the progressive alteration processes in a parent body. Then, the maximum temperature indicated by plagioclase from each chondrite corresponds to the maximum temperature reached during metamorphic processes in parent bodies. The maximum temperatures for Faucett(H5), Mulga north(H6), Holbrook (L6) and Dhurmsala (LL6) are 690, 740, 840 and 840° C, respectively.

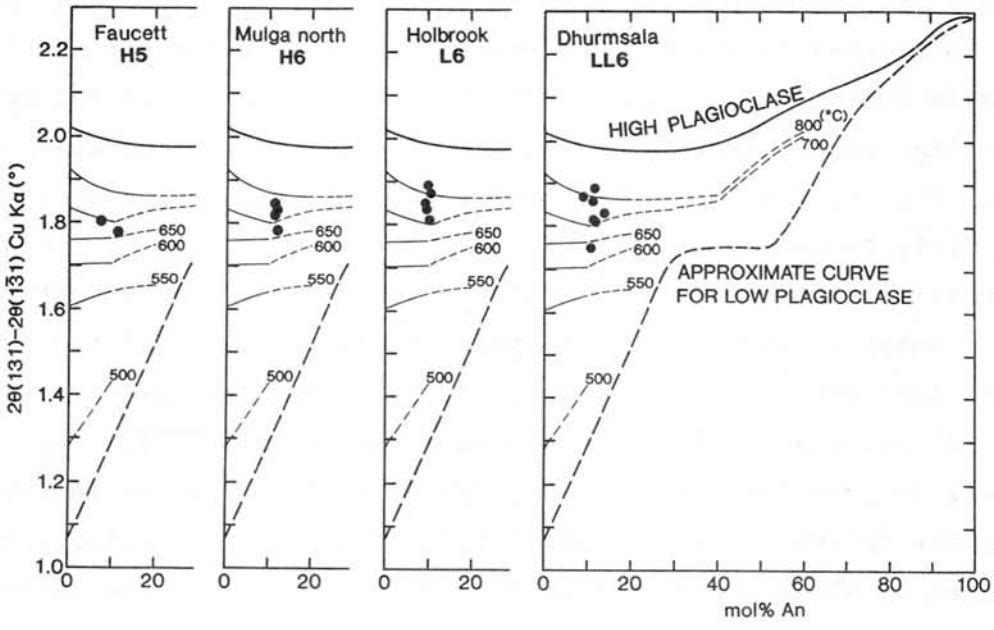

Fig. 3. Plots of chondritic plagioclase on the relation diagram between 131 structural indicator and temperature of synthesis of plagioclase (J. V. Smith, 1972).

A HYPOTHESIS FOR THE SALINITY OF LAKE WATER AND ECONOMIC POTENTIAL OF THE LONAR IMPACT CRATER, INDIA

V. K. NAYAK
Department of Applied Geology, Indian School of Mines, Dhanbad 826004, India

The Indian meteorite impact crater at Lonar ($19^{\circ}58'N$: $76^{\circ}31'E$) in the Deccan Trap tholeiitic basalt flows of the Cretaceous-Eocene age, is an authentic impact crater (Nayak, 1972; Fredriksson et al. 1973). It is an unique feature which is nearly circular with a breach in the north-east, 1830 m diameter, 150 m deep and the crater floor is occupied by a saline lake. Various explanations proposed from time to time (La Touche and Christie, 1912; Pandit et al. 1945; Jhingran and Rao, 1958; Nandy and Deo, 1961; Chowdhury and Handa, 1978) to comprehend the salinity of lake water are critically evaluated. In the past, the origin of the crater and the salinity of lake water have often been treated separately. On the whole, the earlier views pointed out that water from different sources including some suspected juvenile springs, basaltic rocks, evaporation and conversion of sulphate ion to carbonate through the intermediate formation of sulphide, were the factors responsible for the salinity/alkalinity of water in the lake.

The present contribution envisages a new approach in that the origin of the crater and the salinity of lake water are intimately linked and both the aspects are considered together. The crater lake with water spread of about 107 hectares is a closed basin with centripetal drainage and is fed by three perennial springs namely Dhara and Sitanahani in the north-east and Ramgaya in the east. The drilling by the Geological Survey of India, showed that the lake bed is flat, followed upward by about 150 m thick shattered and jointed basalt, 87 m silt, talus and variable depth (0.15 m to 5.5 m) of saline water. The nature of water is Na-CO_3-HCO_3-Cl type with pH about 10 and the concentration of these ions vary with different seasons. The salts are rich in carbonate, bicarbonate and chloride of sodium (Chowdhury and Handa, 1978).

A new idea is postulated in that the salinity of lake water is closely related with the nature of target basalt and the impact by a meteorite. The impact resulted in shock metamorphism, shattering, pulverization and neo-mineralization of the mineral constituents of basalt accompanied by heating of groundwater and perhaps connate water in high pressure-temperature environment. These new conditions resulted in the generation of post-impact hydrothermal system

leading to alteration and solution of neo-minerals like maskelynite etc. as in the case of gabbro of West Clearwater crater, Canada (Bunch et al. 1967). Besides, the zeolites and other secondary minerals of basalt flows may have also contributed to enhance the salinity of water. This concept is further supported by profuse calcareous and zeolitic material, network of carbonate veins and veinlets impregnating the heavily oxidised basalt fragments found within and outside the crater.

The economic resources associated with a number of terrestrial impact structures are the result of relatively rare geologic events (Grieve and Masaitis, 1994). The salt resources occurring at the Lonar impact crater were estimated to be more than 6000 tons (La Touche and Christie, 1912; Pandit et al. 1945). The salts are classified into evaporite category. It is true that the present status of economic potential of salt resources of the Lonar crater needs to be worked out but it is evident that they are intimately linked with the formation of the crater in the basaltic terrain as a result of post-impact hydrothermal system in high pressure-temperature environment followed by evaporation and other factors. All these aspects are discussed in detail and the work is in progress.

References

Bunch, T.E., Dence, M.R. and Cohen, A.J. (1967). Amer. Min., 52, 244-253.

Chowdhury, A.N. and Handa, B.K. (1978). Indian Jour. Earth Sciences, 5, 111-118.

Fredriksson, K., Dube, A., Milton, D.J. and Balasundaram, M.S. (1973). Science, 180, 862-864.

Grieve, R.A.F. and Masaitis, V.L. (1994). Inter. Geol. Review, 36, 105-151.

Jhingran, A.G. and Rao, K.V. (1958). Rec. Geol. Surv. India, 85, 313-334.

La Touche, T.H.D. and Christie, W.A.K. (1912). Rec. Geol. Surv. India, 41, 266-285.

Nandy, N.C. and Deo, V.B. (1961). TISCO Magazine, 8, 144-155.

Nayak, V. K. (1972). Earth and Planet. Sci. Letts., 14, 1-6.

Pandit, V.P., Telang, M.S. and Saletore, S.A. (1945). Jour. Sci. Indust. Res,m 4, 16.

Matrix and chondrule rims in the Tieschitz (H3.6) chondrite

Takaaki Noguchi
Department of Materials and Life Sciences, Ibaraki University,
Bunkyo 2-1-1, Mito 310, Japan

Introduction Tieschitz is a well-known meteorite because it contains "white matrix". It is originally defined as the optically transparent, non-clastic matrix in Tieschitz which has a composition similar to that of some chondrule mesostases (Christophe-Michel-Levy, 1975). However, it is not yet clear what the white matrix is made of. Ashworth (1981), based on TEM observation, showed that the white matrix is composed of coarse plagioclase and nepheline including many inclusions and cracks. Alexander et al. (1989) also performed TEM observation and showed that the white matrix is composed of at least two phases which have similar compositions to plagioclase and amphibole. However, their electron diffraction patterns do not coincide with those of plagioclase and amphibole, respectively. Tieschitz meteorite has been considered to be a product of high temperature accretion (e. g. Hutchison et al., 1979; Bevan and Axon, 1980). Rubin (1995) opposed to their high temperature accretion hypothesis. In this study, petrography and mineralogy of Tieschitz, especially those of matrix and chondrule rims, are described. The origin of the white matrix and the high temperature accretion hypothesis will be discussed briefly.

Petrography and mineralogy **(1) SEM observation** Tieschitz is composed of closely packed chondrules and their fragments, metal and sulfide, and matrix. The larger objects (chondrules and their fragments, and metal and sulfide) are coated by dark, opaque rims. In this meteorite, an opaque matrix occurs as such opaque rims (black matrix: Christophe-Michel-Lévy, 1976 and Ashworth, 1981). Optically transparent white matrix fills the spaces among the larger objects which are coated by opaque rims. Backscattered electron images (BEIs) show that the white matrix in some area contains thin (< 1μm thick), brighter filaments (Fig. 1a). The white matrix often contains voids (typically 5-20 μm across) at or near the boundaries of white and black matrices (Fig. 1b), although there is a possibility that these voids are artifacts during sample preparation. Figure 1 displays that the black matrix is more porous than the white matrix. The black matrix is porous aggregate of fine-grained (< 1 μm) minerals and brighter than the white matrix in BEIs. These photographs show that the black matrix contains a small amount of opaque minerals (tiny bright spots in BEIs).

(2) TEM observation Typical black matrix is composed of densely packed silicates (mainly olivine with a small amount of pyroxene). Chromite and Fe-Ni metal are also rarely observed. Typical grain size of silicates in the black matrix is ca. <200 nm across. Because each crystal stick together due to sintering, the outline of each crystal cannot be delineated well. Because some crystals which sinter together show a preferred orientation, the apparent shapes of matrix crystals are very complicated and their apparent sizes are large (up to <1 μm in length). Si-, Al-, and Na- (and/or Ca-) rich material is sometimes observed among silicate grains. One white matrix sample was observed by TEM. It contains small inclusions and its crystallinity is low.

(3) Composition of the white matrix It has been regarded that the white matrix has a composition similar to that of some chondrule mesostases (Christophe-Michel-Levy, 1975). Chemical compositions of chondrule mesostases, black matrix and white matrix were analyzed and compared. Figure 2a shows that the white matrix has more homogeneous than chondrule

mesostases which contain fine-grained Ca-rich pyroxene, as well as the black matrix which is composed mainly of olivine. Analyses of white matrix are plotted above the albite (or nepheline) - anorthite join in Fig. 2a. The data may indicate that the white matrix contains not only plagioclase and nepheline but also high-Al phase(s). This hypothetical phase may be related to high-Al phase reported by Alexander et al. (1989) in the white matrix. The higher Al content and the more restricted composition of the white matrix than those of chondrule mesostases can also be seen in Fig. 2b. Along with major elements, K_2O concentrations are different among chondrule mesostasis, the black matrix, and the white matrix. K_2O wt % in the white matrix is typically > 0.4, but that in chondrule mesostases and the black matrix is typically < 0.2. Higher K_2O concentration in the white matrix can be seen well in Fig. 3. It is clear that K is concentrated around some chondrules. The K-enriched areas are correspond to the white matrix.

Discussion There are some ideas as the origin of the white matrix. Christophe-Michel-Lévy (1976) suggested that the white matrix was formed by the partial solution and redeposition of chondrule mesostasis. Hutchison et al. (1979) interpreted that the white matrix was a mesostasis that became squeezed out from chondrules while still hot and fluid. Hutchison (1995) proposed that the white matrix was formed by metasomatism on a parent body. If the white matrix had been squeezed mesostasis, the compositional distribution of the white matrix would have been almost the same compositional distribution of chondrule mesostasis. However, as described above (Fig. 2), the composition of white matrix is more restricted than that of chondrule mesostasis. The restricted composition of white matrix result from the lack of Ca-rich pyroxene component. It means that chondrule melts must have been squeezed out after all the chondrule melts crystallized Ca-rich pyroxene. It is also difficult to explain the difference of K_2O concentrations among the white matrix and chondrule mesostasis by the squeezed out hypothesis. Therefore, the squeezed out hypothesis is probably ruled out. According to Hutchison et al. (1979), the white matrix is one of the clues to the high temperature accretion hypothesis. However, as shown above, the white matrix cannot be a clue to the hypothesis. The restricted composition and slight K_2O enrichment of the white matrix may be explained by metasomatism hypotheses. The metasomatism hypotheses, however, are difficult to evaluate, because they did not refer to the composition of metasomatic fluid and to the mechanism of metasomatism in the meteorite parent body. Clues to the metasomatic reactions such as veins and decomposed chondrule mesostasis could not found during SEM observation of chondrules, although voids in the white matrix might be related to the process. Another interpretation is that the white matrix is recondensates from chondrules after chondrule formation. The restricted composition and slight K_2O enrichment of the white matrix may be also explained by this interpretation. However, it is difficult to explain the scarcity of such kind of matrix in other meteorites except for Sharps (Alexander et al, 1989). Although the metasomatic and recondensation hypotheses may be plausible, there are some difficulties for both of them.

References Alexander, C. M. O., Hutchison, R., and Barber, D. J. (1989) Earth Planet. Sci. Lett., 95, 187-207. Ashworth, J. R. (1981) Proc. R. Soc. Lond., A374, 179-194. Bevan, A. W. R. and Axon, H. J. (1980) Earth Planet. Sci. Lett., 47, 353-360. Christophe-Michel-Lévy, M. (1976) Earth Planet. Sci. Lett., 30, 143-150. Hutchison, R., Bevan, A. W. R., Agrell, S. O., and Ashworth, J. R. (1979) Nature, 280, 116-119. Hutchison, R., Bevan, A. W. R., Easton, A. J., and Agrell, S. O. (1981) Proc. R. Soc. Lond., A374, 159-178. Hutchison, R. (1992) Meteoritics, 27, 236-237. Rubin, A. E. (1995) Meteoritics, 30, 568-569.

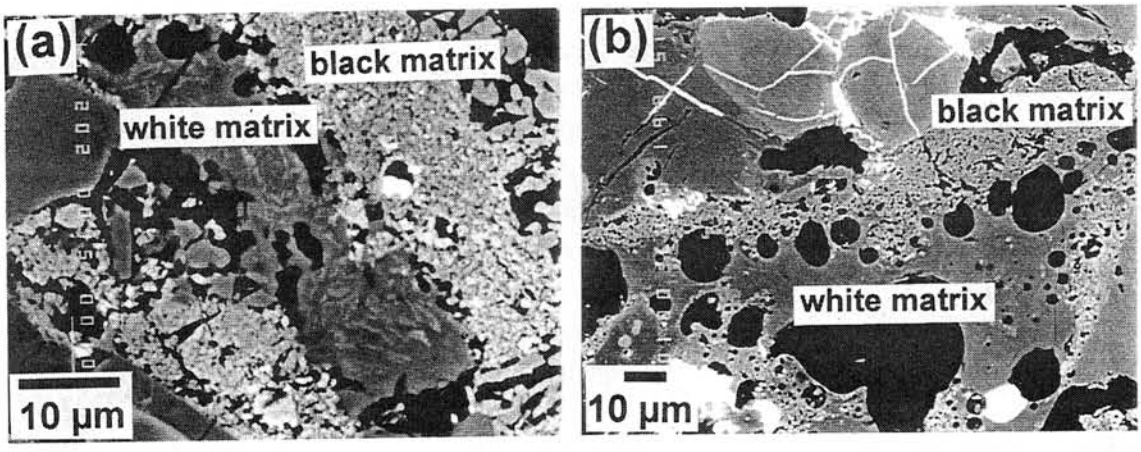

Figure 1 BEI of matrix in Tieschitz. (a) Filaments (brighter than the surroundings) are observed in white matrix. (b) Filaments are rare. There are small voids (5-20 μm across) at the boundary between the black and white matrix.

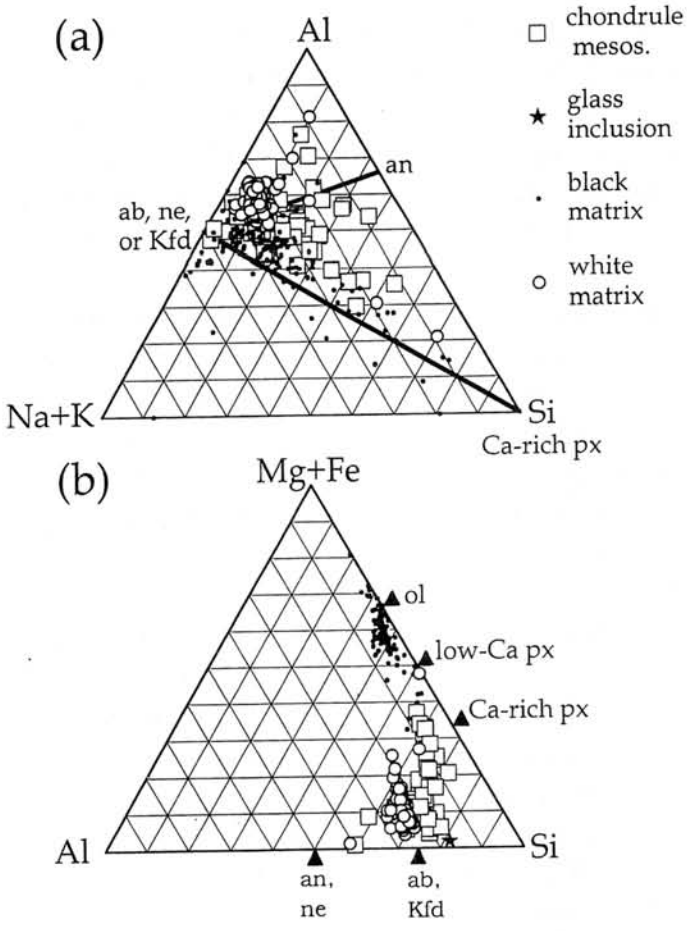

Figure 2 Comparison of chemical compositions of chondrule mesostases, glass inclusion in olivine, the black matrix, and the white matrix. (a) Al-[Na+K]-K (atomic ratio) plot, (b) [Mg+Fe]-Al-Si (atomic ratio) plot.

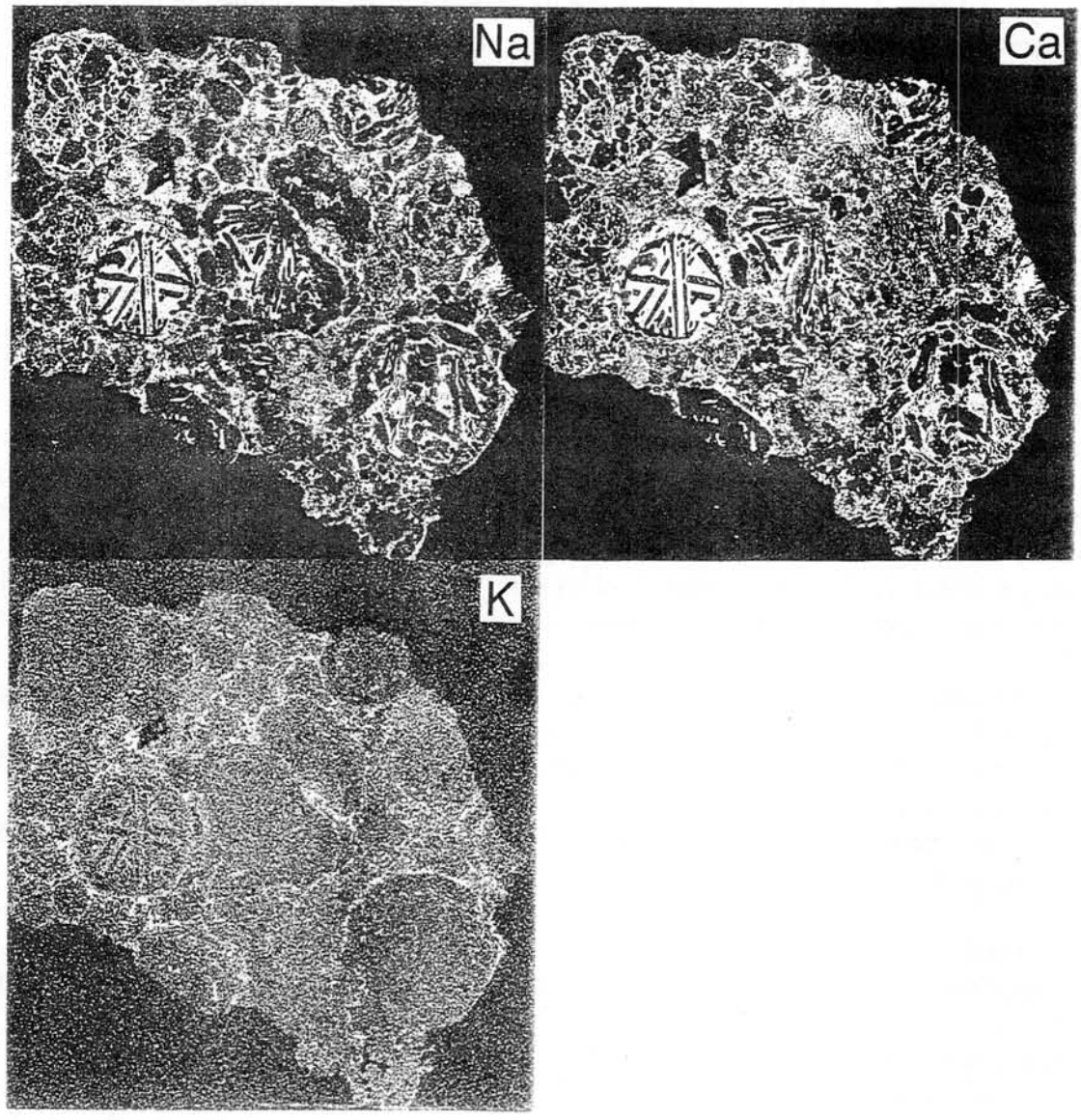

Figure 3 Distributions of Na, Ca, and K in Tieschitz meteorite. Width of each map is 3 mm. It is clear that K is concentrated around some chondrules. Such K-enriched areas are correspond to the white matrix.

Hydrothermal and Heating Experiments on Formation of Nepheline in CAIs: Implications for Aqueous Alteration and Thermal Metamorphism in Parent Bodies.

Koji Nomura and Masamichi Miyamoto

Mineralogical Institute, Graduate School of Science, University of Tokyo, Hongo, Tokyo 113, Japan

Introduction

Ca-Al-rich inclusions (CAIs) in carbonaceous chondrites are of great importance because, on the basis of thermodynamic calculations, their constituent minerals are predicted to be the first phases formed from early solar nebular [e.g., 1]. However, CAIs often include secondary minerals such as nepheline ($NaAlSiO_4$) and sodalite ($Na_4Al_3Si_3O_{12}Cl$) [e.g., 2]. The coexistence of these volatile-rich phases with primary high-temperature phases cannot be readily explained by simple equilibrium condensation. Most previous works suggested that secondary minerals formed by reaction with the solar nebular gas [e.g., 3]. On the other hand, we suggested that secondary minerals in CAIs are produced by aqueous alteration in parent bodies [4]. Especially, secondary minerals such as nepheline, grossular ($Ca_3Al_2Si_3O_{12}$), calcite ($CaCO_3$) and wollastonite ($CaSiO_3$) are suggested to have been produced from gehlenite ($Ca_2Al_2SiO_7$) [e.g., 4]. We further performed hydrothermal experiments on the formation of nepheline which is one of major secondary minerals in CAIs to study aqueous alteration in parent bodies.

In addition, discovery of thermal metamorphosed carbonaceous chondrites [5] suggests that thermal metamorphism after aqueous alteration in parent bodies affect alteration process of CAIs. We also performed heating experiments including thermal analyses to study subsequent thermal metamorphism.

Experimental

Experiments of this study are divided into two categories. One is hydrothermal experiments corresponding to aqueous alteration, and the other is heating experiments corresponding to thermal metamorphism on products obtained by the hydrothermal experiments.

Because the run of gehlenite-H_2O with 1N NaOH solution was performed in our previous studies [4], the experiments on the system gehlenite-Al_2O_3- H_2O-NaOH and gehlenite-SiO_2-H_2O-NaOH were performed to study the effect of Si and Al in fluids on hydration of gehlenite in hydrothermal experiments. The mixtures of gehlenite powder and Al_2O_3 or SiO_2 reagent were prepared by mixing for 24 hours with the weight ratios of (Al_2O_3 or SiO_2) /gehlenite being 8/10, 4/10, 2/10 and 1/10. Synthetic gehlenite studied in this work have been taken from the products of our previous work [4]. Experiments in the system Al_2O_3-SiO_2-H_2O- NaOH were also performed using the Al_2O_3 and SiO_2 reagents to study the products from Na-, Al- and Si-rich fluid in parent bodies. Mixtures of Al_2O_3 and SiO_2 were prepared by mixing for 24 hours with the mole ratios of Al_2O_3/SiO_2 being 8, 4, 2, 1, 1/2, 1/4 and 1/8. Hydrothermal experiments were performed at 200 ℃ for 7 days.

Heating experiments on the analcime and nepheline hydrate obtained by the hydrothermal experiments as starting materials were performed with an electric furnace. Heating temperatures were 400℃, 500℃, 600℃, 700℃ and 800 ℃ and the duration of each run was 24 hours. Thermal analyses including DTA (differential thermal analysis) and TG (thermogravimetric) were also performed to study thermal metamorphism of products obtained by the hydrothermal experiments. About 10 mg of analcime or nepheline hydrate were heated from 30℃ to 1000 ℃

with 10 ℃/min of the ascending rate.

The phases produced by each run were identified by X-ray diffraction (XRD) patterns.

Results

Hydrothermal experiments In the gehlenite-Al_2O_3-H_2O-NaOH and gehlenite-H_2O-NaOH systems, the product was hydrogrossular alone. There was no difference among the products of the runs of gehlenite-Al_2O_3-H_2O-NaOH and gehlenite-H_2O-NaOH systems (Table 1).

In the gehlenite-SiO_2-H_2O-NaOH system, the products were hydrogrossular and 11 Å tobermolite [$Ca_5(Si_6O_{18}H_2) \cdot 4H_2O$] for the 10:1 and 10:2 compositions (Table 1). The XRD peaks of the hydrogrossular were weaker for 10:2 composition than those for the 10:1 composition, whereas those of unreacted gehlenite were stronger. For the 10:4 composition, nepheline hydrate ($NaAlSiO_4 \cdot 1/2H_2O$) was obtained in addition to tobermolite. For the 10:8 composition, analcime ($NaAlSi_2O_6 \cdot H_2O$) and tobermolite were obtained (Table 1). The XRD peaks of analcime were very strong and those of nepheline hydrate disappeared.

In the Al_2O_3-SiO_2-H_2O-NaOH system, analcime crystallized from the $2Al_2O_3 \cdot SiO_2$, $Al_2O_3 \cdot SiO_2$, $Al_2O_3 \cdot 2SiO_2$, $Al_2O_3 \cdot 4SiO_2$ and $Al_2O_3 \cdot 8SiO_2$ with 1N NaOH solution (Table 2). Nepheline hydrate as a major product was obtained from both the $8Al_2O_3 \cdot SiO_2$ and $4Al_2O_3 \cdot SiO_2$ with 1N NaOH solution. The product with 0.1 N NaOH solution was analcime alone (Table 2).

Heating experiments Heating experiments were performed with analcime and nepheline hydrate obtained by the hydrothermal experiments. Although analcime did not change at 400℃, 500℃, 600℃ and 700℃, the presence of nepheline at 800 ℃ shows that analcime dehydrates to form nepheline between 700 ℃ and 800 ℃ (Table 3). Nepheline hydrate did not change at 400℃, 500℃ and 600℃, however, the specific XRD peaks of nepheline appeared at 700 ℃. No peaks of nepheline hydrate were observed at 700 ℃ (Table 3).

The differential thermal curve for analcime gave a broad endothermic peak between 200 ℃ and 400 ℃. The thermogravimetric curve also shows a weight loss between 200 ℃ and 400 ℃. The differential thermal curve for nepheline hydrate gave an endothermic peak at about 230 ℃. The thermogravimetric curve also showed a sharp weight loss between 200 ℃ and 280 ℃.

Discussion

The analcime and/or nepheline hydrate which crystallized from gehlenite-SiO_2 mixtures with 1N NaOH solution coexisted with tobermolite and unreacted gehlenite (Table 1). Since Al was not added in this system, Al leached from gehlenite has contributed to the formation of analcime or nepheline hydrate. Therefore, analcime and/or nepheline hydrate crystallized through the reaction of Al (dissolved from gehlenite), Si (supplied by starting material) and Na (supplied by solution). Analcime which coexisted with gehlenite was obtained from the SiO_2-rich compositions, whereas nepheline hydrate was obtained from the Al_2O_3-rich compositions (Table 1). The results in the system SiO_2-Al_2O_3-H_2O-NaOH also show that nepheline hydrate crystallized from the Al-rich fluid, whereas analcime crystallized from the Si-rich fluid (Table 2). The minerals obtained are dependent on the Al_2O_3/SiO_2 ratio and NaOH content in solution as suggested by the results of the SiO_2-Al_2O_3-H_2O-NaOH system (Table 2). These results suggest that the NaOH content and Al_2O_3/SiO_2 ratio in fluid in parent bodies during aqueous alteration affect the mineral assemblage of secondary minerals in CAIs.

Both analcime and nepheline hydrate were changed to nepheline by the heating experiments. Both analcime and nepheline hydrate stopped decreasing in weight up to 600 ℃, whereas heating experiments have changed both analcime and nepheline hydrate to nepheline between 600 ℃ and 800 ℃ (Table 3). Because the H_2O molecules in both analcime and nepheline hydrate are zeolitic water, the crystal structures of both analcime and nepheline hydrate may remain unchanged until their inversion temperatures to nepheline.

The Na-, Si-rich fluid dissolved gehlenite to become rich in Al enough to crystallize nepheline hydrate and/or analcime by leaching of Al from gehlenite. Whether nepheline hydrate crystallized or analcime from fluid is attributed to the Al/Si ratio and Na content in fluid at the time of crystallization. At the thermal metamorphism stage, nepheline hydrate and/or analcime was converted into nepheline. Nepheline which is often observed to coexist with gehlenite in CAIs [2] may have been produced by this process. Our results imply that some nepheline hydrates and/or analcimes escape dehydration and remain in CAIs due to low-degree thermal metamorphism in parent bodies.

Conclusions

(1) The Na, Si-rich fluid dissolved gehlenite to produce Al-rich fluid enough to crystallize nepheline hydrate and/or analcime.

(2) The Al content in solution in the gehlenite-Al_2O_3-H_2O-NaOH system does not affect the mineral assemblage of products of hydrothermal experiments on gehlenite, whereas the Si content in solution in the gehlenite-SiO_2-H_2O-NaOH system affects the mineral assemblage of products. These results suggest that dissolved ions (e.g., the Al/Si ratio) in fluid in parent bodies affected the mineral assemblage of secondary minerals in CAIs.

(3) Both analcime and nepheline hydrate obtained by the hydrothermal experiments are converted into nepheline by heating experiments. The DTA-TG curves for analcime and nepheline hydrate show that their dehydrations complete up to 400 ℃ and 600℃, respectively. These results suggest that some hydrous minerals produced by aqueous alteration in parent bodies were dehydrated during thermal metamorphism. Our results imply that some nepheline hydrates and/or analcimes escape dehydration and remain in CAIs due to low-degree thermal metamorphism in parent bodies.

Acknowledgments

We thank Dr. K. Tsukimura of Geological Survey of Japan for helpful suggestions.

References

[1] Grossman L. (1972) Geochim. Cosmochim. Acta 36, 597-619.
[2] Tomeoka K., Nomura K. and Takeda H. (1992) Meteoritics 27, 136-143
[3] Grossman L. and Steele I. M. (1976) Geochim. Cosmochim. Acta 40, 149-155.
[4] Nomura K. and Miyamoto M. (1995) Antarctic Meteorites XX, 200-203.
[5] Akai J. (1988) Geochim. Cosmochim. Acta 52, 1593-1599.

Table 1. Experimental conditions and observed phases of products in the gehlenite-Al_2O_3- SiO_2 -H_2O-NaOH system.

Starting Material Ge	Al_2O_3	SiO_2	Solution		Temperature (℃)	Time (hours)	Observed phases
10			NaOH	1N	200	168	Hg
10	1		NaOH	1N	200	168	Hg
10	2		NaOH	1N	200	168	Hg
10	4		NaOH	1N	200	168	Hg
10	8		NaOH	1N	200	168	Hg
10		1	NaOH	1N	200	168	Ge+Hg+ To
10		2	NaOH	1N	200	168	Ge+To+(NH, Hg)
10		4	NaOH	1N	200	168	Ge+To+NH
10		8	NaOH	1N	200	168	Ge+To+Anal

Table 2. Experimental conditions and products in the Al_2O_3-SiO_2-H_2O-NaOH system.

Starting Material	Solution		Temperature (℃)	Time (hours)	Run products
A_8S	NaOH	1N	200	168	NH
	NaOH	0.1N	200	168	Anal
A_4S	NaOH	1N	200	168	NH(Anal,HS)
	NaOH	0.1N	200	168	Anal
A_2S	NaOH	1N	200	168	Anal (HS)
AS	NaOH	1N	200	168	Anal (HS)
	NaOH	0.1N	200	168	Anal
AS_2	NaOH	1N	200	168	Anal
AS_4	NaOH	1N	200	168	Anal
	NaOH	0.1N	200	168	Anal
AS_8	NaOH	1N	200	168	Anal
	NaOH	0.1N	200	168	Anal

Table 3. Experimental conditions and observed phases of heating experiments.

Starting Material	Temperature (℃)	Time (hours)	Observed phases
Analcime	400	24	Anal
	500	24	Anal
	600	24	Anal
	700	24	Anal
	800	24	Ne
Nepheline Hydrate	400	24	NH(Anal, HS)
+ (Anal, HS)	500	24	NH(Anal, HS)
	600	24	NH(Anal, HS)
	700	24	Ne(Anal, HS)

( )	: Minor component		Ge : Gehlenite	$Ca_2Al_2SiO_7$
Anal	: Analcime	$NaAlSi_2O_6 \cdot H_2O$	Hg : Hydrogrossular	$Ca_3Al_2(SiO_4,H_4O_4)_3$
HS	: Hydrosodalite	$Na_8Al_6Si_6O_{24}(OH)_2 \cdot 2H_2O$		
NH	: Nepheline Hydrate	$NaAlSiO_4 \cdot 1/2H_2O$		
Ne	: Nepheline	$NaAlSiO_4$		
To	: Tobermolite	$Ca_5Si_6O_{18}H_2 \cdot 4H_2O$		
A_mS_n	: Mixture of Al_2O_3 and SiO_2	$mAl_2O_3 \cdot nSiO_2$		

Comparative studies of Solar, Q- and terrestrial noble gases, and its implication on the evolution of the solar nebula.

M. Ozima[1,2], R. Wieler[3], B. Marty[4], and F.A.Podosek[1]
[1]MacDonnell Center, Washington University, St Louis, MO63130, USA, [2]Department of Earth and Planetary Physics University of Tokyo, Tokyo 113, Japan, [3]Isotope Geochemistry, ETH, Zurich, CH-8092, Swiss, [4] CRPG-CNRS, Vandeuvre-les-Nancy, France.

Noble gases have been successfully used to resolve the evolution of the Earth, in that important constraints are imposed from comparison of noble gas elemental and isotopic compositions in major reservoirs such as the atmosphere, the crust and the mantle. We discuss that comparative studies of major noble gas components in the solar system also yields fundamental constraints on the evolution of the early solar nebula. As the major noble gas components in the solar system, we consider the solar noble gas which we assume to be best represented by the solar wind noble gas (SW noble gas), and Q-noble gases which are ubiquitous in meteorites. Apart from radiogenic noble gases, heavier noble gases (Ne, Ar, Kr, Xe) in the solar noble gases are essentially the same as those originally incorporated into the primitive solar nebula. However, since helium isotopic ratio changed substantially due to nuclear reactions in the sun, especially due to the deuteron burning, $D(n,\gamma)^3H \rightarrow 3He$, at the early stage of the evolution of the sun, we must make distinction between the pre D-burning He and the post D-burning He.

In Figure 1, we plotted ratios of elemental and isotopic ratios of the Q and SW noble gases against $(m_1/m_2)^{1/2}$. Most of data lie on a nice straight line. This suggests that the Q-noble gases were related to the SW noble gases through Rayleigh distillation. Further interesting is the fact that in plotting Figure 1, we assigned the post D-burning He to the SW helium. Therefore, if the Q-noble gases were indeed derived from the SW noble gases through the Rayleigh distillation, this implies that the solar nebula in a region where meteorites or their parent bodies acquired noble gases was well mixed with the post D-burning He. Noble gas data from terrestrial diamonds also appear to suggest that the Earth acquired the post D-burning He.

In comparing terrestrial noble gases with both solar and Q components we conclude that it is more plausible to derive terrestrial gas from a mixture of the two than from either alone. We therefore also suggest consideration of a model in which the earth acquired its noble gases partly from solar outflow and partly from fractionated gases (the Q component) generated farther from the protosun.

On the basis of the observational constraints, we propose the following scenario for the evolution of noble gases in the solar syste. During and/or soon after the D-burning in the primitive sun, the post D-burning He produced in the sun was fairly well mixed

with the solar nebula. In a region where meteorite parent bodies formed, noble gases underwent the Rayleigh fractionation, whereas the solar nebula nearer to the sun was less subjected to fractionation, perhaps due to less denser nebula density. Therefore, in the terrestrial planet region which is located in an intermediate region, noble gases acquired mixing characteristics of the Q and SW noble gases.

References: [1] Ceruti, H. (1974) *PhD Thesis*, Univ. of Bern. [2] Wieler, R. and Baur, H. (1995) *Astrophys. J. 453*, 987-997. [3] Wieler, R. (1994) In: *Noble Gas Geochemistry and Cosmochemistry, pp 31-41*, (ed. by J. Matsuda), Tera Sci. Publ.Co., Tokyo.

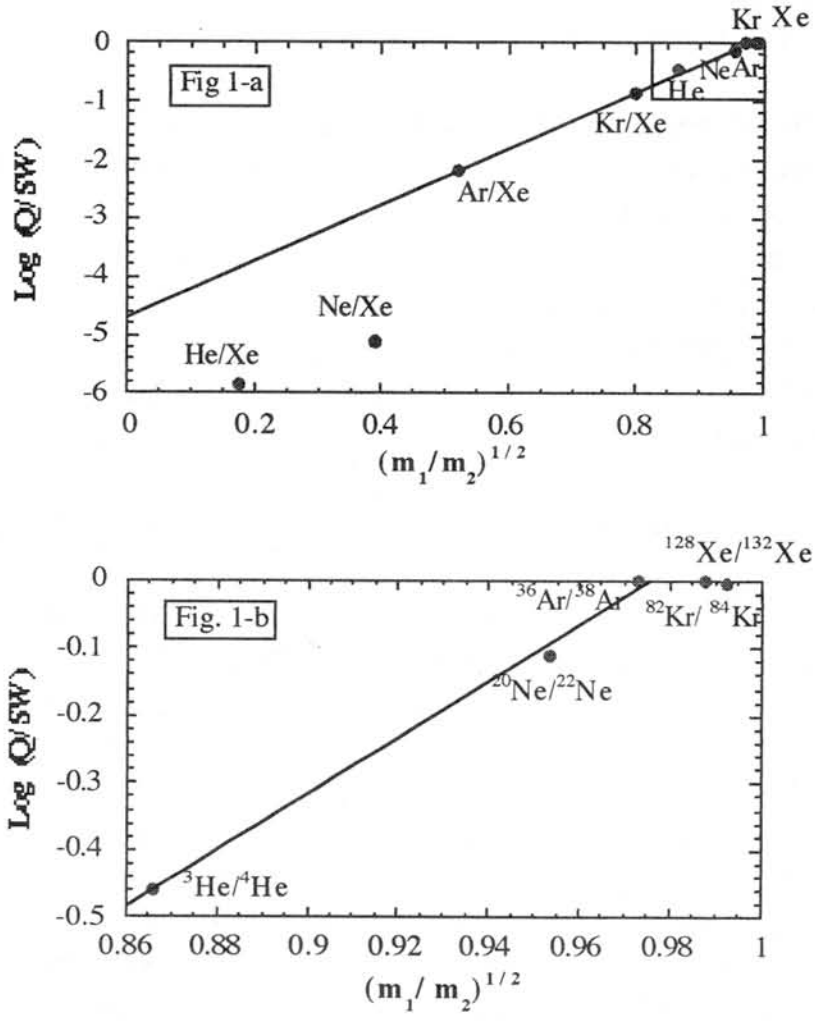

Figure 1. Ratio of elemental and isotopic ratios of Q and SW vs. square root of a mass ratio. Data; He/Ne and Ne/Ar [1], Ar/Kr and Kr/Xe[2], Isotopic ratio[3].

UNUSUAL METAL-RICH CLASTS FROM THE EREVAN HOWARDITE

Rad'ko, L.V.and Ulyanov, A.A.

Geological Department of M.V. Lomonosov Moscow State University, 119899, Moscow, Russia.

During the last years the great interest toward the exploring of breccia meteorites, is increased because it was suggested that there is a possibility of existence in them different clasts, coming from several parent bodies.

The first chemical and mineralogical investigation [1] of Erevan meteorite showed that it is a howardite and a polymict breccia. It was also observed some eucrite-like clasts with different textures [1]; recently M. Nazarov and A. Ariskin [2] found several carbonaceous chondrite lithologies, angrite-like clasts, glassy clasts and clasts containing up to 45 vol. % of metallic iron.

We studied mineralogy of two iron-rich clasts N1 and N475 by EPMA and SEM techniques. In the first clast we found a lot of relative large (up to 30 μm) Ni-poor metal grains and in the second one we observed Ni-rich metal grains. There is a negative correlation between abundances of Ni in the metal phases and FeO content in associated silicates. The electron microprobe analyses of mineral phases are result in weight percent.

Clast N1 (size about 1000*340 μm^2). The metallic phase contains about 0,4 % Ni and ~ 0.1 % Co; covers ~ 45 vol. %. The main silicate minerals are pyroxene (30 vol. %) and plagioclase (20 vol. %); accessories are minute chromite, ilmenite, and silica. The maximal size of main mineral grains decrease in the sequence: Fe-metal (up to 400 μm), pyroxene (up to 200 μm) and plagioclase (up to 150 μm). Pyroxenes are represented by two varieties - Fe-poor ($En_{65}Wo_{2,5}$), containing about 20 % FeO and Fe-rich ($En_{37}Wo_{2,3}$) containing about 35 % FeO (Table 1). Pyroxene grains exhibit often microscopic exsolution but there are also grains without exsolution lamellies. The lamellies has more calcic composition ($En_{35}Wo_{44}$) then the host mineral. The composition of plagioclases (An_{85-87}) are typical for the Erevan matrix (Table 2) [2]. The grains of plagioclase usually contain up to 2 % FeO; the central part of the grains contain more FeO, then the outer part. Chromite grains contain TiO_2 (up to 4.5 %), Al_2O_3 (up to 9.5 %), MgO (up to 1.3 %) and MnO (up to 7 %) (Table 3). Silica is a minor component of the clast (only 4 grains was found). These grains contain up to 2 % FeO (Table 4).

Clast N 475 (size about 600*440 μm^2). The metallic phase contains about 5.0 % Ni and ~ 0.4 % Co; covers ~ 30 vol. %. Clast also contains pyroxene (~ 50 vol. %) and plagioclase (~ 20 vol. %); accessory is minute chromite (Table 3). The maximal size of main mineral grains decrease in sequence: Fe-metal (up to 300 μm), pyroxene (up to 250 μm) and plagioclase (up to 100 μm). Pyroxene contains about 23 % FeO and its composition is $En_{55}Wo_{2,3}$ (Table 1). Plagioclase contains more CaO (An_{90-95}) than one in the clast N1, but it is also typical for the Erevan matrix [2]. Plagioclase grains also contain FeO (0,2 % - 1,1 %) (Table 2).

General condition of formation of these clasts is low values of fO_2 (metallic Fe exist). However because there are differences in contents of Ni in metallic phases and FeO in the silicates between these clasts, we can suggest that these two lithologies were formed in the different parent bodies.

The clast N475 was probably formed of the surface at the meteorite parent bodies and may be represent the matters of the protoregolith breccia. The clast N1 differs significantly in texture, mineralogy and chemistry from the known meteorite matter. Moreover exsolution textures of pyroxenes in clast N1 require annealing for a long period of the time and slow cooling. Clast N1 has probably igneous origin inside an achondrite parent body. A lot of different types of clasts in Erevan howardite suggest the scenario of the origin of breccia meteorites which includes the intensive solid matter exchange between protoplanets and some reservoirs in primary heterogeneous solar nebula.

We thank N.N. Korotaeva and N.N. Kononkova for their technical assistance and M.A. Nazarov for helpfull discussion. This work was supported in part by RFBR grant 96-05-65144.

References: 1. Kvasha, L. and Scripnik, A. (1978) The Erevan meteorite. *Meteoritika* , **37**, p. 80 (in Russion). 2. Nazarov, M.A. and Ariskin, A.A. (1993) The Erevan howardite: petrology of glassy clasts and mineral chemistry. *Lunar Planet. Sci.*, XX1V, p. 1049.

Table 1. Representative analyses of pyroxene.

SiO_2	TiO_2	Al_2O_3	FeO	MnO	MgO	CaO	Cr_2O_3	Wo	En	Fs	Type
clast N1											
47.15	0.06	0.16	33.22	1.00	11.94	1.43	0.05	3.1	35.9	56.0	Fe-rich
52.33	0.17	0.80	16.37	0.58	18.54	10.83	0.41	22.6	51.5	25.9	Fe-poor
49.63	0.34	0.34	18.62	0.70	10.28	19.69	0.40	40.6	29.5	30.0	lamm.
clast N475											
52.97	0.15	0.49	24.65	0.81	19.36	1.31	0.26	0.5	92.4	7.2	Fe-poor

Table 2. Representative analyses of plagioclase.

SiO_2	Al_2O_3	FeO	CaO	Na_2O	K_2O	Or	Ab	An
clast N1								
44.24	33.52	3.65	17.31	1.18	0.10	0.6	7.3	92.1
44.09	34.15	2.65	17.58	1.43	0.11	0.7	5.2	94.1
45.43	34.59	1.07	17.58	1.32	b.d.l.	0.5	9.9	89.6
46.39	30.80	4.78	15.57	2.25	0.21	1.4	15.5	83.1
44.38	32.24	5.18	16.29	1.70	0.21	1.4	8.2	90.4
clast N475								
45.20	33.90	1.15	18.38	1.25	0.12	0.8	7.0	92.3
44.45	34.29	1.19	18.73	1.25	1.00	0.6	4.0	95.4
44.05	34.79	0.84	19.22	1.01	1.00	0.6	2.3	97.1
43.50	35.07	1.11	19.30	0.94	1.00	0.5	0.1	99.3
44.93	35.01	0.26	18.55	1.19	b.d.l.	0.4	6.5	93.2

Table 3. Representative analyses of chromite.

FeO	SiO_2	Cr_2O_3	Al_2O_3	TiO_2	MnO	MgO
clast N1						
34.70	0.39	50.12	9.46	3.40	0.65	1.26
35.90	0.23	48.89	8.56	4.38	0.72	1.24
clast N475						
34.10	0.00	50.57	10.08	2.90	0.70	1.61
39.10	0.43	47.01	7.34	5.17	0.57	0.31

Table 4. Representative analyses of silica (clast N1)

SiO_2	Al_2O_3	FeO	CaO	Na_2O	P_2O_5
96.06	0.58	2.55	0.39	b.d.l.	0.41
98.72	0.00	1.16	b.d.l.	0.12	b.d.l.
98.01	0.50	1.49	b.d.l.	b.d.l.	b.d.l.
97.75	b.d.l.	2.15	b.d.l.	b.d.l.	b.d.l.

* b.d.l = below detection limit

Absorption Bands near 3 μm in Diffuse Reflectance Spectra of Carbonaceous Chondrites: Comparison with C-type Asteroids

K. Sato[1], M. Miyamoto[1], and M. E. Zolensky[2]
[1]*Mineralogical Institute, Graduate School of Science, University of Tokyo, Hongo, Tokyo 113, Japan*
[2]*SN2, NASA/Johnson Space Center, Houston, TX 77058, USA*

Introduction

We measured infrared diffuse reflectance spectra of several carbonaceous chondrites to study surface materials of C-type asteroids. The absorption bands near 3 μm are due to the presence of hydrates and/or hydroxyl ions (OH stretching vibration), and the intensity of the 3 μm band is related to the amount of hydrous minerals in a sample [e.g., 1]. Therefore, absorption features near 3 μm are important to detect the amount or species of hydrous minerals on planetary surfaces such as C-type asteroids, which have been thought to be compositionally similar to carbonaceous chondrites. The two most intensely studied C-type asteroids are the two largest asteroids in the belt, 1 Ceres and 2 Pallas. Reflectance spectra of Ceres and Pallas show broad absorption bands near 3 μm, suggesting the presence of hydrous minerals in their surface materials [2, 3]. Although the spectra of Ceres and Pallas resemble those of CI or CM chondrites, the intensity of the 3 μm bands are weaker than those of CI and CM chondrites. Because thermally metamorphosed carbonaceous chondrites with CI-CM affinities were recently found in the Antarctic meteorite collection, the spectral characteristics of these C-type asteroids should be compared with those of thermally metamorphosed carbonaceous chondrites and C3-5 chondrites.

In this paper, we measured several carbonaceous chondrites in addition to those by [4], and compared the intensity of absorption bands near 3 μm of reflectance spectra of Ceres and Pallas with those of carbonaceous chondrites including the thermally metamorphosed carbonaceous chondrites.

Samples and Experimental Techniques

Newly measured carbonaceous chondrites were Isna (CO3), Maralinga (C4) and Karoonda (C5). Samples of these carbonaceous chondrites weighing approximately 50 mg were ground in a corundum mortar and passed through a 100 μm sieve to obtain powder samples for spectral measurements. Each powder sample was dried in a desiccator for at least 48 hours in order to remove any adsorbed water from the grain surface. A specimen weighing approximately 20 mg was taken from each powder sample and used for the spectral measurements. Diffuse reflectance spectra were measured in dry-air surroundings by the use of a Fourier transform infrared spectrometer (JASCO, FT/IR-300E) equipped with a diffuse reflectance attachment. Spectra were taken over the range from 7900 cm^{-1} (1.27 μm) to 400 cm^{-1} (25 μm) at a resolution of 4 cm^{-1}. An aluminum-coated mirror was used as standard. Diffuse reflectance spectra in [4] were measured under the similar conditions and were taken over the range from 3950 cm^{-1} (2.53 μm) to 400 cm^{-1} (25 μm) at a resolution of 4 cm^{-1}. Details of measurements are described in [5].

Reflectance Spectra of Carbonaceous Chondrites

Reflectance spectra of carbonaceous chondrites exhibit various intensities of absorption bands near 3 μm, caused by hydrous minerals. Generally, molecular water in minerals shows broad absorption bands near 3400 cm^{-1} (2.94 μm) and hydroxyls typically show sharp absorption bands near 3650 cm^{-1} (2.74 μm). In order to compare the intensity of absorption bands near 3 μm of carbonaceous chondrites, we calculated the integrated intensity. The integrated intensity of the absorption bands near 3 μm was calculated as follows: A background curve approximating to a straight line obtained by the least squares fitting was determined by using reflectances from 3950 to 3800 cm^{-1} and from 2600 to 2500 cm^{-1}. After normalizing reflectance data at 2500 cm^{-1}, the integrated intensity was calculated by numerically integrating the spectra from 3800 to 2600 cm^{-1}. Among the measured carbonaceous chondrites, only Maralinga, C4 meteorite, has absorption bands near 2500 cm^{-1}. We, therefore, normalized reflectance data of Maralinga at 2400 cm^{-1} and obtained its background curve by using reflectances from 3950 to 3800 cm^{-1} and from 2450 to 2400 cm^{-1}, in order to avoid the influence of absorption bands near 2500 cm^{-1}.

The CI and CM chondrites show larger values of the integrated intensity than those of thermally metamorphosed carbonaceous chondrites. This is probably due to dehydration of hydrous minerals in the thermally metamorphosed carbonaceous chondrites by thermal metamorphism, consistent with mineralogical observations [e.g., 6]. Orgueil (CI) has the largest value of the integrated intensity among the carbonaceous chondrites measured. CV chondrites have little or no hydrous minerals detectable from the 3 μm band. Renazzo (CR) has a value of the integrated intensity intermediate between the CM and CV. Although the value of the integrated intensity of Renazzo is close to those of the thermally metamorphosed carbonaceous chondrites, the wavenumber position of reflectance minima is different (3630 and 3400 cm^{-1}, respectively). The spectral features of absorption bands near 3 μm of Renazzo are similar to those of the CM or CI chondrites but the amount of hydrous minerals in Renazzo is smaller than that in the CM or CI chondrites.

Reflectance Spectra of C-type Asteroids

1 Ceres has a broad round 3 μm band assigned to "water" and a narrow and weak absorption band centered near 3.1 μm which is superimposed on the much stronger and broader absorption band [7]. The 3 μm "water" feature is strong in the Ceres spectrum, indicating an abundant hydrated silicate species [8]. 2 Pallas has a 3 μm absorption feature that is significantly weaker than the same feature in the spectrum of Ceres, which indicates a much lower abundance of hydrated minerals on its surface [8, 9]. Because of obscuration by terrestrial H_2O, the telescopic reflectance observations do not include the important 2.7 μm region where minerals containing structural or adsorbed water can be distinguished on the basis of the band shape. Therefore, it is difficult to determine mineral species of hydrous minerals on asteroidal surfaces.

Comparison between Carbonaceous Chondrites and C-type Asteroids

Because telescopic reflectance spectra of asteroids between 2.6 and 2.8 μm are not available, we cannot calculate the integrated intensity of the 3 μm band of asteroidal reflectance spectra. Instead of the integrated intensity, we utilized the reflectance ratios

to study the intensity and slope of the 3 μm band. We calculated two reflectance ratios, 2.9/2.53 and 3.2/2.53. The reflectance ratio 2.9/2.53 was calculated by dividing the reflectance at 2.9 μm by that at 2.53 μm. We chose the reflectance at 2.53, 2.9 and 3.2 μm in order to avoid both the gap in the spectral data of asteroids and the absorption bands near 3.4 μm due to organic compounds in meteorites.

There is an excellent negative correlation between the integrated intensity of the 3 μm absorption band and the reflectance ratio 2.9/2.53 for carbonaceous chondrites. The correlation coefficient between these values is -0.996. The integrated intensity of the 3 μm band and the reflectance ratio 3.2/2.53 also have a clear negative correlation. The correlation coefficient between these values is -0.936. Thus, the reflectance ratios, 2.9/2.53 and 3.2/2.53, correlate very well with the integrated intensity of the 3 μm hydration band of carbonaceous chondrites. The increased integrated intensity of the 3 μm absorption bands is evident in the decreased reflectance ratio. The results of the reflectance ratios are consistent with those of the integrated intensity of the 3 μm band and may correlate with the amount of hydrous minerals.

Fig. 1 compares the reflectance ratios, 2.9/2.53 vs. 3.2/2.53 of the carbonaceous chondrites with those of C-type asteroids, Ceres and Pallas. Pallas plots near the crowded region of the thermally metamorphosed carbonaceous chondrites and CR chondrite, Renazzo. Considering the excellent correlation between the reflectance ratios and the integrated intensity of the 3 μm hydration band, this result suggests that the intensity of the 3 μm absorption band in the reflectance spectra of asteroid 2 Pallas is similar to those of the thermally metamorphosed carbonaceous chondrites or a CR chondrite.

Although the 2.9/2.53 ratio of Ceres is similar to those of the thermally metamorphosed carbonaceous chondrites and a CR chondrite, the 3.2/2.53 ratio of Ceres is different. Nevertheless, the overall spectral profile of Ceres is similar to that of the thermally metamorphosed carbonaceous chondrite, Y-82162, in the visible-near IR wavelength region [3]. Since the removal of the asteroidal thermal emission spectra may have an effect on the reflectance at 3.2 μm, further investigations are needed for Ceres.

The four carbonaceous chondrites, Y-793321, Y-82161, Y-86720, and Renazzo share the region near Pallas in Fig. 1 and, thereby, are candidates for the close counterparts of Pallas. The reflectance spectrum of Pallas rises longward of 2.8 μm. The reflectance minima of the thermally metamorphosed carbonaceous chondrites range from 2.9 to 2.95 μm. Among these four carbonaceous chondrites, only Renazzo has its minimum of the reflectance spectra at the shorter wavelength region than 2.8 μm. Although the four carbonaceous chondrites exhibit similarity to Pallas, Renazzo is a best spectral match to Pallas. The position of the reflectance minimum of Renazzo is approximately 2.75 μm (3630 cm^{-1}) which is probably due to the presence of hydroxyls in hydrous minerals.

References

[1] Miyamoto M. (1991) *Geochim. Cosmochim. Acta* **55,** 89-98.
[2] Hiroi T., Pieters C. M., Zolensky M. E. and Lipschutz M. E. (1995) *Meteoritics* **30,** 521.
[3] Hiroi T., Pieters C. M., Zolensky M. E. and Lipschutz M. E. (1995) *Antarctic Meteorites XX*, 72-75.
[4] Miyamoto M. and Zolensky M. E. (1992) *Proc. ISAS Lunar Planet. Symp.* **25th,** 32-35.
[5] Miyamoto M. and Zolensky M. E. (1994) *Meteoritics* **29,** 849-853.

[6] Zolensky M. E., Barrett R. and Browning L. (1993) *Geochim. Cosmochim. Acta.* **57,** 3123-3148.
[7] Lebofsky L. A., Feierberg M. A., Tokunaga A. T., Larson H. P. and Johnson J. R. (1981) *Icarus* **48,** 453-459.
[8] Jones T. D., Lebofsky L. A., Lewis J. S. and Marley M. S. (1990) *Icarus* **88,** 172-192.
[9] Larson H. P., Feierberg M. A. and Lebofsky L. A. (1983) *Icarus* **56,** 398-408.

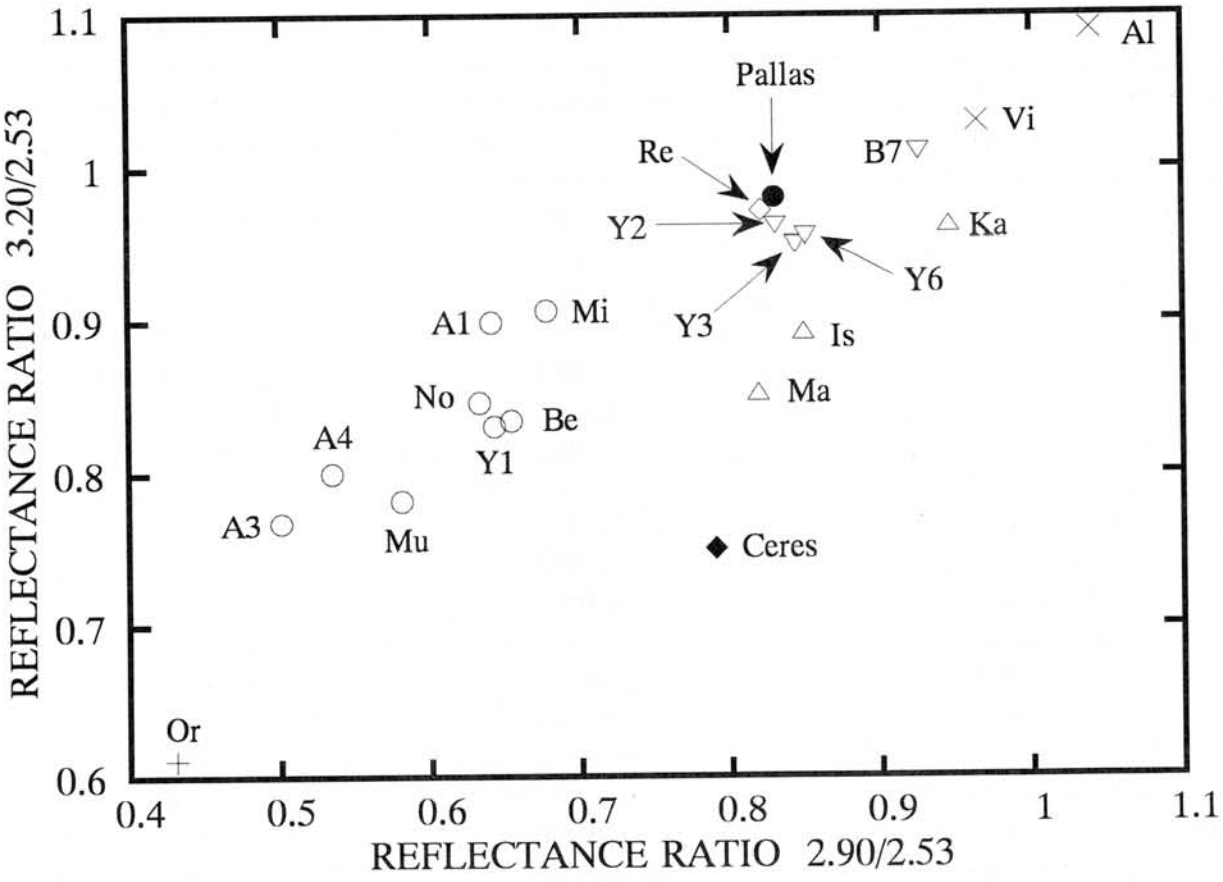

Fig.1. Plots of the reflectance ratio, 2.90/2.53 vs. 3.20/2.53 for carbonaceous chondrites, Ceres and Pallas. ○:CM chondrites, A1: ALH81002; A3: ALH83100; A4: ALH84029; Be: Bells; Mi: Mighei; Mu: Murchison; No: Nogoya; Y1: Y791198. ▽ :Thermally metamorphosed carbonaceous chondrites, B7: Belgica7904(CM); Y2: Y82162(CI); Y6: Y86720(CM); Y3: Y793321(CM). × :CV chondrites, Al: Allende; Vi: Vigarano. ◇:CR chondrites, Re: Renazzo. + :CI chondrites, Or: Orgueil. △:Newly measured carbonaceous chondrites, Ka: Karoonda(C5); Ma: Maralinga(C4); Is: Isna(CO3). ◆: Asteroid 1 Ceres. ●: Asteroid 2 Pallas.

A Preliminary Study of Carbon Isotope Analyses of Individual Hydrocarbon Molecules In Murchison Meteorite.

Jooyoung Sohn and Jongmann Yang
Department of Physics, Ewha Womans University, Seoul 120-750, Korea

$^{13}C/^{12}C$ ratios of hydrocarbon molecules have important informations about the origin of meteorite, the early solar system, prebiotic evolution, and the origin of life. There are good reasons to believe that the meteoritic organic matter was synthesized abiotically in the early solar system. It appears that more than one process contributed to the organic population and that several different environments were involved, possibly including dense interstellar clouds, the solar nebula, and the surface regions of planetesimals[1].

Mueller published the results of his work on the organic component of the Cold Bokkeveld meteorite in 1953[2]. Murchison was found to contain both amino acids and aliphatic hydrocarbons[3].

Two laboratory models have been studied, the Fischer-Tropsch type (FTT) process[4] and the Miller-Urey (MU) synthesis[5], but several other possibilities have been considered in less detail. It is probably fair to say that most investigators believe that multiple processes and environments have contributed to the synthesis of meteoritic organic matter.

A process that has recently become of interest in the context of prebiotic synthesis is the ion-molecule reaction. The occurrence of such reactions in dense interstellar clouds has been extensively investigated[6], but how applicable this work is to conditions in the early solar system is not clear. In such a reaction scheme, an atom or a molecular fragment is ionized by galactic cosmic radiation and can then react with neutral species at a temperature far below than the temperature at which two neutral species could react. It is this property that makes such reactions dominant in dense interstellar clouds, where temperatures are often close to 10K.

The terrestrial organic matters have $\delta^{13}C$ values of about -10 to -40 ‰. The carbon in the Murchison meteorite has the same overall isotopic composition as terrestrial carbon, i.e. a $\delta^{13}C$ value of about -7 ‰[7]. Organic matter, the major carbonaceous phase in carbonaceous chondrites, can be shown from mass balance calculations to have an average $\delta^{13}C$ value of about -9 ‰ in the case of the Murchison meteorite. Relative to terrestrial organic matter, the meteorite organics are isotopically heavy and their $\delta^{13}C$ values are generally more positive or fall at the heavy end of the usual terrestrial range.

A small fraction, probably less than 10%, of the carbon of CM chondrites occurs as a diverse suite of extractable organic compounds[8]. The hydrocarbons of carbonaceous chondrites have been the object of numerous studies. The work done in the meteorite organic chemistry through 1966 was thoroughly reviewed[9]. Subsequent investigations were carried out mainly with the Murchison (CM2) meteorite. Although much effort has been invested in molecular analyses of the hydrocarbons of carbonaceous chondrites, their precise composition has been difficult to establish both because of the complexity of the mixture and the propensity of these meteorites to acquire terrestrial contaminants, the latter being a particular problem with the aliphatic hydrocarbons[10]. Carbon isotopic analyses[3, 11, 12] have been made only on crude hydrocarbon extracts of indefinite composition and with no analytical control on possible contributions by terrestrial contaminants.

But, there were continuous efforts to obtain as precise data as possible. Molecular

and isotopic analyses of total aliphatic, aromatic, and polar hydrocarbons were done[10, 13]. Later, there was the first attempt to determine carbon isotopic ratios of seven individual polycyclic aromatic hydrocarbon molecules[14]. But it is difficult to confirm some anomalies among the seven molecule species.

In this work, we extracted soluble organic matters in the Murchison meteorite(CM2) by benzene and methyl alcohol, which were then separated by silica gel chromatography[15] into predominantly aliphatic, aromatic, and polar hydrocarbon fractions. Each fraction was further separated by gas chromatography(GC) into individual molecule species at temperature range of 40-280℃. Then carbon atoms of the individual molecule species were sequentially oxidized by CuO to carbon dioxide(CO_2). Since water(H_2O) was produced as a byproduct, the oxidized molecules must pass through the water trap which was maintained at -100℃. $^{13}C/^{12}C$ ratios of carbon in resulting carbon dioxide were analyzed by VG Prism II stable isotope ratio mass spectrometer(GC-IRMS).

The precise delta values of hydrocarbons in Murchison meteorite were very difficult to obtain, because of their small quantity. We controlled some experimental factors such as concentration of the solution, split ratio and injection volume in GC, and parameters in IRMS.

$\delta^{13}C$ values of three types of hydrocarbons in Murchison meteorite were increasing in the order of aromatic, polar, and aliphatic[Figure 1] hydrocarbons. Anthracene in aromatic fraction showed the highest $\delta^{13}C$ value of -5.84 ‰ and dibenzopyridine in polar fraction showed the lowest $\delta^{13}C$ value of -58.34 ‰.

ACKNOWLEDGEMENTS

This work was supported by the Basic Science Research Institute Program, Ministry of Education(Korea) and by the National Institute of Polar Research(Japan).

REFERENCES

1. J. R. Cronin, S. Pizzarello, and D. P. Cruikshank, In Meteorites and the Early Solar System, J. F. Kerridge, M. S. Matthews, Eds. (Univ. Arizona Press, 1988), pp. 819-857.
2. Mueller, Geochim. Cosmochim. Acta 4, 1 (1953).
3. K. Kvenvolden, J. Lawless, K. Pering, E. Peterson, J. Flores, C. Ponnamperuma, I. R. Kaplan, and C. Moore, Nature 228, 923 (1970).
4. M. H. Studier, R. Hayatsu, and E. Anders, Geochim. Cosmochim. Acta 36, 189 (1972).
5. S. L. Miller, J. Amer. Chem. Soc. 77, 2351 (1955).
6. E. Herbst, Origins of Life 16, 3 (1985).
7. W. F. Libby, Proc. Natl. Acad. Sci. USA 68, 377 (1970).
8. J. R. Cronin, S. Pizzarello, S. Epstein, and R. V. Krishnamurthy, Geochim. Cosmochim. Acta 57, 4745 (1993).
9. J. M. Hayes, Geochim. Cosmochim. Acta 31, 417 (1967).
10. J. R. Cronin and S. Pizzarello, Geochim. Cosmochim. Acta 54, 2859 (1990).
11. M. H. Briggs, Nature 197, 1290 (1963).
12. R. H. Becker and S. Epstein, Geochim. Cosmochim. Acta 46, 97 (1982).
13. R. V. Krishnamurthy, S. Epstein, J. R. Cronin, and S. Pizzarello, Geochim. Cosmochim. Acta 56, 4045 (1992).
14. I. Gilmour and C. T. Pillinger, Mon. Not. R. Astron. Soc. 269, 235 (1994).
15. W. G. Meinschein, Space Sci. Rev. 2, 653 (1963).

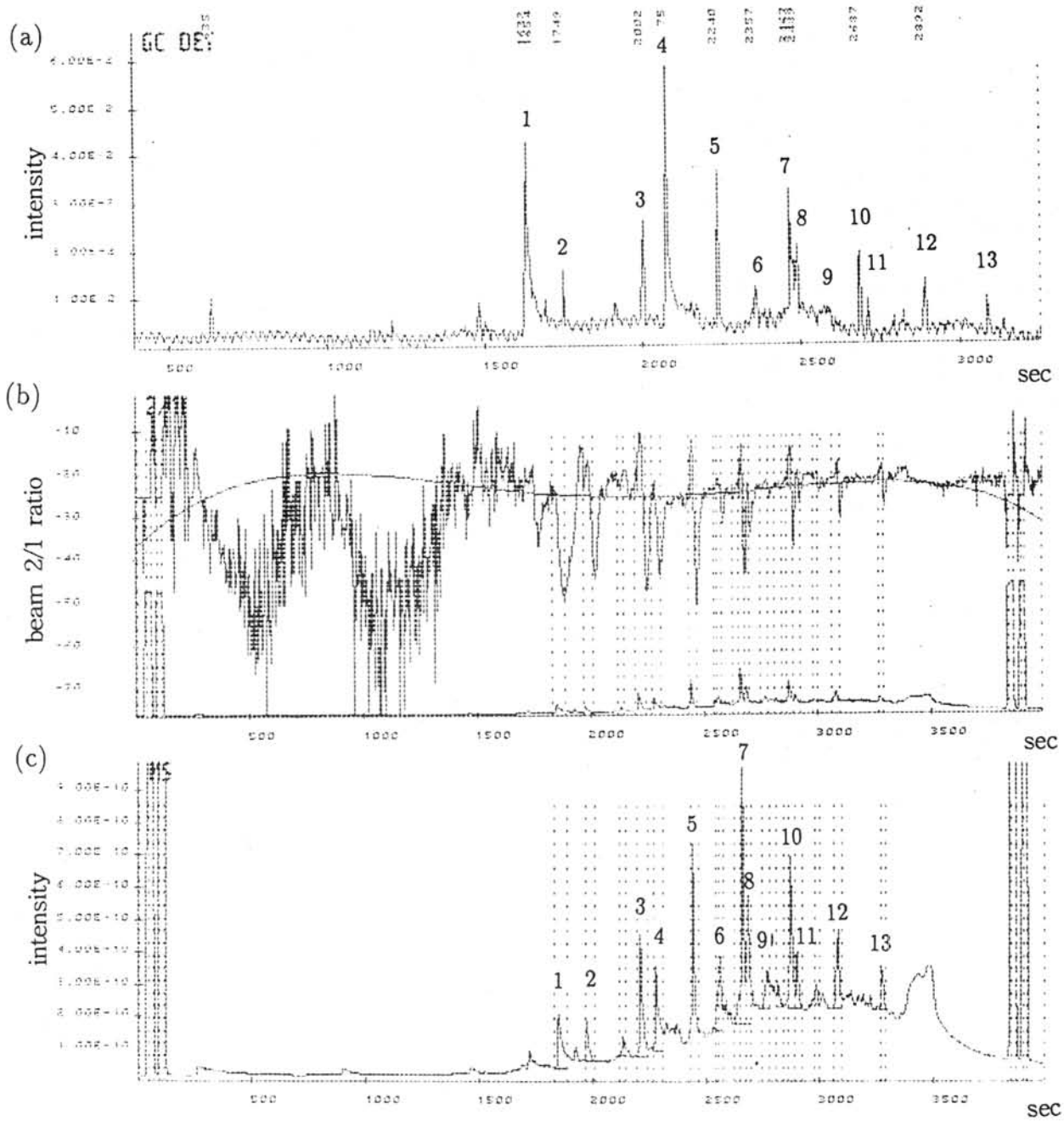

Figure 1. Aliphatic hydrocarbons of the Murchison meteorite, which is a chromatogram of the silica gel hexane fraction of a benzene-methanol extract of the Murchison meteorite. (a) GC chromatogram, (b) C13/C12 ratio, and (c) Mass spectrometer trace. The system used in the analyses is GC-IRMS(Gas Chromatograph - Stable Isotope Ratio Mass Spectrometer; PRISM II) made by VG Isotech.

Exploration of spherules in the Kaba meteorite fall area

P. Solt
Hungarian Geol. Inst. H-1143 Stefánia út 14, Hungary

1.Preface:

In the beginning of investigation of spherules in Hungary in 1994 we suggested field work reviewing some meteorite fall areas In every reports of meteorite fall observations we can hear or-read about detonations, crackings, smoke, etc.,which means thatthere are a lot of little, microscopic particles in the area around the fall. So we had real hope to find some micrometeorites and spherules by collecting soil samples in the area of some well documentated meteorite falls.

2.The Kaba meteorite fall:

Kaba is a village in the Great Hungarian Plain about 200 km east of Budapest. April 15 of 1857 at ten oclock in the evening some inhabitants noticed a fireball coming from south. Mr. Gabor Szilagyi, who also had seen the spectacular event and heard the detonations too, next morning just riding to his farm north of the village, suddenly noticed a black rock flattened into the sandy road. His horse sprang back from the stone. In the evening on the way home Szilagyi digged out the black stone with his friends and carried it to the magistrate of the village. The principal gave the meteorite to the famous Reform College of Debrecen, which town is near to Kaba. The fall is documentated by J.Török/1858/, who was the geography teacher of the College and the first analyses were made by F.Wöhler/1858/. Since then a lot of investigations were made and the meteorite became famous as Kaba III /CV3/ carbonaceous chondrite /A.Hoffer 1928, K.I. Sztrókay 1960,1961, W.R. Van Schmus and J.M. Hayes 1974, L.P. Keller, P.B. Buseck 1990,etc./

3.Field work ;

As the cottage of Szilágyi is already destroyed and the roads and tracks around Kaba changed in the past 140 years, first we had to look for some old maps. In the Library of the Military History Museum in Budapest we could find some excellent documents of military mapping of Hungary 1826-66 and 1861-68., so we could compare the place of the cottage and the roads north from Kaba on modern topographical maps. The possibile meteorite fall area , which we have to investigate is about 40km^2. Our first field work plan consisted of three parts / look the map / :

1. Cross section of the fall direction /1.-2. and 21/27.
2. The area north of Kaba to the cottage of Szilagyi 3.-20.
3. Round the village /28.-52.

The land around Kaba is flat plain with some little lakes, streams and water channels, everywhere sugar beat fields, somewhere fruit gardens. The speed of accumulation of soil is about10 cm in hundred years, so we tried to collect the samples from 10-15 cm deep. Bellow the humusz and soil there are sand and clay from holocene and upper pleistocene. Up to now we collected 52 samples from different places, each sample 1-1,5 kg.

4. Laboratory work:

In the Hungarian Geological Institute from all the samples first the dokumentation samples were separated.After drying, the material was washed with wtaer and then we used hydrogeneperoxide

andhydrochloric acid too for additional cleaning the samples. During sluicing different sieves were used, the finest 60 micron, but we also tried to save the finest, smallest fraction too. We used magnet for to collect the magnetic particles. The sorting and separation was made under microscopes.

5.Results:

After picking we collected up to now more than 400 spherules from 20 to 500 micron / most of them 100-1500 micron in diameter/. The particles are rounded, but also droplets, tear drops, dumb-bell and pear forms occur. There are spherules in matrix too. About one third of the material is magnetic and metallic, one third is glasdsy and one third is scoriaceous.

The distribution of different kinds of spherules in different samples is rathes great, so already we could distinguish the probably fall area / see the map /. To have an exact investigation for the future reconstructionof the Kaba meteorite fall area, sample collection by quadratic method is planned by considering the results of our work. First we have to make lot of chemical analyses of the spherules to distinguish; which are from the Kaba meteorite fall, which are other extaterrestrial ones, which are terrestrials and if there are industrials too. The mineralogical investigations are just made by O.Kákay-Szabó, the mineralogist of the Hungarian Geological Institute.

6.Proposal:

By the results of our investigations we can suggest to other meteorite researchhers, and research groups for meteorite fall reconstructions.

Literature:

Török J. 1858 Ann. Phys. Chem. /Poggendorf/105. p.329.
Wöhler F.1858 Analysis... Sitzungsber.Akad.Wiss.Wien.Math-naturwiss. 33. p.205.
Török J. 1882 Meteorites of the Hungarian Empire. Természettudományi Közlöny XIV. 159. P. 497-514.
Sztrókay K.I. 1960 Neues Jhb. Min. Abh. 94. p. 1284.
Sztrókay K.I. 1961 Acta Geol. Polon. 7. p.57.
Van Schmus W.R., Hayes J.M. 1974 Classification...Geochim.Cosmochim Acta 38. p. 47.
Keller L.P., Buseck P.R. 1990 Aqueous alteration in the Kaba CV3 chondrite. Geochim. Cosmochim. Acta. 54. p. 2113-2120.

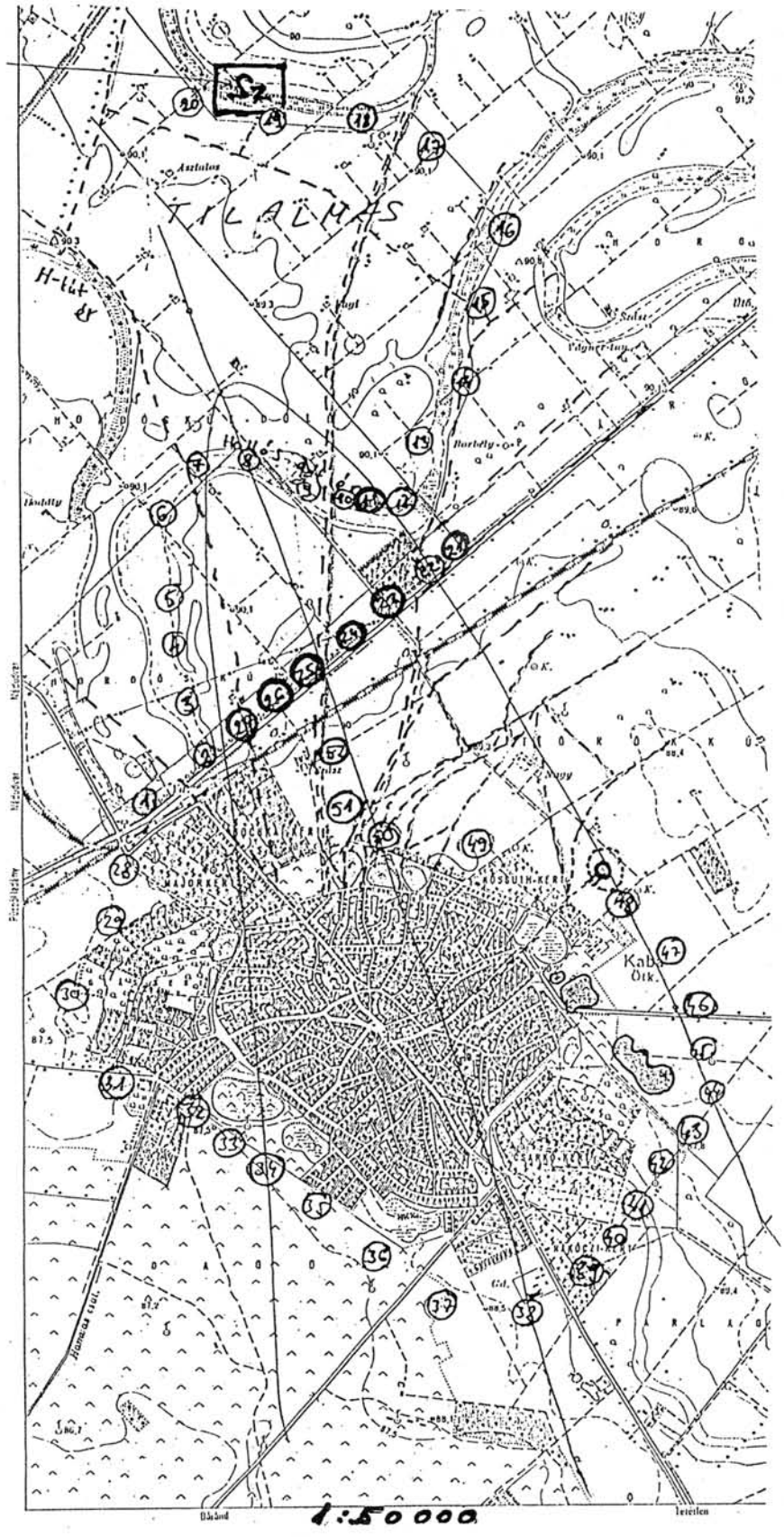

Fig. 1. Map of the Kaba meteorite fall area.

Sz - the site of the Szilágyi cottage, North of Kaba village

---- tracks in 1857

1.-52. Numbers of the sample collecting sites

Mapping of light elements distributions in iron meteorites

Naoji Sugiura

Department of Earth and Planetary Physics, Univ. of Tokyo

Introduction

Microscopic distributions of light elements in iron meteorites were observed with a SIMS (Cameca-6F).

One of the aims of the study is to estimate cooling histories of iron meteorites, analogous to the studies based on nickel distribution in iron meteorites.

Another aim is to elucidate the constitution of the parent bodies based on the abundances of light elements. Light elements are, generally speaking volatile, and hence expected to be lost during the high temperature period of the parent bodies. Therefore, the abundances of light elements are expected to reflect the size of the parent bodies, the duration of the magmatic activity, etc.

This is also a preliminary study for measurements of isotopic compositions of light elements which could be a useful tool for classification.

The only previous studies on microscopic distribution of light elements in iron meteorites are line-profile observations of carbon by e.g. Bashir et al.(1996).

Experimental procedures

Five iron meteorites (Odessa(IA), Squaw Creek(IIA), Sikhote-Alin(IIB), Boxhole(IIIA) and Gibeon(IVA)) have been examined so far. A sample with a size of approximately 1 square cm was polished with diamond paste and set in the sample holder. Cs beam of 10KV was used as the primary ions and the negative secondary ions (H-, C-, CN- and O- together with some of the major negative ions) were extracted at 10KV. The area of the observation (150 micrometer in diameter) was prespattered with a fairly strong (more than 1E-8 A) rastered beam to remove comtamination. A similar rastered beam (more than 1E-8A, with a beam size of about 100 micro meter) was used for the mapping of light elements with RAE (resistive anode encoder). Since the dynamic range of RAE is rather restricted, the intensity of the secondary ions were adjusted by the contrast apertures. Liquid nitrogen trap was used to reduce the effect of contamination. For the observation of a large (150 micrometer in diameter) area with RAE, it is necessary to set the mass resolution to about 500. Due to the low mass resolution, interferences could make spurious results (e.g. O2 vs. S; Si2 vs. Fe etc.). When in doubt,

high mass resolution observation was made in a small area, to make sure which of the interfering species is dominant.

Results

First of all it is important to note that all the light elements studied here (H,C,N and O) are the species which are known for the severe contamination problems. They are the main constituents of the residual gas in the mass spectrometer and also the contamination of the sample surfaces.

In the case of CN-, it was noticed that during the earlier stage of spattering, chlorine signal is well correlated with the CN- signal, which weakened and disappeared after tens of minutes of spattering. Such CN- (and chlorine) is considered to be contamination and disregarded in the following description.

C- signal (mainly contamination) is a little more persistent than CN- (contamination) signal but eventually decreases to a constant small value (unless the area is actually concentrated in carbon), and we think that indigenous distributions are observed. H- and O- signals are still more persistent and stay at a fairly high value after a long time of spattering. We are not sure if the resulting mappings of H- and O- reflect indigenous distributions or not. In any case, if any features are observed, they are described below.

Nitrogen (CN-)

Nitrogen was observed to be enriched in the taenite of Odessa and Boxhole. Such enrichment is expected from the previous studies, but this is the first time that such enrichment was actually observed. Taenite was present in Gibeon but it was not clear if nitrogen is enriched in it, due to the low signal level.

Carbide in Odessa also seems to be somewhat enriched in nitrogen. Carlsbergite (chromium nitride) was observed in the Boxhole (IIIA). Since this mineral has been often reported to be present in IIIA irons (Buchwald ,1975), this is no surprise. But this is the first detection of the presence in the Boxhole and demonstrates that SIMS is indeed a sensitive tool for detecting light elements, in spite of the contamination problems.

Taenite lamella was not observed in other specimens of iron meteorites and therefore CN- signal is generally very weak in the rest of iron meteorites. Sikhote-Alin, however, shows a couple of tiny hot spots of CN- which are not correlated with chlorine. They seems to be some kind of nitride but the identification has not been made yet.

Carbon (C-)

Carbon is enriched in the taenite of Boxhole. Because of the rather narrow band width (less than 20 micrometer) and because of the slight aberration of the ion optics, it is not easy to make a definite statement on the concentration gradient within the taenite. But the first impression is that carbon is concentrated in the middle of the taenite lamella. This is contrary to the observations reported by Bashir et al. and may be the result of rapid cooling of this meteorite. Carbon enrichment was not observed in any other irons except for carbides in Odessa.

Hydrogen (H-)

Hydrogen is observed to be depleted in taenite of Odessa, Gibeon and also Boxhole. Hydrogen is, however, the main residual gas in the mass spectrometer and the observed distribution may be caused by this residual hydrogen gas if it can stick on kamacite better than on taenite. Further studies are needed to clarify this point.

Mottled appearance of hot spots of hydrogen which is correlated with hot spots of Fe, Ni and Co was often observed (Boxhole, Sikhote-Alin and Gibeon). The correlation among these elements are likely a result of the matrix effect due to the presence of hydrogen.

A big question is whether such a hot spot of hydrogen is indigenous or artificial. Further studies are needed to clarify this point, too.

Oxygen (O-)

Odessa taenite appears to be depleted in oxygen. Similar to the case of hydrogen distribution, such apparent enrichment in kamacite could be due to preferential sticking of oxygen on kamacite over taenite. In the rest of iron meteorites, irrespective of the presence or absence of taenite, clear features of oxygen distribution were not observed.

Conclusions

Secondary ion mass spectrometry seems to be quite successful in detecting carbon and nitrogen in iron meteorites. It is yet to be determined if the same statement can be made on hydrogen and oxygen.

References

N.Bashir, J.R.Beckett, I.D.Hutcheon, and E.M. Stolper, Carbon in the metal of iron meteorites, LPS, XXVII,63-64, 1996.

V.F.Buchwald, Handbook of iron meteorites, Univ. of California Press, 1975.

Incongruent evaporation experiments on troilite (2): evaporation rates under low H_2-pressures and kinetics.

TACHIBANA Shogo and TSUCHIYAMA Akira
Department of Earth and Space Science, Osaka University, Toyonaka 560, JAPAN.

Introduction. It is considered that chemical fractionation occurred in the primordial solar nebula had been caused by evaporation and/or condensation processes. Incongruent evaporation of troilite is one of the possible processes for Fe/S fractionation. Evaporation experiments on troilite had been carried out at 1atm with constant hydrogen partial pressure ($p(H_2)$ =0.63atm) [1]. However, to discuss the Fe/S fractionation in the nebula, it is important to know the evaporation behavior of troilite under the primordial solar nebula conditions. So, in this study, evaporation experiments on troilite were carried out under low hydrogen pressures.

Experiments. Troilite was made from a single crystal of pyrrhotite by heating in vacuum with metallic iron powder. Evaporation experiments on troilite under low hydrogen pressures were carried out in the gold image furnace (ULVAC-RHV-E44VHT). The samples were heated at constant temperature 970 °C at total pressures of $p(H_2)=10^{-3}$-10^{-5} atm for 24 to 120 hours. Evaporation experiments on troilite were also carried out at 1atm under several $p(H_2)$ conditions ($p(H_2)$=0.2-1.0 atm) to know $p(H_2)$ dependence of evaporation rates at 1atm. The experiments were done at constant temperatures ranging from 800°C to 970°C for 1 to 19 hours. Hydrogen pressures were controlled by H_2-Ar and H_2-CO_2 mixing gases.

Results. As in the previous experiments [1], troilite evaporated incongruently to form iron residual layers on troilite crystals keeping their original sizes, and these residual layers were porous. The width of the iron residual layer increases linearly with time at constant temperature (a linear rate law), and the linear evaporation rates of troilite were obtained from the width-time data. The evaporation rate constants show the Arrhenius relation, and their activation energy are nearly constant (~80 kJ/mol) under $p(H_2)$=0.2-1.0 atm at 1atm in H_2-Ar mixing gas. The activation energies in H_2-CO_2 mixing gas at 1atm are 94, 111 kJ/mol at $p(H_2)$=0.63, 0.8 atm, respectively. The evaporation rates of troilite did not change by gas flow rate, and seem to be proportional to $p(H_2)^{1.5}$ at 1atm in H_2-Ar mixing gas. On the other hand, change in the evaporation rates of troilite by $p(H_2)$ is small in the low $p(H_2)$ experiments (~$p(H_2)^{0.1}$ dependence). The values of evaporation rates under the low hydrogen pressures are larger than those expolarated from 1atm (Fig.1).

Discussion. Under H_2-rich conditions, the incongruent evaporation reaction of troilite is mainly $FeS(s) + H_2(g) = Fe(s) + H_2S(g)$ if gas species in equilibrium with metallic iron and troilite are taken into consideration. The bulk reaction consists of the following processes, (1) H_2 gas diffusion through the porous residual layer, (2) adsorption and desorption of H_2 gas on the troilite surface, (3) chemical reaction between adsorpted H_2 molecules and the troilite surface, (4) desorption of H_2S gas formed by the surface reaction, (5) H_2S gas diffusion through the porous residual layer, (6) escape of H_2S gas from the residual layer to the surrounding gas phase, (7) formation of the residual iron layer by the diffusion of Fe in troilite. One of these processes should control the rate of the bulk reaction. If the gas diffusion process (1) and/or (5) determines the reaction rate, it is considered that the evaporation would obey a parabolic rate law. So, the process(1) or (5) would not be the rate-determining process. The processes (2) and (4) would not be the rate-determining processes, because adsorption and desorption are generally very fast processes at high temperatures. With regard to the process (6), from the fact that the evaporation rates have a little dependence on the gas flow rate, H_2S gas can easily escape from the residual layer, and the partial pressure of H_2S, $p(H_2S)$, should be small near the surface of residual layers. Hence, the process (6) would not be the rate-determining process. The process (7) should not be a rate-determining process because Fe diffusion in troilite is too fast to explain the experimental rates. Moreover, the $p(H_2)$ dependence cannot be explained by this process because the process (7) probably has a little $p(H_2)$ dependence unless the diffusion coefficient of Fe in troilite, D_{Fe}, depends largely on $p(H_2)$. As a result, the rate-determining process would be the process (3), the surface chemical reaction.

If the surface reaction determines the rates, the evaporation flux of troilite can be calculated by Hertz-Knudsen equation :

$$J_{calc.} = \frac{\alpha\left(p^{e}(H_2S) - p^{surf.}(H_2S)\right)}{\sqrt{2\pi m_{H_2S} kT}},$$

where α ($\leqq 1$) is the evaporation coefficient of FeS, $p^{surf.}(H_2S)$, the partial pressure of H_2S near the troilite surface, $p^{e}(H_2S)$, the equilibrium pressure of H_2S of the reaction ($FeS(s) + H_2(g) = Fe(s) + H_2S(g)$), m_{H_2S}, the mass of the H_2S molecule, and k, the Boltzmann constant. When the value of α is unity, the evaporation process occurs ideally at the maximum rate without any kinetic constrains. The values of apparent α which were obtained in the present experiments at 1atm are much smaller than unity ($\sim 10^{-4}$) (Fig.1). Two possibilities can be considered for the small values of α : (i) the real value of α is not small but ($p^{e}(H_2S)$-$p^{surf.}(H_2S)$) is small, and (ii) α is essentially small. However, the former can be eliminated because the processes (1), (4) and (6) are not the rate-determining processes. Therefore, α is considered to be essentially small. Consideration on reaction

rate constants shows that α depends on the ratio between the rate constant of the surface reaction and that of desorption of adsorpted H_2 molecules. Because the former rate constant is generally much smaller than the latter, α becomes much smaller than unity. Consequently, incongruent evaporation of troilite are extremely constrained by the surface chemical reaction kinetics.

It can be also considered that sulfur evaporates from troilite as S_2 molecule: $FeS(s) = Fe(s) + 1/2S_2(g)$. If the reaction, $FeS+H_2=Fe+H_2S$, occurs ideally, the evaporation flux of H_2S is larger than that of S_2 at $p(H_2)>10^{-5}$atm (Fig.1). However, the reaction, $FeS+H_2=Fe+H_2S$, are kinetically constrained as mentioned above, and the reaction, $FeS=Fe+1/2S_2$, would occur almost ideally without the reaction between adsorpted molecules and the surface of troilite. In this case, it is expected that evaporation flux of S_2 becomes larger than that of H_2S under higher $p(H_2)$ conditions than 10^{-5}atm and the reaction, $FeS=Fe+1/2S_2$, occurs instead of the reaction including H_2 and H_2S. The present experimental data at $p(H_2)=10^{-3}$-10^{-5} atm can be interpreted by the reaction, $FeS=Fe+1/2S_2$. This interpretation agrees with the experimental fact that evaporation rates of troilite under low $p(H_2)$ have few dependences on $p(H_2)$.

Accordingly, it is expected that sulfur would evaporate from troilite as S_2 molecule in the primordial solar nebula, and this could cause Fe/S fractionation.

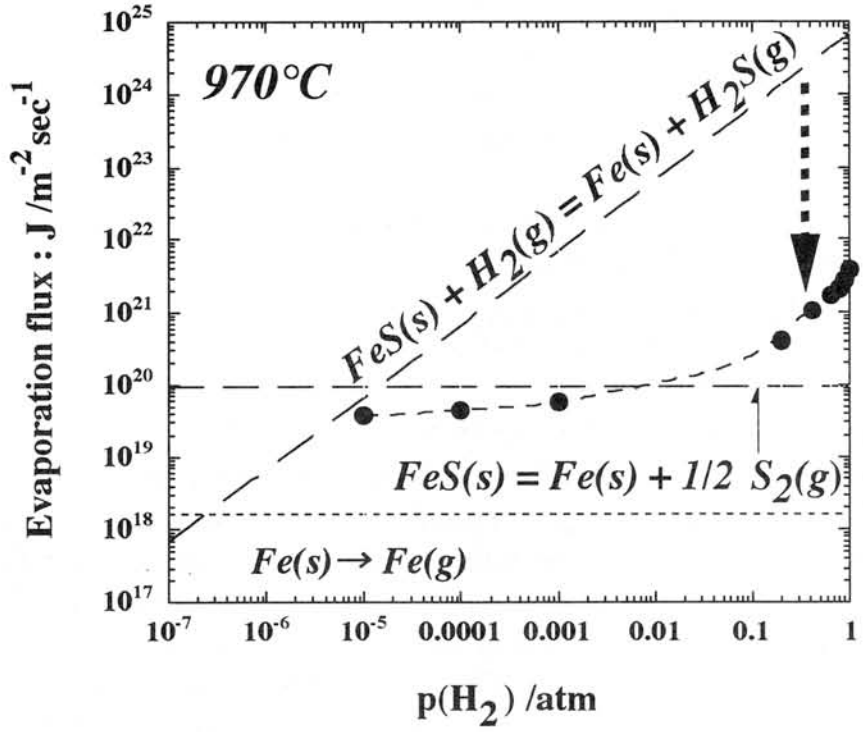

Fig.1
The evaporation flux of troilite at 970°C are plotted against hydrogen pressure, $p(H_2)$. Ideal evaporation rates of H_2S, S_2 and Fe are also plotted as three dashed lines, respectively.

References.

[1] Tachibana, S., A.Tsuchiyama and M.Kitamura, *20th Symp. Antarct. Meteorites (abstract)*, 235-238, 1995.

A POSSIBLE SITE TRAPPING NOBLE GASES IN HAPPY CANYON ENSTATITE CHONDRITE: MICROBUBBLES.

N. Takaoka and T. Nakamura, Dept. Earth & Planet. Sci., Kyushu Univ., Fukuoka 812-81, and K. Nagao, Inst. Study Earth's Interior, Okayama Univ., Misasa, Tottori, 682-01.

Introduction. Primordial noble gases can provide information on formation conditions of meteorites as well as their parent bodies. Carrier phases (or trapping sites) of primordial gases for enstatite (E-) chondrites have not yet been identified, while those for carbonaceous and ordinary chondrites are now known to be carbonaceous matters. The Happy Canyon (HC) E-chondrite is an impact-melt breccia formed probably from the EL-chondrite parent body [1]. We report here results on elemental and isotopic measurements of noble gases released by crushing and by stepped heating pyrolysis of HC bulk samples, and propose microbubbles for a possible site trapping noble gases.

Experimental. A bulk meteorite chip (0.310 g) was crushed in a stainless steel tube by pounding with a magnetic stailess steel piece (22 g), after thorough degassing overnight at 200℃. One step of crushing consists of 100x pounding. Noble gases released in each step of crushing was measured with a modified VG5400 mass spectrometer of Okayama University [2]. Another bulk sample (0.129 g) chipped from the same HC meteorite specimen was heated stepwise and evolved gases were measured with the same mass spectrometer as the crush-released gases were.

Results and discussion. Considerable amounts of trapped Ar, Kr and Xe, and radiogenic ^{129}Xe were released by crushing. More than eight percent of bulk Xe (this work and [3]) appeared by triplicate steps of crushing (Fig. 1). We use hereafter " bulk" gases for gases released by pyrolysis of a bulk sample. The amounts of gases released at each step of crushing are essentially constant (Fig.2a), suggesting that greater amounts of trapped gases could be released by more extensive crushing. Helium and Ne are mostly cosmogenic. Elemental ratios for heavy trapped gases released by crushing are greatly depleted in light elements compared to the bulk: ^{36}Ar / ^{84}Kr / ^{132}Xe = 31.9 /0.68 /1 against 108/1.5 /1 (Fig. 2b).

Ratios of crush-released cosmogenic gases to bulk are very low: 5×10^{-4}, 8×10^{-4} and 2×10^{-3} for ^{3}He, ^{21}Ne and ^{36}Ar, respectively (Fig. 1). The lower release of lighter cosmogenic gases suggests a gas loss by terrestrial weathering. Release of radiogenic ^{40}Ar is also low, 3×10^{-3} relative to the bulk (Fig.1). Both cosmogenic gases and radiogenic ^{40}Ar are in-situ products, thus they are released from the surface newly formed by crushing. The preferential release of trapped gases, therefore, indicates that they do not reside in crystal lattices but at places that are easily destroyed by crushing, such as microbubbles. We

examined thin sections of HC and found many vesicules of ca 2 um across only in enstatite crystals. They are oriented along a plane, suggesting enclosure in fracture.

This finding that considerable parts of trapped gases are contained in microbubbles can give partial solution to questions on host phases of trapped gases and on lack of correlation between trapped gases and petrologic type of E-chondrites [3, 4], although we need more data of crushing experiments for other E-chondrites.

For crush-released gases, $^{3}He/^{4}He$ is actually identical with that for bulk He, but $^{21}Ne/^{22}Ne$ is considerably lower than that for bulk Ne, indicating preferential crush-releasing from Na-rich phases. Isotopic ratios of bulk Xe determined so far for E-chondrites are enriched in heavy isotopes compared to solar Xe [3, 4]. Bulk E-chondrites are expected to contain fissiogenic Xe from ^{244}Pu [3]. The isotopic ratios of crush-released Xe are approximately solar except for ^{129}Xe. Fig. 3 displays the Xe isotopic ratios relative to the solar Xe and plots $^{134}Xe/^{132}Xe$ against $^{136}Xe/^{132}Xe$, suggesting that E-chondrites trapped solar-type Xe.

Impact-melting of HC took place ca. 4.566 Ga ago and the I-Xe age was established, therefore the I-Xe system was closed, during crystallization of the molten portion [1]. A considerable fraction of radiogenic ^{129}Xe (i.e., > 2 % of bulk ^{129}Xe) was crush-released. This is a lower limit of radiogenic ^{129}Xe contained in microbubbles because more steps of crushing could give more gas release. Note the great difference in the crush-released fraction between radiogenic ^{40}Ar and ^{129}Xe, that is, 0.3 % vs 2 % of bulk ^{40}Ar and ^{129}Xe, respectively. This suggests that the cruch-released ^{129}Xe is not in-situ decayed ^{129}Xe in the HC meteorite but inherited ^{129}Xe which was decayed and accumulated prior to the impact-melting. Likely the inherited ^{129}Xe was mixed with trapped gases and occluded in microbubbles by the impact-melting 4.566 Ga ago. The inherited ^{129}Xe could not correlate with ^{128}Xe produced by neutron-capture on ^{127}I. The fraction of neutron-captured ^{128}Xe which correlated with radiogenic ^{129}Xe is only 29.1 % for HC [5].

The extremely low value (: 31.9) for trapped $^{36}Ar/^{132}Xe$ of the crush-released gas can be interpreted by the fractionation hypothesis in microbubbles [6]. According to [6], the elemental ratio R(v) for a silicate sample of bubble density v is given by,

$$R(v)/R(0) = (1 + T_o\, v / T_{Ar}\, S_{Ar}) / (1 + T_o\, v / T_{Xe}\, S_{Xe}) \quad \text{------} \quad (1)$$

where S_X and T_X are solubilities and closure temperatures of X (X=Ar and Xe) for the silicate, respectively. R(v) = 108 for the HC bulk and R(0) = 31.9 for microbubbles. With $S_{Ar} = 2 \times 10^{-5}$ cm^3/g atm, $S_{Xe} / S_{Ar} = 0.15$, $T_{Ar} = 873K$, $T_{Xe} = 1135K$ and $T_o = 273K$ [6], eq. (1) gives $v = 8 \times 10^{-6}$ cm^3/g. This bubble density corresponds to, on average, two microbubbles of

$v = 8 \times 10^{-6}$ cm^3/g. This bubble density corresponds to, on average, two microbubbles of 2 um across in 100 x 100 x 30 um^3.

References: [1] McCoy et al. (1995) Geochim. Cosmochim. Acta 59, 161-175. [2] Miura et al. (1993) Geochim. Cosmochim. Acta 57,1857-1866. [3] Crabb and Anders (1981) Geochim. Cosmochim. Acta 45, 2443-2464. [4] Wacker and Marti (1983) Earth Planet. Sci. Lett. 62, 147-158. [5] Kennedy et al. (1988) Geochim. Cosmochim. Acta 52, 101-111. [6] Takaoka (1994) Noble gas geochemistry and cosmochemistry, ed. Matsuda, J., Terra Sci. Publ. Co. Tokyo, p. 23-29.

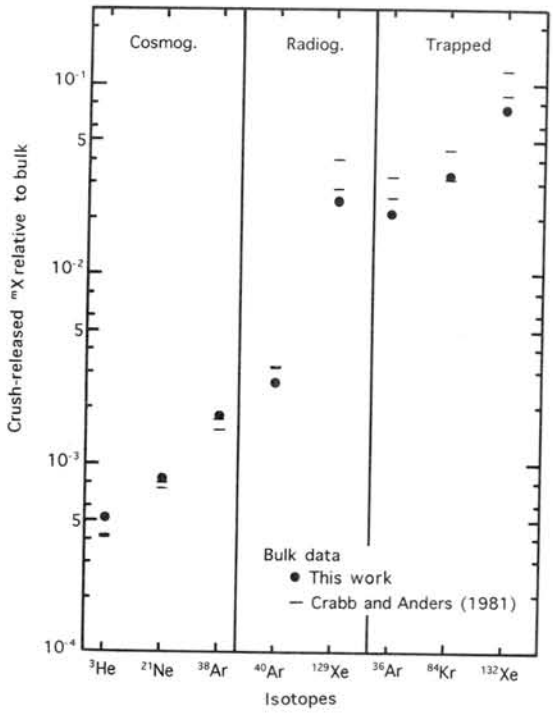

Fig. 1 Crush-released cosmogenic, radiogenic and trapped gases from HC relative to bulk gases

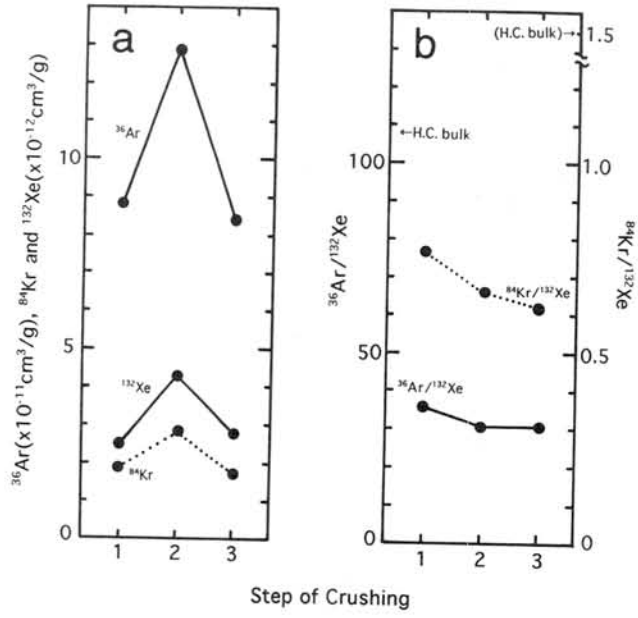

Fig. 2 Releases of trapped ^{36}Ar, ^{84}Kr and ^{132}Xe from HC by crushing.

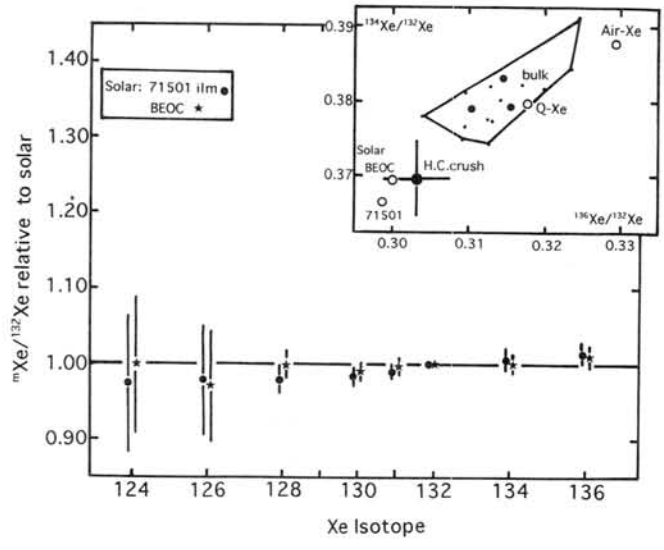

Fig. 3 Isotopic ratios of crush-released Xe relative to solar and 3-isotope plots of ^{134}Xe/^{132}Xe against ^{136}Xe/^{132}Xe.

MINERALOGY OF ASUKA 87 AND 88 EUCRITES AND CRUSTAL EVOLUTION OF THE HED PARENT BODY.

Hiroshi Takeda[1,2], Teruaki Ishii[3], Tomoko Arai[2] and M. Miyamoto[2].
[1]*Research Institute, Chiba Inst. of Technology, 2-17-1 Tsudanuma, Narashino City, Chiba 275, Japan.*
[2]*Mineral. Inst., Graduate School of Sci., Univ. of Tokyo, Hongo, Tokyo 113, Japan.*
[3]*Ocean Research Inst., Univ. of Tokyo, Minamidai, Nakano-ku, Tokyo 164, Japan.*

Introduction

Combined chronological and mineralogical studies of monomict eucrites revealed that these eucrites (ordinary eucrites) experienced extensive metamorphic events in the early history of the crustal evolution [1,2]. However, such events were overprinted by other features such as impacts [2]. Thus, it has been difficult to decipher metamorphic records from the meteoritical studies. Crystalline eucrites may give us more definitive answers, because their mineralogical records were not disturbed by the impact cratering events. In the new Catalog of the Antarctic Meteorites [3] some crystalline eucrites and nearly crystalline eucrites have been described. Preliminary examination of some typical and unique specimens in the Asuka 87 and 88 collections have been reported by Yanai [4]. We report mineralogical examination of such eucrites in connection with our works on the crustal evolution of eucrites [1,5].

Samples and Experimental Techniques

Polished thin sections (PTS) of three Asuka eucrites, A87272,51-2, A881388,54-1 and A881394,52-2 were supplied from the National Inst. of Polar Research (NIPR). The original masses and their preliminary descriptions are given in the Catalog [3]. A87272 (5706 g) is the largest achondrite in the Asuka collections and shows coarse-grained moderately brecciated texture [4]. A881388 (16.92 g) shows a fine-grained crystalline texture. A881394 (70.92 g) shows a coarse-grained granular texture and is classified as a cumulate eucrite. The PTSs were studied by an optical microscope and electron probe microanalyzer (EPMA) JEOL 733 at Ocean Research Inst. (ORI) of Univ. of Tokyo.

Results

Asuka 87272. A brief description is given by Yanai [4] and Takeda *el al.* [6]. Microscopic examination of the PTS ,51-2 shows that it consists of remnant of coarse pyroxene and plagioclase crystals set in much finer, rounded grains of pyroxene (0.01~0.14 mm in diameter) set in continuous matrices of white plagioclase. This texture gives granulitic appearance as was described in some eucrites [7] and suggests recrystallization. The original crystalline texture was disturbed by presumably brecciation event, but in a large scale, the remnant of the original pyroxene and plagioclase crystals can be recognized. A note-worthy feature is that the pyroxene crystals (up to 1 mm long) reveal coarse herrin-bone exsolution textures with thick (up to 35 μm) exsolution lamellae of augite on (001). Much finer (001) lamellae are often found between the coarse (001) lamellae, between which thin (100) exsolution lamellae are observed in the low-Ca host phase. This texture suggests that pigeonite is inverted to orthopyroxene. In the ajacent area, high-Ca pyroxene with fine, dense exsolution on (001) (up to 0.8×0.5 mm in size) are often found, which may be a rim of originally zoned pyroxene in the Ca-Mg-Fe contents. A large ilmenite crystal (0.25×0.12 mm) is rarely found. In the fine-grained granulitic regions, several small rounded graines (0.01~0.14 mm) of ilmenite and chromite are found together often along a line.

The chemical compositions of all pyroxenes in the PTS fall on a tie line between $Ca_2Mg_{37}Fe_{61}$ and $Ca_{44}Mg_{29}Fe_{27}$ in the pyroxene quadrilateral (Fig. 1). This trend is the same as those of the ordinary eucrites [7]. Clouding of pyroxenes is not noticeable. Plagioclase are chemically zoned from An_{87} to An_{90}, preserving the initial crystallization trend. The compositions of chromite $Chr_{71}Ulv_{11}Her_{18}$ are within the ranges of known ordinary eucrites [5].

Asuka 881388. Fine-grained pyroxene crystals 0.03~0.35 mm in diameter are connected to form complex chains and set in a continuous matrix of white plagioclase consisting of polygonal smaller grains (0.05~0.18 mm in diameter). This texture resembles some granulitic eucrites described by Yamaguchi and Takeda [7]. Some lath-shaped plagioclase crystals (up to 0.62×0.12 mm in size) with tiny rounded transparent inclusions can be recognized. The largest pyroxene crystals reach up to 0.5 mm along the longest direction. Augite grains up to 0.24×0.19 mm are present. Exsolution lamellae in pyroxenes are

very fine and appears like striations. Subrounded opaque grains 0.01~0.09 mm in diameter are scattered through out the PTS. Most of them are ilmenite (up to 0.13×0.08 mm). At one corner of the PTS, there is an unusually large opaque grain 0.54×0.61 mm in size with rounded triangular shape and a small tail at one corner. It consists of mostly ilmenite with 1.0~1.6 wt % of MgO and 0.04~0.6 wt % of Cr_2O_3. Chromites with compositions $Chr_{57}Ulv_{31}Her_{13}$~$Chr_{66}Ulv_{17}Her_{16}$ were found at the tail and near the rims. Troilite is found along the rims and one rounded low-Ni Fe metal grain was found in the interior. EPMA studies of pyroxene show that they are homogeneous within the grains and individual grains of pigeonite and minor augite coexist (Fig. 1). The An contents of plagioclase range from 87 to 91.

Asuka 881394. Pale brown pyroxene crystals 0.4 to 1.5 mm in diameter are connected to form a granular texture and white plagioclase fills their interstices. The plagioclase regions are more than 2 mm along the longest direction and consist of rounded smaller crystals 0.1~0.4 mm in diameter (up to 1×0.5 mm). Opaque grains are mostly chromite, but rare troilite is present. Three grains of chromite often bound by crystal faces, up to 0.55×0.30 mm in size are present in plagioclase attached one side to pyroxene. These chromites poikilitically enclose plagioclase and rare pyroxene. Chemical compositions of the exsolved pyroxene analysed by EPMA show that the host $Ca_3Mg_{54}Fe_{43}$ and the lamella augite $Ca_{42}Mg_{40}Fe_{18}$ are well separated (Fig. 2). The thickness of the augite lamellae is about 10 μm. The An contents of plagioclase is very calcic (97~98). Chromite contains 1.6~2.5 wt % of MgO and the composition $Chr_{72}Ulv_{10}Her_{18}$ suggests formation below 800°C [8].

Discussion

The texture and mineral chemistry of three essentially crystalline eucrites described in this paper are not simple products of normal crystallization. The texture of A87272 does not look like an ordinary eucrite. The fact that the degree of pyroxene homogenization of Takeda and Graham [9] is over type 6, suggests extensive thermal metamorphism. The recrystallized texture with secondary augite of the fine-grained portion of A87272 resembles that of granulitic eucrites described by Yamaguchi and Takeda [7]. This granulitic eucrite is comparable to that of lunar highland granulites. The entire texture of A881388 is similar to these granulites. If we extend this idea one step further, the texture of A881394 can be interpreted as a coarse-grained version of A881388, although A881394 has been classified as a cumulate eucrite. We interprete these textures in the light of recent models of the origin of ordinary eucrites [1].

The granulitic texture of A881388 is similar to hipidiomorphic-granular texture of Emmavile [10], but crystallinity of Emmavile is not as good as A881388. The presence of coexisting low-Ca pyroxene and augite is common mineral assemblages of the two eucrites. The discovery of an unusually large rounded grain of ilmenite-chromite-metal-troilite with a tail in comparison with fine-grained dust-free pyroxene and plagioclase indicates that this granulitic texture is not a product of primary crystallization. Formation of chromite-ilmenite in the dust-free granoblastic pyroxene areas in Y792510 has been interpreted as induced by a shock event at high temperature and subsequent thermal metamorphism [5]. The detection of fossil ^{53}Mn in the Y792510 eucrite suggests that the metamorphic event took place in the early history of the HED parent body [5].

The presence of inverted pigeonite with caorse exsolution lamellae in A87272 close to that of the Moore County cumulate eucrite [11] indicates that the metamorphism of the eucritic crust is comparable to the cooling environment of cumulate eucrites on the HED parent body. The exsolution texture of A881394 is not like a typical cumulate eucrite such as Serra de Mage [11], although it is classified as a cumulate eucrite. The *mg* number [= Mg×100/(Mg+Fe) mol %] of A881394 is between cumulate eucrites and ordinary eucrites (Fig. 2). The poikilitic texture of chromite in A881394 suggests rather a metamorphic event. The rounded texture of pyroxene and granoblastic texture of plagioclase are in favor of the granulitic origin. The most important and unusual feature of A881394 is very calcic nature of plagioclase, which suggests affinity to angrites. However, we have to wait trace element data of this interesting achondrite before we further discuss their relationship to other meteorite classes

In order to evaluate fully the significance of these apparently crystalline eucrites, further studies on their isotopic chronology and trace element geochemisty are required. Our present interpretation is that despite their crystalline texture, they migh have experienced extensive metamorphism after the initial crystallization in the early history of the crustal evolution.

We acknowledge the NIPR for supplying us with the sample and the ORI for the EPMA equipment. We thank Drs. A. Yamaguchi, L. E. Nyquist, D. D. Bogard, and Profs. K. Keil, G. J. Taylor and P. Warren for discussion and Mrs. M. Otsuki for technical assistance.

References:

[1] YAMAGUCHI A., TAYLOR G. J., and KEIL K. (1996) *Icarus*, in press.
[2] BOGARD D. D. (1995) *Meteoritics*, **30**, 244-268.
[3] YANAI K. and KOJIMA Y. (1995) Catalog of the Antarctic Meteorites, 230 pp., NIPR, Tokyo.
[4] YANAI K. (1993) *Proc. NIPR Symp. Antarct. Meteorites*, **6**, 148-170.
[5] NYQUIST L., BOGARD D., TAKEDA H., BANSAL B., WIESMANN H. and SHIH C.-Y. (1996) *Geochim. Cosmochim. Acta*, submitted.
[6] TAKEDA H., ISHII T. and MIYAMOTO M. (1996) *Meteoritics and Planet. Sci.* (Abstract of 59th Meteoritical Soc. Meeting, Berlin), submitted.
[7] YAMAGUCHI A. and TAKEDA H. (1995) *Proc. NIPR Symp. Antarctic Metrorites*, **8**, 167-184.
[8] SACK R. O. and GHIORSO M. S. (1991) *Amer. Mineral.* **76**, 827-847.
[9] TAKEDA H. and GRAHAM A. L. (1992) *Meteoritics*, **26**, 129-134.
[10] MASON B. *et al.* (1979) *Smithson. Contr. Earth Sci.*, **22**, 27-45.
[11] MIYAMOTO M. and TAKEDA H. (1995) *Earth Planet. Sci. Lett.*, **122**, 343-349

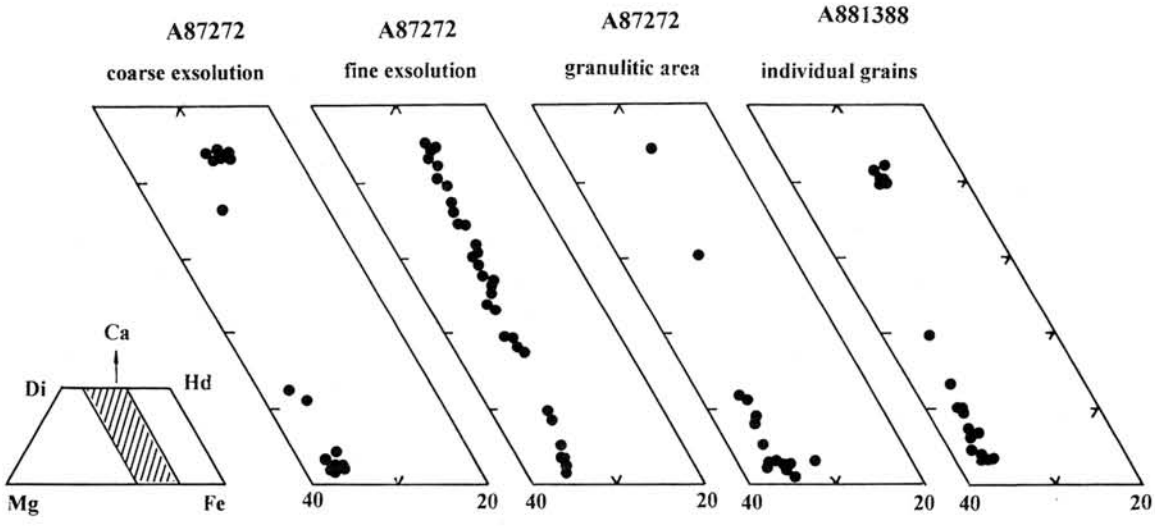

Fig. 1. Parts of the pyroxene quadrilaterals of A87272 and A881388.

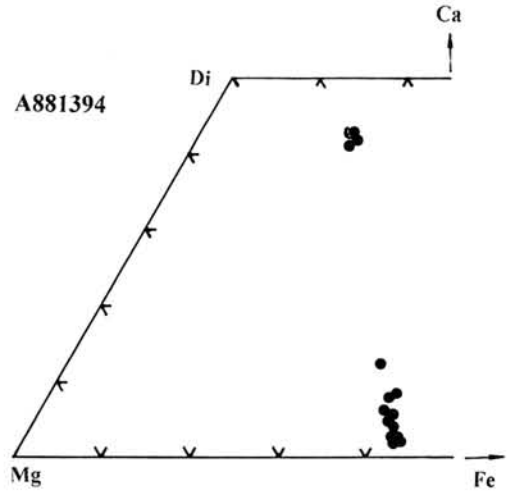

Fig. 2. Mg-rich half of the pyroxene quadrilateral of A881394.

Refractory inclusions in the Yamato-86751 CV3 chondrite

Hajime Takeda [1] and Hideyasu Kojima [2], [1] Department of Polar Science, The Graduate University for Advanced Studies, [2] National Institute of Polar Research, 9-10, Kaga 1-chome, Itabashi-ku, Tokyo 173, Japan.

Yamato-86751 (Y-86751) chondrite has been classified into CV3 [1]. Murakami and Ikeda suggested that the Y-86751 have formed from more oxidized gas than Allende (CV3) by reason of rich in magnetite and Fe content of olivine [2]. They have also suggested that Na contents of refractory inclusions and chondrules are much less than those in the Allende. Many studies have done on the refractory inclusions mainly in the Allende (e.g., [3]), while there are a few studies about those of other chondrites. Most of studies on inclusions in the Allende have suggested that refractory inclusions in the Allende had been suffered secondary alteration resulting from reaction with the nebular gas. Primary phases such as melilite has been consequently replaced by secondary phases such as grossular, anorthite, nepheline and/or sodalite. Especially, "fluffy" type A (FTA's) inclusions in the Allende are heavily altered and contain 70~80 volume per cent of secondary phases [3].

In present work, we studied some inclusions in the Y-86751 using an optical microscope and an electron probe micro analyzer (EPMA), and compared with those in Allende.

In the Y-86751, we have found three refractory inclusions (98-1/I-1, 99/I-1 and 93-1/I-1). They are different in type. 98-1/I-1 is similar to the compact type A inclusions in the Allende in its texture. 99/I-1 is a hibonite-rich inclusion. 93-1/I-1 is an aggregate of spinel-melilite nodule and fine grained fragments of spinel and melilite.

98-1/I-1: This inclusion is relatively large (4.6 mm × 3.7 mm) and its shape seems to be a half of originally oval. It consists mostly of coarse-grained melilites which contain 46~92 % of gehlenite component with minor coarse-grained Ti-rich

pyroxenes and euhedral tiny crystals of spinel. Spinel crystals are scattered in melilites and Ti-rich pyroxenes. Ti-rich pyroxenes contain 16.6~19.1 wt% of Al_2O_3 and 7.5~10.3 wt% of TiO_2. Several modal per cent of melilite is replaced by nepheline. A rim occurs on the outermost of this inclusion. The rim consists of pyroxene layer and olivine layer. The pyroxene layer is very thin (2~3 μm) and consists of Al and Ti poor pyroxene. The olivine layer is thicker than the pyroxene layer and varied in thickness from 2 to 10 μm.

99/I-1: This inclusion consists of core and multi-layered rim. The core consists of hibonite, spinel and melilite, and contains many voids. The hibonite crystals is blue color under an optical microscope like those in the "Blue Angel" from Murchison CM2 chondrite [4]. The rim is distinguished into five layers (layer 1 to 5 toward outside) by mineral assemblages. Layer 1 contains perovskite in addition to mineral assemblages of the core. Melilites in the core and the layer 1 are mostly of gehlenite. Layer 2 consists of melilite which is coarser in size than that in the layer 1. Melilites in the layer 2 are slightly richer in akermanite contents than those in the core and the layer 1. Layer 3 consists of spinel and pyroxene. Layer 4 consists of pyroxene only. Pyroxenes in the layer 3 contain 18~25 wt% of Al_2O_3 and 4~12 wt% of TiO_2, while those in the layer 4 contain less than 7 wt% of Al_2O_3 and 2 wt% of TiO_2. Layer 5 consists of olivine which contains less than 1.5 wt% of FeO. Secondary alteration which is reported in the Allende type A inclusions has not yet observed in this inclusion.

93-1/I-1: This inclusion (4.3 mm × 3 mm in size) consists of spinel-melilite nodules and fine-grained fragments of spinel and melilite. The nodule has spinel in a core and melilite in a rim. Spinel shows compositional zoning in Fe perpendicular to some cracks. Fine grained fragments of spinel usually show high Fe contents. As a result of map analysis by EPMA, sodium is distributed among the fine grained fragments but not exists in the nodule. In a part of this inclusion, it is observed the texture that is resemble to FTA's in the Allende [5]. In this part, anorthite is observed

as secondary phase replacing melilite.

As mentioned above, refractory inclusions in the Y-86751 contain less amount of alteration products compared with those in the Allende. This observation is consistent with that bulk chemical compositions of refractory inclusions in the Y-86751 show less Na contents than those in the Allende [2]. On the other hand, the matrix in the Y-86751 shows high Na content compared with that in the Allende [2]. Na contents for bulk chemical compositions of both chondrites are nearly same [6]. If the secondary phases in refractory inclusions had formed by reaction with the gas which have produced the matrix, inclusions in the Y-86751 may had not experienced sufficient reactions with the gas.

References

[1] Yanai K. and Kojima H. (1987) *Photographic Catalog of the Antarctic Meteorites.* [2] Murakami T. and Ikeda Y. (1994) *Meteoritics 25, 115-125.* [3] MacPherson G. J. et al. (1988) *In "Meteorites and The Early Solar System", Univ. of Arizona Press 746-807.* [4] Armstrong J. T. et al. (1982) *GCA. 46, 575-595.* [5] MacPherson G. J. and Grossman L. (1983) *GCA 48, 29-46.* [6] Yanai K. and Kojima H. (1995) *Catalog of Antarctic Meteorites.*

Chondrule rims of secondary origin in the Vigarano CV3 carbonaceous chondrite

I. Tanimura, K. Tomeoka and T. Kojima

Department of Earth and Planetary Sciences, Faculty of Science, Kobe University, Nada, Kobe 657

INTRODUCTION

Type 3 chondrites are commonly regarded as being the least affected by parent-body process and thus petrologically the most primitive among the various chondrite types. However, recent studies showed evidence that some CV3 chondrites have experienced various secondary processes [e.g.,1-3]. Especially, resent studies of dark inclusions (DIs) [4,5] suggested that intensive aqueous alteration and subsequent thermal dehydration may have occurred locally on the CV parent body. These studies have aroused considerable controversy in the recent years. We here present the results of detailed mineralogical and petrographic study of chondrule rims in the Vigarano CV3 carbonaceous chondrite. Chondrule rims are generally believed to have been formed by accretion of dust to chondrule surfaces in the solar nebula [e. g., 6]. Our major purpose is to find the effects and the extent of secondary process, if any, in chondrule rims in Vigarano. We found evidence suggesting that part of chondrule rims in Vigarano were formed by secondary process that probably occurred on the meteorite parent body.

RESULTS AND DISCUSSION

Vigarano CV3 chondrite has highly brecciated texture; it consists of millimeter to submillimeter clasts. In addition to chondrules and CAIs, it contains abundant small mineral fragments, many of which are probably fragmented chondrules and CAIs. Chondrules commonly have rims of various thicknesses (20-200 μm), which consist mainly of fine grains (<5 μm in diameter) of Fe-rich olivine (Fa45-60) and minor Fe-Ni metal, Fe sulfide and magnetite. Lesser amounts of Mg-rich olivine, enstatite and hedenbergite also occur. The rims are more uniform in grain size and composition than the matrix.

We found several chondrule rims that are compositionally and mineralogically different from the common olivine-rich rims. Defocused electron beam analysis shows that they are consistently lower in analytical total (80-85 wt.%) than olivine-rich rims (~90 wt.%). S contents are especially high, approximately four times as high as the average S content of other rims. The rims are composed mainly of two materials; one occurs as irregular-shaped grains (<5 μm in diameter) that appears bright in back-scattered electron (BSE) images, and the other fills interstices of the bright grains and is dark. The bright grains compositionally resemble serpentine (24-35 wt.% SiO_2, 23-41 wt.% FeO, 15-30 wt.% MgO, 2.6-7.2 wt.% Al_2O_3), and the dark grains resemble saponite (22-35 wt.% SiO_2, 19-35 wt.% FeO, 9-21 wt.% MgO, 3.5-7.8 wt.% Al_2O_3, 0.9-2.2 wt.% CaO); the latter may correspond to the saponite reported from Vigarano by previous workers [7,8]. Other minor minerals include magnetite, Mg-rich olivine (Fa1-5), Fe-rich olivine (Fa90-95), enstatite, hedenbergite, spinel, Fe-Ni metal and Fe sulfide. The serpentine-like material occasionally encloses grains of Mg-rich olivine, enstatite and spinel, suggesting that it was formed by replacing these minerals.

Similar aggregates consisting of the serpentine-like and the saponite-like grains also occur as clasts (40-400 μm in diameter) without chondrules. They commonly contain small (20 - 50 μm in diameter) fragments of CAIs. One clast (~150 $\times$ 400 μm) coexists with a relatively

large CAI fragment (~400 μm in largest dimension). S contents of these clasts are very high, as high as those in the phyllosilicate-bearing chondrule rims. The mineralogical and textural similarities between the chondrule rims and the clasts suggest common origin. We suggest that the phyllosilicate-bearing chondrule rims are part of a preexisting matrix in a chondrite before fragmentation. Some portions of the preexisting matrix were probably incorporated as independent clasts.

We found another unusual chondrule rim (<50 μm in thickness) that appears to have been formed by replacing a chondrule (~700 μm in largest dimension). The rim consists mostly of fine, elongated to fibrous grains (~0.1 μm wide and <5 μm long) of Fe-rich olivine (Fa64-70) and minor irregular-shaped grains (<20 μm in diameter) of Mg-rich olivine, enstatite, Ca-rich pyroxene, Fe-sulfide, Fe-metal and magnetite; all of these minor minerals also occur within the chondrule. EDS analysis of the olivine shows relatively high Ca, Al and Cr (~1.1 wt.% CaO, ~1.3 wt.% Al_2O_3, ~0.41 wt.% Cr_2O_3). These morphological and compositional characteristics of Fe-rich olivine in the rim are very similar to those in the chondrule pseudomorphs in some dark inclusions (DIs) [4,5]. The chondrule pseudomorphs in the DIs are interpreted to have been formed by aqueous alteration and subsequent dehydration of chondrules on the meteorite parent body. We suggest that this chondrule rim was probably formed by similar process. In this case, however, aqueous alteration was not so intense that the chondrule was partly replaced only at its margin by phyllosilicate, which was later dehydrated and transformed to Fe-rich olivine. The minor minerals in the rims described above (Mg-rich olivine, enstatite, Ca-rich pyroxene etc.) are probably unaltered remnants of chondrules.

The present study shows that at least part of chondrule rims in Vigarano have texture and mineralogy that can not be explained by direct accretion of dust on chondrule surfaces in the solar nebula. Some chondrule rims appear to be fragmented remnants of a preexisting matrix of a chondrite that has experienced aqueous alteration. One chondrule rim appears to have been formed by partial replacement of chondrules, i.e. aqueous alteration and subsequent dehydration, thus having a history similar to some DIs. At present, we can not be certain whether the secondary processes occurred *in situ* on the meteorite parent body or not. However, it seems to be certain that the aqueous alteration and dehydration process is not limited to DIs but is more prevalent in Vigarano than previously thought. We suggest that the chondrule rims of secondary origin would potentially provide new aspects of information regarding secondary processes on the CV parent body.

Acknowledgements - We thank Drs. G.J. MacPherson and M. Prinz for providing Vigarano samples. This work was supported by Grant-in-Aid of the Japan Ministry of Education, Science and Culture (No. 06403001).

REFERENCES:

[1] Tomeoka K. and Buseck P.R. (1990) Geochim. Cosmochim. Acta 54, 1745-1754.
[2] Keller L.P. and Buseck P.R. (1990) Geochim. Cosmochim. Acta 54, 2113-2120.
[3] Krot A.N., Scott E. R. D. and Zolensky M. E. (1995) Meteoritics 30, 748-775.
[4] Kojima T., Tomeoka K. and Takeda H. (1993) Meteoritics 28, 649-658.
[5] Kojima T. and Tomeoka K. (1996) Geochim. Cosmochim. Acta 60, in press.
[6] Metzler K., Bischoff A. and Stöffler D. (1992) Geochim. Cosmochim. Acta 56, 2873-2897.
[7] Graham A.L. and Lee M. (1992) Lunar Planet.Sci. XXIII, 435-436 (abstract).
[8] Zolensky M.E., Barrett R. and Browning L. (1993) Geochim. Cosmochim. Acta 57, 3123-3148.

Did alteration of chondrule mesostasis occur in the nebula or on the parent body ? : Preliminary laser ablation study of Allende chondrule HN-3

Mariko Terauchi[1], Noboru Nakamura[1,2], Keisuke Nagao[3] and Tomoki Nakamura[4]

[1]Graduate School Science and Technology, and [2]Faculty of Scinece, Kobe university, Nada, Kobe 657,

[3]Institute for Earth's interior, Okayama University, Misasa, Tottori 682-01

[4]Faculty of Science, Kyushu University, Hakozaki, Fukuoka 812-81

Introduction

Chondrules are considered to have formed through the melting events at high temperature, but they are enriched in volatile alkali metals. Abundant alkali-rich phases such as nepheline and sodalite have been reported for chondrules from carbonaceous chondrites, typically Allende (CV3) [1,2]. They have been explained by reactions of chondrule mesostasises with nebula gases [1,2] or by later low temperature alteration on their parent body. In order to obtain time constraints on the locaiton of alteration (nebula or parent body), we investigate whether chondrules have ^{129}Xe excess produced by in situ decay of ^{129}I.

Sample and analytical procedures

We collected a large barred-olivine chondrule (HN-3 ; weight = 18.8392 mg, diameter = 3 mm ~) from the Allende (CV3) meteorite. It was cut into a few parts for experiments ; 1) preparation of a "thick" section for petrographic observation, and noble gases analyses by laser ablation and 2) analyses of Rb-Sr isotopes. A "thick" section was first examined for the texture using scanning electron microscope (SEM) and the chemical compositions were obtained using energy dispersive spectoscopy (EDS). After petrographic observations, we selected laser shot locations covering major constituent phases, olivine, pyroxene, and mesostasises (MS) which are locally replaced by nepheline and/or sodalite,

and Cr-spinel. We tried to analyze noble gases trapped in different phases separately by fusing specific portions. Since the laser beam was relatively broad (~120μm), the ablated portions were mostly mixtures of a few phases such as mesostasis and olivine. Isotopic compositions of noble gases were measured at Institute for Study of the Earth's Interior, Okayama University. We are planning to analyse Rb-Sr isotopic compositions for the second portion of HN-3 using the mass spectrometry (MAT 262).

Results

Results for isotopic compositions of noble gases after blank correction are shown in Table 1.

Using He data for which blank corrections are minor (< 4 %), the amounts of laser ablated materials are estimated to be about 6μg in weight (see Table 1). Correlation between ($^{21}Ne/^{22}Ne$) and ($^{20}Ne/^{22}Ne$) is shown in Figure 1. The neon isotopic compositions of Allende chondrule HN-3 are plotted on mixing line between Ne A and spallation. Figure 1 indicates that there is no difference in neon isotopic compositions among samples.

The Xe contents in each ablated portion are mostly blank levels except for ^{129}Xe isotope. It is interesting that four samples (MS-5, MS-7, Ol-1, Cr-sp) which are located in the outer portion of the chondrule tend to have higher radiogenic ^{129}Xe. Particularly, it is worth noting that one sample (MS-5) indicates ^{129}Xe excess distinct from air composition.

Disscusion

Since chondrules are considered to have been melt droplets formed at high temperature, it does not seem that volatile I and Xe have been introduced from outside. The SEM observation indicates that mesostasises of HN-3 chondrule are locally replaced by nepheline and/or sodalite, suggesting that the chondrule was subjected to low temperature alteration and the outer portion including MS-5 was more extensively altered. The problem we are interested in is whether the alteration reactions took place in the solar nebula or their parent body. If alteration of Allende chondrules took place in Allende parent body, then ^{129}Xe excess is not probably observed because most of extinct nuclide ^{129}I have decayed

out. If ^{129}Xe excess is observed, the alteration reactions are more favorablely explained to have taken place in the solar nebula. The higher ^{129}Xe concentrations as observed for four outer portion samples, particularly for MS-5, suggests that ^{129}I has been still alive during alteration of Allende chondrule HN-3. Although our results do not rule out possibility that the alteration reactions occurred in the very early stage on the parent body, it is more likely that alteration of HN-3 chondrule took place in the solar nebula. Due to large blank correction, ^{129}Xe excess for HN-3 is close to the merge of analytical limit. In order to confirm present results, we are looking for chondrules with larger sizes of nepheline or sodalite which gains an advantage of $^{129}Xe/^{132}Xe$ ratios over blank.

Acknowledgments :

We thank Tomoko Kojima for assistance of SEM observations, and Professor Hiroshi Nagasawa for providing us with the Allende samples including a large chondrule HN-3. Research was supported by Grant for Basic Science Research Project of the Sumitomo Foundation to K.Nagao and T.Nakamura.

References :

[1] Y.Ikeda & M.Kiumura, Proc.NIPR Symp. Antarct. Meteorites, 8, 97-122, 1995

[2] M.Kiumura &Y.Ikeda, Proc.NIPR Symp. Antarct. Meteorites, 8, 123-138, 1995

[3] K.Nagao & T.Abe, J. Mass Spectrom. Soc. Jpn, Vol. 42, No. 1,1994

[4] M.Ozima & Frank A. Podosek, noble gas geochemistry

Table 1. Results of laser ablation analyses of noble gases
for Allende chondrule HN-3

Sample	sampling location	weight [a] (μg)	^{4}He-rad [b] (10^{-5}cc/g)	^{3}He/^{4}He	^{21}Ne-cosm (10^{-8}cc/g)	^{40}Ar-rad [c] (10^{-5}cc/g)	^{129}Xe-rad [d] (10^{-12}cc/g)
MS-5	outer	6.1	3.1	0.00250 ±.00016	1.4	2.6	210
MS-7	outer	6.3	1.9	0.00407 ±.00022	1.7	2.8	100
MS-3	inner	4.8	3.6	0.00218 ±.00014	1.3	4.4	10
Ol-1	outer	6.6	1.3	0.00608 ±.00027	1.5	3.7	80
Px-1	inner	6.5	2.8	0.00279 ±.00012	1.4	3.6	30
Cr-sp	outer	6.7	1.7	0.00450 ±.00019	1.3	5.4	90

Weight [a] : calculated assuming that ^{3}He content in Allende samples is 8 x 10^{-8} cc/g
^{4}He-rad [b] = ([^{4}He] -5 [^{3}He]) / weight
^{40}Ar-rad [c] = ([^{40}Ar] - [^{40}Ar-blank]) / weight
^{129}Xe-rad [d] = ([^{129}Xe] - [^{129}Xe-blank]) / weight
MS-5, MS-7 : alkali-rich mesostasis, MS-3 : alkali-poor mesostasis
Ol-1 : olivine-rich, Px-1 : high Ca pyroxene-rich, Cr-sp : Cr spinel-rich

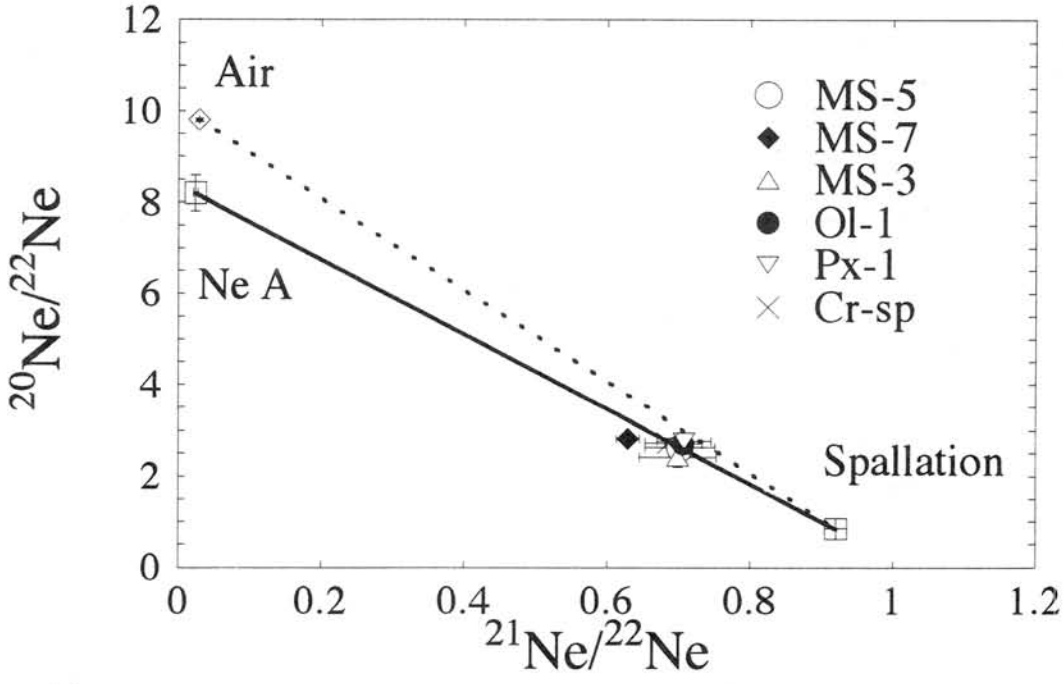

Figure 1. Correlation between (^{21}Ne/^{22}Ne) and (^{20}Ne/^{22}Ne)
Neon A composition is characteristic of carbonaceous chondrites which display elemental abundances in the planetary pattern, and "Ne A" is now synonomous with ' planetary A' [4].

Trace elements of Antarctic meteorites by INAA (II)

Shigeko Togashi[1], Hikari Kamioka[1], Mitsuru Ebihara[2], Keizo Yanai[3] Hideyasu Kojima[4] and Hiroshi Haramura[4]

1) Geological Survey of Japan, Higashi, 1-1-3, Tsukuba, Ibaraki 305.
2) Tokyo Metropolitan University, Minami-Ohsawa, Hachioji, Tokyo 192-03.
3) Iwate University, 4-3-5 Ueda, Morioka, Iwate 020.
4) National Institute of Polar Research, Kaga 1-9-10, Itabashi, Tokyo 173.

The non-magnetic separates of ordinary chondrites show the different characteristics corresponding to chemical groups (Togashi et al 1994). In this study, magnetic separates of various chemical groups were analyzed by instrumental neutron activation analysis. The metal phases were separated from ALH 769 (L6) with a magnet and chemicals, and were analyzed to characterize the magnetic separates from ordinary chondrites.

According to Rambaldi(1977a,b), kamacite and taenite are present in the coarse metal fraction, and in the intermediate-fine metal fractions, respectively. For purification of kamacite in this study, the large grains (about 1 mg) were hand picked, treated in hot HF for two minutes. The impurity of surface was removed physically.

The non-magnetic fraction of ALH 769 (L6) was treated with hot HF for ten minutes. The residue was analyzed by INAA.

The samples were irradiated in an S-pipe of JRR-4 reactor at JAER1 for 6 hours with a neutron flux of 5.5 X 10^{13}/cm^2·sec. Chemical standards for Os, Ir and Au, rock standards JP-1 for Ni and Cr, and JB-1 for other elements were irradiated simultaneously with the samples. The abundance of elements was determined with a high-purity Ge gamma-ray detector (ORTEC GEM20180) of Geological Survey of Japan (Tanaka et al., 1988). The neutron flux for small size (a few mg) samples was not the same as that for the reference standards because of the difference in counting geometry, and the variation reached up to 20 %. For such a case, total abundance of major elements is normalized to 100%; siderophile elements for metal separates are calculated assuming total Fe and Ni are 100%. The concentration of Ni in the kamacite separates are 5.1-5.5 % after the correction. The concentrations of Ni in the kamacite were observed to be 6.0-6.5 % with EPMA.

The results are consistent with the data for taenite and bulk metal from L6 chondrite (Kong et al.1995). Kamacites are plotted in the lower-Ir extent of the trends for the taenite and bulk metal (Fig.1a &b). The randomly sampled small size (less than 10 mg) metal mixtures are scattered along the mixing line between taenite and kamacite. This shows large sample size (more than 10 mg) is essential to get precise bulk metal compositions.

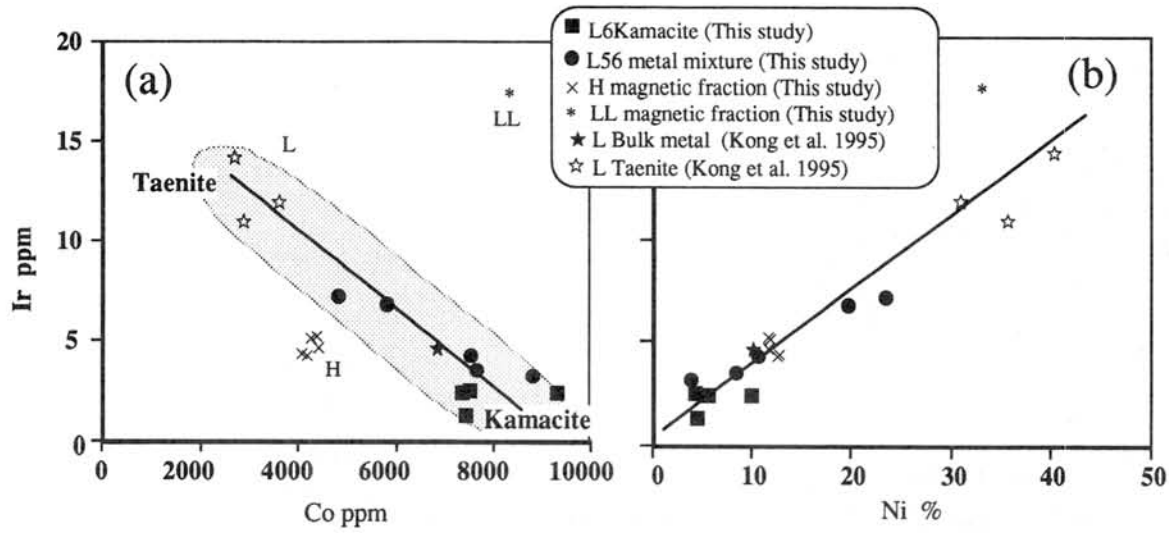

Fig.1 Ir-Co and Ir-Ni diagram for magnetic fraction.

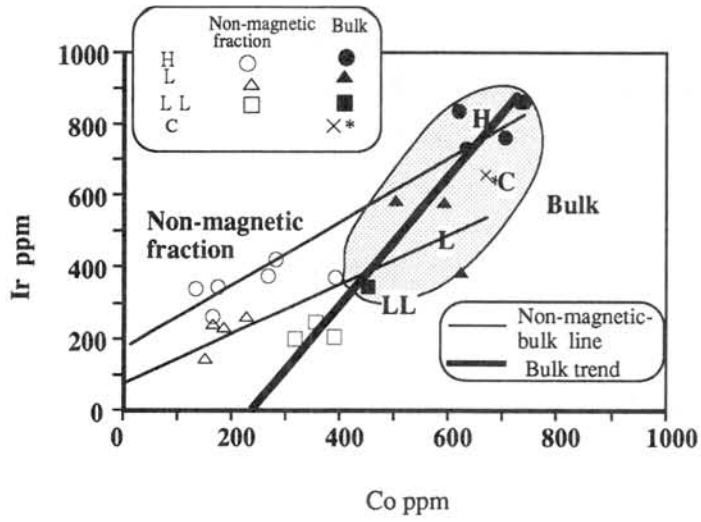

Fig.2 Ir-Co diagram for non-magnetic fraction and bulk chondrite.

The Ir-Co diagram indicates that the concentrations of Ir in metal phases of L chondrite correlate negatively with those of Co (Fig.1a), whereas the concentration of Ir in non-magnetic and bulk samples of the different types of chondrites correlates positively with those of Co (Fig.2) The negative correlation of Ir-Co in metal phases is governed by the subsolidus distribution rule during cooling process of the chondrite. The positive correlation of Ir-Co in bulk chondrites is caused by the difference in the ratio of lithophile and siderophile elements during condensation. The positively correlated line of bulk chondrites does not through the origin of Fig 2. This indicates that Ir/Co ratio of the primitive materials of the chondrites should have a variety.

The concentrations of Ir and Co in non-magnetic portions of the samples are lower than the bulk compositions of ordinary chondrites (Fig. 2). Most data for non-magnetic portions of L and H chondrite are plotted above the lower extent array defined by bulk compositions of ordinary chondrites. Consequently, small minerals which accommodate significant amounts of Ir are included in the non-magnetic fractions. The concentrations of Ir in the non-magnetic fraction of H chondrites are higher than that of L chondrites.

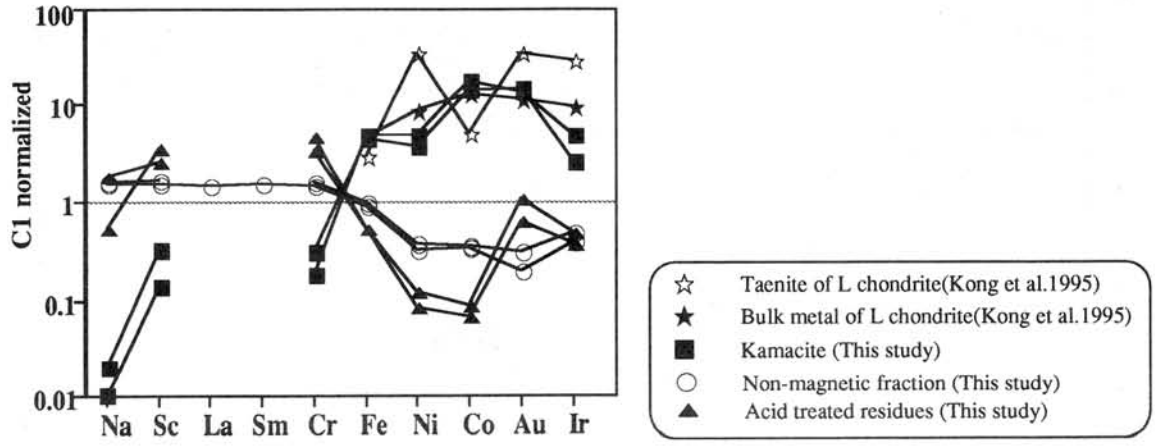

Fig.3 C1 chondrite normalized values for metal, non-magnetic fraction and acid treated residues.

The acid-treated residues from non-magnetic fractions are rich in Sc, Cr and Au (Fig.3), indicating a relatively high concentration of chromite. However, the residue is not enriched with Ir compared with non-magnetic fraction. Thus, the Ir-rich phase is still not detected, despite the inferred existence.

Kong P., Ebihara, M., Endo, K and Nakahara, H.(1995) Proc. NIPR Symp. Antarct. Meteorite, 237-249.

Rambaldi,E.R.(1976)Earth Planet.Sci,Lett.31,224-238.

Rambaldi,E.R.(1977a)Earth Planet.Sci,Lett.33,407-419.

Rambaldi,E.R.(1977b)Earth Planet.Sci,Lett.36,347-358.

Rambaldi,E.R.,Cendales, M., and Thacker, R.(1978)Earth Planet. Sci, Lett. 40,175-186.

Tanaka, T., Kamioka, H.,Yamanaka.,K.(1988) Bull. Geol. Surv. Japan.

Togashi, S., Kamioka, H. Ebihara, M.,Yanai, K., Kojima, H.(1994) Trace elements of Antarctic meteorites by INAA(I) Abstr. NIPR Symp. Antarct. Meteorite, 81-83.

Yanai, K (1979) Catalog of Yamato meteorites.

Yanai, K and Kojima, H. (1987) Photographic catalog of the Antarctic meteorites. NIPR, Tokyo.

EXPERIMENTAL SHOCK METAMORPHISM OF THE MURCHISON CM2 CARBONACEOUS CHONDRITE

K. Tomeoka[1], Y. Yamahana[1], F. Mizumoto[1] and T. Sekine[2]

[1] Department of Earth and Planetary Sciences, Faculty of Science, Kobe University, Nada, Kobe 657.

[2] National Institute for Research in Inorganic Materials, 1-1 Namiki, Tsukuba, Ibaraki 305.

INTRODUCTION

Collision-induced hypervelocity impact is a common, fundamental process in the early evolution of the meteorite parent bodies, and so an understanding of shock metamorphism of meteorites is greatly important to resolve many problems concerning the history of the meteorite parent bodies. While ordinary chondrites show a wide range of shock effects [1], carbonaceous chondrites having been affected by high shock pressures are rare [2], and the shock effects on these meteorites are relatively unknown. Compared to ordinary chondrites, carbonaceous chondrites contain higher proportions of porous matrix. Shock effects on such porous and multiphase materials are extremely heterogeneous and the amount of post-shock heat is much larger than nonporous material [3]. In addition, CI and CM chondrites in particular are rich in volatiles and contain large amounts of water (10-20 wt% H_2O). It remains to be known how these volatile- and water- rich, porous meteorites will react to high shock pressures.

In order to gain our knowledge about the shock history of carbonaceous chondrites, we believe experimental research is a necessary step. The previous shock experiments of the Allende CV3 chondrite [4] demonstrated that chondrules are flattened in the plane of shock front by shock pressures in the range 10-20 GPa. In the present study, we attempted shock experiments of the Murchison CM2 chondrite. Murchison contains a larger volume fraction of porous matrix and is richer in volatiles than Allende, and therefore these meteorites are expected to respond differently to shock compression. The Murchison samples were shocked at 7, 11, 21, 26, and 30 GPa. The previous petrographic study of Scott et al. [2] reported that 22 out of 23 CM2 chondrites are shock stage S1 (up to 5 GPa) with one stage S2 in the classification of Stöffler et al. [1]. The shock pressures adopted for the present experiments correspond to the S2-S4 level, and thus they are much higher than those experienced by the existing CM2 chondrites. The major purposes of our study are to know how the Murchison CM2 chondrite will be mineralogically and chemically affected by shock pressures for stage S2-S4 and also to compare the results to those of the Allende shock experiments [4].

MATERIALS AND METHODS

The shock recovery experiments were performed by using a single stage 30-mm bore propellant gun at the National Institute for Research in Inorganic Materials. The target is a disk of Murchison, 8-10 mm in diameter and 2-3 mm in thickness, encapsuled in a cylindrical container made of stainless steel, 24 mm in diameter and 30 mm in length. The projectiles are a 12-mm-thick plate made of stainless steel SUS304 and a 3-mm-thick plate made of aluminum, both bedded at the front of a polyethylene sabot. The peak shock pressure produced in the target sample is regarded as an equilibrated value with that of the target assembly and is determined from the velocity of the projectile measured just before impact and the Hugoniots of the stainless steel and aluminum. Details of shock-experimental procedures are described in Sekine et al. [5].

We first undertook to shock Murchison at 5, 10, and 20 GPa, which correspond to the

highest pressure values estimated for shock stages S1, S2 and S3, respectively. 10 and 20 GPa are approximately the same pressures adopted for the previous Allende shock experiments [4]. The resultant peak pressures calculated by the measured velocities in the present experiments turned out to be 7, 11, and 21 GPa, respectively. After we found evidence of incipient melting and evaporation from the sample recovered from 21 GPa, we further undertook to shock Murchison at 25 and 30 GPa in order to see details of transition in the 20-30 GPa pressure range (stage S4). The resultant peak pressures calculated by the measured velocities are 26 and 30 GPa, respectively.

Polishied thin sections were made from each recovered sample by cutting along the shock compaction axis and studied by using an optical microscope, a scanning electron microscope (JEOL JSM-5800) equipped with an energy-dispersive X-ray spectrometer. We here present the results of detailed mineralogical and petrographic studies of the recovered samples shocked at 7, 11 and 21 GPa. The studies of 26-GPa and 30-GPa samples are in progress, and the results will be shown at the symposium.

RESULTS

Natural Murchison (Before shock; comparison to CV3)

Murchison CM2 chondrite consists of smaller chondrules and a higher volume fraction of matrix (~64 %) [6] than CV3 chondrites (40-50 %). Murchison is richer in volatiles including water (~12 wt% H_2O) [7] than CV3 chondrites (<2 wt%). The matrix of Murchison consists largely of hydrous minerals, mostly Mg-Fe serpentine and tochilinite, while the matrix of CV3 chondrites consists mostly of olivine. PCP is a major constituent of the CM2 matrix. It is a complex aggregate (typically 20 to 80 μm in diameter) consisting mainly of two phases, tochilinite and cronstedtite, and the proportion of these phases varies widely between and within PCP grains [7-9].

Impact at 7 GPa

Olivine grains in some chondrules show irregular fractures and undulatory extinction, but such olivines are rare. Otherwise no significant changes in texture and mineralogy are observed. These features are consistent with shock stage S2 [1]. Chondrule flattening and preferred orientations are not obvious.

Impact at 11 GPa

Most chondrules are slightly flattened and show appreciable preferred orientation nearly perpendicular to the compaction axis. The mean aspect ratio of 50 chondrules is 1.23, which is smaller than the aspect ratio (1.34) of chondrules in the Allende sample shocked at the same pressure [4]. Part of olivine grains in chondrules are irregularly fractured and show undulatory extinction, while others show no such textures. These features of olivine are consistent with shock stage S2 and are similar to those observed in the Allende sample recovered from 11 GPa [4]. The matrix is considerably compacted, and PCPs show minor deformation.

Impact at 21 GPa

Chondrules are more flattened and show more pronounced preferred orientation than those in the 11-GPa sample. The mean aspect ratio of 41 chondrules is 1.48, which is again considerably smaller than that (1.62) for chondrules in the Allende sample recovered from the same pressure. Almost all olivines in chondrules are heavily fractured and show undulatory extinction. Olivines with parallel planar fractures with a spacing of several tens of microns also occur. These features of olivine are consistent with shock stage S3 and are similar to

those observed in the Allende sample recovered from 21 GPa [4]. The matrix is more greatly and more homogeneously compacted than that of the 11-GPa sample. Especially PCPs are strongly deformed.

An important change observed in this sample is that minor melting occurs in the outer portions of the disk sample (to 2-3 mm from the edge). Relatively thick melt veins (30-120 μm in width and <1.2 mm in length) occur along flat, thick cracks running at angles of 40-60° to the compaction axis. They branch into thinner veins (5-20 μm in width), forming a complex network. The melts contain a high density of tiny spherules of Fe-Ni metal and Fe sulfide (0.5-3 μm in diameter) as well as small grains of olivine and low-Ca and high-Ca pyroxenes. Wall-rock xenoliths are also included. The matrix of xenoliths is characteristically wrinkled, suggesting volume shrinkage due to dehydration. The veins contain abundant bubble-like voids (1-20 μm in diameter), indicating evaporation of volatiles. The melts compositionally resemble the matrix except that they are distinctly more enriched in S and Ca.

A melt pocket (60x400 μm in area) also occurs near the edge of the disk sample. The internal texture and mineralogy of the melt pocket are similar to the melt veins except that it contains more abundant metal. The metal occurs as aggregates (20-80 μm in diameter) of small domains filled with fine veinlets of Fe sulfide, suggesting they were once melted. The matrix of this melt pocket is compositionally very heterogeneous.

A thin section contains an unusual area (~2x3 mm), in which most PCPs show texture suggesting strong heating. They appear to be partially melted and contain bubble-like voids (1-3 μm in diameter) especially in tochilinite-rich areas, suggesting that evaporation, probably of water, occurred. Because no such texture is observed in PCPs in other areas, this particular area may have been more strongly heated than other non-melting areas.

DISCUSSION

The present experiments show that chondrule flattening and foliation occur in the plane of shock front by shock pressure in the Murchison CM2 chondrite. These changes are not readily recognizable by a single shock at 7 GPa, but it becomes obvious at 11 GPa or above. Chondrule flattening and foliation are evidently related to collapse of pores in the matrix, and they at such low pressure can be explained by the high porosity and the high volume proportion of the matrix of Murchison. From the results of the present experiments and those of Allende [4], it can be concluded that chondrule flattening and foliation are important features characteristic of shock compression for type 2-3 carbonaceous chondrites, and should be added as one of shock features indicating shock stage S3 or above.

The present experiments also confirm that the degree of chondrule flattening increases in accordance with the intensity of shock pressure. So, the degree of chondrule flattening can be used as a more precise measure of shock pressures for type 2-3 chondrites. The aspect ratios of Murchison chondrules are found to be smaller than those of Allende chondrules at both 11 and 21 GPa, indicating that the degree of chondrule flattening is different between chondrite types. Chondrule flattening is probably related to multiple factors such as porosity of matrix, chondrule-size distribution, proportion of chondrule to matrix, constituent minerals of chondrules and matrix, so the cause for the differences in chondrule flattening can not readily be explained.

It has become evident that incipient local melting takes place at 21 GPa in Murchison. Relatively thick shock veins are formed along major flat cracks oblique to the compaction axis, indicating that they were essentially formed by frictional heating. The melts are mostly formed by fusion of the matrix material. The abundant bubble-like voids in the melts indicate that evaporation of volatiles, including H_2O in phyllosilicate and tochilinite, took place at the same time of melting. Experiments of Tyburczy et al. [9] showed that Murchison starts to

devolatilize at an initial shock pressure of ~11 GPa which corresponds to the lower limit of stage S4, consistent with the present results. The melts are variable in composition but have a common characteristic, i.e. they are consistently enriched in S and Ca relative to the matrix, indicating that these particular elements could be readily mobilized and incorporated in the melts by shock melting. S and Ca are probably derived from tochilinite and calcite that are widely dispersed as fine grains in the matrix.

An important difference from the results of the Allende shock experiments [4] is that shock melting and evaporation occurred in the Murchison sample recovered from 21 GPa, while no such evidence was found in the Allende sample recovered from the same pressure. The difference indicates higher post-shock heat was produced in the Murchison sample than in the Allende sample, probably due to the higher fraction of porous matrix of Murchison. This may be related to the fact that CM2 chondrites shocked to stage S2 or above are nearly absent, while a major fraction (6 out of 13) of CV3 chondrites are shocked to stages S3 and S4 [2], as discussed later.

Scott et al. [2] pointed out heterogeneous distribution of coarse-grained olivine chondrules indicative of shock stage S2 in Murchison, and suggested that about 10-20% of the chondrules and fragments were shocked to stage S2 before they were assembled. The present study shows that petrographic characteristics of shock stage S2 such as irregular fractures and undulatory extinction can be produced by a single shock at 7 and 11 GPa, but their distributions are highly heterogeneous. This is probably because of heterogeneous shock effects due to intrinsic porosity variations, which Scott et al. also suggested. Therefore it is not necessary to consider preaccretionary shock events to explain the heterogeneity of shock effects in the S2 level, though our study does not exclude that possibility.

To explain why highly shocked carbonaceous chondrites are rare, Scott et al. [2] suggested that carbonaceous chondrites shocked above 20-30 GPa (S3-S4 level) escape from parent bodies, due to explosive expansion of shocked materials on pressure release, and form particles that are too small to survive as meteorites. Especially, CM2 chondrites are almost exclusively in stage S1. We currently have not had enough data to check this hypothesis, but the present experiments appear to indicate that drastic change, involving melting and evaporation, starts to take place at ~20 GPa, and thus to support the idea of Scott et al. [2]. A more confident conclusion will be given in the near future (at the symposium) after detailed investigation of the samples recovered from 26 and 30 GPa.

Acknowledgments - This work was supported by the Grant-in-Aid of the Japan Ministry of Education, Science and Culture (No. 06403001).

References

[1] Stöffler D., Keil K. and Scott E.R.D. (1991) *Geochim. Cosmochim. Acta* **55**, 3845-3967.
[2] Scott E.R.D, Keil K. and Stöffler D. (1992) *Geochim. Cosmochim. Acta* **56**, 4281-4293.
[3] Stöffler D., Bischoff A., Buchwald V and Rubin A.E. (1988) *Meteorites and the Early Solar System*, 165-202, Univ. Arizona Press.
[4] Nakamura T., Tomeoka K., Sekine T. and Takeda H. (1995) *Meteoritics* **30** 344-347.
[5] Sekine T., Akaishi M., Setaka N. and Kondo K. (1987) *J. Mat. Sci.* **23**, 3615-3619.
[6] McSween H.Y. (1979) *Geochim.. Cosmochim. Acta* **43**, 1761-1770.
[7] Fuchs L.H., Olsen E. and Jensen K.J. (1973) *Smithson. Contrib. Earth Sci*. **10**, 1-39.
[8] MacKinnon I.D.R. and Zolensky M. (1984) *Nature* **309**, 240-242.
[9] Tomeoka K. and Buseck P.R. (1985) *Geochim. Cosmochim. Acta* **49**, 2149-2163.
[10] Tyburczy J.A., Frisch B. and Ahrens T.J. (1986) *Earth Planet. Sci. Lett.* **80**, 201-207.

DECAY RATES OF Na CHARACTERISTIC X-RAY INTENSITIES DURING ELECTRON BEAM IRRADIATION ON SHOCK-LOADED ALBITE: A POTENTIAL SHOCK BAROMETER

TSUCHIYAMA Akira[1], SYONO Yasuhiko[2], and FUKUOKA Kiyoto[2]
1) Department of Earth and Space Science, Osaka University, Toyonaka 560, JAPAN 2) Institute for Material Research, Tohoku University, Sendai 980, JAPAN.

Introduction: Shock features, such as shock melting, shock veins, mosaicism and undulatory extinction of minerals, are usually seen in meteorites as a result of hypervelocity collisions on their parent bodies. There are many studies to estimate shock degrees or shock pressures by using such features (*e.g.*, [1]). However, most of the estimations are qualitative or semi-quantitative because presence or absence of such shock textures are used as criteria.

Plagioclase is a common mineral in equilibrated chondrites and eucrites. It has been known that mosaicism and planar deformation features are developed in plagioclase by shock, and maskelynite is formed by more intensive shock (*e.g.*, [1]). It has been also known that the characteristic X-ray intensity of Na in shocked plagioclase decreases in time during electron beam irradiation. If relation between the decreasing rates of the X-ray intensities and shock pressures is known, shock pressures of natural plagioclase can be estimated quantitatively. In the present study, shock-loading experiments were done on albite, and the relation was obtained to examine a possibility of the new shock barometer.

Experiments: A low albite single crystal ($An_{1.0}Or_{1.1}$) was used as starting materials for the experiments (10 mm in diameter and 2 mm in thickness) . Shock-loaded experiments were done using a propellant gun at Tohoku University [2]. The shock pressures (30.1, 39.0 and 49.2 GPa) were estimated from the measured flyer plate velocities.

Polished thin sections of the recovered specimens were prepared for observation under an optical microscope and electron irradiation experiments. The decreasing rates of the Na characteristic X-ray intensities were measured with an electron probe microanalyzer (JEOL-733) at Osaka university. Changes in the intensities were measured for every 5 seconds with 5 second intervals (5/5 sec run) during electron beam irradiation. 10/10, 10/20, 10/50 sec runs were also made depending on the decreasing rates. The accelerating voltage was 15 kV, and specimen current was 12 nA. During the measurements the focused electron beam was scanning with magnification of x1000 (thus, the area of 8x8 μm^2 region was irradiated by the scanned beam) . Other magnifications were also applied to check irradiation size effect. Powder X-ray diffraction patterns were obtained to examine crystalline states and Al-Si ordering of the specimens.

Results and discussion: With increasing the shock pressure, apparent strain of the specimens increased, from 0.1, 0.3 to 0.4 at 30.1, 39.0 and 49.2 GPa, respectively. Under an optical microscope, all the specimens have birefringence, and no amorphous region was observed even in the 49.2 GPa specimen. Shock veins and mosaicism were commonly observed. Peak heights of the X-ray diffraction patterns decreased significantly by the shock, and the peak/back ground ratios decreased (the amount of so-called "X-ray amorphous" states was increased) with increasing the shock pressure. The value of $\Delta 2\theta_{131}$ (about 1.1 deg; low albite) was not changed by the shock.

Examples of the change in the X-ray intensity of Na, I, in time, t, are shown in Fig.1. It was assumed that the intensity is decayed exponentially with time toward a base intensity, I_0,

$$I = I_0 + (I_1 - I_0)\exp(-\lambda t), \qquad (1)$$

where I_1 is the initial intensity, and λ is the decay constant. Linear regression of $\ln(I - I_0)$ to t was done for each $I - t$ data set. In this procedure, λ, I_0, and I_1 were obtained by maximizing the r-factor of the regression. The Na intensities decreased first, but sometimes increased with further electron beam irradiation (Fig.1b). Decrease of sample current was always accompanied with the increment of the intensity, and thus charge up of the specimen due to damage by the electron irradiation might cause this increment although the reason is uncertain exactly. Because of the increment the regression was made on the data of $I > I_{max}/e$. When the intensity increased at $I > I_{max}/e$, the regression was made on the data of $I > I_{min}$. The measured data were commonly fitted well by regression curves, indicating that Eq.(1) is a good assumption, except for some data with small λ values (starting material and some portions in 30.1 GPa specimen). Measurements with different irradiation areas show that λ seems to be inversely proportional to the area.

The decay constants, λ, measured at different positions were scattered in the same specimen. The scatter suggests that degree of shock changes locally at different positions. Therefore, bulk properties, such as powder X-ray diffraction, Raman and IR spectra, and thermoluminescence (TL), may be represented by summation of the properties throughout a specimen, in which degrees of shock are locally different.

An average of 7-22 measurements of the λ values in each specimen is plotted against the shock pressure in Fig.2. The decay constant increases with increasing the shock pressure although the scatter is large. The present results indicate that degrees of shock of natural samples can be estimated by this method. Especially, it should be noted that the estimation is possible within a spacial resolution of

about 10 μm. In fact, shock degrees in an eucrite estimated by this method are consistent with micro-TL results [3].

As discussed above, the present method has potential to use as a quantitative shock barometer. For further study, we have to check (1) effect of the chemical composition of plagioclase, and (2) whether or not maskelynite has similar λ - shock pressure relation. Calibration of the absolute shock pressure due to specimen size effect in shock-loading experiments should be also done.

References: [1] Stöffler *et al.* (1991) *G.C.A.*, **55**, 3845-3867. [2] Goto and Syono (1984) in "Materials Science of the Earth's Interior" ed. Sunagawa, pp.605-619, Terra Sci. Pub. Co. [3] Ninagawa *et al.* (1996) Japan Earth and Planetary Science Joint Meeting.

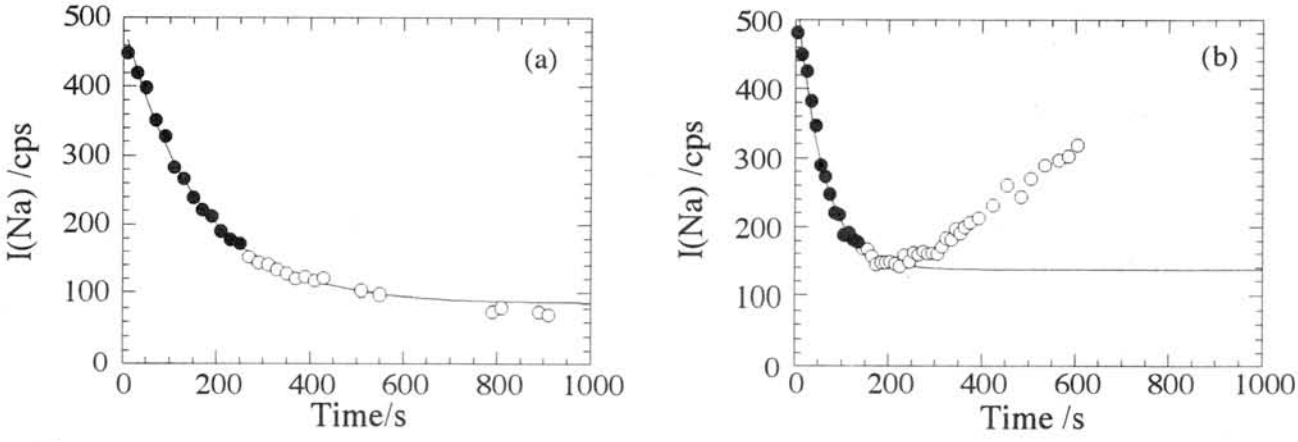

Figure 1. Change in Na characteristic X-ray intensities by electron beam irradiation to the area of 8x8 μm^2. Regression curves are also shown. Data used for the regressions are shown by solid circles. (a) 30.1 GPa, λ=0.00634 s^{-1}, r=0.99741. (b) 49.2 GPa, λ=0.0180 s^{-1}, r=0.99294.

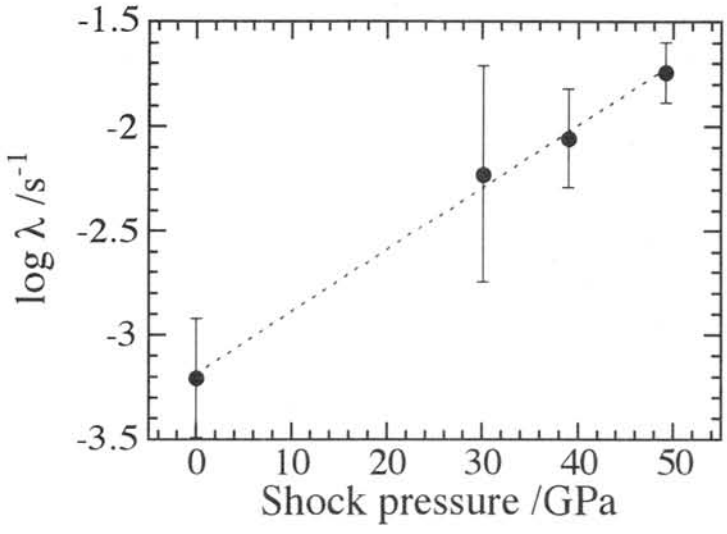

Figure 2. Average decay constants of Na-intensities, λ, with electron beam irradiation area of 8x8 μm^2 plotted against the shock pressure.

Preliminary Study of 7 Antarctic Ordinary Chondrites (H, L):A Petrographical and Mineral Chemical Comparison with Chinese Modern Falls

WANG Daode and WEN Wei

Guangzhou Institute of Geochemistry, Chinese Academy of Sciences,Guangzhou,P.R.China

Introduction

Comparative studies of Antarctic and non-Antarctic meteorites demonstrated many differences between these two populations, including terrestrial ages, average mass, trace element contents, and abundance of rare and unique types of meteorites [Freundel, et al., 1986; Dennison, et al., 1986; Dennison and Lipschutz, 1987; Koeberl and Cassidy, 1991]. Studies on some Antarctic achondrites and carbonaceous chondrites also revealed deviations in petrography and mineral chemistry from that of the non-Antarctic counterparts [Paul and Lipschutz, 1989; Tomeoka, et al., 1989; Lipschutz and Samuels, 1991; Takeda, 1991]. However, little comparative work was conducted on petrography and mineralogy of ordinary chondrites. Although some differences could be post-terrestrial (weathering effects, paring, and collecting method, etc.), the others were considered to be pre-terrestrial in origin. Different parent populations or Meteoroid Steams were proposed to explain these differences [Koeber and Cassidy, 1991]. In this paper, we report petrography and mineral chemistry of 7 Antarctic H, L chondrites and compare the results with 22 Chinese modern falls (CMFs).

Samples

The Antarctic meteorites studies in this work are ALH77004 (H4), Yamato74193 (H5), ALH76006 (H6), ALH77214 (L3), Yamato75271 (L5), ALH76001 (L6) and ALH76009 (L6). They are compared with 22 CMFs including 9 H5, 4 H6, 1 L4 and 8 L6 chondrites. All of these CMFs fell within 40 years to now and experienced little weathering.

Petrology and mineral chemistry

H-group: The three Antarctic H chondrites show no evidence of being significantly shocked, however, somewhat weathered. Except of major silicates of olivine and pyroxenes, abundance of plagioclase, chromite and phosphates obviously increases from H4 to H6 but in range of the 13 CMFs of H-group. In spite of clear outline of chondrules, presence of glass in chondrules and fine-grained matrix indicative of a classification of type 4, ALH77004 is rather homogeneous in mineral chemistry. The PMD values of Fa-content of olivine and Fs-content of low-Ca pyroxene in ALH77004 are 2.4 and 2.7, respectively, compatible with Yamato74193 (1.7 and 1.7) and ALH76006 (2.7 and 1.4). Furthermore, analysis of coexisting olivine and low-Ca pyroxene indicates well equilibrium of ALH77004 (Figure 1). Figure 1 also demonstrates similar compositions of olivine and low-Ca pyroxene between the 3 Antarctic chondrites and the 13 CMFs. Ni-content of kamacite (ALH77004: 6.15±0.39; Yamato74193: 6.08±0.24; ALH76006: 6.15±1.04) is somewhat more scatter than the Co-contents (4.18±0.03; 4.19±0.04; 0.55±0.07, respectively). The Co-, Ni-contents of kamacite of the three Antarctic H chondrites are plotted in range of the CMFs too. Plagioclase shows variation in Or-content with average composition of $Ab_{87.9}Or_{3.6}$ in ALH77004, $Ab_{82.5}Or_{5.6}$ in Yamato74193 and $Ab_{81.7}Or_{5.2}$ in ALH76006, similar to that of the CMFs. Figure 2 shows positive relevance of Fa-content of olivine and Co-content of kamacite, again, the three Antarctic H chondrites are plotted in range of the 13 CMFs.

L-group: ALH77214 (L3) shows obvious weathering. Chondrules have sharp outline and contain nearly clear glass. Troilite is significantly more abundant than metal. All metal

grains are kamacite and no taenite countered in this study. Kamacite has quite constant Co-content (0.8±0.07) but variable Ni-content (3.86±0.72). Olivine (Fa25.7±10.7) and low-Ca pyroxene (Fs13.4±3.9) are heterogeneous from grain to grain. Some grains of olivine in porphyritic olivine chondrules are normally zoned with Fa-content increasing sharply from core (14.4-15.4 mol%) to rin (35.1-44.8 mol%). Both of Yamato75271 and ALH76009 were moderately shocked as indicated by presence of maskelynite. Undulose extinction, breakdown of silicate crystals are also common. In addition, wormly intergrowth between kamacite and taenite is generally found in Yamato75271. ALH76001 shows only breakdown of silicate grains, without noticeable undulose extinction nor the other shocked features. Olivine is homogeneous not only in individual meteorites also among them (the mean Fa-content are 24.9, 24.8 and 24.8 mol%, respectively). In addition, Fs-contents of low-Ca pyroxene of the three Antarctic meteorites are same (21.9 mol%). The compositions of olivine and low-Ca pyroxene of the Antarctic L chondrites are plotted in a more narrow range than the CMFs (Fig.1). Kamacite contains 0.83±0.26wt%Co, 6.54±0.89wt% Ni in Yamato75271, 0.95± 0.14wt% Co, 5.63±1.01wt% Ni in ALH76001 and 0.92±0.07wt% Co, 6.06 ±0.33wt% Ni in ALH76009, overlapping range of the 9 CMFs of L-group. Compositions of maskelynite in the two shocked Antarctic L chondrites show a different trend in comparison with plagioclase in the other meteorites. The maskelynite shows a well defined negative relationship between Or- and Ab-contents with a nearly constant An-content, while negative relationship between An- and Ab-contents of the plagioclase in the other samples. The average compositions of plagioclases (or maskelynite) are Ab83.7±1.9Or6.0±2.1 in Yamato75271, Ab83.6±1.9Or4.4. ±1.2 in ALH76001 and Ab84.6±1.1Or5.4±1.0 in ALH76009.

Discussion and conclusions

1. Many Significant deviations between Antarctic and non-Antarctic H and L-group chondrites were demonstrated. A Study of bulk compositions of these 7 Antarctic samples also revealed significant differences of some trace elements in comparison with their counterparts of the CMFs (For H-group, Co, Sb, Cs, Au, Se, Zn, Th and U were higher in the former than the later. For L-group, Au, Se, Th and U were lower in the former than latter) [Zhong, et al., 1995]. However, we found no meaningful difference in petrography and mineral chemistry between the 7 Antarctic meteorites and their counterparts of the 22 CMFs. Since these CMFs fell within a relatively short period (40 years), it seems reasonable to consider them coming from same H or L population, respectively, hence an ideal reference for Antarctic meteorites that fell within a period upto one million years. The well overlapping of the 7 Antarctic samples with the CMFs, studied in this work, suggests that there is probably little difference in petrography and mineral chemistry among the supposed meteorite populations. However, more Antarctic meteorites especially those with large terrestrial ages are required to be studied in the future in order to make any conclusion.

2. The petrographical features and mineral chemistry (e.g. mean values and deviations of Fa-content of olivine, Fs-content of low-Ca pyroxene, Co-content of Kamacite) confirm classification of the 7 Antarctic ordinary chondrites.

Acknowledgements: Samples of the 4 Antarctic meteorites were supplied by NIPR.

References: Dennison, J. E., et al. (1986) Nature 319, 390-393; Dennison, J. E. and Lipschutz, M. E. (1987) GCA 51, 741-754; Freundel, M., et al. (1986) GCA 50, 2663-2673; Koeberl, C. and Cassidy, W. A. (1991) GCA 55, 3-18; Lipschutz, M. E. and S. M. (1991) GCA 55, 19-34; Paul, R. L. and Lipschutz, M. E. (1989) Z. Naturforsch 44a, 979-987; Spitz, A. H. and Boynton, W. V. (1988) Meteoritics 23, 302-303; Takeda, H. (1991) GCA 55, 35-

47; Tomeka, K., et al. (1989) Proc. NIPR 2, 36-54; Zhong et al. (1995), Antarctic Research Vol.7 No.3, 49-54 (in Chinese).

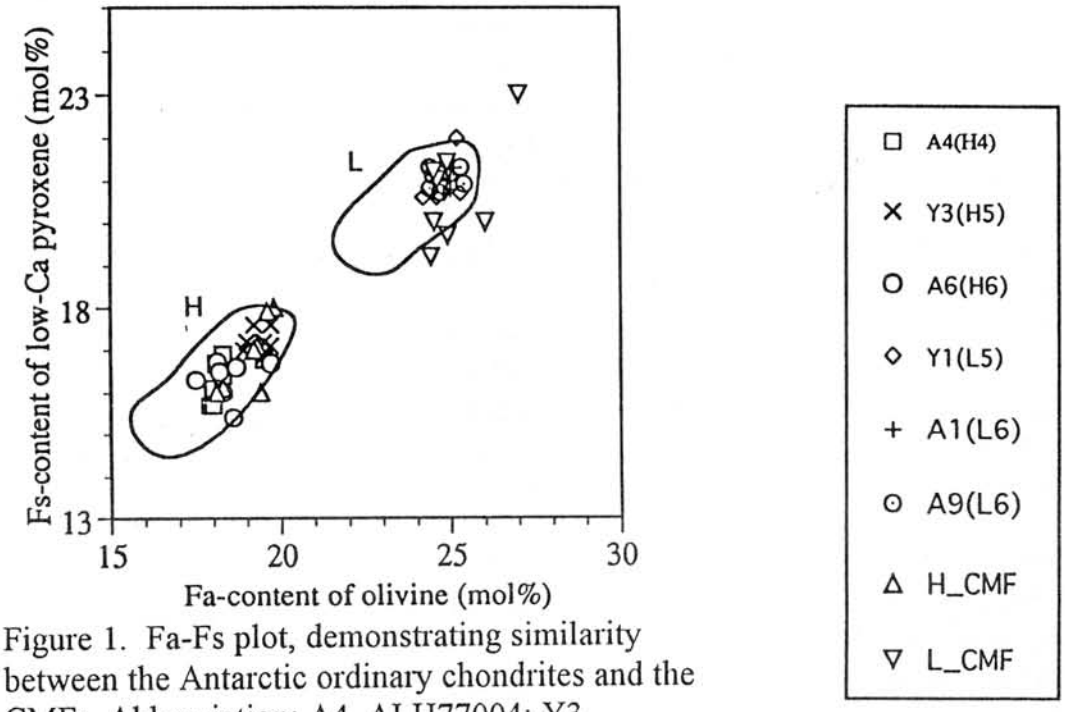

Figure 1. Fa-Fs plot, demonstrating similarity between the Antarctic ordinary chondrites and the CMFs. Abbreviation: A4, ALH77004; Y3, Yamato74193; A6, ALH76006; Y1, Yamato75271; Al, ALH76001; A9, ALH76009.

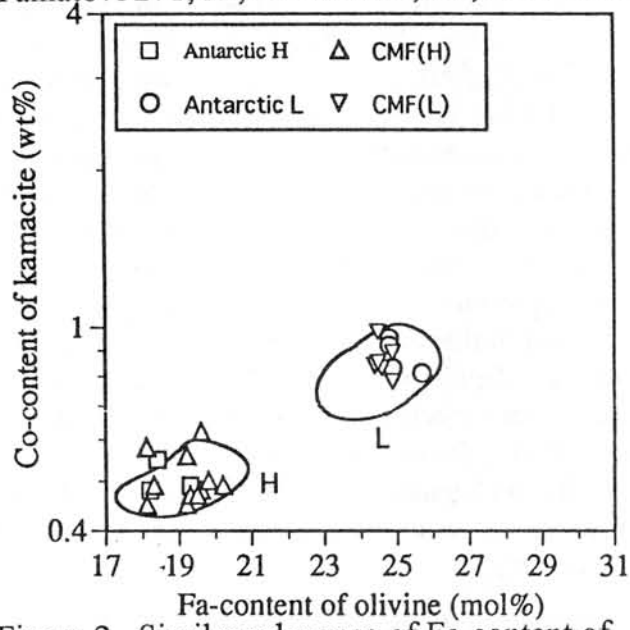

Figure 2. Similar relevance of Fa-content of olivine with Co-content of kamacites between the Antarctic ordinary chondrites and the CMFs.

COMPOSITIONAL-PETROLOGIC INVESTIGATION OF EUCRITES AND THE QUE94201 SHERGOTTITE

PAUL H. WARREN[1,2], GREGORY W. KALLEMEYN[2], TOMOKO ARAI[1], and KENTARO KANEDA[1]

[1]Mineralogical Institute, University of Tokyo, Hongo, Tokyo 113, Japan
[2]Institute of Geophysics and Planetary Physics, UCLA, Los Angeles, CA 90095-1567, USA

Introduction We have studied bulk compositions and mineralogy of several unusual eucrites and the bulk composition of the QUE94201 shergottite. Bulk compositions were determined using standard UCLA methods: INAA, RNAA (for Ni, Zn, Ge, Cd, Re, Os, Ir and Au), and fused-bead EPMA (major elements + Ti). Mineral compositions were studied using EPMA at the University of Tokyo. We have not yet completed RNAA for some samples (those showing no Re and Os data in the Table).

QUE94201: In agreement with [1], we find that this basaltic shergottite (BASH) shows some remarkable similarities to EET79001, especially the "b" portion of EET79001 (the portion with a fairly typical BASH texture). CI-normalized data for incompatible elements are shown in Fig. 1 (data for other BASHes from literature, except Th in EET79001b, from our own work in progress). Also, concentrations of Na, Mg, Al, Ca, Sc, Cr and Ni, all show a close resemblance to EET79001b. However, Ti is much higher, V is much lower, and Si is slightly lower, in QUE94201. A very close match would be surprising, because cosmic-ray exposure evidence [e.g., 2] suggests that EET79001 was launched in a separate martian cratering event from all other SNC meteorites. It will be interesting to see if RNAA siderophile element data, when they become available, show further evidence of EET79001-QUE94201 similarity.

Polymict (?) eucrites: All of the eucrites of this study feature extremely low siderophile concentrations (Table). In the cases of ALH81001 and LEW87010, these new data are difficult to reconcile with previous classification of these eucrites as polymict [3]. The textures are not obviously polymict (both are essentially unbrecciated, although ALH81001 is to an unusually high degree porphyritic), so these samples were apparently deemed polymict in the sense of being impact melts. They should be reclassified as normal igneous (compositionally "pristine") eucrites.

PCA91007, the second unbrecciated vesicular eucrite: Until now, the only known vesicular eucrite (discounting cavities of uncertain origin in heavily brecciated samples) was Ibitira. Interpretation of Ibitira is complicated by its unusually intense metamorphic history. PCA91007 is not as vesicular as Ibitira, but the small (roughly 5 mm^2) thin section we studied features at least 5 (possibly 8 or more) approximately spherical cavities, with diameters of 50-150 (-300?) μm. The section is extremely irregular in shape, so possibly a few larger vesicles are present but not identifiable. Unlike Ibitira, PCA91007 has been only moderately metamorphosed. Pyroxene compositions are fairly well equilibrated (with exsolution lamellae typically about 1 μm wide), but the original texture is essentially preserved. This texture is more uniformly fine grained (typically 0.05-0.1 mm, longest grain is an acicular pyroxene, 500×30 μm) than in any other known eucrite. ALH81001 has an even more fine-grained groundmass, but also features a major proportion of relatively coarse, phenocryst-like pyroxene grains. Thus, PCA91007 represents the best case for a eucrite that has been quenched to preserve the composition of a former HED-asteroidal melt. This composition is not highly unusual. Unlike Ibitira, PCA91007 shows no significant depletion of alkalis relative to typical eucrites (Fig. 2). Incompatible elements are also at typical noncumulate eucrite concentrations. The mg# ratio (37 mol%) is significantly lower than that of Ibitira (42).

Asuka-881394, a volatile-depleted cumulate eucrite: The medium-grained granular texture of As-881394 [4] is possibly altered from the original igneous texture, and difficult to categorize in terms of cumulate vs. noncumulate origin. However, based on low incompatible element contents and high mg#, we infer it is a cumulate. Even so, its extremely low concentrations of volatile elements (Fig. 2) seem remarkable. The Ga/Al ratio (0.010×CI) is also exceptionally low. This sample tends to blur the distinction between eucrites and angrites. However, many significant differences vs. angrites remain. For example, the Fe/Mn ratio (34) is typical for eucrites, and only 0.4× the lowest Fe/Mn among angrites.

EET87548, an extraordinarily pyroxene- and chromite-rich cumulate eucrite: PTS EET87548,11 contains 67.9 vol% pyroxene (px), 29.3 vol% plagioclase (pl), 1.1 vol% chromite (cm), and 1.7 vol%

other phases (mainly silica and Fe-metal). This mode features more than twice the cm content of any other eucrite, and ties with Binda for the highest px/pl ratio among eucrites. The high cm content is reflected in exceptionally high bulk-rock contents of Cr and V (Fig. 3). Augite exsolution lamellae in px are up to 35 μm wide. Three of the chromites contain bands of ilmenite, up to about 4 μm wide. These bands probably formed by exsolution, because they are unusually Cr-rich for eucritic ilmenites, their host cm's are compositionally distinctive (vs. band-free cm), and in one case a crack that crosses the cm grain disappears as it crosses the ilmenite band (implying that the band formed after brecciation of the cm).

The high cm content of EET87548 strongly confirms previous conjectures [e.g., 5] that cm may be a cumulus phase in some eucrites. The extremely low incompatible element contents of this rock imply that if it formed by any reasonably simple cumulus process from any conceivable eucrite-related magma, only about 4 wt% can have come from trapped liquid. In such a case, there is practically no way to generate a rock with twice the cm content of normal eucrites, unless the cm is at least partly cumulus in origin.

Origins of cumulate eucrites: Stolper [6] argued long ago that some cumulate eucrites probably formed from parent melts more ferroan (low mg#) than any known eucrite. This conclusion has been supported by further cumulate eucrite discoveries [7]. Recently, however, Treiman [5] has criticized this conclusion, arguing that most cumulate eucrites crystallized from "normal eucritic" magmas, not significantly more ferroan than Nuevo Laredo, which has bulk-rock mg# = 33 mol%. As an historical aside, by inclusion of [7] among five papers criticized for "flawed" modeling "from mineral analyses" and "without consideration of magma trapped among the crystals," Treiman [5] seriously misrepresented [7]. Treiman's model addressed primarily a relatively REE-rich (Sm = 0.28 μg/g; we assume that Sm is a representative incompatible element) analysis of Serra de Magé. The modeling approach of [7], which is basically identical to that later adopted by Treiman [5], agrees in predicting that such a sample (Serra de Magé) must have formed with 11 wt% trapped liquid (TL), from a parent melt with mg# (32 mol%), assuming the melt's Sm content was roughly 2-3 μg/g — a close match to Nuevo Laredo (33 mol% and 2.3 μg/g). However, the same modeling approach predicts that EET87548 formed with only 3.6-3.7 wt% TL (very definitely <<10 wt%), and its parent melt had mg# = 28-29 mol%. This model includes a slight adjustment for diminution of the bulk-rock mg# associated with the cumulus cm. The parent melts of Y791195 and RKPA80224, modeled by the same technique (in these cases the TL contents are much higher) require even lower mg#. For Moama and Medanitos (both adcumulates like EET87548, with very low TL) the implied parent melts are similar to that implied for Serra de Magé. All of the known cumulate eucrites except Binda appear to have crystallized from melts with mg# as low as, or considerably lower than, the extreme low-mg# end of the noncumulate eucrite compositional range.

References: [1] Mittlefehldt D. W. & Lindstrom M. M. (1996) *LPS XXVII*, 887-888. [2] Eugster O. et al. (1996) *LPS XXVII*, 345-346. [3] Grossman J. N. (1994) *Meteoritics 29*, 100-143. [4] Yanai K. et al. (1995) *Catalog of the Antarctic Meteorites*. [5] Treiman A. H. (1996) *LPS XXVII*, 1337-1338. [6] Stolper E. (1977) *GCA 41*, 587-611. [7] Warren P. H. & Kallemeyn G. W. (1992) *Meteoritics 27*, 303-304.

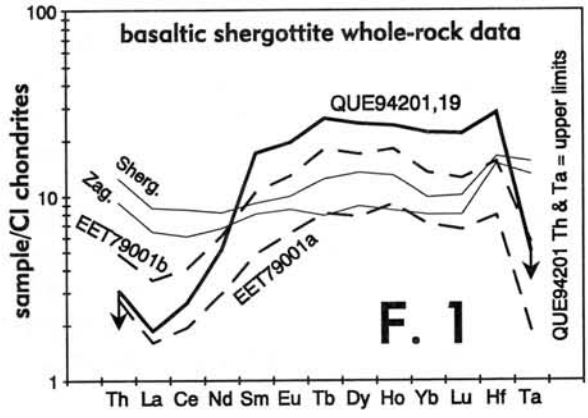

Table: Whole-rock concentrations of 38 elements in eucrites and QUE94201, determined by INAA, RNAA and fused bead EPMA.

	mass	Na	Mg	Al	Si	K	Ca	Sc	Ti	V	Cr	Mn	Fe	Co	Ni	Zn	Ga	Ge	Sr	Zr	Cd	Ba
	mg	mg/g	mg/g	mg/g	mg/g	mg/g	mg/g	µg/g	mg/g	µg/g	mg/g	mg/g	mg/g	µg/g	µg/g	µg/g	µg/g	ng/g	µg/g	µg/g	ng/g	µg/g
As-881394,56a	273	0.63	52	79	245	*0.04*	78	20.6	0.92	82	2.62	2.96	91	7.8	<30	17	*0.9*	---	*58*	<32	---	<32
ALH81001,16a	185	---	---	---	---	---	---	---	---	---	---	---	---	---	3.0	2.34	---	15.2	---	---	25	---
EET87548,7a	341	1.33	81	31.0	232	*0.12*	49	31.0	1.27	109	7.6	5.1	163	12.1	<26	<5.1	*0.70*	---	<35	<61	---	<23
EET87548,7b	344	1.19	84	32.2	232	*0.11*	47	31.3	1.29	141	8.0	5.3	164	11.5	3.4	1.13	*0.50*	27	<43	<48	*3.6*	<15
LEW86002,10a	375	3.04	41	65	228	0.25	69	28.1	3.6	66	2.11	4.40	150	6.0	<18	<3.1	1.32	---	*82*	*62*	---	*28*
LEW86002,10b	400	3.35	---	66	---	0.26	70	29.5	2.7	64	2.14	4.40	*142*	5.3	0.47	1.61	1.54	0.75	*66*	<110	<4	*37*
LEW87010,6	171	3.32	40	68	229	0.33	70	31.3	4.0	81	2.38	4.7	149	6.4	*0.40*	0.70	*1.48*	1.3	*81*	*48*	<0.8	*30*
PCA91007,4	328	3.41	36	69	233	0.34	74	30.6	4.4	68	2.03	4.14	141	6.0	<19	25	*1.31*	---	*94*	*69*	---	<33
RKPA80204,14	319	3.07	41	68	230	0.51	73	29.9	4.6	85	2.20	4.41	144	3.9	*0.48*	1.12	*1.50*	1.5	*53*	<73	<400	*24*
RKPA80224,6	132	3.33	43	72	227	*0.35*	72	28.4	3.0	77	2.28	4.49	149	5.1	<59	---	*1.60*	---	*74*	<70	---	*35*
RKPA80224,7	218	3.33	39	72	229	*0.43*	72	30.7	2.2	69	2.38	4.36	142	5.8	*1.50*	1.59	*1.55*	2.0	*100*	<61	<4.2	*26*
Ya-791186;88a	270	3.69	*46*	61	234	0.51	70	28.8	5.3	62	2.73	4.30	143	4.2	*0.49*	0.9	*1.01*	10.5	*85*	*79*	<10	*55*
Ya-791195;73a	235	2.77	45	72	238	0.31	72	29.0	1.33	72	2.15	4.20	125	6.0	*1.21*	0.92	<3	---	*66*	<32	<10	*<20*
Ya-82037,64	372	2.87	*41*	72	238	0.27	73	28.4	1.50	73	2.02	4.37	134	6.4	1.19	1.64	<2.6	3.8	*63*	50	12	*23*
QUE94201,19	305	10.3	38	51	220	*0.32*	81	49	11.7	124	1.03	3.72	145	24.4	<40	108	26	---	*59*	*94*	---	<41

	La	Ce	Nd	Sm	Eu	Tb	Dy	Yb	Lu	Hf	Ta	Re	Os	Ir	Au	Th	U	mg#
	µg/g	µg/g	µg/g	µg/g	µg/g	µg/g	µg/g	µg/g	µg/g	µg/g	µg/g	ng/g	ng/g	ng/g	ng/g	µg/g	µg/g	mol%
As-881394,56a	0.40	1.08	<2	0.29	0.27	0.085	<2	0.36	0.061	0.215	<0.05	---	---	<1.7	<0.7	<0.04	<0.1	56.6
ALH81001,16a	---	---	---	---	---	---	---	---	---	---	---	*0.006*	*0.011*	0.0082	0.031	---	---	---
EET87548,7a	0.167	<0.44	<1.4	0.140	0.200	*0.041*	<2.2	0.37	0.062	<0.11	<0.06	---	---	<2.6	<2.3	<0.061	<0.11	53.3
EET87548,7b	*0.20*	<0.46	<1.0	0.137	0.184	*0.063*	<1.9	0.37	0.064	<0.063	<0.066	0.006	*0.0040*	0.0032	0.038	<0.057	<0.10	54.1
LEW86002,10a	1.62	5.3	*2.1*	1.02	0.54	0.23	<2.3	1.22	0.191	0.90	0.121	---	---	<1.0	<0.8	0.24	<0.14	38.8
LEW86002,10b	1.75	5.9	*2.6*	1.15	0.57	0.26	<6	1.34	0.207	0.96	0.123	*0.0011*	*0.0036*	*0.0005*	0.0097	0.26	<0.09	---
LEW87010,6	2.81	5.9	4.3	1.60	0.64	0.37	<6	1.72	0.27	1.01	0.144	*0.0041*	*0.0028*	*0.0009*	*0.013*	0.27	<0.14	38.1
PCA91007,4	3.04	8.6	*5.7*	2.16	0.68	0.49	*3.1*	2.08	0.32	1.44	0.174	---	---	<2.8	<0.38	0.38	<0.15	37.1
RKPA80204,14	2.51	6.6	*4.1*	1.34	0.67	0.32	*2.2*	1.47	0.24	1.29	0.149	*0.0069*	*0.0052*	0.0065	0.046	0.30	0.07	39.8
RKPA80224,6	1.51	*4.0*	*2.6*	0.87	0.73	0.27	<2.4>	1.60	0.25	0.82	<0.08	---	---	<5	<3	*0.15*	<0.2	39.8
RKPA80224,7	2.31	5.4	4.2	1.30	0.67	0.31	<2.8>	1.77	0.28	0.97	*0.102*	*0.0042*	*0.0135*	*0.0021*	*0.0158*	*0.25*	<0.06	38.5
Ya-791186;88a	3.07	9.2	5.7	1.82	0.77	0.44	*3.1*	1.99	0.30	2.04	0.27	*0.006*	<0.006	<0.002	*0.032*	0.49	*0.13*	42.6
Ya-791195;73a	0.50	1.86	1.18	0.35	0.45	0.10	---	0.52	0.083	0.24	<0.08	*0.0024*	<0.02	*0.005*	<0.013	<0.06	<0.07	45.2
Ya-82037,64	2.08	5.3	*3.7*	1.33	0.58	0.35	*2.1*	1.46	0.223	0.97	*0.08*	*0.0013*	*0.0015*	*0.0006*	0.015	*0.12*	<0.07	41.1
QUE94201,19	0.44	1.63	*2.4*	2.55	1.09	0.93	6.1	3.5	0.54	3.4	<0.08	---	---	<2.4	---	<0.09	---	37.5

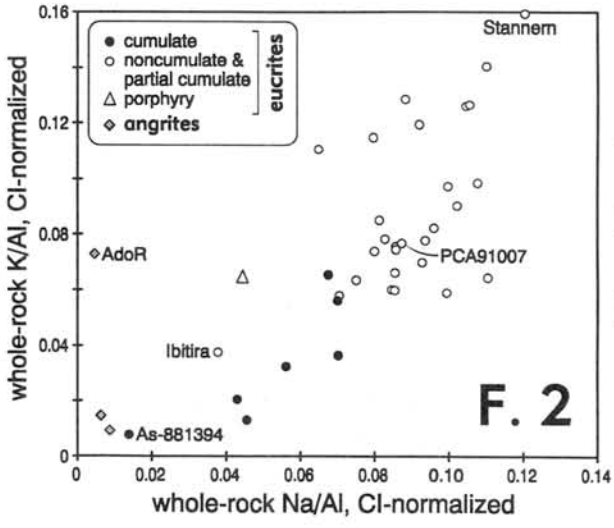

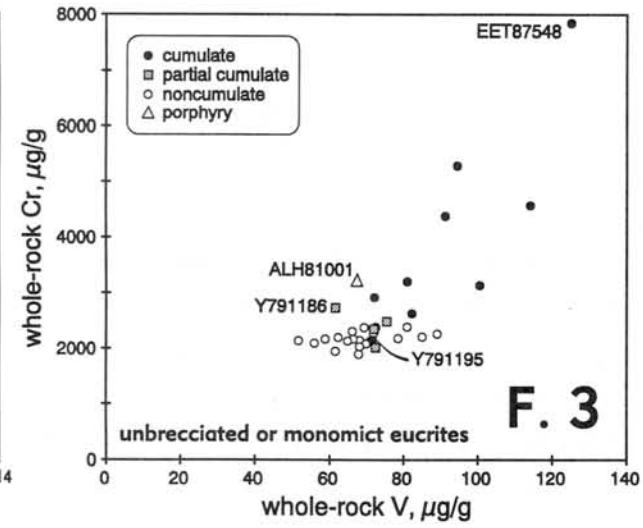

Meteoritic Sampling of the Asteroid Belt

John T. Wasson
University of California, Los Angeles, CA 90095 USA

Calculations indicate that 90% of the meteorites exit the Asteroid Belt via the 3:1 mean-motion resonance near 2.5 AU, and that most 10-km-size asteroids are fragments of moderate-size asteroids having original diameters >40 km. A much smaller fraction of the meteorites escape the inner portion of the Belt by other mechanisms, particularly the ν_6 resonance with the precession of Saturn's orbit. Because 80% of observed-fall meteorites are ordinary chondrites (OC), it follows that a similar fraction of the strong asteroids near 2.5 AU have OC compositions. Because no moderate-size asteroids with semi-major axis **a** between 2.4 and 2.6 AU have Q-type, OC-like reflection spectra, it follows that an overwhelming fraction of these asteroids have degraded spectra.

The most common spectral classes are C and S. If most asteroids having diameters >40 km have been compacted and heated enough to make their rocky materials as tough as a typical (L-group) OC chondrite, it follows that, at 2.4<**a**<2.6 AU, most S and C asteroids have OC interior compositions. Alternatively, roughly half the asteroids exiting at 2.5 AU may be CM or CI chondrites that are less efficiently sampled because of atmospheric or space-survival biases. In this case, only ≈40 % of the meteoroids exiting at the 3:1 resonance are ordinary chondrites, and the S asteroids are sufficient to account for the flux.

Basalts such as eucrites show deep pyroxene absorptions at 940 and 1900 nm because they have high FeO contents. However, observations on lunar maria show that the same high FeO contents make it easy to darken and redden basaltic regoliths by solar-wind irradiation and micrometeorite impact. The accretion of dust, especially dark, cometary dust, adds additional obscuration. One should therefore not expect that the intact, regolith-covered surfaces of asteroids that were covered with basalts ≥4 Ga ago would show sharply defined spectra having deep absorptions today. It is probable that there are numerous basalt-covered asteroids other than Vesta in the inner portion of the Asteroid Belt, and that the HED meteorites originated on one of these that is much closer to a resonance than is Vesta, which requires implausibly high launch velocity of 1 km s^{-1}.

The anomalously sharp reflection spectrum seems to require a recent resurfacing of Vesta. Only 0-2 other asteroids with D>40 km show basaltic reflection spectra. It is therefore of special import that the Binzel and Xu survey of small, Vesta-family (≤10 km) asteroids showed 20 to have well defined spectra with deep 940-nm absorptions. It seems probable that these "vestoids" were created in the impact event that resurfaced Vesta.

Although the hypothesis that the vestoids and the HED meteorites were ejected from Vesta in the same event has an appealing simplicity, there are major dynamical and mass-balance problems with this picture. Assuming a chondritic composition and 50% incorporation of Al into a eucritic crust, one obtains a mean original thickness of basalt of ≈11 km. It is unlikely that the impact of a large, 130-200 km projectile, as envisioned by Binzel and Xu, would leave basalt rather than mantle and projectile materials as the main rock type exposed on the surface. A still more severe problem is associated with launching 5-10 km fragments off Vesta with separation velocities of 0.9-1.0 km s^{-1}, necessary to account for the most distant vestoids and to inject material into the 3:1 resonance; cratering theory predicts far smaller separation velocities for large ejecta, and Vickery found evidence that km-size ejecta consist of clusters of 10-100 m objects that may be gravitationally unbound.

A simple and seemingly more plausible model is that the Vesta family asteroids are mainly fragments of a projectile that disintegrated during a grazing impact. If the impact generated a dust cloud that coated Vesta and the fragments of the impactor, all would show similar spectra even though their interior compositions probably differ. The dust may have mostly originated in the regolith of Vesta.

The main asteroidal dust band observed by the IRAS satellite has orbital parameters similar to those of the Vesta-family asteroids. It may have been mainly formed in the same collisional event that produced the Vesta family. Its presence supports the idea of a recent coating of dust on the surfaces of these bodies. Estimates by C. Chapman of the age of Vesta's surface based on comparisons with the reflection spectra of the Ida S asteroid by the Galileo spacecraft suggest that the resurfacing of Vesta occurred about 10 Ma ago.

In summary, the three largest classes of meteorites, the H, L and LL ordinary chondrites, appear to originate on asteroids located near 2.5 AU; the absence of OC reflection spectra on any large asteroids in this region is strong evidence that most asteroidal spectra have been degraded. This argument indicates that there can be numerous basalt-covered asteroids with degraded spectra. One of these that is located near a resonance is the probable source of the HED meteorites.

Na-REDISTRIBUTION IN THE MELT PHASE OF YANZHUANG METEORITE

XIE Xiande and CHEN Ming
Guangzhou Institute of Geochemistry, Academia Sinica, Guangzhou 510640, China

Introduction

Many chondrites contain shock-produced melt veins or pockets. It could be understood that the shock-induced melting of chondrites would result in the loss of some volatile elements by vaporization during cooling of melt. Evident Na-loss of shock melt veins has been reported in some L and H chondrites. Among the L6 chondrites, the loss of 25 wt% and 35 wt% Na were revealed in the veins of Apt and Vouillé [1], 30 wt% Na in the early vein of Chantonnay [2]. The veins in the Barbotan (H5) and Charsonville (H6) chondrites have lost 46 wt% and 50 wt% Na, respectively, in contrast to their unmelted chondritic materials [3]. Here we report a special case found in a severely shocked and reheated Yanzhuang H6 chondrite. Our study revealed that volatile element Na in the shock-induced melt phase of the meteorite has not obviously depleted.

Samples and Experimental Methods

The Yanzhuang (H6) chondrite is a Chinese meteorite fall that was severely shocked and reheated in an extraterrestrial impact event [4], and it is intersected by many melt veins (Fig. 1) and melt pockets.

Several polished thin sections containing both melt phase and unmelted chondritic materials were prepared for petrology, mineralogy and microprobe analyses. Several shock-metamorphosed facies were extracted from the meteorite for compositional measurement by instrumental neutron activation analysis (INAA).

Results and Discussion

1. Shock-metamorphosed facies

Four shock-metamorphosed facies were identified in the meteorite. Facies A: lightly deformed chondritic materials characteristic of mechanical deformations of minerals. This facies makes up about 40 vol% meteorite. Facies B: brecciated materials that most minerals especially the silicates were heavily deformed or broken into fine-grained fragments. This facies makes up about 20 vol% meteorite. Facies C: blackened and partially melted chondritic materials. The facies occur in neighboring melt veins and melt pockets. Plagioclase was melted; troilite, metal and pyroxene were partially melted. Solid state recrystallization of olivine and pyroxene had produced. This facies make up about 10 vol% meteorite. Facies D: melt phase including melt veins and pockets (Fig.1). It consists of microcrystalline olivine and pyroxene, silicate melt glass, metal-troilite eutectic nodules ranging in diameter from 0.1 to 10 mm. The facies makes up about 30 vol% meteorite.

2. Na in the shock-metamorphosed phases

Analyses by INAA indicate following Na-contents: 7020 ppm in facies A, 6010 ppm in facies B, 6600 ppm in facies C, 6600 ppm in facies D. It shows that Na content of melt phase

has not evidently depleted in contrast with other shock facies and with the average H chondrite fall (6380 ppm). Minor difference of Na content (<15 %) among different shock facies could be due to sample selection and experimental conditions.

Both high-Ca and low-Ca pyroxenes are encountered in the melt phase, and low-Ca pyroxene is predominant. The low-Ca pyroxene in the melt phase has heterogeneous compositions from grain to grain in contrast to the homogeneous compositions of low-Ca pyroxenes of chondritic material. These microcrystalline pyroxenes crystallized from shock-induced silicate melt contain high concentrations of Al_2O_3, Cr_2O_3, CaO and Na_2O, for example 0.1 to 2.7 wt% Al_2O_3, 0.1 to 1.3 wt% Cr_2O_3, 0.7 to 4.5 wt% CaO and up to 0.19 wt% Na_2O. Microcrystalline olivine in the melt phase has the same composition as the olivine of chondritic material, and only some grains contain slightly high CaO up to 0.28 wt.%.

A number of phosphate inclusions were found in metal-troilite eutectic nodule (Fig.2). These phosphate inclusions occur within the troilite as fine-grained spherule inclusions from 2 to 8 μm in diameter, and contain 48 to 58 wt% FeO, 2 to 5 wt% MnO and up to 4.55 wt% Na_2O (Fig.3). Among the identified phosphate inclusions, the majority of them contain high contents of Fe, Mn and Na. Na contents of them range from 1.32 to 4.55 wt% Na_2O which show a continuum of compositions (Fig. 3). The Fe-Mn-Na phosphate (~ 4 wt% Na_2O) has the formula $(Na,Ca,K)_2(Fe,Mn)_8(PO_4)_6$. Na-bearing Fe-Mn phosphates (1.32 - 3.72 wt% Na_2O) would be a mixture of graftonite (Fe-Mn phosphate) and Fe-Mn-Na phosphate. The phosphate in chondrite is mainly accessory mineral whitlockite which contains only up to 3 wt% Na_2O. Phosphate inclusions occurring in the kamacite, taenite and troilite in the chondritic material have not been identified. During shock event, chondrite was melted, and volatile elements Na and P released from the decomposed whitlockite and plagioclase concentrated to the shock-induced Fe-Ni-S melt at high pressures and high temperatures. P combined with Fe, Mn and Na, and formed phosphate which occur as inclusions within troilite.

The melt phase of Yanzhuang contains about 3 to 5 % silicate melt glass occurring among recrystallized olivine, pyroxene, metal and troilite. The dimensions of melt glass are too small to conduct microprobe analysis. EDX measurement shows that the glass has very heterogeneous compositions with 50 to 90 wt% SiO_2, 3 to 15 wt% Al_2O_3, 0.5 to 15 wt% FeO, 0.5 to 30 wt% MgO, 1 to 5 wt% Na_2O, 1 to 4 wt% CaO.

3. Na behavior in the melt phase

Na is easy to mobilize from minerals by vaporization during heating. Experimental vaporization of the Holbrook L6 chondrite showed that Na vaporization occurs at 800 - 1250 °C [5]. The shock pressures and post-shock temperatures in the brecciated areas (facies B, 350 to 850 °C), blackened and partially melted areas (facies C, 850 to 1300 °C), and melt phase (facies D, >1500 °C) of Yanzhuang were high enough to release Na from minerals into vapor phase. However, Na was not lost from the melt phase. Our explanations for the Na reservation are: (1) because the melt phase are surrounded by the high pressure and high temperature shock facies both blackened and partially melted areas and brecciated areas thus having lower temperature and pressure gradients, Na vapor could not be transported quickly from the melt phase to the surrounding areas. (2) shock compression reduced the meteorite porosity especially those severely metamorphosed facies, thus preventing most volatile elements in the melt phase from mobilization. (3) The cooling rates of melt phase of Yanzhuang were 6 - 30

°C/sec in the veins and 100 - 400 °C/sec in the pockets in the interval 950 - 1400 °C/s[6]. Fast cooling of melt phases reduced the mobilization of volatile elements and froze these elements.

Although there is no evident depletion of sodium in the melt phase of Yanzhuang, Na-redistribution has taken place. First, Na along with other volatile elements such as Mn and P (or PO_4^{-3}) concentrated in the Fe-Ni-S melt at high pressure and high temperature. During rapid cooling, phosphorus, on one hand, was solidified in the metal dendrites as solid solutions [6]; on the other hand, P, Fe, Mn, and Na crystallized as Fe-Mn and Fe-Mn-Na phosphates. Second, minor amount of Na was solidified into crystallized low-Ca pyroxene, resulting in slightly high Na-content in the pyroxenes. Third, the remaining Na was frozen in silicate melt glass.

References

[1] Dodd, R.T. & Jarosewich, E. (1982) *Earth Planet.Sci.Lett.*, 59, 355-363. [2] Dodd, R.T. et al. (1982) *Earth Planet.Sci.Lett.*, 59, 364-374. [3] Semenenko, V.P. et al. (1992) *Lunar Planet. Sci. XXIII*, 1263-1264. [4] Xie Xiande et al. (1994) *Chinese J. Geochem.*, 13, 39-45. [5] Gooding, J.L. & Muenow, D. (1977) *Meteoritics*, 12, 401 - 408. [6] Chen Ming et al. (1995) *Meteoritics*, 30, 28-32.

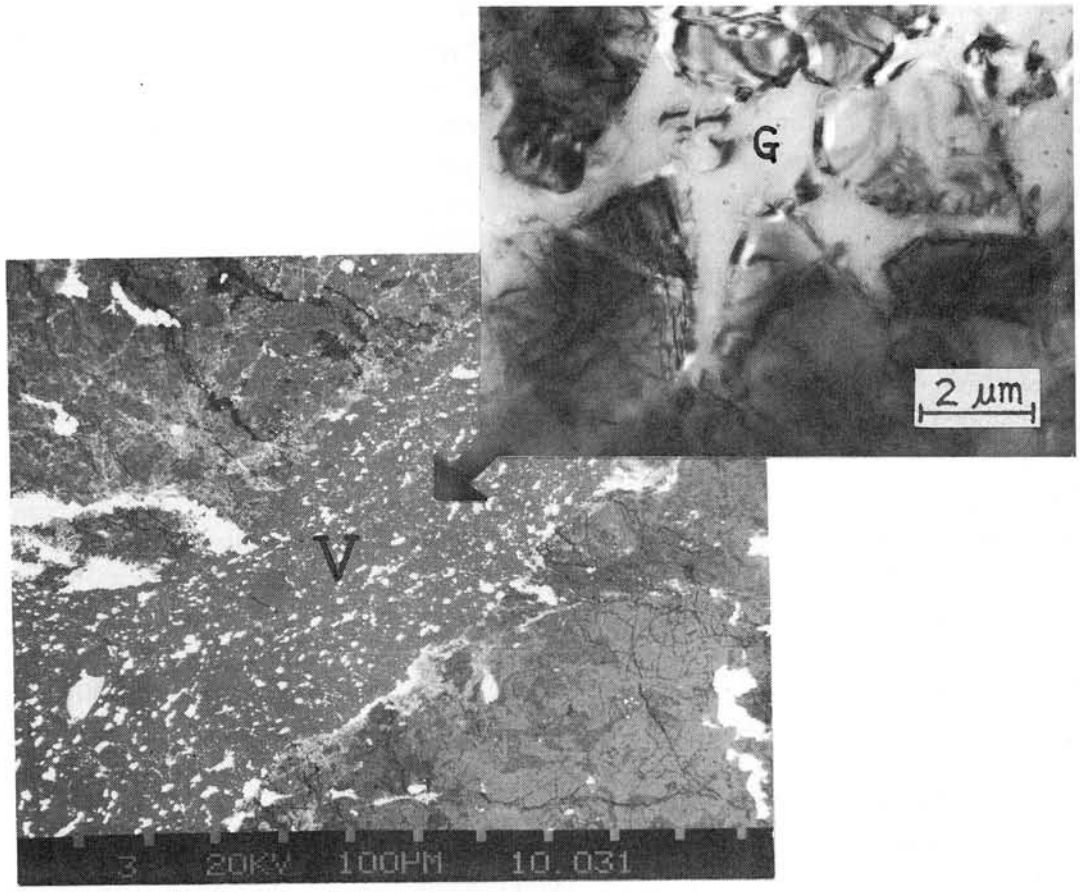

Fig.1 Severely shocked and reheated Yanzhuang meteorite which consists of unmelted chondritic material and shock-produced melt veins (V). The melt phase is composed of microcrystalline olivine and pyroxene, silicate melt glass (G), metal and sulfide.

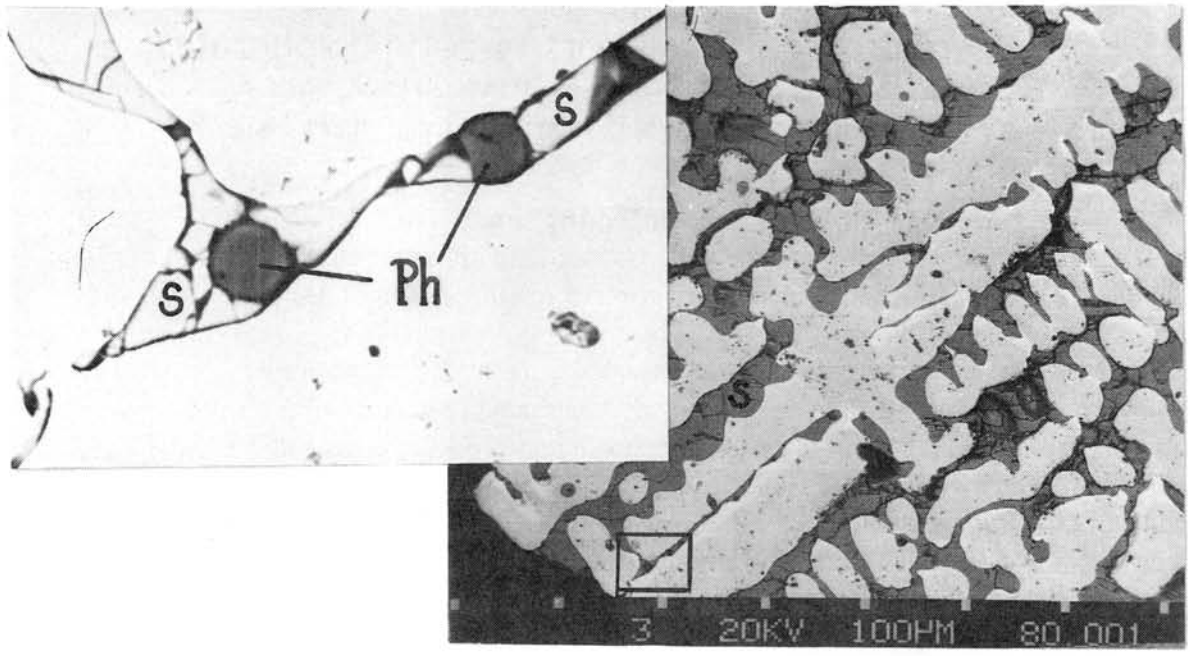

Fig.2 Back-scattered electron image showing an Fe-Mn-Na phosphate spherule inclusion (Ph) within troilite (S) of metal-troilite eutectic nodule in a shock vein.

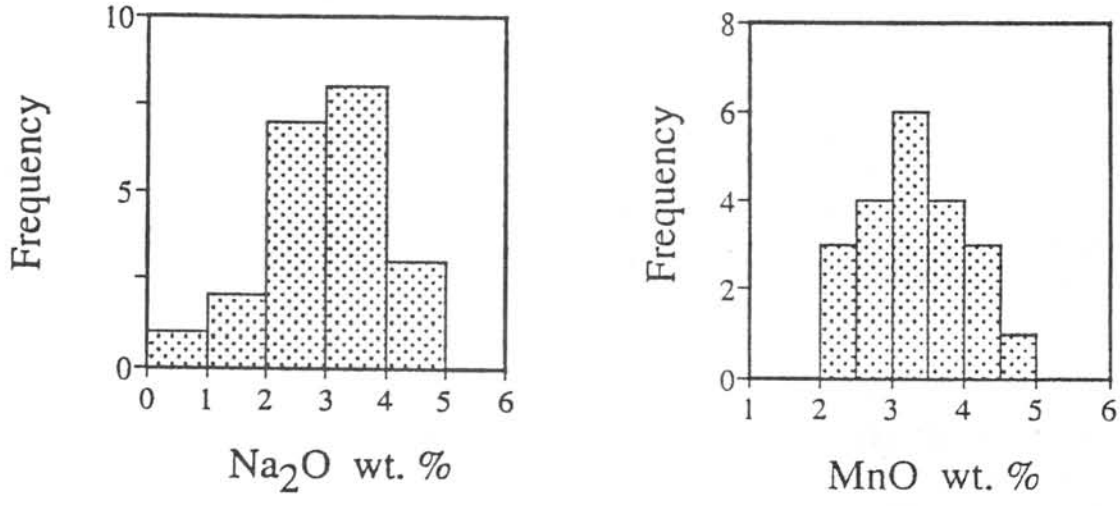

Fig.3 Compositional characteristic diagrams showing the frequencies of Na_2O and MnO contents of analyzed phosphate grains.

Information on precursors of S-type spherules

T. Yada, W. Nozaki, T. Nakamura, M. Sekiya, and N. Takaoka
Dept. Earth & Planet. Sci., Kyushu Univ., Fukuoka 812-81

1, Introduction

Spherules are spherical particles which are found in deep-sea sediments, Greenland and Antarctic ice, and sedimental rocks. Their size ranges from 20 to 1000 μm in diameter. Three types of spherules are found: Iron (I) type, Stony (S) type, and Glassy (G) type. They have been identified as extraterrestrial materials, for examples, from the concentration of Ir (Millard and Finkelman, 1970) and the abundance of a cosmogenic nuclide, ^{53}Mn (Nishiizumi, 1983). However, it is difficult to identify their precursor materials since spherules melted during their atmospheric entry. Steele et al. (1985) indicate that S-type spherules are similar to C1 and C2 chondrites from minor elements of relict olivine grains. From their work, precursors of some of S-type spherules included forsterite grains which have same origin as those of C1 and C2 chondrites. From studies of interplanetary dust particles (unmelted extraterrestrial dust, called shortly as IDPs), on the other hand, it is indicated that hydrous (chondritic smooth) IDPs are similar to C1 or C2 chondrites in their mineralogies, though some differences exist (Schramm et al., 1989). Most of micrometeorites, unmelted extraterrestrial dusts found in Greenland and Antarctic ice, also show mineralogies of olivine and pyroxene similar to those of C2 chondrites (Robin et al., 1990). With all these observation, it is concluded at least that most of extraterrestrial dust accreting to the earth now are material strongly related to C1 or C2 chondrites in mineralogy and chemistry. Further studies of extraterrestrial dust will lead us to understanding of primordial planetary materials and the history of early solar system.

We researched relict grains in S-type spherules in order to have more information on their precursors.

2, Experiments

S-type spherules we examined are collected from deep-sea sediments offshore Hawaii, 5800 m depth. About 200 spherules are separated by a hand magnet, washed by purified water, and handpicked. Then we performed EPMA observation of their surfaces and cross sections. Among 13 polished S-type spherules, 4 of them included relict forsterite grains. We analyzed the center of relict grains for chemical compositions. We also performed line analysis from the center to the edge of relict grains (for example, Fig. 1) which are large enough to analyze several points across the grains.

3, Results

The center of relict olivine grains shows $<Fa_5$ in composition. Their analysis data on CaO and Cr_2O_3 are shown in Fig. 2. For comparison, those of C1~3 chondrite are also exhibited. This graph shows that relict grains overlap C1, C2 chondrites in minor elements composition. Especially, most of the points are in the C1 chondrite region.

Results of line analysis of relict grains are shown in Fig. 3. This graph shows that MnO and Cr_2O_3 tend to diffuse out of crystal and FeO, Al_2O_3, CaO, and NiO have a trend to diffuse into the crystal. From this result, silicates surrounding the relict grains were supposed to melt and the melt silicate could be more abundant in Fe, Al, Ca, and Ni and less in Mn and Cr than the forsterite.

Diffusions of these elements occurred by heating during their atmospheric entry. From Fa

distribution of a relict grain of a S-type spherule of 160 μm in diameter, its cooling rate was estimated to be 55 °C/s, from the peak temperature of 1800 °C (Yada et al., 1996).

4, Numerical simulation

Cooling rates of micrometeoroids entering atmosphere can estimate also by application of our numerical simulation of I-type spherules to S-type. Basic equations of the simulation are essentially same as Love and Brownlee (1991). We start calculations from 200km in altitude. A meteoritic sphere of initial radius r_0 comes into atmosphere at initial entry speed v_0 with angle θ_0 from the local vertical at the starting point. Equation of energy conservation is

$$\pi r^2 \cdot \rho_{air} v dt \cdot \frac{1}{2} v^2 \cdot \varepsilon_{th} - 4\pi r^2 \sigma T^4 \cdot \varepsilon_{em} dt + L \cdot 4\pi r^2 dr \cdot \rho_{mat} - \frac{4}{3}\pi r^3 \rho_{mat} C_P dt = 0, \quad (1)$$

where r is radius of spherule, ρ_{air} is density of air at altitude it exists, v is spherule's speed, ε_{th} is transform efficiency from kinetic energy to heat, σ is the Stefan-Boltzmann constant, T is its temperature, ε_{em} is radiative efficiency, L is latent heat of iron, ρ_{mat} is density of the meteoritic material, C_P is specific heat capacity of the meteoritic material at constant pressure. ε_{th} and ε_{em} are assumed to be 1 here. The first term of left-hand side expresses relative kinetic energy of atmospheric atom on the spherule's route. The second term stands for radiative heat loss from the surface. The third term signifies heat lost by evaporation. The fourth term is heat capacity of a spherule. The fourth term is supposed to be small, so we also ignore it.

If a spherule loses its mass only by evaporation, the equation of mass balance is written

$$4\pi r^2 dr \cdot \rho_{mat} = -\frac{P(T)\sqrt{m}}{\sqrt{2\pi kT}} \cdot 4\pi r^2 dt, \quad (2)$$

where $P(T)$ is saturated vapor pressure of the meteoritic material at T, m is mean molecular mass of the meteoritic material and k is the Boltzmann constant.

The equation of momentum is

$$\frac{4}{3}\pi r^3 \rho_{mat} \frac{d\boldsymbol{V}}{dt} = \frac{4}{3}\pi r^3 \rho_{mat} \boldsymbol{g} - \frac{1}{2} C_D \rho_{air} v \pi r^2 \boldsymbol{V}, \quad (3)$$

where $\boldsymbol{V}$ is velocity of spherule, $\boldsymbol{g}$ is gravity acceleration vector and C_D is drag constant which is 2 in supersonic situation (Adachi et al., 1976). This equation shows that derivative of a spherule's momentum with respect to time is balanced with the force by terrestrial gravitation and air resistance.

On the basis of equation (1)-(3), we calculate for time dependence of velocity, altitude, spherule's radius and temperature using the Runge-Kutta method. Then At each initial conditions, we calculate cooling rates between peak temperatures and 1100 °C on the assumption that the cooling rates are constant. For data on air density at given altitude, we use the U. S. Standard Atmosphere (1976). Vapor pressure and latent heat of meteoritic material is from Öpik (1958). Mean molecular weight of meteoritic material is set 45 from Hashimoto et al. (1979).

From the results of simulation, cooling rates of 55 °C/s result from only the case of high entry angle and low entry speed. We will constrain cooling rates applicable to that of the relict grain more strictly from considering peak temperatures and final sizes of spherules.

References

Adachi, I., Hayashi, C. and Nakazawa, K. (1976), Progr. Theor. Phys., 56, 1756-1771.

Hashimoto, A., Kumazawa, M., and Onuma, N. (1979), Earth Planet. Sci. Lett., 43, 13-21.

Love, S. G. and Brownlee, D. E. (1991), Icarus, 89, 26-43.

Millard, Jr, H. T. and Finkelman, R. B. (1970), J. Geophys. Res., 75, 2125-2134.
Nishiizumi (1983), Earth Planet. Sci. Lett., 63, 223-228.
Öpik, E. J. (1958), Physics of Meteor Flight in the Atmosphere. Interscience, New York.
Robin, E., Michel-Levy, N. C., Bourot-Denise, M., and Jéhanno, C. (1990), Earth Planet. Sci. Lett., 97, 162-176
Schramm, L. S., Brownlee, D. E., and Wheelock, M. M. (1989), Meteoritics, 24, 99-112
Steele, I. M., Smith, J. V., and Brownlee, D. E. (1985), Nature, 313, 297-299
U. S. Standard Atmosphere. (1976): U. S. Gonvt. Printing Office, Washington, DC., 227p.
Yada, T., Nakamura, T., Sekiya, M., and Takaoka, N. (1996), Proc. NIPR Symp. Antarct. Meteorites, 9, in press.

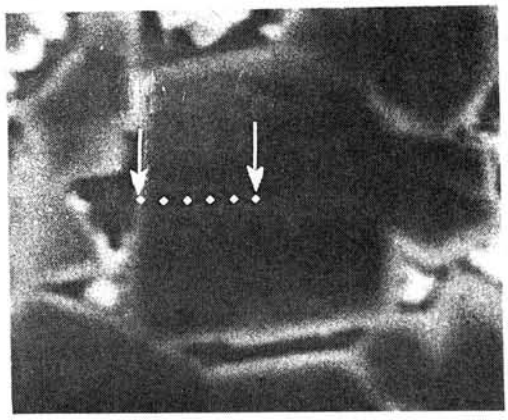

Fig. 1 A EPMA backscattered electron image of a relict forsterite grain in a S-type spherule. The grain's width is 10 μm. White spots are analytical points whose data are shown in Fig. 3.

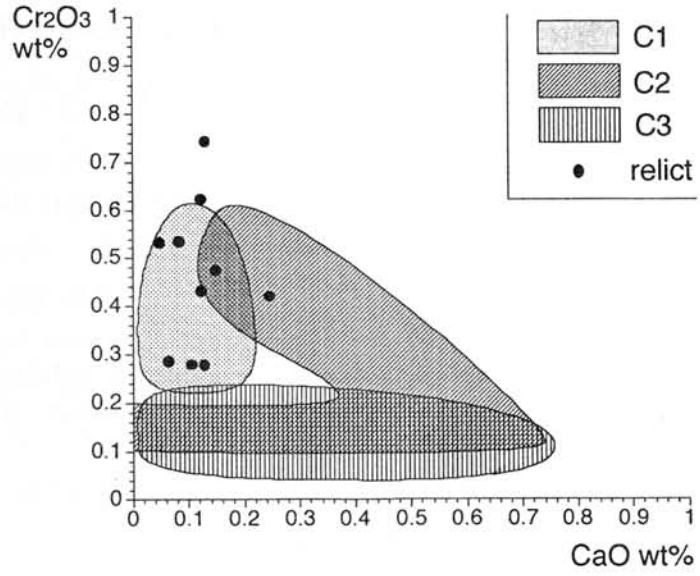

Fig. 2 Analytical data of relict grains in S-type spherules plotted on a CaO-Cr2O3 diagram. The data overlap those of forsterites in C1 chondrites.

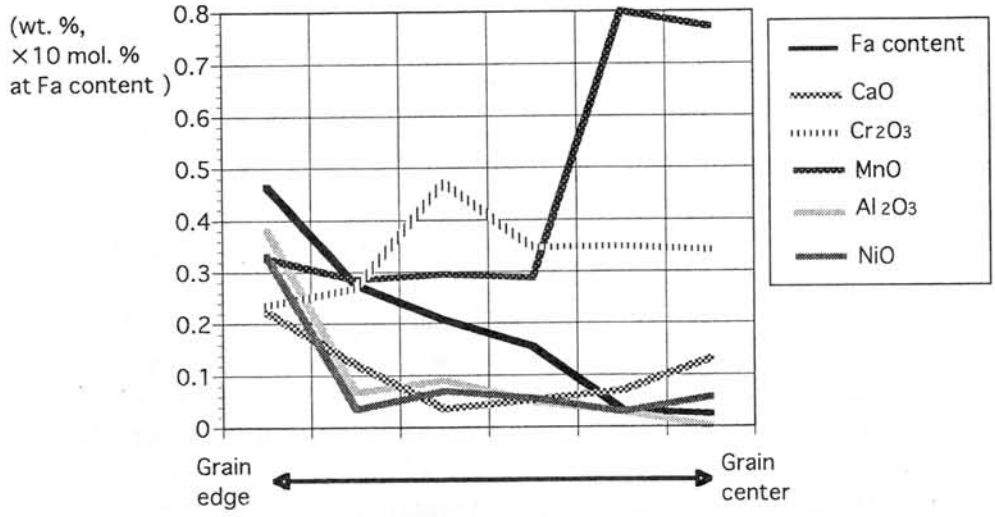

Fig. 3 Minor elements Compositions from edge to center of the relict grain shown in Fig. 1. The center of the grain shows forsterite in composition and is richer in MnO and Cr2O3 than the edge of the grain.

ORIGIN OF UNIQUE CHONDRITIC IMPACT MELT ROCKS, RAMSDORF (L) AND YAMATO-790964 (LL). A. Yamaguchi, E.R.D. Scott, and K. Keil; Hawaii Institute of Geophysics and Planetology, SOEST, University of Hawaii at Manoa, Honolulu, HI 96822, USA.

Introduction

Impact-melt rocks commonly occur in ordinary chondrites as clasts in fragmental and regolith breccias, but rarely as whole rocks [1, 2, 3]. Impact melt rocks or melt breccias resulting from whole rock melting are the highest form of shock alteration [2]. To better understand the origin of the rare impact melt rocks, we have studied the unique impact melt rocks, Ramsdorf and Yamato (Y) -790964. Detailed studies of those rocks were provided by [4] and [5]. Both impact melts appear to have formed fairly recently: ~0.5 Ga for Ramsdorf [6] and ~1.0-1.2 Ga for Y-790964 [5].

Results

Ramsdorf

There are two lithologic types in Ramsdorf: impact melt portion and chondritic portion (Fig. 1a). The impact melt portion has been studied by [4]; [7] described the portion that retained a prominent chondritic texture despite extensive melting (~90 vol%). At high magnification, however, there is little difference between the impact melt portion and the chondritic portion.

The igneous matrix of the chondritic portion, which is texturally identical to the matrix of the impact melt portion, shows typical melt texture comprising equant, euhedral olivines (10-30 μm in size), subhedral pyroxenes (~80 μm in size) that poikilitically enclose olivines, and interstitial glass. This melt texture is essentially the same as the texture observed in parts of other impact melt rocks [e.g., 1, 10, 12]. However, grain sizes and modal composition of the minerals are variable in PTSs (Fig. 1a), and this local textural heterogeneity accounts for the macroscopically prominent chondritic texture. The chondritic portion contains ~65 vol% of igneous textured melt matrix, ~12% of fine granular olivines and ~13 vol% of pyroxene laths (see below). If the granular olivines and pyroxene laths crystallized from the impact melt as we infer, the volume of the impact melt in the chondritic portion is ~90 vol%.

The large relict olivines (~100-800 μm in size) in both portions have irregular shapes and are surrounded by fine-grained granular (recrystallized?) olivines (< 20-30 μm in diameter) and/or melt matrix. The relict olivines in the chondritic portion often show mosaicism (S3-4) and sometimes contain polygonal smaller olivines and traces of melt. Relict (?) olivines in the impact melt portion, on the other hand, often show granular texture (~40 μm in size) with 120° triple junctions. The shock effects in the olivines vary from unshocked (S1) to slightly shocked (S3), which are relatively lower than those in the chondritic portion . Olivine compositions vary from $Fa_{21.3-24.4}$. The olivine relict crystals are enriched in CaO (0.21-0.29 wt%), compared to other ordinary chondrites. The tiny euhedral and granular olivines (<20 μm in diameter) in the impact melt matrix show generally lower CaO concentrations (0.07-0.30 wt%). The pyroxenes show lath to irregular shapes with closely spaced mechanical twins (<2 μm spacing). Microphenocrysts (~80 μm in size) in the melt matrix show extensive Ca-zoning from core to rim ($Wo_{2.4}Fs_{18.5}$-$Wo_{24.3}Fs_{15.2}$). Pyroxene laths in pyroxene-rich chondrule ghosts are slightly zoned ($Wo_{2.2}Fs_{15.9}$-$Wo_{6.7}Fs_{18.5}$) as in the Ca-poor part of the microphenocryst. The interstitial materials are feldspathic glass as in the impact melt portion [4]. Metal-troilite in all portions shows melt textures [4, 8].

Y-790964

Y-790964 is a very heterogeneous impact melt rock (Fig. 1b), containing abundant vugs [5; 9]. No well-defined lithic clasts are observed in our PTS (Y-790964, 81-3). Several chondrule ghosts are observed. Modal compositions of minerals and crystal shapes and sizes of olivine and pyroxene vary (Fig. 1b). The fine-grained igneous matrix is mixed with varying proportions of olivine relicts (see below) and a few chondrule-like materials. Vugs are very

abundant (~15 vol%) in Y-790964. Unlike vugs in basaltic lava, these vugs are irregularly shaped and some contain protruding pyroxene laths.

The relict olivines are abundant (~20 vol%) and are characterized by their large size (< 1.5 x 0.5 mm) and numerous dusty inclusions (troilite and metal) along healed cracks. These olivines often show weak mosaicism and mottled extinction, suggesting shock stage S3-4. Some relicts contain fine polygonal olivine crystals (<10-20 μm in size) as in Ramsdorf, which may have nucleated and grown in the solid state. Some portions of the relict olivines are mostly replaced by granular olivines. Euhedral olivine is generally tiny (<20-30 μm in size) and associated with pyroxene laths and feldspathic glass. Pyroxene is generally lath-shaped, and unlike olivines seldom contains opaque veins. Pyroxene crystals show extensive zoning (e.g., $Wo_{1.9}En_{73.0}$-$Wo_{32.6}En_{51.0}$). Olivines are enriched in CaO and FeO compared to normal LL-chondrites [5].

Comparison between Ramsdorf and Y-790964 and their thermal histories

The impact melt rocks, Ramsdorf and Y-790964 have several unique characteristics, distinct from other impact melts [e.g., 2, 10]. The relict olivine grains in Ramsdorf and Y-790964 show relatively lower shock features (S1~3-4) than those expected from evidence of whole rock melting (i.e., >S6). This may be a result of annealing. [11] suggested that if the shock pressure is greater than about 56 Ga (about 44 Ga if porous), annealing occurs and healed microfractures and broadening of mosaicism are observed. He also suggested that post-shock thermal history strongly affects the degree of annealing. Judging from the abundant impact melt in Ramsdorf and Y-790964 and slower cooling relative to shock experiments, the annealing temperature and time were such that severely shocked relict olivines recovered. Indeed, the presence of newly formed polygonal crystals in the relict olivine crystals may require annealing at high annealing temperature. This recrystallization may not be comparable to shock recrystallization described by [2]. Rather, they formed by annealing of shock fractured olivine by impact heating. Higher CaO (~0.1-0.3 wt%) and lower FeO contents in the relict olivines, compared to the matrix olivines and other ordinary chondrites, may be due to rapid equilibration with the impact melts at high temperatures [5]. This redistribution of Ca and Fe in impact melt clasts is not common. Most pyroxenes, however, are chemically zoned to varying degrees, suggesting that they crystallized from the impact melt. Chemically zoned pyroxenes are common in the impact melt portion of, for instance, Chico and Shaw [10, 12]. Vugs are virtually absent or too small to identify in Ramsdorf, probably implying that the Ramsdorf precursor was a solid rock. As suggested by [5], on the other hand, the vesiculate features of Y-790964 may result from a regolith-like precursor [13]. If so, the shock pressure that Y-790964 experienced was ~30-35 GPa [14].

The post-shock equilibration temperatures of Ramsdorf and Y-790964 could have been as high as the melting temperature of pyroxene (~1400-1600 °C) and below that of olivine (~1600 °C). These estimates are higher than that given by [5] who argued for equilibrium melting. The post-shock temperature of Ramsdorf may have been slightly higher than that of Y-79 because of the higher melt in Ramsdorf (> 90 vol% cf. 80 vol% in Y-790964). For Ramsdorf, cooling rates during crystallization of metal are ~1 x 10^{-3} °C/sec based on the zoning of metal [15] and 0.1 °C/sec (1400-950 °C) based on the spacing of the arms on metallic dendrites [8]. [5] estimated a cooling rate of ~0.01 °C/sec for the Y-790964 impact melt, based on the Fe diffusion profile observed in the relict olivines. Similar mineral chemistry in olivine suggests that cooling rates of Ramsdorf and Y-790964 are similar. However, the mesostasis of Ramsdorf is glass [4] while that of Y-790964 is microcrystalline, suggesting that Y-790964 cooled somewhat slower. These cooling rates suggest that these impact melts were ~ several tens of cm in diameter when they cooled.

Origin of the unique impact melt textures

Textures of impact melt rocks vary from completely igneous to complex mixture of clasts and melt. [16] suggested that the density and distribution of crystals present at the initiation of cooling can drastically affect the texture of the crystallized product. He also suggested that the nucleation sites could be micron to sub-micron relicts. Apparently, the Ramsdorf and Y-790964 impact melts crystallized from impact melt with numerous nuclei and fragments. The

heterogeneous chemical compositions of the impact melts formed on asteroid by in situ melting and rapid cooling may reflect limited mixing. Even metal-troilite in these impact melts could not segregate during the melting event. In the most extreme case, the prominent chondritic texture of Ramsdorf visible at low magnification was preserved because of minimum mixing [7]. In summary, those impact melts rapidly crystallized from chemically heterogeneous melt containing numerous nuclei and fragments.

Geologic setting

[17] performed computer simulation of impact cratering on asteroids and found that most strongly heated and melted particles are also strongly accelerated and thus escape from the body. The high post-shock equilibrated temperature (thus highly shocked) and rapid cooling rate of Ramsdorf and Y-790964 imply that they cooled in bodies several tens of cm in size, which were possibly ejected after whole rock melting near the center of the impact crater. The impact melts, Ramsdorf and Y-790964 may have been ejected from the LL and L parent bodies by the impacts that melted them and reaccreted into smaller bodies, as was suggested for the L chondrites by [18]. The Y-790964 impact melt rock may also have survived in reaccreted ejecta until more recent minor collisional events that delivered to Earth.

References

[1] Scott E. R. D. et al. (1986) Lunar Planet. Sci. 17, 785-786. [2] Stöffler D. et al. (1991) Geochim. Cosmochim. Acta , 55, 3845-3867. [3] Rubin A. E. (1995) Icarus 113, 156-167. [4] Begemann F. and Wlotzka F. (1969) Geochim. Cosmochim. Acta 33, 1351-1370. [5] Okano O. et al. (1990) Geochim. Cosmochim. Acta, 54, 3509-3523. [6] Bogard D. D. et al. (1976) J. Geophys. Res. 81, 5664-5678. [7] Yamaguchi A. et al. (1996) Lunar Planet. Sci. 27, 1467-1468. [8] Scott E. R. D. (1982) Geochim. Cosmochim. Acta 46, 813-823. [9] Miyamoto M. et al. (1984) J. Geophys. Res., 89, 11581-11588. [10] Bogard D. D. et al. (1995) Geochim. Cosmochim. Acta 59, 1383-1399. [11] Bauer (1979) Proc. Lunar Planet. Sci. Conf. 10, 2573-2596. [12] Taylor G. J. et al. (1979) Geochim. Cosmochim. Acta 43, 323-337. [13] Schaal R. B. et al. (1979) Proc. Lunar Plaent. Sci. 10, 2543-2571. [14] Stöffler D., et al. (1988) Meteorites and the Early Solar System (eds. J. F. Kerridge and M. S. Matthews), pp. 165-202. Univ. of Arizona Press. [15] Smith and Goldstein (1977) Geochim. Cosmochim. Acta 41, 1061-1072. [16] Lofgren G. (1977) Proc. Lunar Planet. Sci. Conf. 8, 2079-2095. [17] Love S. G. and Ahrens T. J. (1996) Lunar Planet Sci. 27, 777-778. [18] Haack H. et al. (1996) Icarus 119, 182-191.

(a) Ramsdorf. (b) Y-790964.

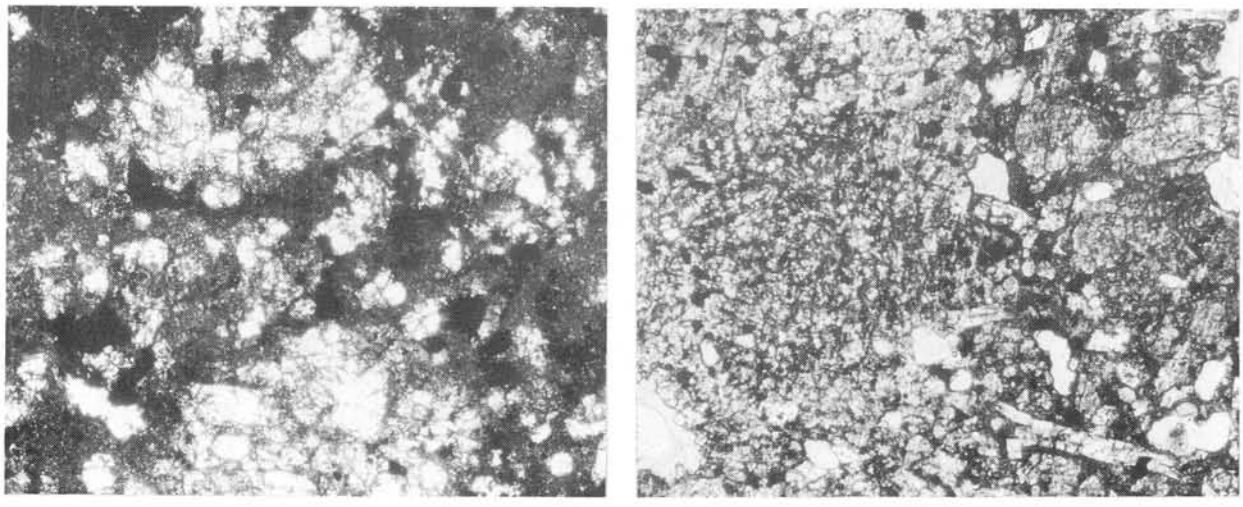

Figure 1. Photomicrographs of Ramsdorf (a) and Y-790964 (b), showing heterogeneous impact melt textures. Widths of field are 1.6 mm. Plane light.

Measurements of Evaporation rates of Sodium and Potassium from Silicate Melts

[1]Atsuko YAMANAKA, Akira TSUCHIYAMA, Shogo TACHIBANA and [2]Katsuyuki KAWAMURA

[1]Department of Earth and Space Science, Faculty of Science, Osaka University, Toyonaka 560, JAPAN

[2]Department of Earth and Planetary Science, Tokyo Institute of Technology, Tokyo 152, JAPAN

Chondrules had been formed as isolated droplets of molten or partially molten materials. It has been known that alkalis volatilize easily from silicate melts at high temperatures. However, contents of Na in chondrules are not so depleted compared with C1-chondrites or the cosmic abundance. This problem has been one of the important restrictions for discussing conditions of chondrule formation [1]. Experiments were conducted on the volatilization of Na from silicate melts with chondrule composition and conditions of chondrule formation has been discussed based on the experiments [2]. However, evaporation rates of Na has not been known systematically under different conditions with different composition. In fact, different evaporation rates were reported in different composition [3]. In this study we try to construct a new tequnique to measure vaporization rates of alkalis from silicate melts using a thermobalance. In this tequnique, a volatilization rate can be obtained from mass loss in a single experiments, and a lot of data could be accumulated.

Melts with simple compositions were used in the experiments as a first step. Na_2O-SiO_2 glass (Na_2O = 23.56 wt%, SiO_2 = 74.13 wt%, liquids temperature = 800℃) and K_2O-MgO-SiO_2 glass (K_2O = 36.8 wt%, MgO = 10.3 wt%, SiO_2 = 52.9 wt%, liquidus temperature = 1200℃) were prepared as starting materials for the experiments. High temperature mass balance (SETARAM TG-92; upper limit of the temperature is 1750℃ and identification limit is 1 μ g) was used in the experiments. Each sample was held on the Pt wire loop, and heated at constant temperature ranging from 1300℃ to 1500℃ in an Ar flow at 1 atm or in low vacuum. It was confirmed from comparison between mass loss and chemical analysis of the recovered sample that the measured volatilization mass are loss of Na_2O and K_2O by volatilization (volatilities of Na_2O and K_2O are much higher than those of MgO and SiO_2). Some of recovered samples were analyzed with electron probe micro-analyzer (JEOL-733). Distribution of Na and K in the samples were homogeneous.

An example of mass loss during heating is shown in Fig. 1. As shown in the example, volatilizations of Na and K did not occur lineary with time both in Ar flow and vacuum (Fig. 1). The averaged volatilization rates increased with increasing temperature. The non-linear evaporation behavior would be explained by diffusion of the elements in the melts. However,

the homogeneous distribution of Na and K eliminate this possibility.

The non-linear evaporation can be also explained by the compositional change in a melt by the evaporation. The volatilization rate of Na, J, can be expressed by Hertz - Knudsen equation:

$$J = \frac{\alpha\left(p^e - p\right)}{\sqrt{2\pi m k_b T}} \qquad (1)$$

where α is the vaporization coefficient, m the mass of a gas molecule, k_b is the Boltzmann constant, and T the temperature. p and p^e are the partial and equiriburium pressure of the element.

If we assume that (1) p are negligibly small compared to p^e, and (2) activity coefficient of the element in a melt is constant (Henry's law), the volatilization rate of Na or K, J, can be expressed from eq.(1) as follows:

$$J = kAC \qquad (2)$$

where k is a constant, A is the surface area of the melt, and C is concentration of the element in the melt. It was reported by [2] that eq. (2) was satisfied in their experiments. However the present results cannot be fitted by eq. (2). To discuss our experimental results change in equilibrium vapor pressure by changing chemical composition of the melt, and change in vapor pressure in a gas due to evaporation were taken into consideration. We assumed that

$$p_e = p^e{}_0 - f_1 g \qquad (3)$$

$$p = p_0 + f_2 g \qquad (4)$$

where g is the measured volatilization mass loss, and f_1 and f_2 are positive constants. Suffix 0 denotes initial value. Eq. (3) is reasonable for small mass loss when the relation between activity and concentration reported by Rego et al.[4] is considered. Eq. (4) indicates the effect of volatilized Na remaining around melting sample to prevent from further volatilization of elements. From eqs. (1)(3)(4) we can obtain :

$$g = \frac{p_0^e - p_0}{f_1 + f_2}\left\{1 - \exp\left[-A\alpha\sqrt{\frac{m_{Na}}{2\pi k_b T}}\left(f_1 + f_2\right)t\right]\right\} \qquad (5)$$

Experimental data were fitted well by eq. (5) (Fig. 2). If A is known, and α is assume to be unity, we can obtain $p^e{}_0 - p_0$ and $f_1 + f_2$ from the fitting. In the experiments in an Ar flow, it is expected that $p_0 > 0$ and $f_2 > 0$. On the other hand it is expected that $p_0 \sim 0$ and $f_2 \sim 0$ in vacuum because the evaporated Na should be evacuated. In this case, we can obtain $p^e{}_0$ and f_1. Comparison between $p^e{}_0$ obtained from the present experiments and that calculated from activity data [5] for the Na_2O-SiO_2 melt will be made.

References

[1] Grosmann J.N. (1988) 9.3. Formation of chondrules, in "Meteorites and the early solar

system" ed. J. F. Kerridge and M. S. Matthews, pp680-696. [2] Tsuchiyama A. Nagahara H. and Kushiro I. (1981) Geochim. Cosmochim. Acta, ***45***, 1357-1367. [3] Shimaoka T. and Nakamura N. (1991), Proc. NIPR Symp. Antarct. Meteorites, 2, 252-267. [4] Rego D. N., Sigworth G. K. and Philbrook W.O. (1985) Metal. Trans., ***16B***, 313-327.

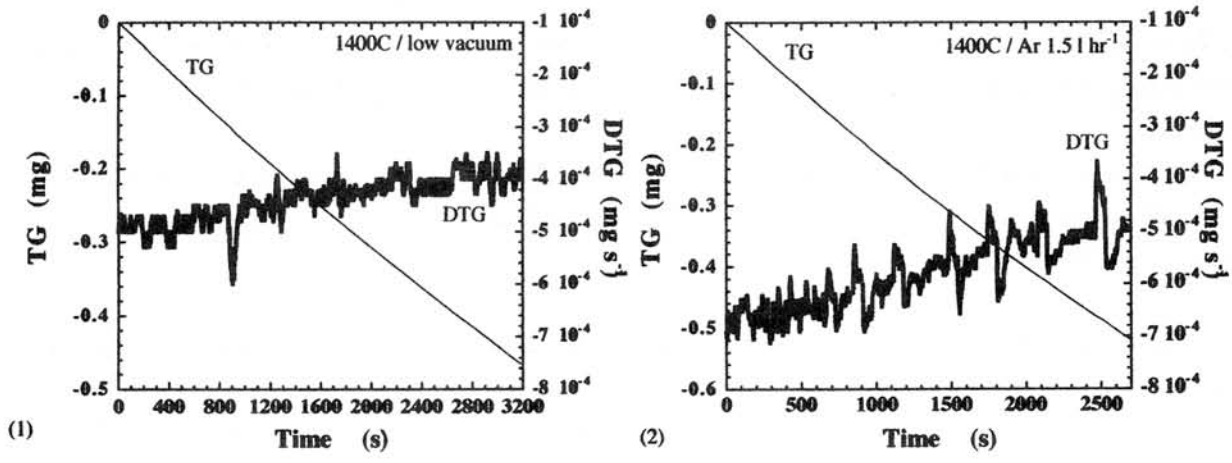

Fig. 1. the volatilization mass loss, TG, and time differential of TG, DTG, plotted against time. (1)Na_2O-SiO_2 at 1400℃ and (2)K_2O-MgO-SiO_2 at 1400℃

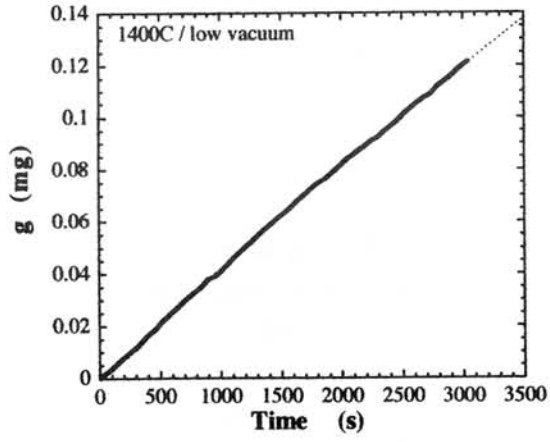

Fig. 2. Comparison of experimental data of volatilization mass loss g, vs. time, t, with fitting curve by eq. (5) Na_2O-SiO_2 at 1400℃.

HYPERVELOCITY IMPACT EXPERIMENTS USING ANTARCTIC MICROMETEORITES

Hajime Yano[1], Cécile Engrand[2] and Michel Maurette[3]

1. Planetary Science Division, Institute of Space and Astronautical Science, 3-1-1 Yoshinodai, Sagamihara, Kanagawa, 229 Japan

2. Naturhistorisches Museum, Mineralogische Abteilung, Postfach 417, A-1014, Vienna Austria

3. Centre de Spectrométrire Nucléaire et de Spectrométrire de Masse, Bâtiment 108, F-91405, Orsay-Campus France

Introduction

Interplanetary dust particles (IDPs) in size range of ~50-500 μm are considered as a major contributor for a mass accretion of extraterrestrial material on the Earth of ~2×10^{10} g per year, whereas stratospheric IDPs (1 μm < diameter (d) < 50 μm) and conventional meteorites (< 10^{10} g) make up only 1 % of the total mass [1]. Blue lakes in Greenland and ice sheets in Antarctica provide high concentrations of IDPs (specifically called "micrometeorites") in such a larger size range [2, 3]. In addition, Antarctica is the most remote land from major industrial nations and continental winds keep the surface snow dry and ultra-clean. Unlike the micrometeorites from Greenland blue lakes, Antarctic micrometeorites (AMM) thus concentrate in "cryconite-free" blue ice sheets and provide complementary insights of extraterrestrial material collected from other terrestrial environment (i.e., stratosphere and deep sea sediments) and the Low Earth Orbit (LEO).

Micrometeorite Collection in Antarctica

Since 1983, extraction of AMMs from deep ice cores (depth ~100-700 m) had been attempted by the Japanese Antarctica expedition team, as a by-product of a paleo-climatic survey near Mizuho Station, Asuka Station and the Advance Camp [4, 5]. Yet small volumes of ice cores were much less efficient to collect AMMs than filtering melt water of shallow ice [3]. In 1988, a "micrometeorite factory" was constructed near the French station at Cap-Prudhomme. Steam generators were used to deliver water jets into a 2-3 m deep hole and made a melt pocket on the blue ice sheet. The stream of melt water was filtered with four stainless steel sieves of 25, 50, 100 and 400 μm size holes. Since 1990, Maurette *et al.* have extracted ~40,000 AMMs from 360 t of blue ice [6]. The most dominant size group is 50-100 μm in which 10 % of grains are extraterrestrial. Unmelted or partially melted ("scoria") chondritic AMMs were a factor of 4 more than melted spherules. In the 100-400 μm range, this trend reverses.

Sample Processing

All samples used for this work were extracted from ~1 m^3 ice collected in the expedition of January 1994. Initial processing was carried out at Orsay, France in November 1994. Fourteen unmelted or scoria AMMs (d ≈ 100-400 μm) were separated from terrestrial grains and contamination, cross sectioned, polished, mounted on an epoxy and coated with Au-Pd sputtering for SEM/EDX studies (Fig. 1). Prior to sputtering, all the samples were investigated their morphology and optical properties at Canterbury, U.K. They appeared either black, glassy (olivine-type green-to-yellow colour) or shiny metallic colours due to thin (~1 μm) magnetite rim. Melted AMMs in 50-100 μm and 100-400 μm size ranges were then gathered about 300 each. SEM/EDX analyses were performed for 5-6 samples from each range but no size dependence of morphological and compositional variations was found.

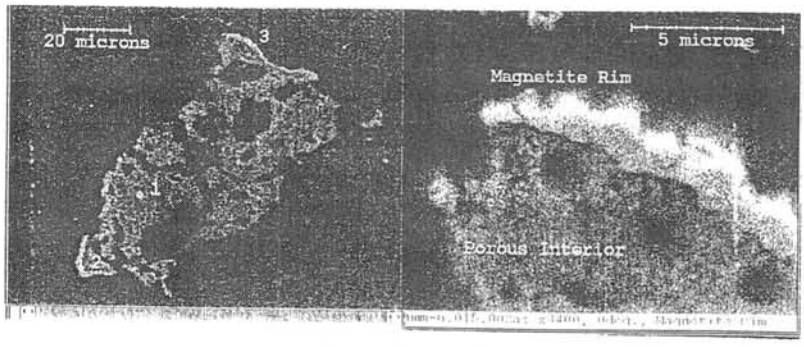

Figure 1. Cross sectional view of a "scoria" porous AMM of 94 μm x 44 μm in size (left). Magnetite rims are seen around edges (right).

Hypervelocity Impact Experiments

In order to study survivability and analogue for physical and chemical alterations of micrometeoroids impacted on retrievable LEO satellites such as SMM, LDEF, EuReCa, HST solar array and SFU [7], we performed hypervelocity impact (HVI) experiments using AMMs as projectiles. Except few examples using meteorite powders or "artificial IDPs" [8], this was the first HVI experiments that ever employed real micrometeorites and gave both glass and Al targets identical impact conditions. These could only be achieved by the "shot gun" technique using a two stage light gas gun (LGG), which were more abundant and larger than stratospheric IDPs. Two identical targets were made for the 50-100 μm sized melted AMMs and mixed shards of enstatite and albite ("Ens+Alb") and these projectiles were loaded into split sabots. Each target had both ~6 mm-thick aluminium (Al) and glass plates. The melted AMMs were mostly spherical to ellipsoids with median d ≈ 75 μm. The Ens+Alb shards were irregular-shaped and the size range spread in ~10-100 μm with the peak of the distribution of ~20 μm.

Analytical Results

The impact experiments were successfully performed at 5.39±0.05 km/s for melted AMMs and 5.17 ±0.05 km/s for Ens+Alb shards, both from normal impact angle. All craters on Al thick targets have traceable amounts of residues of projectiles. For the AMMs, either unmelted fragments or melted large pieces often occupy the bottom of the craters (Figs. 2 and 3), proving that fragmented AMMs in this size range easily survive impacts at ~5 km/s (considerably lower than actual impacts in space).

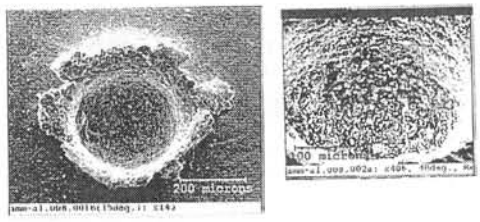

Figure 2. A crater (Dc = 309.6 μm x 295.0 μm) formed by a melted AMM impact on a thick Al target in the LGG simulation (left). Unmelted fragments of the impactor occupy the bottom of the crater (right).

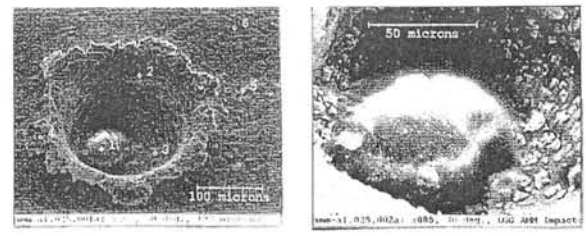

Figure 3. A crater (Dc = 193.9 μm x 193.2 μm) formed by a melted AMM impact on a thick Al target in the LGG simulation (left). A large melted piece of the impactor is embedded at the crater bottom (right).

Since the depth (P) to diameter (Dc) ratio of impact craters is known as an indicator of impactor density, P/Dc of craters by these two projectile types on thick Al targets were examined. Each group was sub-divided by circularity (Ci = semi-major axis / semi-minor axis) as "circular" (1/Ci < 1.05) and "elongated" (1/Ci ≥ 1.05). For circular craters, both exceeded P/Dc = 0.5, being consistent with the space samples [7]. Shallow craters are mostly elongated as fragmentation of porous AMMs occurred at impact incidence and projectile mass was scattered before developing sufficient crater depth. This mechanism could be applied to fluffy meteoroid impacts on spacecraft, even at a normal angle.

Also unmelted and melted AMMs were analysed with SEM/EDX (beamed 25 kV at 100-300 seconds). Figure 4 shows bulk elements detected from each IDP type collected in the terrestrial environment. "Asuka" is uncontaminated terrestrial grains from the surface snow of Antarctica for comparison [5]. Despite poor statistics of AMM data, the difference between terrestrial and extraterrestrial samples is evident. High presence of Cl for unmelted AMM is due to epoxy in which the particles were embedded. Maurette *et al.* [6] reported that AMMs often depleted Ca, Ni, Co, S and sometime Mg and Mn. However, unmelted AMMs agree well with stratospheric IDPs except substantial depletion of S. Supposing their parent bodies are the same, this implies that the atmospheric friction and chemical interaction with ice water did not change most of the compositions of unmelted AMMs, contradicting the prediction of the current atmospheric entry theory [9]. The S depletion is not surprising because it has a low vaporisation point (780 K) and can be oxidised easily (H_2S). The lack of S in unmelted AMMs implies that they experienced the peak temperature above 780 K or kept in ice melt water long enough to dissolve S at least from the surface reachable by EDX beam. Melted AMMs are enriched Al, Ca and Ti, possibly due to the interaction with terrestrial elements in blue ice. However the interior exposed by degassing cavities sometimes retained C, suggesting some carbonaceous components could be still trapped inside.

Both AMM and Ens+Alb impact residues show enrichments of S, C and Ti with the depletion of Mg and Ni comparing to the stratospheric IDPs ("Cosmic" type recorded in NASA Cosmic Dust Catalog (CDC) [10]). Such depletion is consistent with space impacts (Fig. 5). The target materials (Al and glass) did not affect their EDX results. The majority of AMM impact remnants showed Fe associated with S. The presence of S after HVI became as high as the stratospheric IDPs and again consistent with LDEF's Al experiment tray clamps on its 12 peripheral faces [7]. It is reasonable to imagine that survived impact fragments of FeS and other S-bonded minerals from both LDEF Al clamps and AMM impacts are exposed from the interior of impactors, rather than outer shells which could be completely melted or

vaporised. On the contrary, the Au target for CME [11] on the trailing face of LDEF was so dense and hard that kinetic energy induced by HVI well-exceeded complete vaporisation of S. Some other fragments contained Cl, K, P or/and Na with Fe, S and Si. Such light elements might have been penetrated and enriched inside AMMs by interaction with melted water during processing the ice. These embedded elements might be revealed after breaking up. Note, however, that the presence of Mg, Si and S on the Al clamps may be partially due to the anodisation. K, Na and Cl on the clamps can be from maritime contamination at NASA Kennedy Space Centre.

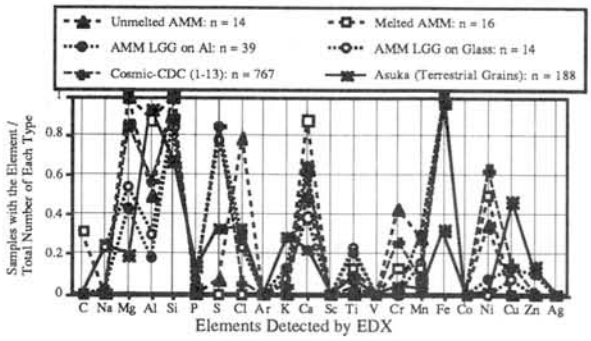

Figure 4. Elements detected by EDX for "un-impacted" AMMs, impact residues of melted AMMs on thick Al and glass targets and stratospheric IDPs with terrestrial grains.

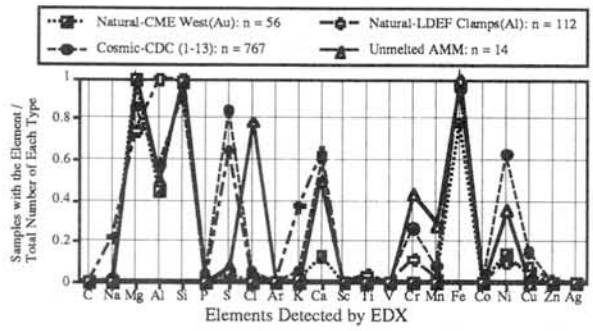

Figure 5. Elements detected by EDX for "un-impacted" IDPs (Unmelted AMMs and CDC-Cosmic) and Natural impact residues on LDEF's CME Au plate and Al clamps.

Discussion

Since this study is based upon statistical approach, only the "bulk" trend of different IDP groups are discussed. In the future, individual AMMs should be analysed and compared with stratospheric and LEO IDPs. Impact experiments using unmelted AMMs segmented in half are particularly important. Elemental ratios between a non-impacted half of the unmelted AMMs and impact residues formed by another half will enable us to follow impact-induced chemical alteration of each AMM.

When we apply empirical equations to estimate impactor size from HVI features, both bulk density and incident velocity must be correctly assumed. In the past, bulk densities of micrometeoroids were estimated from (1) micro-craters on lunar rocks and (2) meteor observations and (3) fractal models of the particle morphology. Direct measurements of densities of stratospheric IDPs are still in progress [12, 13]. Love *et al.* [13] showed their densities would change upon melting. This effect and the discovery of large (> 100 μm) unmelted AMMs caution that the current atmospheric entry theory does not satisfactorily explain the alteration mechanism of IDPs. The bulk density of AMMs also should depend on the degree of heating of the particle because a re-homogenised particle (e.g., glassy sphere) is denser than unmelted one made of fine grained matrix. On the other hand, melted AMMs can also have large internal cavities by degassing volatiles. Thus it is the next logical step to make density measurements of both unmelted and melted AMMs and modify the atmospheric ablation theory. Such efforts entail to decode HVI features on LEO spacecraft more precisely.

Conclusions

Due to their abundance and large size, AMMs are not only extraterrestrial samples that complement other IDP types but also excellent projectiles for HVI simulations of meteoroid impacts in the near Earth space. Fragments of melted AMMs survive impact velocity at ~5 km/s as a lower limit of meteoroid impacts on LEO spacecraft with analysable residues left for EDX. Trends of bulk elements of stratospheric IDPs, unmelted and melted AMMs and space impact residues are all similar but some depletion and enrichments occur by unique physical and/or chemical effects albite in each collection site. Future Antarctic expedition teams are encouraged to excavate them in every possible occasion.

References

[1] Grün, E. *et al.*: *Icarus,* **62,** 244-272, (1985); [2] Maurette, M. *et al.*: *Nature,* **328,** 699-702, (1987); [3] Maurette, M. *et al.*: *Nature,* **351,** 44-46, (1991); [4] Higashi, A. and Fujii, Y.: *Annal. Glaciol.*, **20,** 73-79, (1994); [5] Yano, H.: **BSc. Thesis**, International Christian University, Tokyo, Japan, (1991); [6] Maurette, M. *et al.*: In Analysis of Interplanetary Dust, *(edit.)* Zolensky, M.E. *et al.*, AIP Press, 277-289, (1994); [7] Yano, H.: **Ph.D. Thesis,** University of Kent at Canterbury, Kent, U.K., (1995); [8] Zolensky, M.E. *et al.*: *Abst. Lunar Planet Sci. Conf.*, **21,** 1381-1382, (1990); [9] Brownlee, D.E.: In Cosmic Dust, *(edit.)* McDonnell, J.A.M., John Wiley & Sons, 295-336, (1978); [10] CDPET: Cosmic Dust Catalog, NASA/JSC, Houston, Texas, U.S.A., **1-14,** (1981-1994); [11] Bernhard, R.P. *et al.*: *Proc. Third LDEF Post-Retrieval Symp.*, **NASA CP-3275,** 401-413, (1995); [12] Flynn, G.J. and Sutton, S.R.: *Abst. Lunar Planet. Sci. Conf.*, **21,** 375-376, (1990); [13] Love, S.G., Joswiak, D.J. and Brownlee, D.E.: *Abst. Lunar Planet. Sci. Conf.*, **24,** 901-902, (1993).

MINERALOGY OF NEW PRIMITIVE ACHONDRITES, Y8005 AND Y8307 AND THEIR DIFFERENTIATION FROM CHONDRITIC MATERIALS

Keiko Yugami[1], Hiroshi Takeda[2], Hideyasu Kojima[3] and Masamichi Miyamoto[1]
1) Mineralogical Institute, Graduate School of Science, University of Tokyo, Hongo, Tokyo 113, Japan
2) Research Institute, Chiba Institute of Technology, Tsudanuma, Narashino, Chiba 275, Japan
3) National Institute of Polar Research, Kaga, Itabashi-ku, Tokyo 173, Japan

Introduction

Discoveries of many primitive achondrites from Antarctica contributed to deducing the general trends of differentiation from the chondritic source materials [*e.g.* 1, 2]. In this paper, we describe additional two samples, which will give us additional insight into the origin of primitive achondrites. There are some sub-groups in the primitive achondrites. The oxygen isotope compositions of primitive achondrites indicate that the parent body of winonaites and IAB irons and of acapulcoites and lodranites are different [3]. The silicate minerals of winonaites are in general richer in Mg than those of acapulcoites and lodranites [1]. Lodranites are distinguished from acapulcoites mainly by criteria of that they are coarser grained and depleted in plagioclase.

Yamato (Y) 8005 and Y8307 are mineralogically classified as primitive achondrites [4, 5] although they have not been studied in details. In this paper, we studied Y8005 and Y8307 to gain additional information on mode of distribution of mafic and opaque minerals. We also studied extensively recrystallized H chondrite Y75008 (H7) for comparison with primitive achondrites.

Samples and Techniques

We studied polished thin sections (PTSs) Y8005,51-3, Y8307,51-2, Y75008,2-3, Y74025,52-4 and Y75305,52-2. These samples were supplied from National Institute of Polar Research. Y8005 were studied by electron probe microanalyzer (EPMA) at Ocean Research Institute and Geological Institute, University of Tokyo. Two dimensional chemical mapping analysis (CMA) techniques of EPMA have been applied to Y8005, Y8307, Y75008, Y74025 and Y75305. Modal abundances of minerals of Y8005, Y8307 and Y75008 were obtained from CMA. Y8005 is classified as a winonaite [4] by its texture and mineralogy. The oxygen isotope composition of Y8005 has not been determined. Y8307 is classified as a primitive achondrite [5]. Y74025 is a winonaite [1, 6]. Y75305 is classified as a winonaite [1, 7] but its oxygen isotope composition is unique [8]. Y75008 is an H7 chondrite [9].

Results

Y8005 The modal abundance of minerals of Y8005 are shown in Table 1. The silicate minerals of Y8005 are very fine-grained (0.02-0.2 mm). The Mg/Fe distribution of orthopyroxene and olivine show zoning (increase towards the rims). The average *fe#* (Fe×100/(Fe+Mg) atomic ratio) of cores of olivine grains is 2.1 and that of orthopyroxene ($En_{96.6}Fs_{2.0}Wo_{1.5}$) is 1.9. The Ca content of plagioclase of Y8005 ($An_{11.2}$) is much lower than other winonaites [1]. Fig. 1 shows the distribution of FeNi metal and troilite in Y8005. PTS Y8005,51-3 is characterized by presence of a very large opaque grain (5.7 mm^2, 8 vol% of the PTS). which is mainly kamacite (Ni 6.36 wt%) including shreibersite (Ni 41.4 wt%) and taenite grains. Cr in troilite is 0.37 wt% and it is similar to other winonaites [1, 10]. The large metal grains (except for the extremely large one) have complicated shapes that resemble the opaque grains in Elephant Moraine (EET) 84302 [2,

11]. Y8005 rarely include medium-sized opaque grains and large opaque grains in Y75305 and Y8005 are mainly FeNi metal and most troilite grains exist as smaller grains between silicate minerals. Our new data of Y74025 show that medium opaque grains are abundant and the largest opaque grain of Y74025 is mainly troilite. Our data of Y75305 shows that distribution of opaque minerals are similar to Y8005.

Y8307 The modal abundance of minerals of Y8307 are shown in Table 1. It is similar to typical acapulcoites such as Allan Hills (ALH) 77081 and ALH78230 [11], and is slightly coarser grained (about 0.3 mm in diameter) than them. The largest olivine grain is about 0.8 mm across. Some fault-like lines can be seen in the PTS. It dose not include pyroxene grains with dusty cores like those of Acapulco and EET84302 [2] (coarser grained members of acapulcoites). Orthopyroxene grains with a small amounts of dusty inclusions in Y8307 show CaO zoning similar to orthopyroxene grains with dusty cores in Acapulco and EET84302 [12]. The augite distirbutes heterogeneously and is concentrated in some zones, whereas the distribution of plagioclase ($An_{15.0}$) is homogeneous. No Fe/Mg zoning of pyroxene or olivine was detected. The average *fe#* of olivine is 10.7 and that of orthopyroxene ($En_{88.4}$ $Fs_{9.9}$ $Wo_{1.6}$) is 10.1.

Y75008 The modal abundance of minerals of Y75008 are shown in Table 1. The average *fe#* of olivine is 18.6 and that of orthopyroxene ($En_{79.9}Fs_{16.1}Wo_{4.0}$) is 16.8. The grain sizes of minerals are similar to those of Y8307. Y75008 includes orthopyroxene with cores that have lower CaO content than rims. The chromite grains in Y75008 show Al_2O_3 zoning. Al_2O_3 increases at first and then decreases from the core to the rims.

Discussion

Y8307 has modal abundance and chemical compositions of minerals typical of acapulcoites. Y8307 is almost identical to ALH77081 and ALH78230 and is less similar to Acapulco. Y8005 can be classified as a winonaite on the basis of mineral chemistry. The distribution of opaque minerals of Y8005 is more similar to Y75305 than Y74025.

The presence of an extremely large metal grain suggest that Y8005 may represent the transitional state from chondrites to iron meteorites. There is considerable difference between distributions of FeNi metal and troilite in winonaites. The final classification is rest on the oxygen isotopic compositions. The mineral assemblages of silicates and phosphates portions of primitive achondrites are plotted in the Pyroxene-Olivine-(Plagioclase + phosphate) pseudo-ternary diagram (Fig. 2) [13]. Y8005, Y8307 and Y75008 are plotted in the area of acapulcoites and winonaites. Y75008 is closer to acapulcoites and lodranites than H6 plotted in the figure (FIG. 2) of [6]. General trends of deviation of winonaites from the chondritic assemblages are away from the olivine corner, but Y8005 is closer to the olivine corner than other winonaites.

On the basis of coarser mafic mineral inclusion in fine-grained matrix in Winona, Benedix et al [14] proposed a destruction and reassembly model. Similar texture found in Y8005 is not as pronounced as that of Winona and no relationship can be seen between the distribution of coarse grains and those of augite and plagioclase, and the fault-like lines. The complex shapes of metal cannot be interpreted as clasts of metallic cores. These coarse-grained portions of silicates can be interpreted as growth of coarser-grained mafic silicates during recrystallization using larger grains in the original chondrites as nucleus crystals. We do not need to invoke reassembly of differentiated clast of silicate material by reassembly. However, there may be such cases in other meteorites. Impact excavation and mixing are another possibility. The heterogeneous distribution

of materials in Y8005 and EET84302 [2] support the idea that local heterogeneity of materials in the parent bodies can explain the variety of primitive achondrites [11].

References: [1] Kimura M. et al. (1992) Proc. NIPR Symp. Antarct. Meteorites, 5, 165-190. [2] Takeda H. et al. (1994) Meteoritics 29, 830-842. [3] Clayton R. N. et al. (1992) LPSC. XXIII, 231-232. [4, 5, 6, 7, 8] NIPR (1995) Catalog of the Antarctic Meteorites, 148, 153, 81, 94, 90. [9] Mayeda T. K. and Clayton R. N. (1989) NIPR Symp. Antarct. Meteorites Abstract., 172. [10] Graham A. L. and Hutchison R. (1977) Mineral.Mag., 41, 201-210. [11] Yugami K. et al. (1995) NIPR Symp. Antarct. Meteorites Abstract., 280-283. [12] Yugami K. et al. (1994) Proc. 27th ISAS Lunar Planet. Symp., 120-123. [13] Prinz M. et al. (1983) LPSC XIV, 616-617. [14] Benedix G. K. et al. (1996) LPSC XXVII, 95-96.

Table 1. Modal abundances of minerals of Y8005, Y8307 and Y75008.

	Y8005	Y8307	Y75008
Orthopyroxene	28.5	37.1	42.9
Augite	5.5	11.9	2.2
Olivine	18.9	23.4	18.7
Plagioclase	8.1	13.8	4.9
Ca-Phosphate	+	0.8	0.4
FeNi metal	12.5	3.6	3.7
FeNi oxides	16.8	4.6	19.2
Troilite	8.3	4.6	6.8
Schreibersite	0.6	0.0	0.0
Daubreelite	0.7	0.0	0.0
Chromite	0.0	0.2	1.3

Fig. 1. The distribution of FeNi metal and Troilite of Y8005,51-3. The gray portions are FeNi metal and black portions are troilite.

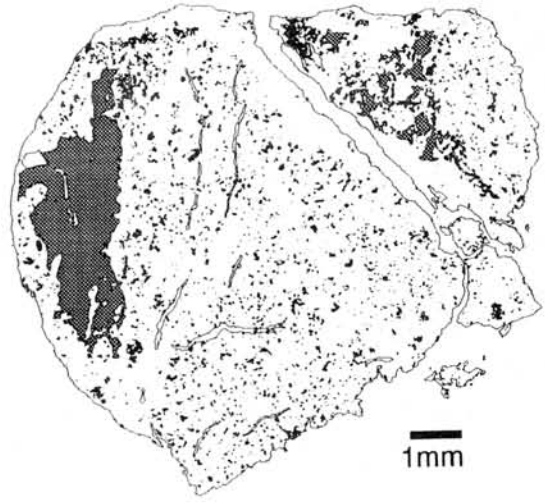

Fig. 2. The mineral assemblages of silicates and phosphates portions of primitive achondrites plotted in the Pyroxene-Olivine-(Plagioclase + phosphate) pseudo ternary diagram [13]. Data of acapulcoites, lodranites and winonaites are from [1, 2, 11].

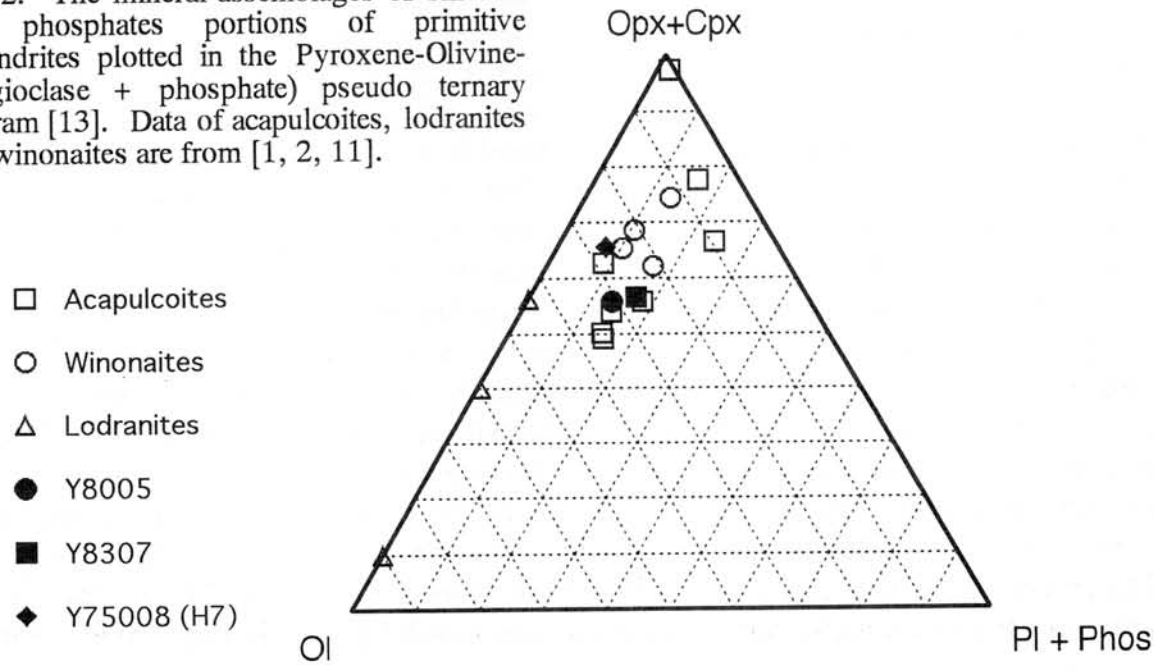

INTERACTION BETWEEN CHONDRULES AND MATRIX IN CHONDRITES: EVIDENCE FROM THE YAMATO-82133 (H3) CHONDRITE

Nina G. Zinovieva, Olga B. Mitreikina, and Lev B. Granovsky

Department of Petrology, Faculty of Geology, Moscow State University, Lenin Gory, Moscow 119899, Russia

The matrix of the Yamato-82133 ordinary chondrite (H3) is a heterogeneous fine-grained aggregate of a strongly oxidized aluminum-sulfide-silicate-iron material with numerous silicate fragments. Basing on the textural and compositional features, the matrix material can be classified into three main varieties: fine-grained sulfide-silicate-iron matter, aluminum-iron matter [1, 2], and nearly pure iron (with or without troilite). The matrix has a patchy texture like taxitic, in which areas richer in silicates are variably saturated in oxidized iron-troilite or purely iron material.

The fine-grained sulfide-silicate-iron material (Fig. 1) consists of fine-grained (submicroscopic) aggregates of olivine of constant composition (f = FeO/(FeO + MgO) = 0.40 - 0.43) cemented by iron oxides. Widespread are thin grains of troilite, whitlockite and Cl-apatite. The fine-grained silicate-iron material penetrates into chondules of various composition along a network of capillary fractures and results in rims of olivine (Fig. 2), whose iron mole fraction increases toward the matrix. The matrix material forces apart mineral fragments and cements brecciated chondrule fragments.

The interaction between the matrix material of the Yamato-82133 chondrite (H3) both chondrules of all petrochemical types, and the silicate material of hercynite-kamacite objects (HKO) [3] depends on their compositions. Olivine grains at chondrule boundaries and fragments of olivine grains in the matrix recrystallize and simultaneously increase their iron mole fraction up to that of the matrix olivine. The pyroxene of the chondrules and fragments of pyroxene grains in the matrix interact in two manners. Grains of magnesian pyroxene (f = 0.04 - 0.19) are replaced either by ferrous olivine or by troilite-pyroxene aggregates. If ferrous olivine forms, its iron mole fraction is controlled by the magnesium content of the primary pyroxene (magnesium contents of the primary pyroxene and newly formed olivine are the same) and increases toward the matrix up to 0.43. In cases when the pyroxene is replaced by a fine-grained troilite-pyroxene aggregate, the overall iron mole fraction of this aggregate is weakly variable (f = 0.69 - 0.72), whatever the composition of the pyroxene (whose f ranges from 0.04 to 0.50) interacting with matrix. Explanations of these two distinct interaction patterns between the pyroxene and the matrix was found when a tabular grain of magnesian pyroxene had been detected in the matrix. A part of this tabular grain is replaced by ferrous olivine, whereas the rest of this grain is transformed into a troilite-pyroxene aggregate. As is seen in Fig. 3, the olivine develops along the contact of pyroxene with kamacite, while troilite-pyroxene aggregates form at the contacts between pyroxene and troilite. As follows from the comparison of their bulk compositions, in the former case, Mg remains inert, Fe is introduced, and Si slightly extracted from the system, whereas in the latter case, Fe and Si behave as in the previous case, Mg is removed, and S added to the system. Inasmuch as both the olivine and troilite-pyroxene aggregate develop as pseudomorphs after the same pyroxene grain, the

probability of the origin of one or another rim is described by the schematic reaction: $Ol_{0.28} \Rightarrow Px_{0.30} + Tr$, which is primarily controlled by the activity of sulfur that seems to have increased Mg mobility.

The interaction between the sulfide-metallic matrix and silicate material is most vividly expressed at the boundary with silica-pyroxene chondrules, where a metasomatic zonation forms:

$$\underset{1}{Silica + Px_{0.25}} \mid \underset{2}{Px_{0.60}} \mid \underset{3}{Px_{0.40} + Tr} \mid \underset{4}{Ol_{0.30} + Km \pm Tr} \mid \text{sulfide-metallic matrix}$$

$$\overset{\text{S, Fe}}{\longleftarrow} \qquad \overset{\text{Si}}{\longrightarrow}$$

The occurrence of such a zoning suggests that the solid material of the chondrules and their fragments was extensively reworked by iron- and sulfur-rich fluids. The primary assemblage $Silica + Px_{0.25}$ is preserved in the core of the chondrule (Fig. 4), it gives way to more ferrous pyroxene ($Px_{0.60}$) in zone 2 and then to assemblages of less ferrous pyroxene with troilite in zone 3. Sometimes the monomineral pyroxene zone is absent, and the primary assemblage ($Silica + Px_{0.25}$) occurs in an immediate contact with the troilite-pyroxene assemblage, which may be controlled by the activity of sulfur. The next zone (zone 4) is composed of the assemblage $Ol_{0.30} + Km \pm Tr$ and results from active assimilation of the silicate material of the chondrule by the matrix. The removal of silica promotes the development of the outermost *Ol-Km* zone with a simultaneous increase in the iron mole fraction of the olivine toward the matrix, with the maximum ($f = 0.43$) values occurring at its boundary.

The increase in the iron mole fraction of olivine in the outer rims on chondrules reflects the more oxidized conditions at the contact with the matrix. The replacement by the matrix material is often so active that the silicate material of chondrules and their fragments remain merely as rounded or irregular formed relics, which are also zoned (Fig. 1, right). Therewith the matrix material shows various chemical aggressiveness of with respect to chondrules of various types. The pyroxene-rich chondrules are replaced more actively than the olivine-rich, up to nearly complete replacement of the pyroxene chondrules, a phenomenon seemmingly caused by the greater chemical differences between the pyroxene and, particularly, silica-pyroxene chondrules, on the one hand, and the volatile-rich sulfide-metallic matrix, on the other.

Because the iron mole fraction of olivine becomes constant at the boundaries of chondrules of all types, in the extensively oxidized HKOs occur in the matrix, and in relic olivine grains in the matrix, on the one hand, whilst the overall iron mole fraction of the troilite-pyroxene aggregates is also constant ($f = 0.69 - 0.72$) at the boundaries of silica-pyroxene chondrules, at the boundaries of single pyroxene grains with the matrix, and around pyroxene grains in extensively oxidized HKO, on the other hand, the interaction process of the matrix with silicate chondrules and their fragments seems to have proceeded at equilibrium. Noteworthy, by the interaction time, both the silicate chondrules and HKO had became solid.

FIGURE CAPTIONS: Fig. 1. The fine-grained silicate-iron matrix material. Interaction between matrix, on the one hand, and olinine-pyroxene chondrule (left), and silicate fragments, on the other hand. Fig. 2. Contact of a *Silica-Px* chondrule (17) with matrix material. *Ol* - olivine; *Tr + Px* - Tr-Px aggregate; *Px* - pyroxene. Fig. 3. Tabular grain of magnesian pyroxene (black) partly replaced by a troilite-pyroxene pseudomorph (at the contact with troilite) and partly by ferrous olivine (at the contact with kamacite). *Tr* - troilite; *Km* - kamacite. Fig. 4. Zoning resulted from the interaction between a silica-pyroxene chondrule (22) with the material of matrix. 1 - *Silica-Px* chondrule; 2 - monomineral *Px* zone; 3 - *Tr - Px* zone; 4. *Ol-Km ± Tr* zone.

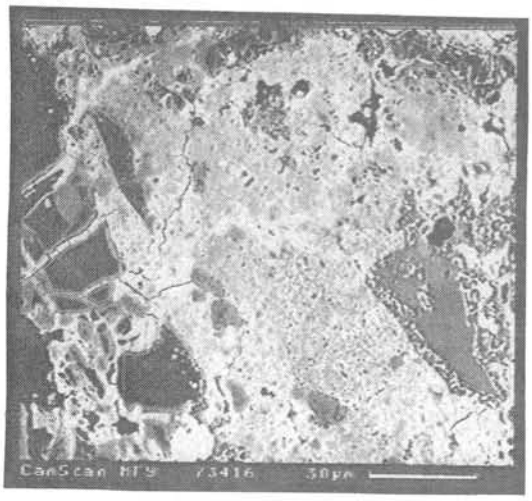

Fig. 1.

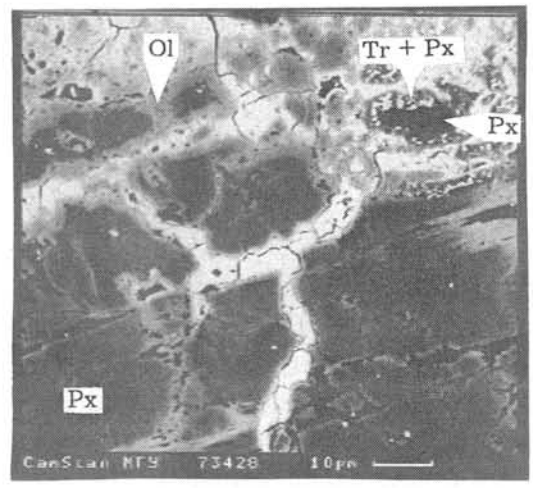

Fig. 2.

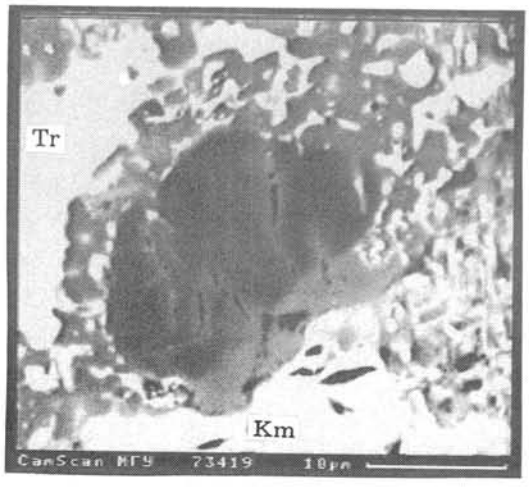

Fig. 3.

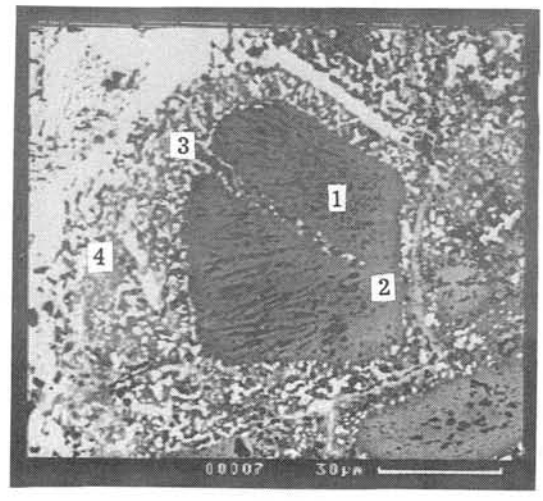

Fig.4.

ACKNOWLEDGMENTS: We are grateful to National Institute of Polar Research (Tokyo) for loaning the Antarctic Meteorite samples. This work was supported by Russian Foundation for Basic Research, grant 96-05-65387.

REFERENCES: [1] Zinovieva *et al.* (1996) *LPS XXVII*, 1499-1500; [2] Zinovieva *et al.* (1996) *Intern. Conf. Regularities of the Earth crust evolution*, (in press, in Russian); [3] Zinovieva *et al.* (1996) *21th Symp. Antarct Meteorites* (Abstr.), this volume.

ORIGIN MECHANISM OF HERCYNITE-KAMACITE OBJECTS: EVIDENCE FOR LIQUID IMMISCIBILITY PHENOMENA IN THE YAMATO-82133 (H3) ORDINARY CHONDRITE

Nina G. Zinovieva, Olga B. Mitreikina, and Lev B. Granovsky
Department of Petrology, Faculty of Geology, Moscow State University, Lenin Gory, Moscow 119899, Russia

Systematic studies of chondritic objects allowed us to recognize several lines of textural and petrologic evidence for their melt-related origin. This concept required support from experimental modeling of chondritic textures and the identification of those features of natural objects which could provide witness to equilibrium between the chondrule and matrix compositions.

The possibility of liquid immiscibility in chondrite material was demonstrated in experiments on its melting in vacuum [1], melting at pressures ranging from 6 to 30 kbar [2], and melting, in reduced conditions, of materials chemically approximating chondrites [3]. Experiments on iron-silicate liquid immiscibility in picritic glass were performed in graphite crucibles; before melting, Fe, S, and Ni were added to the glass to make its composition close to that of chondrite. The experiments have demonstrated that, first, the iron-silicate liquid immiscibility of the melt is characterized by equilibrated chondrules and matrix, as it follows from the systematic correlation between the chemistry of the silicate chondrules and Fe-Ni phase in the matrix (phenomenon known as the Prior rule), and, second, the iron-sulfide immiscibility occurs if the system contains carbon, a natural condition required by iron-sulfide liquid immiscibility, which can be inferred from textural phase relationships of not only chondrites but also iron meteorites.

Detailed studies of the Yamato-82133 ordinary chondrite (H3) provided have furnished further support for that the processes in the chondrules and matrix were identical and proceeeded in equilibrium. Hercynite-kamacite objects (HKO), which we discovered earlier and described in [4, 5], are specific of the Yamato-82133 chondrite. These are regular hercynite-kamacite textures, which sometimes also contain corundum. In addition, the mineral assemblage usually includes whitlockite or Cl-apatite. Kamacite of these textures strongly dominates over hercynite and, particularly, over corundum. The two latter minerals have a triangular habit, which is determined by fractures cutting the kamacite at angles of 60° to one another (Fig. 1). HKO are common in the chondrite matrix, in which they occur interstitially between silicate chondrules (Fig. 2) and sometimes develop rounded aggregates resembling chondrules (Fig. 3) or veinlets in chondrules. These also occur in the chondrules as rounded droplets in olivine and pyroxene grains or in interstices between them (Fig. 4). Sometimes, the hercynite-kamacite droplets coalesce to form dumbbells (Fig. 5). The droplets are typically zoned (Fig. 6): the cores consist of hercynite-kamacite aggregates, sometimes in assemblage with corundum. Rounded aggregates of taenite are normally restricted to the marginal portions of the droplets; taenite and hercynite-free kamacite sometimes crystallize within HKO, with the hercynite-kamacite aggregate occurring interstitially. The core of the droplets are ubiquitously surrounded by whitlockite or Cl-apatite, sometimes with chromite, rims. The outermost zone consists of a monomineral olivine aggregate, whose olivine is more ferrous

than that in the chondrules, and forms pseudomorphs after pyroxene and olivine phenocrysts of the chondrule. The contours of primary grains can be readily perceived in the olivine rim. HKOs sometimes contain, although very seldom, troilite and have in this case a *Tr* + *Px* outer rim instead of an olivine one. The chondrules typically show very specific textures, in which silicate crystals are oriented toward the centers of the kamacite-hercynite droplets, whose melt crystallized after the silicate melt did and was partly squeezed into interstices between silicate grains. The origin of these textures was controlled by the immiscible separation of the chondrule melt into a formerly equilibrated silicate melt and a essentially metallic (with Al and, seldom, S) liquid rich in fluids. The richness of the hercynite-kamacite melt in fluids is substantiated by that the crystalline chondule material is metasomatized around HKOs (it contains olivine pseudomorphs after pyroxene in outer olivine rims). The alterations of the silicate material in chondrules by fluid equilibrated with HKO is similar to the interaction between the chondrules and matrix described in this same chondrite [6].

Noteworthy, the texture, mineral assemblage, and phase chemistries of HKO are analogous within the chondrules and matrix. The occurrence of the typical for this meteorite fragments of the matrix material in chondrules with specific features of liquid immiscibile separation into magnesian-silicate and aluminum-iron constituents illustrates the general mechanism of the iron-silicate immiscible separation in chondritic melts. Even if the origin of hercynite-kamacite melt in the matrix could be explained by impact melting (although the olivine and pyroxene in nearby chondrules and their fragments in the fine-grained matrix show no signs of impact metamorphism and, thus, contradict to this concept), textures indicative of the immiscible separation into magnesium-silicate and aluminum-iron constituents within the chondrules definitely argue for the liquid immiscibility of the chondrite melt.

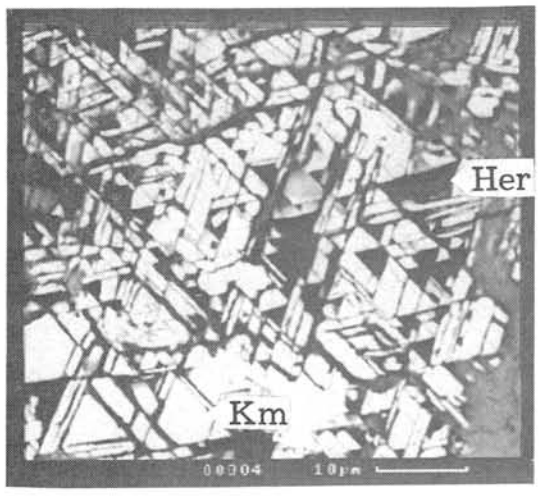

Fig. 1.

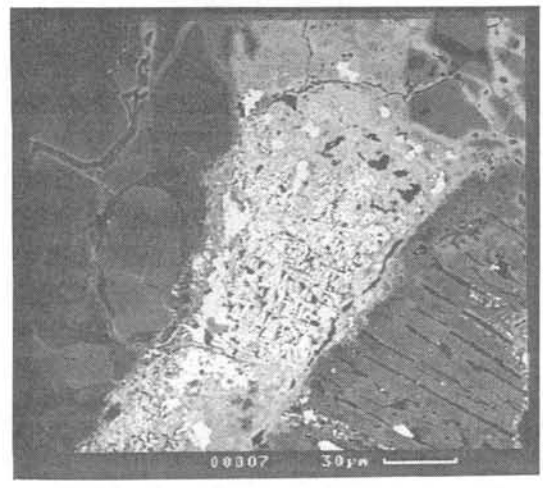

Fig. 2.

FIGURE CAPTIONS:

Fig. 1. Texture of a hercynite-kamacite aggregate. *Km* - kamacite, *Her* - hercynite, gray - iron oxides.

Fig. 2. Hercynite-kamacite aggregate cementing silicate chondrules.

Fig. 3. Chondrule-like hercynite-kamacite aggregate in the matrix.
Fig. 4. Abundant hercynite-kamacite droplets in a pyroxene-olivine porphyritic chondrule.
Fig. 5. Hercynite-kamacite dumbbells in a porphyritic pyroxene-olivine chondrule.
Fig. 6. Hercynite-kamacite droplet in a pyroxene-olivine porphyritic chondrule (fragment of Fig. 4). *Km* - kamacite, *Her* - hercynite, *Wt* - whitlockite, *Tn* - taenite, *Ol* - olivine.

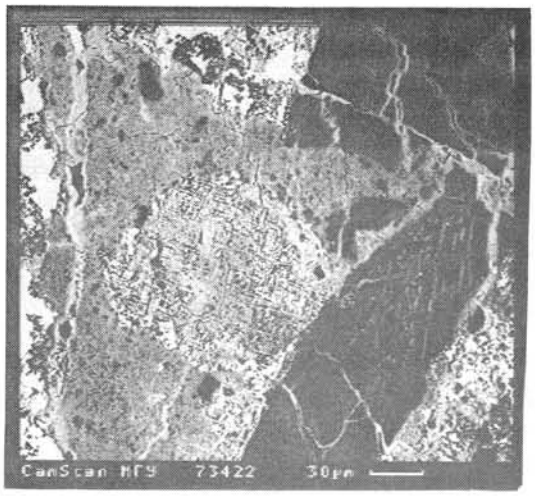

Fig. 3.

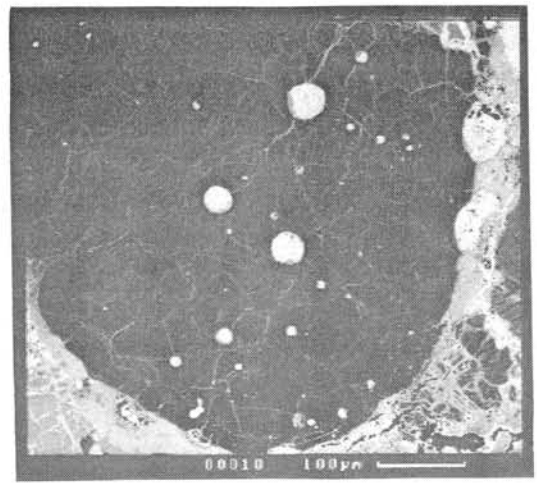

Fig. 4.

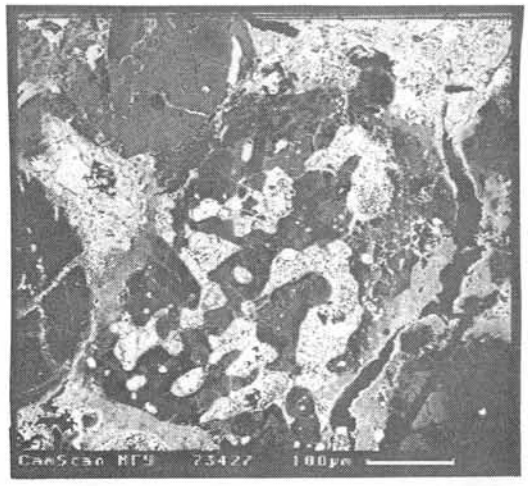

Fig. 5

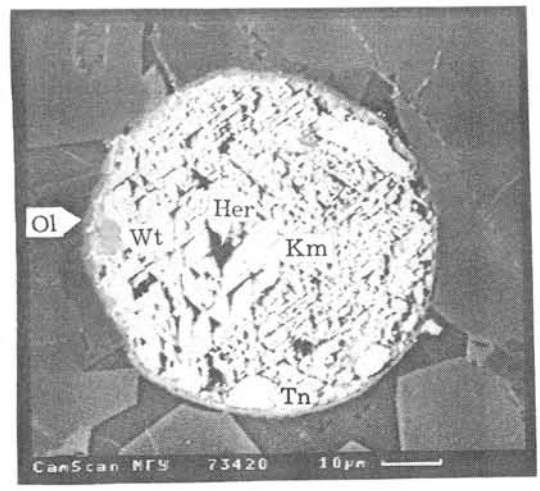

Fig. 6.

ACKNOWLEDGMENTS: We are grateful to National Institute of Polar Research (Tokyo) for loaning the Antarctic Meteorite samples. This work was supported by Russian Foundation for Basic Research, grant 96-05-65387.

REFERENCES: [1] Zinovieva *et al.* (1995) *Vestnik Mosk. Universiteta*, ser. 4, **5**, 42-50, (in Russian); [2] Takahashi (1983) *Proc. NIPR 8th Symp Antarct. Meteorites*, Sp. Is., 30, 168-180; [3] Marakushev *et al.* (1995) *Experiment in geosciences*, v. 4, **3**, 1-5; [4] Zinovieva *et al.* (1996) *LPS XXVII*, 1499-1500; [5] Zinovieva *et al.* (1996) *Intern. Conf. Regularities of the Earth crust evolution* (Abstr.), (in press, in Russian); [6] Zinovieva *et al.* (1996) *21th Symp. Antarct. Meteorites* (Abstr.), this volume.

AUTHOR INDEX

AUTHOR INDEX